GEOLOGICAL EVOLUTION OF TWO CRUSTAL SCALE SHEAR ZONES

PART I: THE RAND THRUST COMPLEX, NORTHWESTERN MOJAVE DESERT, CALIFORNIA

PART II: THE MAGDALENA METAMORPHIC CORE COMPLEX, NORTH CENTRAL SONORA, MEXICO

Thesis by
Jonathan Alan Nourse

In Partial Fulfillment of the Requirements
for the Degree of
Doctor of Philosophy

California Institute of Technology
Pasadena, California

1989
(Submitted May 18, 1989)

ACKNOWLEDGMENTS

The two field studies described below would not have been possible without the guidance and support of my thesis advisor, Professor Leon T. Silver. Lee recognized my inclination for field geology, and was instrumental in nurturing my interest in deformed crystalline rocks. Through his broad based experience and geological insight I was introduced to two exciting and regionally relevant tectonic problems.

Financial support for field and laboratory research came primarily from Silver, through grants awarded by the National Science Foundation and Arco, Inc. Some of my field expenses were covered by two grants from Sigma Xi. A Caltech student loan made it possible for me to purchase a used field vehicle.

Field mapping was carried out with the assistance of several adventurous friends. The field assistance of Allison Bent during one hot July weekend in the Rand Mountains is gratefully acknowledged. Paul Stubbe spent two weeks in Sonora helping me traverse some highly inaccessible country. With Bridget Jensen and the aid of her Jeep Cherokee I was able to explore a large region of northern Sonora. Steve Wickham and Ann Bykerk-Kauffman offered insightful field observations during separate trips to Mexico. Never to be forgotten, the advice and mechanical wizardry of Andy Gaynor were critical factors in my struggles to keep the truck running through thick and thin.

My understanding of regional geology and tectonics was greatly enhanced by discussions with numerous field geologists. These persons include Lee Silver, Tom Anderson, Gordon Haxel, Steve Reynolds, Steve Naruk, George Gehrels, Andy James, Eric James, George Smith, Chris Smith, Barbara

John, Joanne Stock, Jack Stewart, Jaime Roldan-Quintana, Jose Luis Rodriguez-Castaneda, Tito Rey Montano, Gordon Gastil, Kees de Jong, Cesar Jacques-Ayala, Juan Carlos Garcia, and Carlos Gonzalez-Leon.

Drafting of the illustrations was facilitated by equipment and supplies graciously provided by Jan Mayne. In Hermosillo, geologists at the Instituto de Geologia kindly allowed me access to their library and drafting room. Structural data were compiled by means of a stereonet program written by Richard Allmendinger. Strain data were plotted using a computer program devised by Declan de Paor. Janet Teshima, Rob Ripperdan, Eric James, and Charlie Rubin educated me on some of the fine points of the Macintosh system.

Lastly, my parents, Ann and Alan Nourse deserve special thanks for years of support. Their financial assistance and moral encouragement made my tenure as a graduate student immeasurably easier.

ABSTRACT

The geology and structure of two crustal scale shear zones were studied to understand the partitioning of strain within intracontinental orogenic belts. Movement histories and regional tectonic implications are deduced from observational data. The two widely separated study areas bear the imprint of intense Late Mesozoic through Middle Cenozoic tectonic activity. A regional transition from Late Cretaceous-Early Tertiary plutonism, metamorphism, and shortening strain to Middle Tertiary extension and magmatism is preserved in each area, with contrasting environments and mechanisms. Compressional phases of this tectonic history are better displayed in the Rand Mountains, whereas younger extensional structures dominate rock fabrics in the Magdalena area.

In the northwestern Mojave desert, the Rand Thrust Complex reveals a stack of four distinctive tectonic plates offset along the Garlock Fault. The lowermost plate, Rand Schist, is composed of greenschist facies metagraywacke, metachert, and metabasalt. Rand Schist is structurally overlain by Johannesburg Gneiss (= garnet-amphibolite grade orthogneisses, marbles and quartzites), which in turn is overlain by a Late Cretaceous hornblende-biotite granodiorite. Biotite granite forms the fourth and highest plate. Initial assembly of the tectonic stack involved a Late Cretaceous? south or southwest vergent overthrusting event in which Johannesburg Gneiss was imbricated and attenuated between Rand Schist and hornblende-biotite granodiorite. Thrusting postdated metamorphism and deformation of the lower two plates in separate environments. A post-kinematic stock, the Late Cretaceous Randsburg Granodiorite, intrudes deep levels of the complex and contains xenoliths of both Rand Schist and mylonitized Johannesburg? gneiss.

Minimum shortening implied by the map patterns is 20 kilometers.

Some low angle faults of the Rand Thrust Complex formed or were reactivated between Late Cretaceous and Early Miocene time. South-southwest directed mylonites derived from Johannesburg Gneiss are commonly overprinted by less penetrative north-northeast vergent structures. Available kinematic information at shallower structural levels indicates that late disturbance(s) culminated in northward transport of the uppermost plate. Persistence of brittle fabrics along certain structural horizons suggests a possible association of late movement(s) with regionally known detachment faults. The four plates were juxtaposed and significant intraplate movements had ceased prior to Early Miocene emplacement of rhyolite porphyry dikes.

In the Magdalena region of north central Sonora, components of a pre-Middle Cretaceous stratigraphy are used as strain markers in tracking the evolution of a long lived orogenic belt. Important elements of the tectonic history include: (1) Compression during the Late Cretaceous and Early Tertiary, accompanied by plutonism, metamorphism, and ductile strain at depth, and thrust driven? syntectonic sedimentation at the surface. (2) Middle Tertiary transition to crustal extension, initially recorded by intrusion of leucogranites, inflation of the previously shortened middle and upper crustal section, and surface volcanism. (3) Gravity induced development of a normal sense ductile shear zone at mid crustal levels, with eventual detachment and southwestward displacement of the upper crustal stratigraphy by Early Miocene time.

Elucidation of the metamorphic core complex evolution just described was facilitated by fortuitous preservation of a unique assemblage of rocks and structures. The "type" stratigraphy utilized for regional correlation and strain analysis includes a Jurassic volcanic arc assemblage overlain by an Upper

Jurassic-Lower Cretaceous quartz pebble conglomerate, in turn overlain by marine strata with fossiliferous Aptian-Albian limestones. The Jurassic strata, comprised of (a) rhyolite porphyries interstratified with quartz arenites, (b) rhyolite cobble conglomerate, and (c) intrusive granite porphyries, are known to rest on Precambrian basement north and east of the study area. The quartz pebble conglomerate is correlated with the Glance Conglomerate of southeastern Arizona and northeastern Sonora. The marine sequence represents part of an isolated arm? of the Bisbee Basin.

Crosscutting structural relationships between the pre-Middle Cretaceous supracrustal section, younger plutons, and deformational fabrics allow the tectonic sequence to be determined. Earliest phases of a Late Cretaceous-Early Tertiary orogeny are marked by emplacement of the 78±3 Ma Guacomea Granodiorite (U/Pb zircon, Anderson et al., 1980) as a sill into deep levels of the layered Jurassic series. Subsequent regional metamorphism and ductile strain is recorded by a penetrative schistosity and lineation, and east-west trending folds. These fabrics are intruded by post-kinematic Early Tertiary? two mica granites. At shallower crustal levels, the orogeny is represented by north directed thrust faulting, formation of a large intermontane basin, and development of a pronounced unconformity. A second important phase of ductile strain followed Middle Tertiary? emplacement of leucogranites as sills and northwest trending dikes into intermediate levels of the deformed section (surficial volcanism was also active during this transitional period to regional extension). Gravitational instabilities resulting from crustal swelling via intrusion and thermal expansion led to development of a ductile shear zone within the stratigraphic horizon occupied by a laterally extensive leucogranite sill. With continued extension, upper crustal brittle normal faults (detachment faults) enhanced the uplift and tectonic denudation of this

mylonite zone, ultimately resulting in southwestward displacement of the upper crustal stratigraphy.

Strains associated with the two ductile deformation events have been successfully partitioned through a multifaceted analysis. R_f/ϕ measurements on various markers from the "type" stratigraphy allow a gradient representing cumulative strain since Middle Cretaceous time to be determined. From this gradient, noncoaxial strains accrued since emplacement of the leucogranites may be removed. Irrotational components of the post-leucogranite strain are measured from quartz grain shapes in deformed granites; rotational components (shear strains) are determined from S-C fabrics and from restoration of rotated dike and vein networks. Structural observations and strain data are compatable with a deformation path of: (1) coaxial strain (pure shear?), followed by (2) injection of leucogranites as dikes (perpendicular to the minimum principle stress) and sills (parallel to the minimum principle stress), then (3) southwest directed simple shear. Modeling the late strain gradient as a simple shear zone permits a minimum displacement of 10 kilometers on the Magdalena mylonite zone/detachment fault system. Removal of the Middle Tertiary noncoaxial strains yields a residual (or pre-existing) strain gradient representative of the Late Cretaceous-Early Tertiary deformation. Several partially destrained cross sections, restored to the time of leucogranite emplacement, illustrate the idea that the upper plate of the core complex has been detached from a region of significant topographic relief. 50% to 100% bulk extension across a 50 kilometer wide corridor is demonstrated.

Late Cenozoic tectonics of the Magdalena region are dominated by Basin and Range style faulting. Northeast and north-northwest trending high angle normal faults have interacted to extend the crust in an east-west direction. Net

extension for this period is minor (10% to 15%) in comparison to the Middle Tertiary detachment related extensional episode.

TABLE OF CONTENTS

LIST OF ILLUSTRATIONS

Oversize Figures

Appendices (available from author)

MOTIVATION AND SCOPE OF STUDY

A diversity of well exposed thrust faults and detachment faults in southern California, western Arizona, and northwestern Mexico provide potential constraints on the Late Mesozoic through Cenozoic tectonic history of the southwestern Cordillera. These low angle faults mark the locus of intense shearing, planes of failure along which significant displacements have occurred during regional shortening and/or extension of the middle and upper crust. Deformational fabrics developed in rocks adjacent to these faults record the cumulative imprint of large scale crustal movements. Crosscutting structures at many scales define the relative kinematic sequence as well as the geometry of the associated strain. Shear zones can thus be related to regional tectonic events. The intent of my thesis is to explore these relationships through the application of multiscale geological observations.

In the succeeding chapters, rocks involved in two important crustal scale shear zones are analysed in detail. The movement history of each shear zone is interpreted and then integrated into a regional tectonic framework. The models developed offer fresh insight into the tectonic evolution of the southwest Cordillera.

Complete documentation of a shear zone movement history should address the following questions:

(1) What rocks are affected by the shear zone, and what is its geographic extent?

(2) How much displacement has occurred?

(3) What was the direction of motion, and how does it relate to the larger

scale tectonic environment and regional stress regime?

(4) When was the main phase of movement?

(5) Has the shear zone been reactivated? If so, when and where did these reactivations take place, and what was their tectonic significance?

(6) At what temperature and depth did faulting occur, and how did these conditions evolve with time?

(7) To what degree did deformation within the shear zone approach a simple shear strain geometry?

(8) How does the shear zone movement history bear on the tectonic evolution of the region?

All of these questions are considered in my efforts to understand the movement histories of two quite dissimilar shear zones exposed in widely separated areas of the southwest Cordillera. The two study areas (shown in Figure 0.1) encompass low angle fault systems which developed within an evolving continental margin. The **Rand Thrust Complex** records a history of Late Cretaceous overthrusting followed by at least one episode of reactivation in a probable extensional environment. The **Magdalena Metamorphic Core Complex** preserves a brittle-ductile normal sense shear zone which evolved in response to regional extension of a previously shortened (and inflated?) Middle Mesozoic through Middle Cenozoic crustal section. These conclusions are based largely upon field observations and visual measurements performed on rock samples in the laboratory. My research technique involved the mapping of rocks and structures at many scales, and the comparison of highly deformed rock assemblages to undeformed equivalents. As with most geological research, the story is not yet complete, but this work serves as a basis for future studies.

Figure 0.1: Map showing location of the Rand Thrust Complex and the Magdalena Metamorphic Core Complex. Stippled areas represent the lower plates of metamorphic core complexes. Hachured lines indicate major Middle Tertiary detachment faults. Barbed lines are thrust faults. LA = Los Angeles; SD, San Diego; m, Mexicali; Y, Yuma; A, Ajo; P, Phoenix; T, Tucson; N, Nogales; C, Caborca; M, Magdalena; Ca, Cananea.

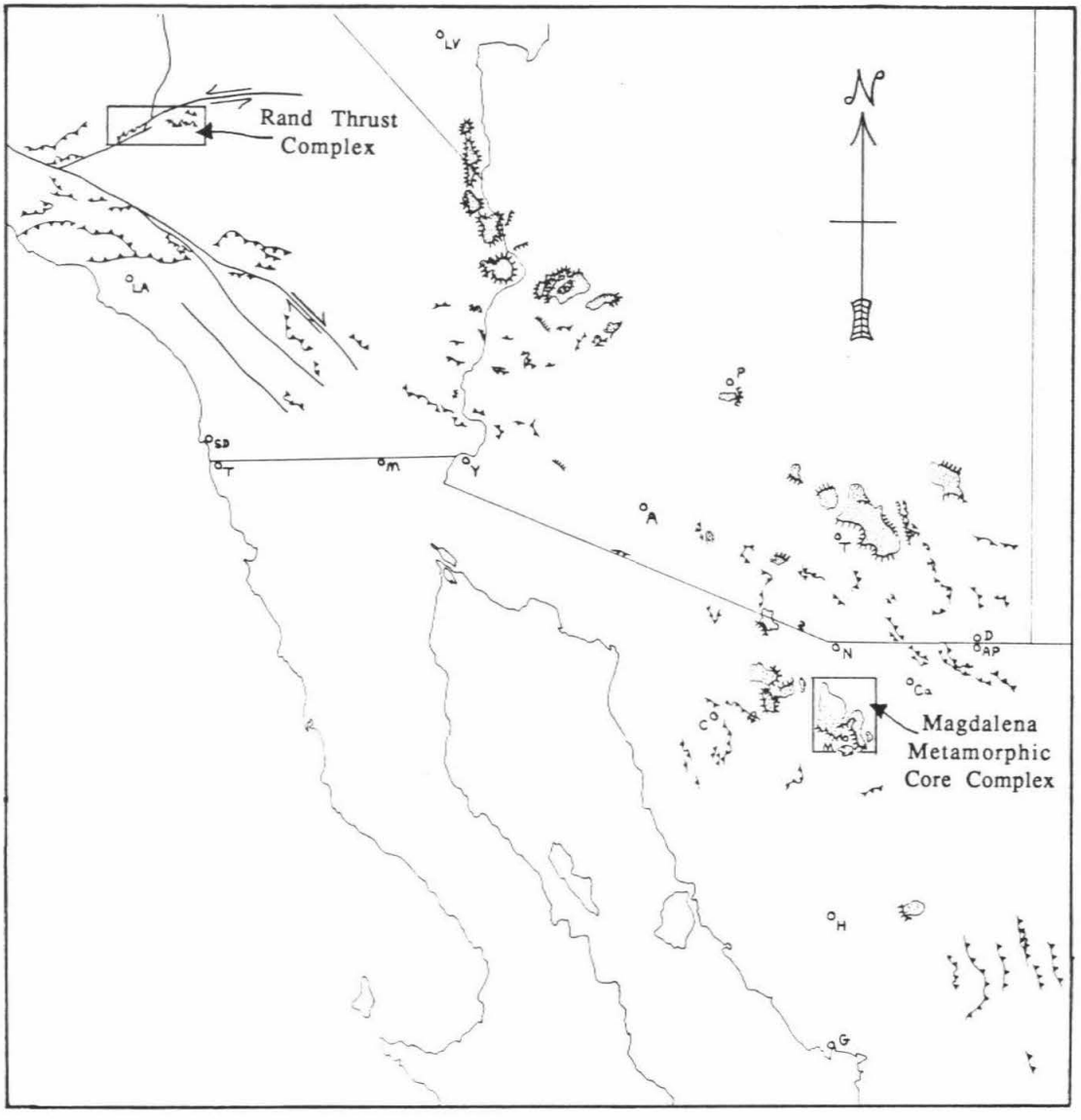

Figure 0.1

PART I:

THE RAND THRUST COMPLEX

CHAPTER 1

INTRODUCTION

In the northwestern Mojave desert a tectonic stack of at least four distinctive plutonic and metamorphic terranes is exposed along the crest of a faulted basement antiform. The four crystalline masses are separated by low angle faults which can be traced for tens of kilometers. This structural assemblage (hereafter referred to as the Rand Thrust Complex) has been offset left laterally about 60 kilometers by the Neogene Garlock Fault system. On a more regional scale, the Rand Thrust Complex shares a common structural setting with several other low angle fault systems exposed in widely scattered basement uplifts of southern California and southwestern Arizona (see Figure 1.1). Each of these fault complexes reveals a lower plate of schist derived from an oceanic protolith, structurally overlain by one or more plates of continental crystalline rock. The schist bodies comprise the deepest exposed structural levels of a large portion of the southwest Cordillera. The sequence of tectonic events leading to their present disposition is a controversial subject of critical importance to reconstructions of this region.

The multiplate tectonostratigraphy described below was first proposed by Lee Silver during his leadership of a Caltech advanced mapping class (in which I was an active participant). Silver was also first to suggest the correlation of specific components of the Rand Thrust Complex to schists, gneisses, and granites of the southern Sierra Nevada. The ideas and geological intuition of my thesis adviser thus played an important role in focusing my field research and providing a regional tectonic context for the structural and

Figure 1.1: Map showing two offset portions of the Rand Thrust Complex, the regional distribution of Pelona/Orocopia/Rand Schist, exposures of the Vincent/Chocolate Mountains thrust system, and important Neogene faults (heavy dark lines). Modified from Haxel and Dillon, 1978.

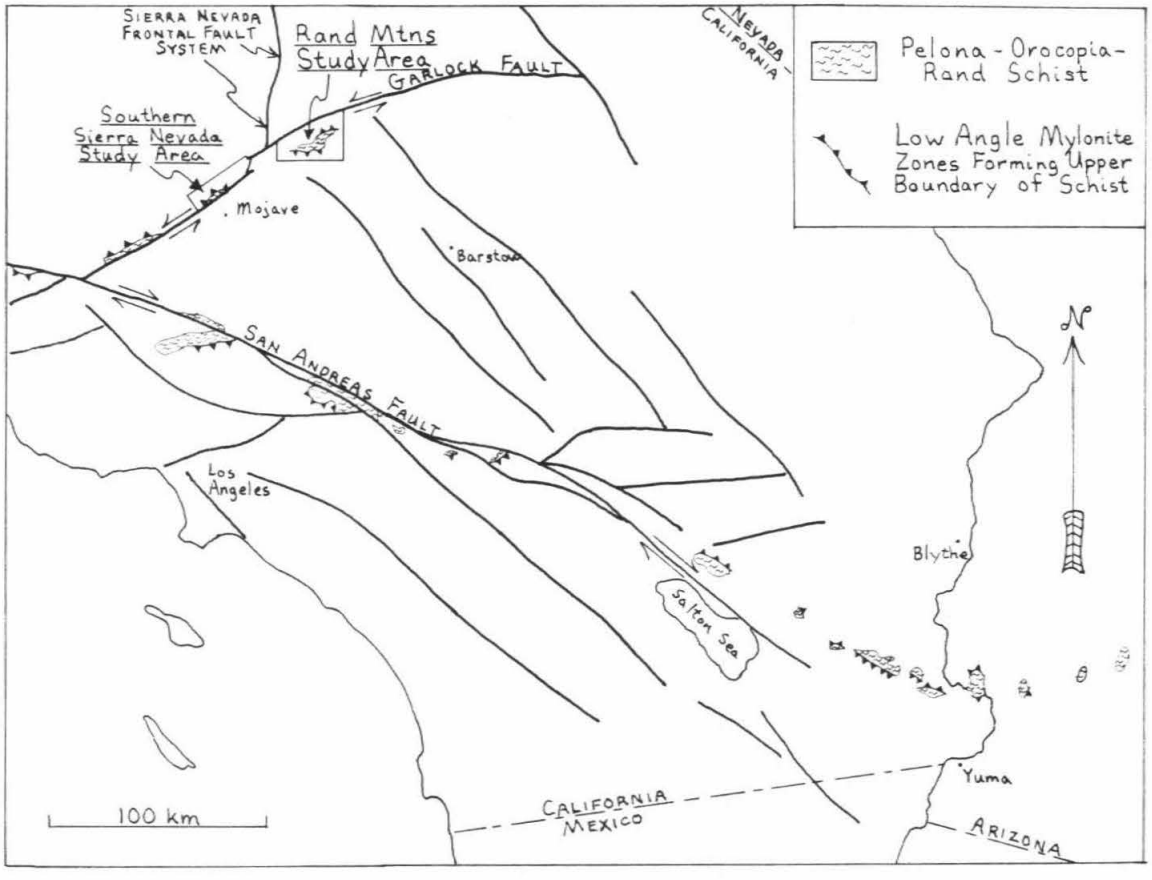
SIERRA NEVADA FRONTAL FAULT SYSTEM
Rand Mtns Study Area
GARLOCK FAULT
NEVADA
CALIFORNIA
Pelona - Orocopia - Rand Schist
Low Angle Mylonite Zones Forming Upper Boundary of Schist
Southern Sierra Nevada Study Area
Mojave
Barstow
SAN ANDREAS FAULT
Los Angeles
Blythe
Salton Sea
Yuma
100 km
CALIFORNIA
MEXICO
ARIZONA
N

Figure 1.1

kinematic analysis outlined below. A well preserved portion of the complex centered in the Rand Mountains was the target of my research during several excursions to the area between 1983 and 1988. Block faulted fragments of a correlative tectonostratigraphy in the southern Sierra Nevada were mapped in reconnaissance during the same time period.

The bulk of this portion of the dissertation addresses diverse mylonites and cataclasites from the Rand Mountains. These sheared rocks record a history of late Cretaceous to Middle Tertiary tectonic events which were responsible for assembly of the Rand Thrust Complex. Multiple overprinting of structures attests to the complexity of relative movements between various structural levels of the tectonic stack. Pre-thrusting fabrics within the two lowest plates provide insight into separate, earlier phases of regional metamorphism and deformation.

The movement history of the Rand Thrust Complex is developed in the following discussion. A regional tectonostratigraphy is defined and structures associated with three low angle faults are analysed at mesoscopic and microscopic scales. Directions of displacement are constrained by a variety of kinematic indicators. The sequence of fault motion is interpreted from crosscutting field relationships. Finally, absolute timing of the deformational sequence is bracketed by a number of well dated intrusive units which were emplaced during various stages of evolution of the complex.

PREVIOUS STUDIES

The Rand Mountains have been the subject of geological investigation since gold was discovered locally in 1893. The Rand Schist and associated rocks were first mapped for purposes of mineral resource evaluation (see early

reports by Hess, 1909; Hershey, 1912; Hulin, 1925; and Dibblee, 1952). Subsequent comparison of the Rand Schist to better known exposures of Pelona/Orocopia Schist in southwestern California (Dibblee, 1967; and Ehlig, 1968) sparked a renewed interest in the area by tectonics enthusiasts. Several workers have noted similarities in structural setting between the Rand/Pelona/Orocopia schists and their tectonically overlying gneissic and plutonic rocks (Dibblee, 1967; Ehlig, 1968; Vargo, 1972; Silver et al., 1984; Silver and Nourse, 1986; Postlethwait and Jacobsen, 1987). This peculiar structural association is believed to represent an important regional tectonic event which may have structurally underplated a large portion of the southwest Cordillera with an oceanic terrane.

A variety of models have been proposed to explain the present structural geometry of the northwestern Mojave desert. Haxel and Dillon (1978) interpret the Rand Schist as a window through a regional thrust system which hypothetically extended across southern California and southwestern Arizona. In their two alternative models, the Pelona-Orocopia-Rand Schists were contemporaneously overthrust by continental crystalline rocks during either east directed subduction or the closing of a back arc or intra-arc basin. Silver (1986) proposed the correlation of lithologies and structures in the Rand Mountains to those exposed in the southern Sierra Nevada, and suggested their involvement in large scale detachment of part of the Sierran batholith. Postlethwait and Jacobson (1987) argue that the Rand thrust originally formed in a subduction zone, but has subsequently been reactivated as a low angle normal fault.

The ultimate test of these tectonic models is reconstruction of the crustal terranes involved. This requires the documentation of piercing points in conjunction with kinematic analysis of the terrane bounding shear zones.

Constraints on the direction, magnitude, and timing of important low angle fault movements in the Rand Mountains are evaluated below.

GENERAL GEOLOGICAL SETTING

The four plates of the Rand Thrust Complex are best exposed in the Rand Mountains near the mining communities of Johannesburg, Red Mountain, and Randsburg, California (see Figure 1.2). Outcrops of all structural levels are preserved at various positions along the crest and flanks of an east trending antiform. The two lowest plates of the complex are intruded by a granodiorite stock in the vicinity of Randsburg. All but the uppermost plate are intruded by a family of felsite dikes which emanate from a hypabyssal intrusive center located midway between Randsburg and Johannesburg. The crystalline complex is unconformably overlapped by a thick section of middle to upper Tertiary sedimentary and volcanic rocks that comprise most of the nearby Lava Mountains. Folding of this section and the underlying basement rocks was contemporaneous with deposition.

The present level of exposure in the Rand Mountains is due in part to uplift along a major east-northeast trending normal fault that bounds the range on its northwest side. Less significant normal faults with structural throws of tens and hundreds of meters disrupt the crystalline complex along north and northeast trends.

Structurally disturbed components of the Rand Thrust Complex are preserved along the prominent range front of the southern Sierra Nevada, immediately north of the Garlock Fault, 10 to 15 kilometers northeast of Mojave, California (see Figure 1.3). As in the Rand Mountains, the crystalline assemblage in this area is intruded by felsite dikes and overlain by Tertiary sedimentary and volcanic rocks. Also, northeast and east-northeast striking

Figure 1.2: Geologic Map of the Rand Mountains and vicinity. After Hulin, 1925, Smith, 1964, and Dibblee, 1952, 1967.

Figure 1.3: Geologic sketch map of a portion of the southern Sierra Nevada. Based in part on mapping by Dibblee, 1952. Symbols as in Figures 1.2, 2.1-2.2.

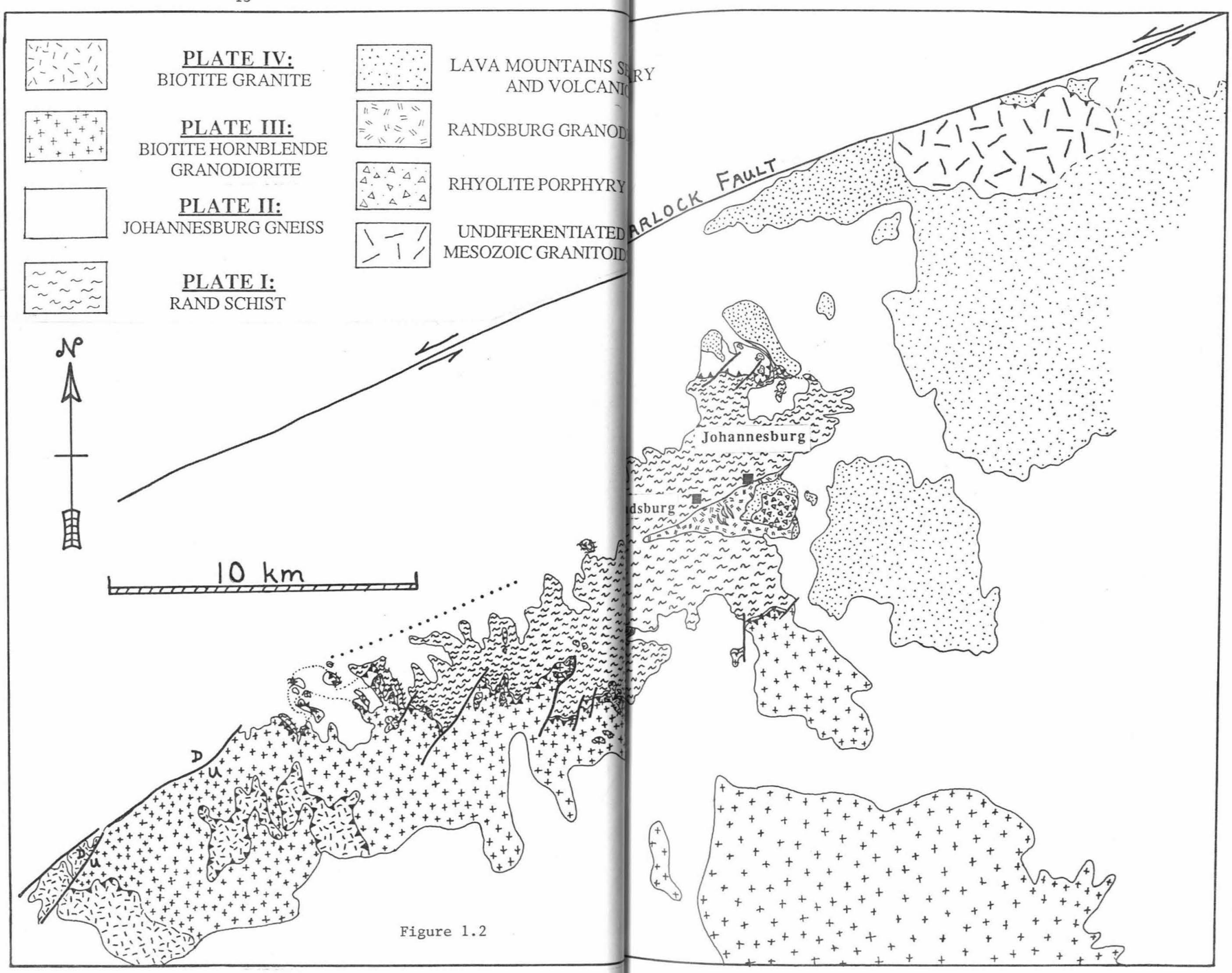
PLATE IV:
BIOTITE GRANITE
PLATE III:
BIOTITE HORNBLENDE
GRANODIORITE
PLATE II:
JOHANNESBURG GNEISS
PLATE I:
RAND SCHIST
LAVA MOUNTAINS SE RY
AND VOLCANI
RANDSBURG GRANOD
RHYOLITE PORPHYRY
UNDIFFERENTIATED
MESOZOIC GRANITOID
ARLOCK FAULT
Johannesburg
dsburg
N
10 km
D
U
D
U

Figure 1.2

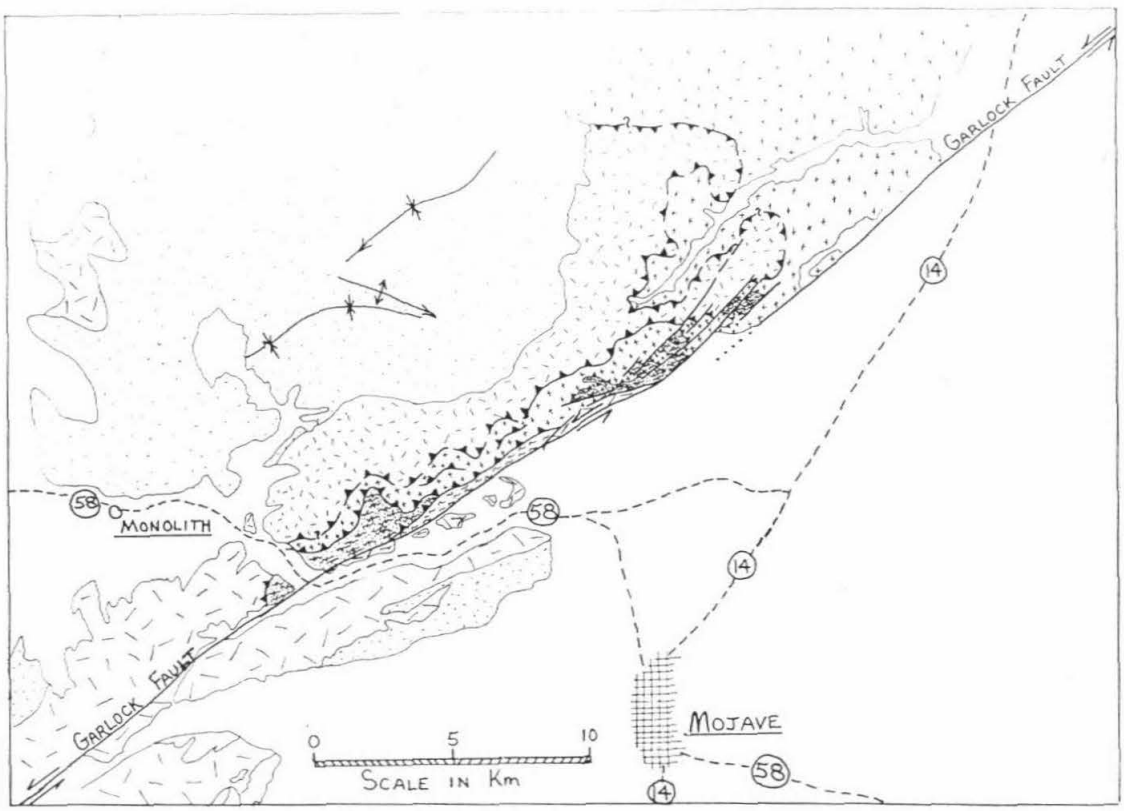
GARLOCK FAULT
14
58
MONOLITH
58
14
GARLOCK FAULT
0
5
10
SCALE IN Km
MOJAVE
58
14

Figure 1.3

normal faults have downdropped the tectonic stack in a stairstep fashion. Some of these faults may record minor amounts of left lateral slip sympathetic to motion along the Garlock Fault zone. Late Cenozoic tectonics of this region reflect the kinematic interaction between a left step in the Garlock Fault and a system of normal faults that bound the eastern Sierra Nevada (see Figure 1.1).

CHAPTER 2

DEFINITION AND DISTRIBUTION OF TECTONOSTRATIGRAPHY

Figures 2.1 and 2.2 summarize tectonostratigraphic relationships preserved in the two offset segments of the Rand Thrust complex. These diagrams integrate the field observations and geological mapping of several workers, including myself, Silver et al. (1984), Silver (1986), Dibblee (1967), Smith (1964), and Hulin (1925). My geologic map of the south flank of the Rand Mountains Antiform is compiled at 1:16,000 scale in Plates 1A and 1B. Sample locations are also plotted on this map. Sample descriptions are compiled in Appendix A. In the following discussion, each component of the tectonostratigraphy is described in structural sequence, from the lowest exposed structural levels to the highest.

PLATE I

The lowest exposed plate of the Rand Thrust Complex is Rand Schist. The schist occupies the stuctural core of a regional east trending fold hereafter referred to as the Rand Mountains Antiform. The dominant lithologic constituent of Plate I is a gray, well foliated plag-musc-qtz-ep-chl±bio±gt schist This rock is commonly associated with less foliated dark green to black mafic schists composed of amphibole and plagioclase. 4 centimeter to 5 meter thick interlayers of purple quartzite with varying amounts of musc-gt-mgt±crossite are locally abundant. Rare marble is present in thin lenses (Hulin, 1925). The protoliths of these metamorphic rocks were probably marine graywackes, basalts, cherts, and limestones. Collectively they are

Figure 2.1: Generalized tectonostratigraphic relations in the Rand Mountains study area.

Figure 2.2: Generalized tectonostratigraphic relations in the southern Sierra Nevada study area.

GENERALIZED TECTONOSTRATIGRAPHY
(RAND MOUNTAINS AREA)

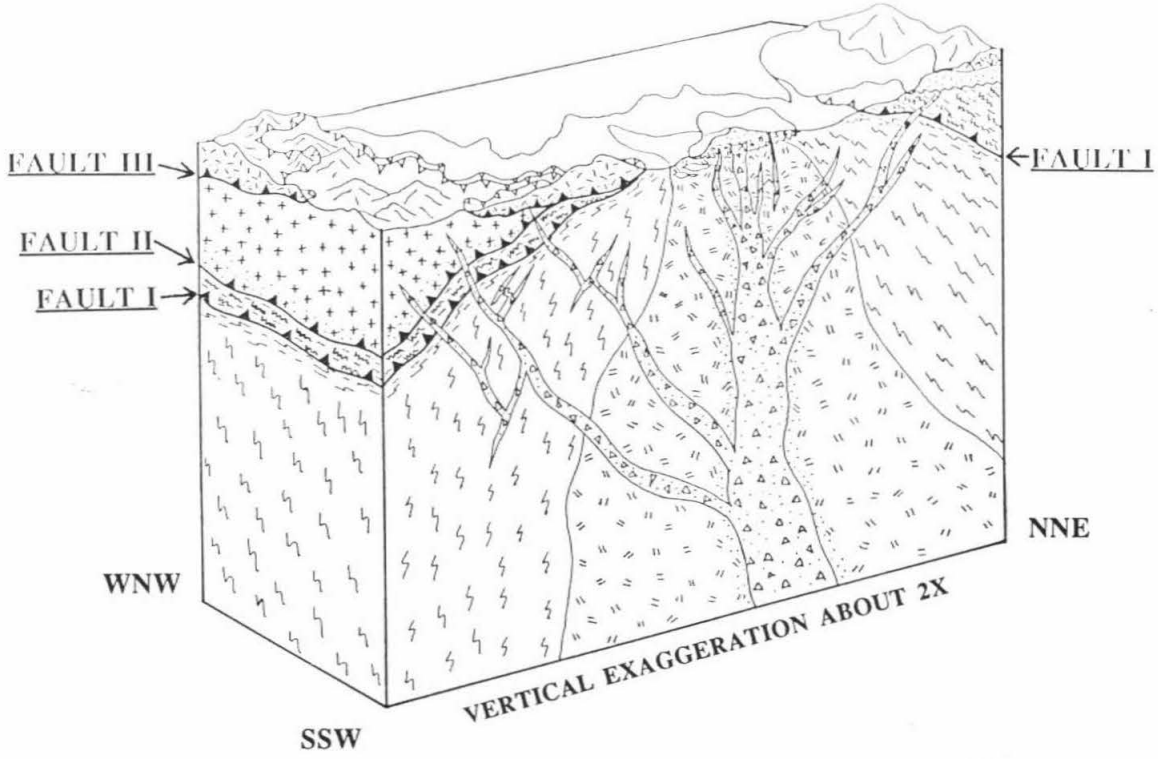

PLATE IV:
BIOTITE GRANITE

PLATE III:
BIOTITE HORNBLENDE GRANODIORITE

PLATE II:
JOHANNESBURG GNEISS

PLATE I:
RAND SCHIST

LAVA MOUNTAINS SEDIMENTARY AND VOLCANIC SERIES

RANDSBURG GRANODIORITE

RHYOLITE PORPHYRY

UNDIFFERENTIATED MESOZOIC GRANITOIDS

Figure 2.1

GENERALIZED TECTONOSTRATIGRAPHY
(SOUTHERN SIERRA NEVADA AREA)

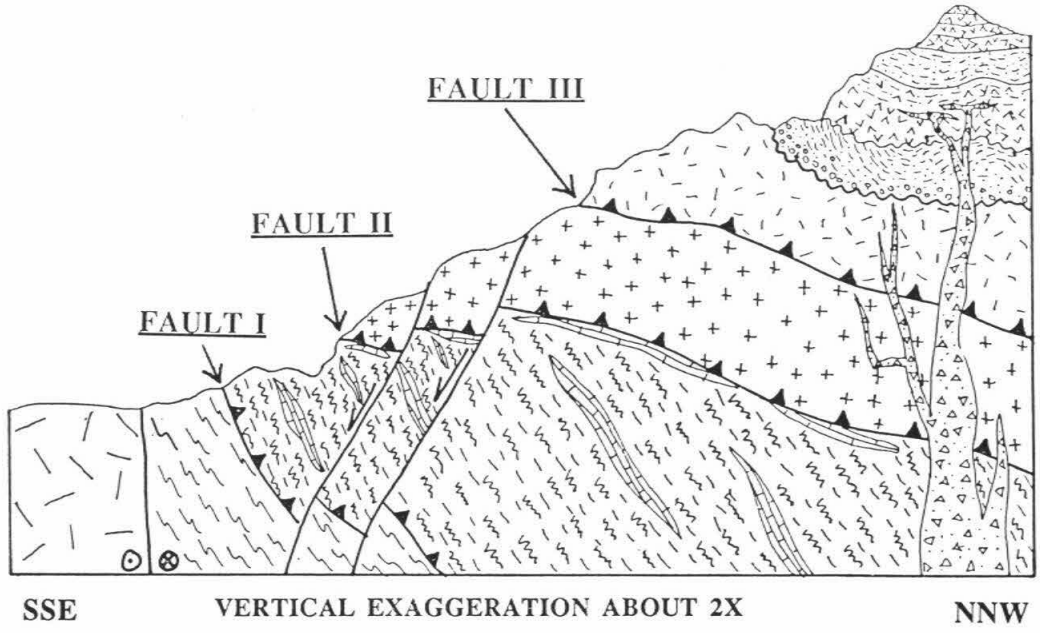

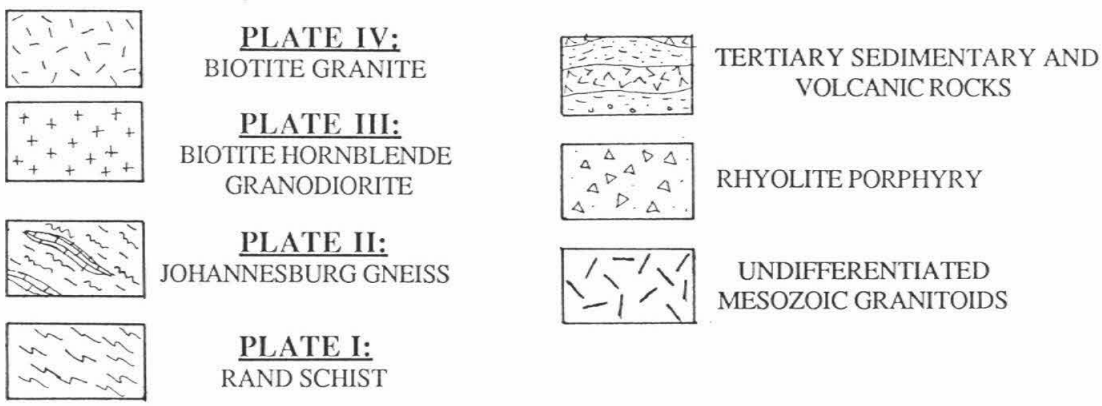

Figure 2.2

interpreted to be a metamorphosed trench/oceanic basin assemblage. A similar environment of accumulation has been suggested for the protoliths of the Pelona, Orocopia, and Chocolate Mountain schists of southeastern California and southwestern Arizona (Haxel and Dillon, 1978). These interpretations are supported by a variety of trace element and isotope studies (Bennett and DePaulo, 1982; Dawson and Jacobson, 1986; Haxel and Tosdal, 1986; Haxel et al., 1987).

A narrow slice of Rand Schist occurs north of the Garlock Fault, where it appears to dip beneath higher grade gneisses (see Figure 1.3; see also Ross, 1982). Most primary tectonic contacts in the area are disturbed. This Rand Schist exposure is the deepest structural level of the Rand Thrust Complex in the immediate area. It serves as an approximate piercing point to the axial trace of the Rand Mountains Antiform.

The Rand Schist contains abundant veins of coarsely crystalline white bull quartz that range in thickness from 4 centimeters to 2 meters. These veins tend to occur as discontinuous sheets concordant to the schistosity of their host rock. Occasionally, the veins cut sharply across the schistosity. Away from Fault I they exhibit no deformational fabric. These bull quartz veins are interpreted to be late stage mobilizates of silica emplaced during the final stages of prograde metamorphism. Ross (1982) arrived at a similar interpretation for bull quartz veins in the Rand Schist of the southern Sierra Nevada.

The Rand Schist exhibits some internal variation in metamorphic grade. Postlethwait and Jacobsen (1987) report systematic trends in the compositions of amphiboles extracted from the mafic schists. Apparently, sodium rich crossite occurs at the deepest structural levels whereas calcium rich hornblende is found at shallower levels. These authors also cite variations in

bulk metamorphic assemblage which indicate that lower parts of the Rand Schist are metamorphosed to blueschist-transitional-greenschist facies while upper portions are at albite-epidote-amphibolite grade (see also Jacobson and Sorensen, 1986). They argue that the vertical metamorphic zonation in the Rand Schist was acquired during deformation in a subduction zone environment.

PLATE II

Plate I is structurally overlain by crystalloblastic gneisses of higher metamorphic grade and differing deformational history. Named the Johannesburg Gneiss by Hulin (1925), this unit consists of well foliated, locally mylonitic orthogneisses of granitic to dioritic composition intercalated with marbles and quartz rich metasedimentary rocks. A 900 meter thick section of the garnet-amphibolite grade assemblage is exposed in its type locality north of Johannesburg (see Figure 2.3). In this area all original lithological contacts have been transposed into a north dipping compositional layering. A fault contact with structurally lower Rand Schist dips concordantly beneath Plate II at an angle of 55^{o} or less (see Figures 2.1 and 2.3).

On the south flank of the Rand Mountains Antiform, remnants of Johannesburg Gneiss occur as a thin (0 to 35 meters) tectonic slice sandwiched between Plates I and III. Here, all constituents of the gneiss are overprinted by mylonitic fabrics. A fine grained marble tectonite frequently occupies the lowest structural position of Plate II, and commonly, a thicker, more coarsely crystalline marble layer occurs at the highest level.

Probable displaced lithologic equivalents of Plate II occur on the north side of the Garlock Fault (see Figures 1.3 and 2.2). Here, garnet bearing orthogneisses, marbles, amphibolites, sparse quartzites, and abundant

Figure 2.3: Geologic map of the northern Rand thrust. Map units as follows: rs = Rand Schist, jogn = Johannesburg Gneiss, undifferentiated, mgm = mafic gneiss component of jogn, vertical ruled pattern = marble component of jogn, stippled pattern = quartzitic component of jogn, gr = cataclatic leucogranite, Tp = Early? Miocene rhyolite porphyry, Tv = undifferentiated Tertiary volcanic and sedimentary rocks, Qv = colluvial cover derived from Tertiary volcanic rocks, Q = alluvium.

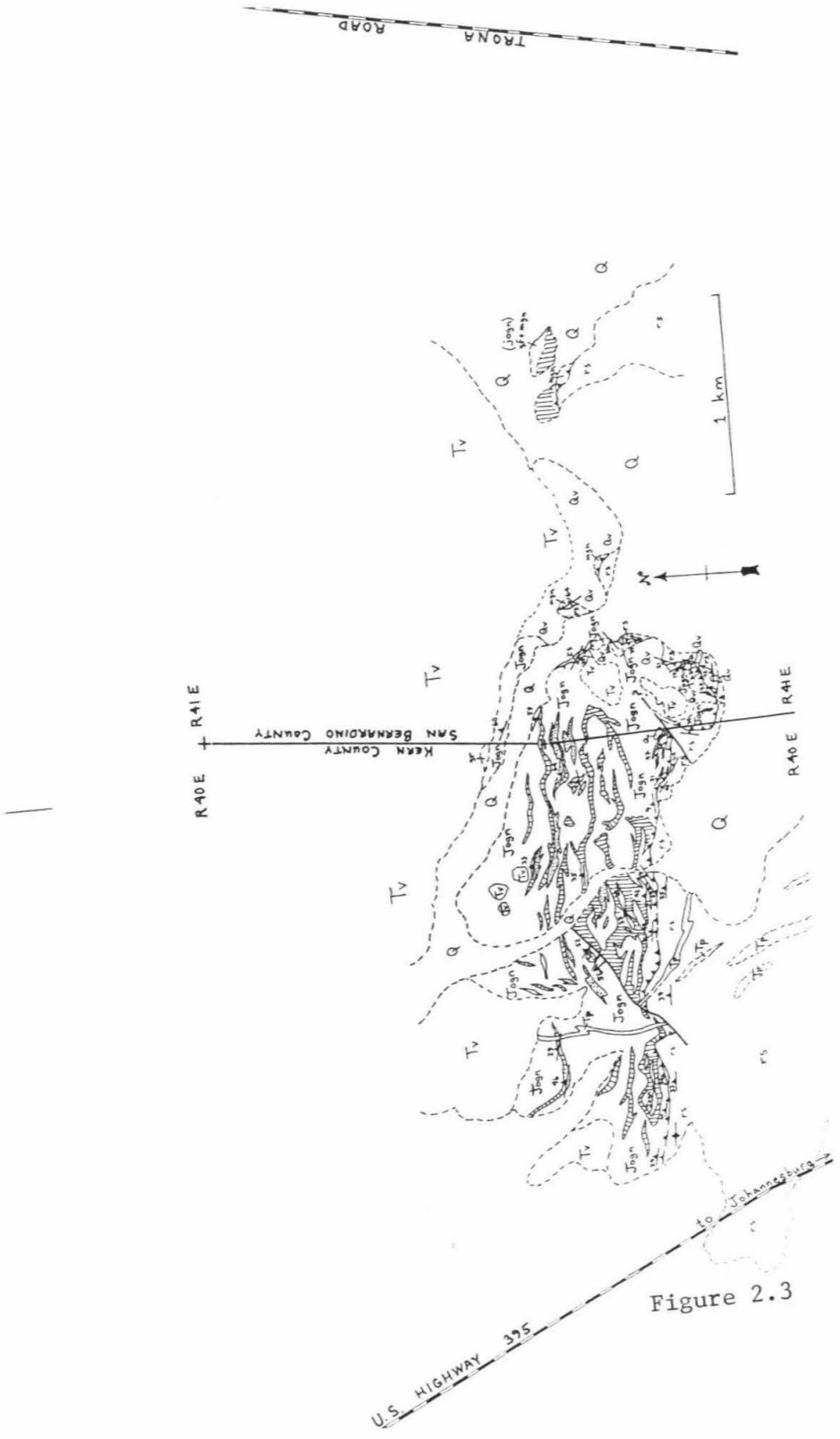
TRONA ROAD
1 km
N
KERN COUNTY
SAN BERNARDINO COUNTY
R40E
R41E
R40E
R41E
Tv
Q
Qv
Jogn
U.S. HIGHWAY 395
to Johannesburg

Figure 2.3

mylonites are exposed as discontinuous fault slices in the lower portions of canyons draining the range front. Despite significant disruption by Neogene faulting and recent landsliding, it is possible in several areas to delineate a shallow north dipping fault contact between the gneisses of Plate II and a structurally higher granodiorite of Plate III. Frequently the contact is marked by a 1 to 15 meter thick layer of coarsely crystalline marble. In many places this low angle fault surface is clearly discordant to steep foliations in the underlying gneisses.

The rocks of Plate II may correlate with a similar group of high grade gneisses exposed to the northwest in the Tehachapi Mountains. These gneisses have been mapped in reconnaissance by Sharry (1981) and Ross (1982). Their U/Pb, Rb/Sr, and oxygen isotopic systematics were studied by Saleeby and Sams (1987). The Tehachapi Mountains gneiss complex includes a variety of garnet+pyroxene bearing orthogneisses of dioritic to granitic composition, with associated metasedimentary screens of pelitic, calcareous, and quartzofeldspathic material. Deep seated Early Cretaceous regional metamorphism of this assemblage culminated in the emplacement of several 100±5 Ma tonalitic plutons (Saleeby and Sams, 1987; Sams and Saleeby, 1988). The resemblance of these rocks to constituents of the Johannesburg gneiss is striking, as is their close proximity to a fault bounded slice of Rand Schist.

PLATE III

Plate II is structurally overlain in the Rand Mountains and in the southern Sierra Nevada by a medium grained porphyritic granodiorite. This rock varies in composition from hornblende-biotite-sphene quartz diorite or tonalite at deep structural levels to biotite quartz monzonite at shallow levels. It is commonly cut by leucocratic dikes or veins of aplite and pegmatite.

Dioritic xenoliths occur frequently. The geometry of Plate III is truly plate-like. Its structural thickness ranges from 0 to 500 meters over an exposed area of greater than 500 square kilometers.

In contrast to Plates I and II, Plate III is not penetratively deformed. However, irregular zones of intense cataclasis and chloritic alteration are present in the lowest (and sometimes the highest) structural levels of the granodiorite. True mylonitic textures are restricted to narrow, isolated shear zones. These localized deformational fabrics probably reflect movement along boundary structures during the tectonic emplacement and/or reactivation of Plate III.

Silver et al., (1984) report an age of 84±3 Ma for a hornblende-biotite-sphene granodiorite component of Plate III, based on U/Pb systematics on zircon. This age is interpreted as the primary crystallization age of the granodiorite.

PLATE IV

Scattered remnants of an orange weathering leucocratic biotite alkali granite with a maximum thickness of 50 meters structurally overlie Plate III in the southern Rand Mountains. A larger (greater than 750 meters thick) mass of a similar granite forms the highest component of the tectonic stack in the southern Sierra Nevada. The granite consists of a medium grained porphyritic phase with coarse quartz intruded by dikes of fine grained aplite. Biotite in the older phase is often completely replaced by iron oxide. The aplite resembles some of the dikes which cut Plate III. In one place, the porphyritic phase is intruded by a dike of medium grained biotite granodiorite similar to nearby parts of Plate III. Plate IV is therefore interpreted to be older than Plate III.

Nowhere in the mapped area was a **primary** intrusive contact observed between Plates III and IV, due to the persistance of a hydrothermal alteration zone in the lower 5 to 35 meters of the granite. Parts of the granite are commonly replaced by hematite, calcite, and silica, and the feldspars may be sericitized. Primary plutonic textures are locally overprinted by cataclasis and vein filling of fracture networks. This mappable alteration zone forms a resistant ledge which everywhere parallels a subhorizontal contact with structurally deeper Plate III.

A 1 to 5 meter thick ductile shear zone marked by quartz rich mylonites is preserved at the base of Plate IV in one area of the southeastern Rand Mountains (see Plate 1B). This subhorizontal fault cuts down section toward the northeast. Here and at several other locations, Plate IV appears to impinge upon Plate I.

RANDSBURG GRANODIORITE

South and west of Randsburg a small (8 km^2) stock of porphyritic biotite-hornblende granodiorite intrudes the Rand Schist. In addition to abundant inclusions of schist, the granodiorite contains two large, elongate xenoliths of layered gneiss composed of highly sheared hornblende diorite, marble, and quartzite (see Plate 1B). These rocks are tentatively interpreted to be pendants of mylonitized Johannesburg Gneiss. Accepting this correlation, the field relations suggest that the granodiorite has intruded into the lowermost two plates of the Rand Thrust Complex.

The Randsburg Granodiorite is essentially undeformed. However, in one place (structurally above the sheared gneiss pendants), the rock is cut by irregular, discontinuous shear zones. These shear zones are apparently localized along narrow (less than 1 cm wide) veins which are mineralized with

epidote, chlorite, and quartz. Minor northeast directed displacements across the shear zones were observed occasionally.

Southeast of Johannesburg the granodiorite is intensely hydrothermally altered along its contact with a younger porphyritic rhyolite plug. Feldspars are completely altered to clay, and the mafic minerals are obliterated over a zone at least 100 meters wide.

Silver (1986) obtained a U/Pb age of 79±1 Ma on the Randsburg Granodiorite. This is probably the best estimate for the true time of crystallization. Younger K/Ar ages of 74.2±1.9 Ma (from hornblende) and 18.2±0.5 Ma (from biotite) reported by Kistler and Peterman (1978) probably reflect thermal disturbance of the granodiorite during emplacement of the nearby hypabyssal intrusive center (see below). Kistler and Peterman also report an initial strontium value of .7066 and a Rb/Sr age of 90 Ma for the same rock. The Sr_i number implies a significant contribution from a cratonal source region. The discordant Rb/Sr age may reflect nonideal mixing between two or more source materials and/or complications due to the Early Miocene thermal reactivation.

RHYOLITE PORPHYRY

In the Rand Mountains, the Rand Thrust Complex is intruded by a family of porphyritic felsite pipes, dikes, and sills. These hypabyssal rocks are dominantly rhyolitic in composition, but include some quartz latites and dacites (Hulin, 1925). A large rhyolite pipe, exposed 1-2 km southeast of Johannesburg, has imparted an intense alteration halo to its country rocks. Dikes which appear to extend radially outward from this pipe are frequently observed to intrude Plates I, II, and III. One felsite dike sharply cuts across Fault I on the north flank of the Rand Mountains Antiform. Rhyolite

porphyry also intrudes into the lower portion of a Middle to Late Tertiary sedimentary and volcanic section which unconformably overlies deep structural levels of the Rand Thrust Complex (see next section).

The age of the rhyolite porphyry in the Rand Mountains is constrained indirectly. Shallow emplacement of porphyries into the Randsburg Granodiorite has apparently caused the thermal resetting of biotite in the latter rock to 18.2±0.5 Ma (K/Ar, Kistler and Peterman, 1978). The lowermost beds of the Rosemond Series/Bedrock Springs Formation (see Hulin, 1925 and Smith, 1964), which contain clasts of Rand Schist and Randsburg Granodiorite, are intruded by rhyolite. Stratigraphically higher pyroclastic rocks and conglomerates of the Bedrock Springs Formation, dated at Early to Middle Pliocene, contain clasts of rhyolite (Smith, 1964). Emplacement of the porphyries therefore postdated uplift and erosion of the Rand Schist and the Randsburg Granodiorite, but preceded Early Pliocene deposition of locally derived clastic debris. Based on the above evidence, the age of the rhyolite porphyry is believed to be Early Miocene.

A lithologically similar family of porphyritic rhyolite dikes intrudes all levels of the Rand Thrust Complex exposed in the southern Sierra Nevada. These porphyries have not been radiometrically dated, but they exhibit stratigraphic relationships similar to those observed in the Rand Mountains. In the Cache Peak area, the lower beds of a thick Tertiary sedimentary and volcanic sequence are intruded by rhyolite porphyry (Dibblee, 1967). These hypabyssal rocks are contemporaneous with rhyolitic flow breccias and tuffs which underlie sandy siltstone in the middle part of the Tertiary section. Fossiliferous strata from the latter horizon have been dated at Middle Miocene (Buwalda, 1916, 1954). The rhyolite dikes which cut the Rand Thrust Complex in the southern Sierras are thus also assigned an Early to Middle Miocene age.

SEDIMENTARY AND VOLCANIC OVERLAP SEQUENCE

A thick (as much as 4 km) Tertiary section of clastic sedimentary and volcanic rocks overlaps contrasting structural levels of the Rand Thrust Complex in the Rand Mountains and in the southern Sierra Nevada. These strata have been mapped separately and assigned different formational names in the two areas, but probably can be correlated over large areas of the northwestern Mojave desert.

In the Rand Mountains, a folded sequence of conglomerates, sandstones, siltstones, tuffs, and rare gypsum (originally named the "Rosemond Series" by Hulin, 1925) unconformably overlies the Rand Schist and the Randsburg Granodiorite east of Randsburg (see Plate 1B). Hulin demonstrated that deposition of part of the Rosemond Series was contemporaneous with the local emplacement of rhyolite porphyries (see previous section). A section of andesite flows, agglomerates, and tuffs, mapped by Hulin as "Red Mountain Andesite" overlies the Rosemond Series in angular unconformity along the crests of the Lava Mountains and on Red Mountain.

Smith (1964) remapped and subdivided the sedimentary and volcanic strata of the Lava Mountains, and discovered some vertebrate fossils in the middle part of the section. The type section of Smith's Bedrock Springs Formation, exposed in the central Lava Mountains, was assigned an Early to Middle Pliocene age. The stratigraphic relationship of this dominantly arkosic and conglomeratic section to the part of Hulin's Rosemond Series exposed near Randsburg is uncertain. However, the type Bedrock Springs Formation contains clasts of rhyolite and granodiorite, suggesting that it correlates with the **upper** beds of the Rosemond Series in the Randsburg area. Two stratigraphically higher volcanic units mapped by Smith (the Almond

Mountain Volcanics and the Lava Mountains Andesite) are essentially equivalent to Hulin's Red Mountain Andesite. Both units have been assigned Late Pliocene ages by Smith.

Folds in the Lava Mountains strata (as mapped by Smith, 1964) trend east northeast. Smith describes a marked angular unconformity between the Bedrock Springs Formation and the overlying Almond Mountain Volcanics, which have in turn been folded. Thus, deformation of the Lava Mountains section occurred after Early Pliocene time and continued during accumulation of the Late Pliocene volcanic rocks.

In the Cache Peak area of the southern Sierra Nevada, Tertiary strata unconformably overlap Plate IV of the Rand Thrust Complex (see Figure 1.3). The oldest unit, the Witnet Formation, is composed of unfossiliferous arkosic sandstone and micaceous siltstone with subordinate conglomerate, including a basal granite cobble conglomerate (Buwalda, 1954; Dibblee, 1967). This unit has been assigned an Early Tertiary age (Buwalda, 1954; Dibblee, 1967). The Witnet Formation is overlain in pronounced angular unconformity by tuffs and volcaniclastic sandstones of the Kinnick Formation. The dominantly pyroclastic lower and middle members of this formation are devoid of fossils, but sandy siltstones of the upper member have yielded Middle Miocene vertebrate fossils (Buwalda, 1916, 1954) and early Middle Miocene plant fragments (Savage et al., 1954). The Kinnick Formation is conformably overlain by conglomeratic sandstones, siltstones, and shales of the Bopesta Formation (Buwalda, 1954), which in turn are overlain by thick (up to 1 km) andesite flows. The lower and middle parts of the Bopesta Formation have yielded Late Miocene vertebrate fossils (Buwalda, 1916; Savage et al., 1954).

Reconnaissance mapping by Dibblee (1967) indicates that Tertiary strata of the Cache Peak area have been folded about east and east northeast

trending axes. Because the Bopesta beds are affected, this folding event is at least as young as Late Miocene. An earlier local deformational event is also implied by stratigraphic relations along the southern margin of the Tertiary section (near its contact with the Plate IV granite. Here, steeply north northwest dipping, locally overturned beds of the Witnet Formation are overlapped by the shallow north dipping Kinnick Formation (see Dibblee, 1967, Figures 59-60). Significant tilting of the Witnet strata therefore took place sometime in the Middle Tertiary before pre-Middle Miocene deposition of the lowermost Kinnick beds.

Correlations of Tertiary strata between the Rand Mountains and the southern Sierras are difficult to make precisely. However, it is interesting that the ages and succession of rock types are similar in both areas. Also, both regions have experienced post-Late Miocene folding along similar trends. Together, the two Tertiary sections represent the accumulation of clastic and volcanic debris in a tectonically active continental setting. The Tertiary strata overlap the Rand Thrust Complex in both areas, placing an upper bound on the timing of tectonic juxtaposition. It is clear that by Middle Tertiary time the Rand Mountains segment of the complex had been unroofed to much deeper structural levels than the southern Sierra Nevada segment.

CHAPTER 3

STRUCTURAL AND KINEMATIC ANALYSIS

The contacts separating the four plates of the Rand Thrust Complex are interpreted to be low angle faults (hereafter referred to as Faults I, II, and III). Associated with these faults are abundant exposures of mylonites which reflect the movement history of the shear zone network as well as the evolution of deformational conditions. These mylonites are the focus of the following structural analysis. As research proceeded and as more plates were recognized, kinematic complexities became quite apparent, particularly with regard to the reactivation of early phase structures. Indeed, it appears that low angle faulting within the complex took place along different structural levels at different times, followed interfering trajectories, and occurred under a variety of crustal conditions. Still, a consistent pattern of tectonic fabrics and kinematic indicators places important constraints on the movement history.

Mapping of portions of the four plates and their tectonic boundaries was carried out at a scale of 1:16,000. Structural elements were measured and oriented samples collected at all levels of the tectonic stack. About 120 thin sections were analysed petrographically. Quartz c-axis orientations were measured in seven samples. A progressive sequence of fabric development demonstrated by crosscutting structures is described below. The structural and kinematic data are summarized in Figures 3.1 through 3.6. Structures and fabrics are addressed systematically from the deepest to the shallowest levels of the tectonic stack. A discussion of mesoscopic structures is followed by a

description of microstructures.

MESOSCOPIC STRUCTURES AND PETROGRAPHY

Plate I: The most conspicuous structure within the Rand Schist is a moderate to strong schistosity which parallels a mesoscopic compositional layering. This schistosity appears to be a transposition foliation developed during the flattening and shear of the schist protoliths. It is generally concordant with the attenuated limbs of early isoclinal folds. At map scale the schistosity defines an antiform with a subhorizontal east trending axis. At outcrop scale, a variety of folds deform the schistosity. Fold styles are complicated and variable, as are the fold axis orientations. Two discordant lineations are frequently observed, one or both of which may correspond to the axes of millimeter to centimeter scale kink folds. I did not study the internal structures of the Rand Schist in detail (see Hulin, 1925; Dibblee, 1967; Vargo, 1972; and Postlethwait and Jacobsen, 1987 for further discussion).

Away from Fault I, the main body of Rand Schist is characterized by prograde metamorphic mineral asssemblages and crystalloblastic textures. A foliation is defined by preferred orientation of muscovite and chlorite in the quartzofeldspathic schists, and by suparallel alignment of amphibole and flattened plagioclase in the mafic schists. In gt-musc±crossite quartzites, coarse, elongate, slightly undulose quartz grains lie parallel to the mica foliation. Porphyroblasts of plagioclase, epidote and rare garnet within the grayschist component of Plate I appear to be in textural equilibrium with their matrix minerals. Dynamic strain overprinting is restricted to the immediate vicinity of Fault I.

Fault I: Directly beneath Plate II, all structures of the Rand Schist are

transposed into a penetrative mylonite zone. An abrupt contact with structurally higher Johannesburg Gneiss is commonly delineated by a thin (less than 2 meters wide) layer of finely laminated marble mylonite. Approaching this contact from below, the upper 1 to 3 meters of Plate I becomes intensely foliated and lineated. Abundant quartzite mylonites within this structural interval display a pronounced millimeter scale ribbon foliation.

Mylonites derived from the Rand grayschist are characterized by finely comminuted layers of feldspar and phyllosilicate transected at low angles by shear bands filled with chlorite and iron oxide. Quartz grains are drawn out into coarse, undulose ribbons. Garnet porphyroclasts are frequently displaced and rotated along chlorite filled fractures. A late set of kink folds and mineralized fractures cut the mylonitic foliation at high angles.

Stretching lineations associated with Fault I are defined by streaks of quartz, feldspar, and muscovite on the surfaces of quartz rich lithologies, and by elongate clusters of resistant calcsilicate material in the marble mylonite. These lineations are shallow and consistently oriented within a given geographic domain.

Plate II: The gneisses of Plate II exhibit a great diversity of structures which reflect their complex deformational history. On the north dipping limb of the Rand Mountains Antiform a crude compositional layering is defined by 1 to 10 meter thick lenticular masses of orthogneiss, marble, and quartzite. This layering is concordant with north dipping foliations observed within individual constituents of the Johannesburg Gneiss. Mylonitic fabrics occur throughout the section, but are best developed near the fault contact with underlying Rand Schist. Away from Fault I lineations are poorly developed. Mesoscopic folds of variable orientation and vergence are present at all

structural levels.

On the south dipping limb of the Rand Mountains Antiform a highly attenuated sheet of Johannesburg Gneiss is imbricated between Plates I and III. The dominant structure here is a penetrative, shallowly dipping mylonitic foliation (S_1) which overprints most earlier fabrics of Plate II (see Figures 3.1 and 3.2a). S_1 probably represents early differential movement between Plates I and III. In the thicker Plate II exposures of the southwest Rand Mountains, blocks of garnet-amphibolite grade orthogneiss retain their prograde metamorphic foliation (S_0). This fabric is often rotated at low angles to S_1 in the surrounding mylonites. S_1 is generally parallel to Fault I. A strong stretching lineation (L_1), marked by elongate quartz, feldspar, amphibole, or mica, is best developed in quartz rich lithologies. L_1 is shallow and displays a measurable fluctuation in direction between various geographic domains (see Figure 3.1). In general, stretching lineations within Plate II trend more southwestward than those measured in the immediate vicinity of Fault I.

A second, obliquely oriented lineation (L_2) observed in the southern Rand Mountains corresponds to the axes of millimeter scale kink folds which deflect S_1. L_2 may also mark the axes of larger scale asymmetric folds. Some overturned folds are truncated by miniature thrust ramps oriented at about 30^o to S_1. These mesoscopic folds display a wide variety of vergence directions (see Figure 3.3). They probably represent late differential movements between Plates I and III.

All ductile structures within Plate II are overprinted by brittle fabrics. S_1 is transected at high angles by discontinuous fractures filled with quartz, calcite, limonite, or chlorite. These fractures often display minor (less than 1 centimeter) offsets in both normal and reverse senses.

Figure 3.1: Geographic distribution of mylonitic structures (S_1 and L_1) in the Rand Mountains study area. For each geographic domain the left hand stereonet shows stretching lineations while the right hand stereonet shows poles to mylonitic foliation.

Figure 3.2a: Compilation of poles to mylonitic foliation (S_1) in the Rand Mountains study area.

Figure 3.2b: Compilation of stretching lineations (L_1) in the Rand Mountains study area.

Figure 3.1

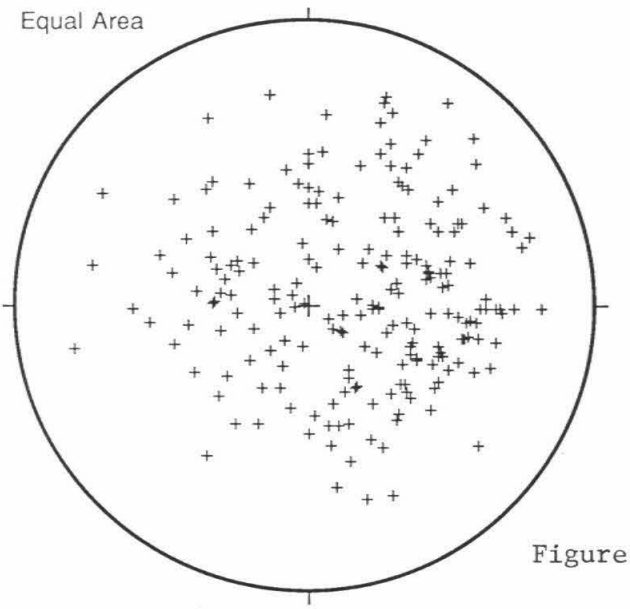

Figure 3.2a

Southern Rand Thrust
Compilation of Poles to Foliation (S1)
N=272

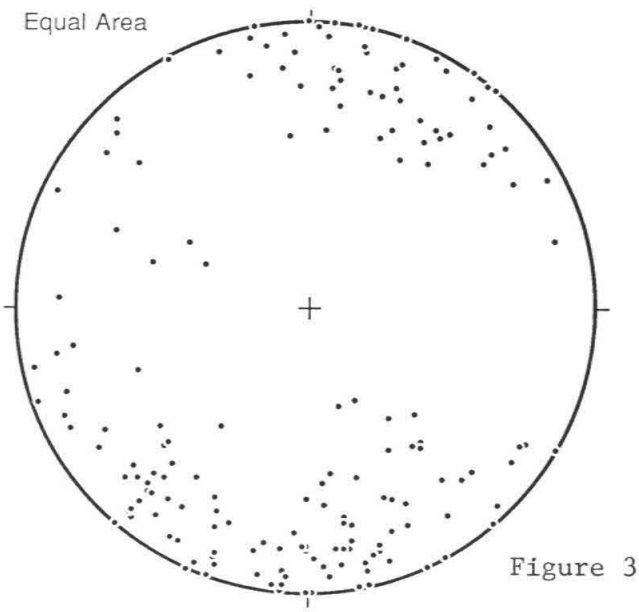

Figure 3.2b

Southern Rand Thrust
Compilation of Lineations (L1)
N=197

A retrograde mineral assemblage is associated with the mylonitic fabrics of Plate II. Hornblende is replaced by fibrous actinolite and chlorite. Feldspars are pervasively sericitized. Garnets are fractured and filled with chlorite. White mica and chlorite are localized along mylonitic shear bands, and frequently show offset or rotation. These disequilibrium textures imply that mylonitic deformation within Plate II accompanied fracturing and alteration of the host rocks in a fluid rich environment. Deformational conditions probably did not exceed greenschist facies.

Faults II and III: Narrow zones of cataclasis and hydrothermal alteration are encountered directly above Faults II and III. Within these 5 to 50 meter wide structural intervals, primary plutonic textures are modified by cataclastic, and locally, mylonitic fabrics. The alteration is most visible in Plate III where the conversion of hornblende and biotite to chlorite gives the rock a distinctive green color. Feldspar and sphene crystals are brittlely fractured and mechanically abraded. Quartz grains may be slightly undulose, but are not noticeably recrystallized. Microbreccias veined with epidote, chlorite, quartz, and calcite are common.

Rare occurrences of mylonites within Plate III are confined to the highest and lowest structural levels. In outcrop these orthogneisses exhibit a strong foliation marked by elongate, flazered quartz grains and flattened lense of comminuted feldspar. Exposures with mesoscopic kinematic information were encountered in two places: (1) Directly above Fault II in the south central Rand Mountains a 1 meter wide mylonite zone hosted in granodiorite dips steeply (71^{o}) north-northeast. This shear zone is apparently truncated by Fault II (and Fault I) at depth. The mylonitic foliation is disrupted by centimeter scale asymmetric folds which verge southwest. (2) Nearby, but at a

higher structural level (within a few meters of a Plate IV klippe), an outcrop of mylonitic granodiorite with a strong northeast (043°) lineation was observed. In this exposure northeast dipping chlorite filled shear bands consistently transect a subhorizontal quartz-feldspar foliation at an angle of 25°. In accordance with Berthe, et al. (1979) and Simpson (1984, 1986), this S-C fabric yields a top-to-the-northeast sense of shear.

Lineated quartz rich mylonites occur along the base of Plate IV in the southeastern Rand Mountains. Some of these mylonites are composed of 100% finely recrystallized quartz. A shallow, east dipping foliation in these rocks is defined by lamellae of extremely fine grained phyllosilicate and feldspar which alternate with pure quartz on a submillimeter scale. This foliation is affected by centimeter and millimeter scale asymmetric folds and "mini-thrusts" which were observed to verge north and west (see Figure 3.3). Well developed stretching lineations trend NNE-SSW, at high angles to most of the mesoscale fold axes. The upper level shear zone has apparently overridden the south-southwest dipping mylonites localized along Fault I. In this immediate area, Plates II and III have been tectonically thinned or cut out altogether, and the structurally deeper mylonites carry a contrasting SSE-NNW stretching lineation (see Figure 3.1)

Figure 3.3: Equal area stereonet showing axes and vergence directions of small scale folds affecting the mylonitic foliation, Rand Mountains study area. Sample locations are plotted on Plates 1A and 1B.

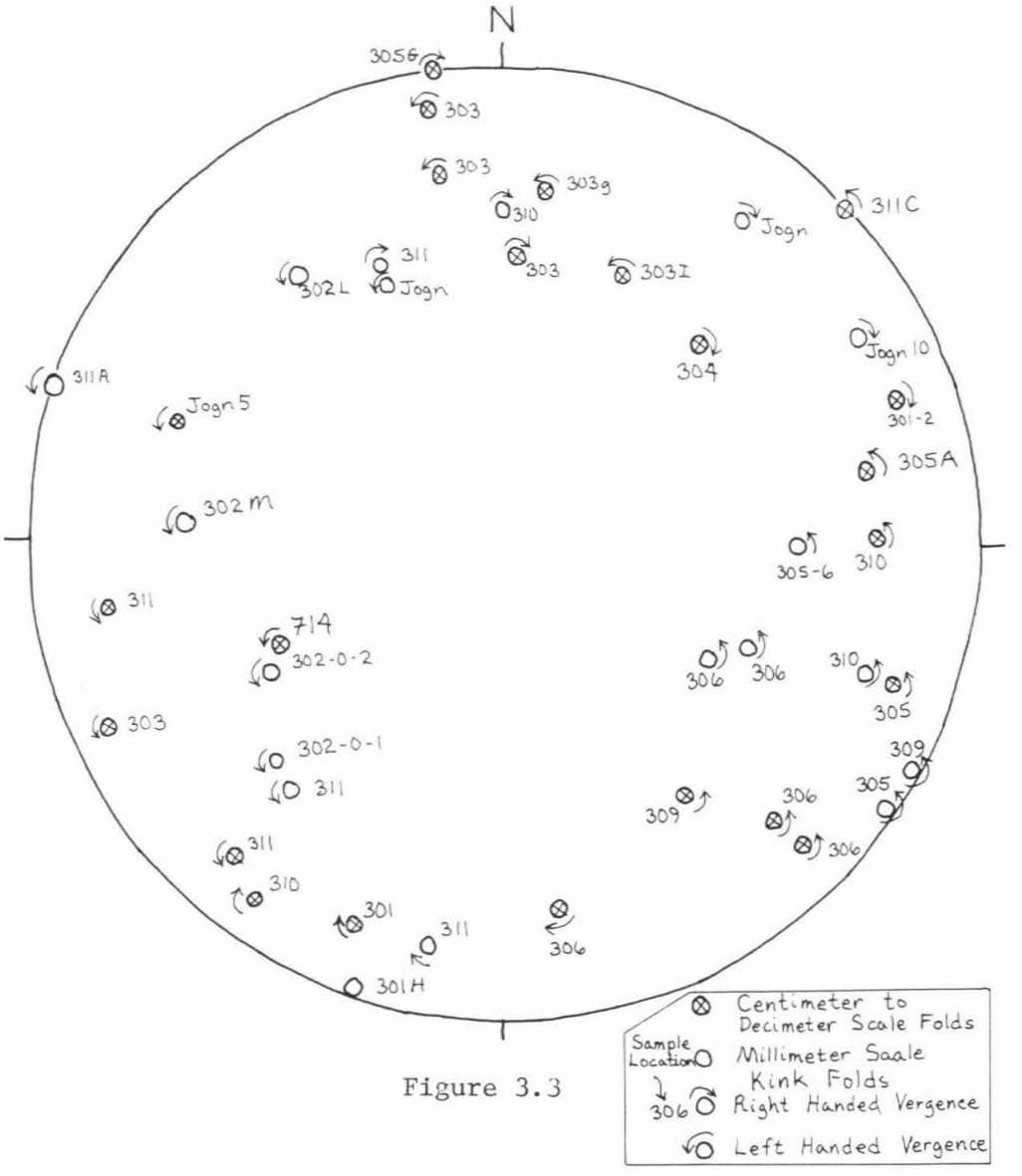
N
305G
303
303
303g
310
311C
Jogn
311
302L
Jogn
303
303I
304
Jogn 10
311A
Jogn 5
301-2
305A
302 m
305-6
310
311
714
302-0-2
306
306
310
305
303
302-0-1
309
311
309
306
305
306
311
310
301
311
306
301H
Centimeter to Decimeter Scale Folds
Sample Location
Millimeter Saale Kink Folds
306
Right Handed Vergence
Left Handed Vergence

Figure 3.3

MICROSTRUCTURES

Thin sections of 45 mylonite samples were studied to characterize their microstructural evolution and interpret the sense of movement along various levels of the Rand Thrust Complex. Samples were collected throughout the southern Rand Mountains, where the complete tectonostratigraphy is preserved. It is convenient to describe the samples in three sets, based on structural position: **Set I** includes samples of mylonitic schist and quartzite collected from the uppermost 3 meters of Plate I. **Set II** includes a variety of Plate II mylonites. **Set III** includes samples from the quartz mylonite zone localized along Fault III.

Most thin sections were cut perpendicular to the mylonitic foliation and parallel to the stretching lineation. This plane corresponds to the XZ plane of the finite strain ellipsoid (Simpson, 1988). A few sections were cut perpendicular to both the foliation and lineation, affording a view of the YZ plane. Three dimensional sectioning of the associated hand specimens indicates that the lineation reflects a true elongation of residual feldspar porphyroclasts, and the foliation marks a flattening of feldspars and quartz as well as a preferred orientation of phyllosilicates and amphiboles.

Set I Mylonites: Mylonites derived from three distinctive Rand Schist lithologies occur directly beneath the marble mylonite layer that marks Fault I. Most common is the Rand grayschist, which displays a remarkable microfabric transition over a 3 meter interval. An upward increase in dynamic strain intensity is defined by several criteria: (1) feldspars are reduced in grain size, (2) feldspar and epidote are converted to porphyroclasts by means of fracturing and mechanical abrasion, (3) a mylonitic foliation

(S_1), defined by elongate feldspars or feldspar aggregates and subparallel domains of stretched quartz (frequently ribbon-like) is developed, (4) quartz domains are dynamically recrystallized into finer subgrains, and (5) the deformational fabric is enhanced by conjugate sets of chlorite filled shear bands (C) which transect S_1 at low angles and commonly display minor normal offsets. These shear planes are sometimes asymmetrically disposed about S_1 and variable in intensity. In two samples (#522 and #607), a shallow (5° to 15°) north dipping set of C planes dominates a steeper (40°) south dipping set.

Purple sheared quartzites (metacherts) containing up to 25% garnet, 10% muscovite, 5% magnetite, and 3% feldspar are interlayered with the mylonitic grayschists. In these rocks a strong foliation (S_1) is defined by medium to fine grained elongate quartz ribbons which may be dynamically recrystallized into extremely fine subgrains. A marked elongation of the ribbon grains observed in YZ sections implies that a significant component of flattening strain was important during deformation. Extension of garnet porphyroclasts parallel to S_1 is initially accommodated by normal sense displacement along intragrain fracture networks preferrentially oriented at high angles (greater than 65°) to the foliation. Progressive rotation of these fractures toward the foliation plane has resulted in pronounced elongation (up to 500%) of some garnets. The sense of displacement on these fractures is antithetic to the prevailing shear direction (Paschier and Simpson, 1986; Simpson, 1986). Two samples (#301 C and #525) with rotated and displaced garnets indicate a south or southwest sense of shear, while three samples (#521 B, D, and E) yield a northward direction.

S_1 is commonly transected at 10° to 25° angles by normal sense shear bands (C planes) which are delineated by stringers of wispy chlorite. This S-C fabric is highly asymmetric in seven samples of mylonitic metachert. Four

samples (#521 B, D, and E, and #303 L) are consistent with a northward sense of shear, while three samples (#301 C, #525, and #729) display a southward component of rotation.

Intensely sheared white bull quartz veins are frequently encountered in the Fault I mylonite zone. These samples of pure quartz exhibit spectacular ribbon structures in thin section. Various stages of ribbon evolution, breakdown, and subsequent dynamic recrystallization are well preserved. Early generation (Phase I) ribbons were apparently derived from very coarse quartz grains. Individual ribbons ranging in width from 1/2 to 2 millimeters maintain a constant optical orientation across the entire thin section. Ribbon boundaries are sharply defined by optical discontinuities and may be marked by stylolites. Phase I ribbons often display longitudinal parting along subparallel glide? planes which eventually become the boundaries of narrower Phase II ribbons. Both Phase I and Phase II ribbons may be dynamically recrystallized into domainal mosaics of fine subgrains. Individual subgrains within a domain maintain the same **optical** orientation as their parent ribbon.

Shear bands are not well developed in the mylonitic quartz veins. However, in six samples, the long axes of slightly elongate recrystallized subgrains collectively define a secondary foliation (S_2) which is inclined to S_1 at angles of 5^o to 30^o. This asymmetric subgrain shape fabric indicates that recrystallization of the host ribbon grains took place in a noncoaxial strain environment (Burg, 1986). Five of the samples (#604 A and B, #602, #532, and #524) yield a top-to-the-south sense of shear, while one sample (#714) displays an opposite sense of movement. It should be noted, however, that these shape fabrics are only useful for constraining the latest increment of the finite strain history (Burg, 1986; Simpson, 1986).

C-axis orientations of quartz ribbons from two samples of mylonitic metachert (#301-C and #303L) and three samples of sheared bull quartz (#309-A, #309-E1, and #524) were measured optically on a universal stage. The resultant fabrics are shown in Figure 3.4. All measurements are plotted as lines on the lower hemisphere of equal area stereonets. The plots are oriented so that the XY plane corresponds to the quartz ribbon foliation and the X direction coincides with the northward component of lineation. Sample #303 L is noticeably less deformed than the others. Its lineation is poorly defined and the quartz grains are only partially drawn out into ribbons. Hence, this sample may record the partial inheritance of an earlier fabric (acquired during the initial metamorphism of the Rand Schist?).

In general, strong preferred orientations are displayed by slightly asymmetric crossed girdle fabrics. The girdles intersect about the Y axis, indicating that the mesoscopic structural elements of the sample coincide with the axes of the strain ellipsoid (Bouchez, 1977). The occurrence of discrete maxima at shallow and intermediate angles implies that the preferred orientation resulted from dislocation glide along basal and rhombohedral slip planes, respectively. These planes are believed to be active under low temperature, possibly high P_{H2O} conditions (Lister, 1979). The narrow "opening angle" between the two outer maxima is also consistent with low temperature (greenschist facies) deformational conditions (Lister, 1979).

The presence of two crossed girdles indicates that coaxial strain was important during development of the preferred orientation (Lister, 1977). However, the five fabrics are slightly asymmetric in their skeletal outlines, and in some cases, their density distributions. In all samples the prominant girdle is tilted slightly northward with respect to the foliation. Strikingly

Figure 3.4: Quartz c-axis fabrics for seven samples of mylonitic quartzite collected from various structural positions in the southern Rand Mountains. In these equal area stereonet plots, the mylonitic foliation plane (S_1) is oriented EW, and Z is normal to the foliation. X marks the direction of the stretching lineation (L_1). The contours represent 1, 3, 5, 7, 9, 11, and 13 times uniform distribution (Kalsbeek Counting Net method). See also discussion in text. Sample locations are plotted on Plates 1A and 1B.

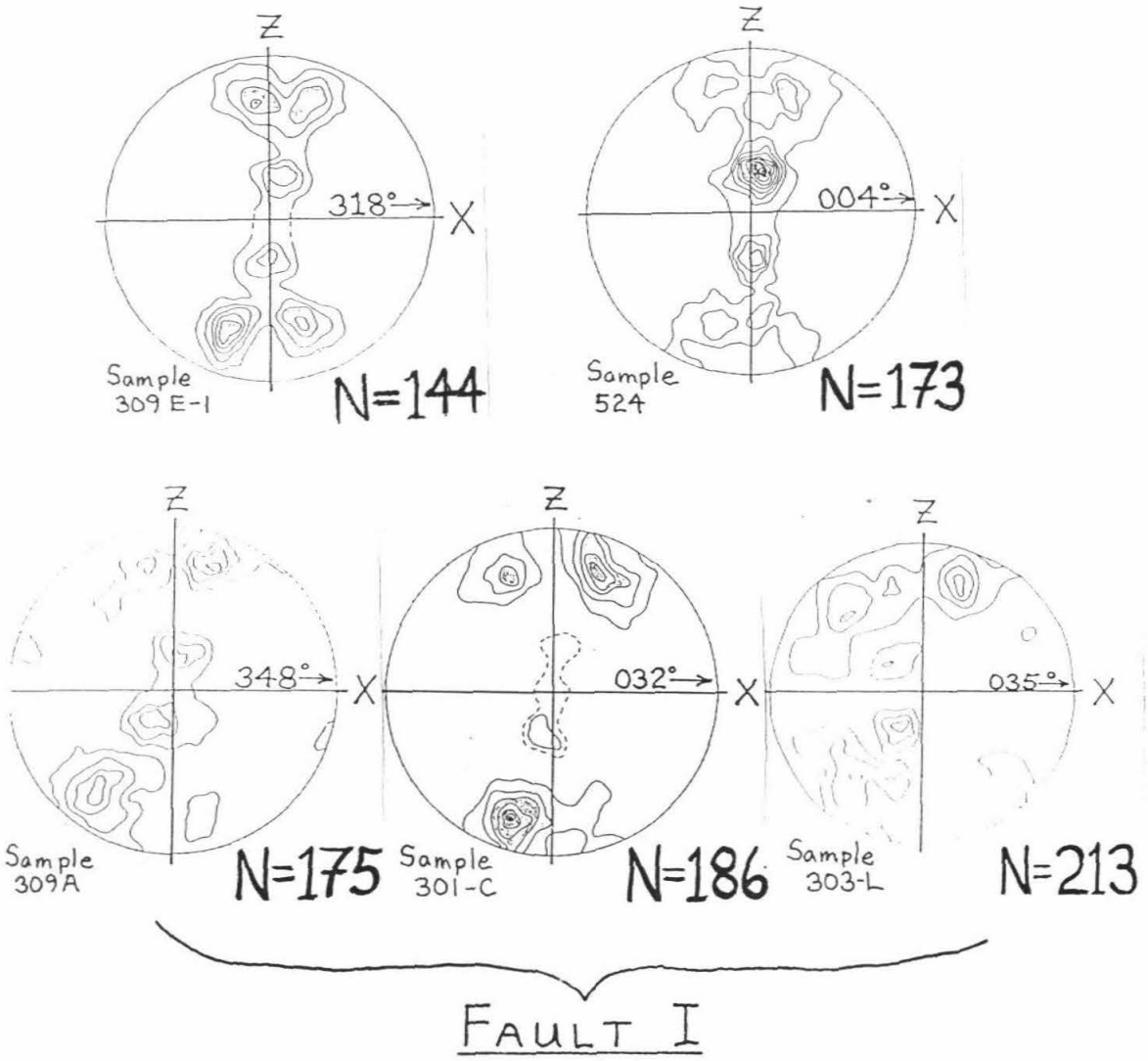

FAULT I

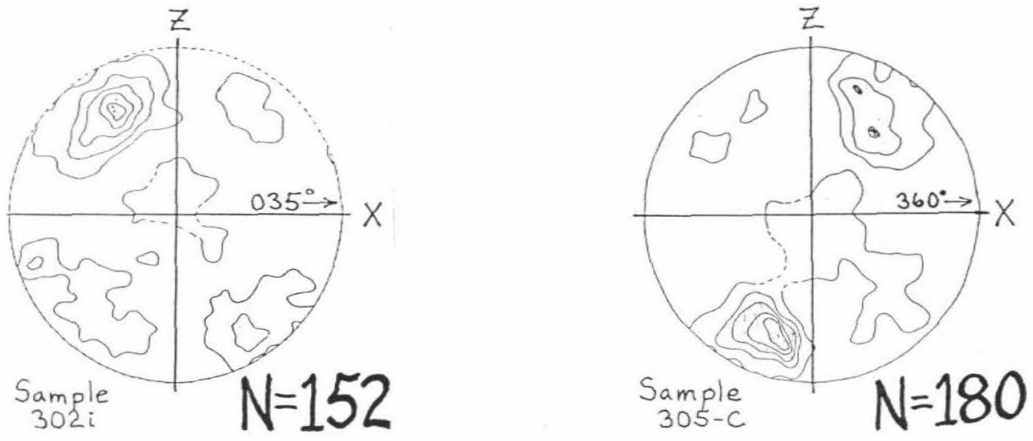

PLATE II

Figure 3.4 FAULT III

similar c-axis fabrics were published by Postlethwait and Jacobson (1987) for quartzites sampled from shallow structural horizons of the Rand Schist in the southern Rand Mountains. The northward asymmetry reflects a north directed component of noncoaxial deformation (Lister, 1977; Simpson and Schmidt, 1983). Unfortunately, this kinematic interpretation must be qualified. As with the quartz subgrain shape fabrics desribed earlier, skeletal outlines are sensitive to late stage strain perturbations, and probably reflect only the last phase of deformation (Paschier, 1983; Burg, 1986). These c-axis fabrics therefore can only be used to document late movements on Fault I. The inferred northward transport direction is consistent with other late microstructures observed at the same structural levels (see below).

All of the Set I mylonites are disturbed by at least two generations of late microfractures. These fractures are healed by veins of fine grained, statically recrystallized quartz. Fractures oriented at high angles (greater than 50^{o}) to the foliation often display minor reverse offsets which dominantly verge to the north. In quartz rich mylonites the microfaults have induced millimeter scale kinking of the ribbon foliation. On the mesoscale these kinks correspond to intrafolial folds with axes at high angles to the stretching lineation (see Figure 3.3).

Set II Mylonites: Samples in this suite include garnet bearing quartz dioritic gneisses, finely laminated marbles, and a variety of quartzofeldspathic mylonites and ultramylonites which appear to have been derived from K-feldspar and quartz rich garnetiferous granite orthogneisses. All are components of Plate II. Only the latter group yielded microfabrics suitable for kinematic analysis.

The quartzofeldspathic mylonites are characterized by subrounded to

ovoid porphyroclasts of feldspar and rare garnet isolated within a strongly foliated matrix of comminuted feldspar and finely recrystallized quartz. The foliation is enhanced by irregular stringers of chlorite and rare biotite, and by tails of fine crushed feldspar which trail from the long axes of the porphyroclasts. In six samples (#303 B, #302 H1, # 302 M2, #302 O1, #302 I, and #303 E), this fabric is cut by normal sense shear planes which dip consistently 10^{o} to 15^{o} southwest relative to the mylonitic foliation. The shear bands also deflect spindle shaped white micas (aka "mica fish", see Lister and Snoke, 1984) in a sense consistent with southwest directed simple shear. Long axes of porphyroclasts are back tilted relative to the foliation in the same sense as the mica fish. Finally, elongate domains of dynamically recrystallized quartz exhibit an asymmetric subgrain shape fabric (Burg, 1986) which reflects a late stage southwest directed noncoaxial strain component.

Not all samples display a strong southwestward asymmetry. In many cases the mylonitic foliation and the shear bands are virtually parallel, and displaced strain markers record conflicting senses of offset. Extreme shear strains are implied by the exceptionally fine grain size of the matrix and by the coincidence of the S and C planes.

Two samples (#304 B and #304 D) show evidence for late northeast directed shear. Discrete, northeast vergent shear bands transect and offset a earlier formed mylonitic foliation. These samples were collected from an area of the south central Rand Mountains where the mylonites of Plate II are complexly folded, and shortening along mesoscale thrust ramps of variable orientation is frequently observed.

A quartz c-axis fabric measured from one quartz rich ultramylonite (#302 I) displays a strong single girdle inclined at 55^{o} to the foliation plane (see Figure 3.4). The southwestward tilt of the girdle reflects a southwest

simple shear component consistent with other microstructural evidence observed in this sample.

Set III Mylonites: Quartz mylonites from the base of Plate IV in the southeastern Rand Mountains exhibit a strong foliation (S_1) defined by layers of extremely fine biotite and chlorite that separate domains of dynamically recrystallized quartz. Recrystallization has occurred at the expense of previously strained ribbon grains which are sometimes preserved as "ghosts." The fine quartz subgrains are elongate with their major axes inclined at oblique angles to S_1. In all twelve samples analyzed, this oblique subgrain shape foliation (S_2) dips south-southwestward relative to S_1, indicating that recrystallization took place in a north-northeast directed noncoaxial shear regime. Within a given sample, the angle between S_1 and S_2 varies inversely as a function of subgrain aspect ratio; i.e., the most elongate grains are inclined to S_1 at the lowest angles. This angular variability probably represents fluctuations in shear strain within different domains of the sample (Burg, 1986).

C-axis orientations of recrystallized quartz subgrains from one sample (#305 C) were measured optically. The contoured fabric (see Figure 3.4) displays a single girdle inclined at about 60° to S_1. The asymmetry of this fabric may be interpreted as additional evidence for late north-northeast directed simple shear along Fault III.

SUMMARY OF STRUCTURAL AND KINEMATIC SEQUENCE

The structural features described above record the cumulative history of crustal movements that resulted in the present disposition of the Rand Thrust Complex. At each structural level, mylonitic foliations and stretching

lineations define the orientation of the bulk finite strain ellipsoid, and shear sense indicators provide the dominant direction of noncoaxial rotation, if any. Where two or more deformational events have left an imprint in these rocks, the tectonic sequence must be interpreted from crosscutting structures and fabrics. Some early shear zone fabrics may have been obliterated during evolution of the complex. Nevertheless, the spatial and temporal distribution of kinematic indicators is sufficient to differentiate at least two important movement episodes.

Figures 3.1 and 3.2 summarize the mesoscopic mylonitic foliations (S_1) and lineations (L_1) measured at various locations in the Rand Thrust Complex. Figure 3.1 shows the geographic distribution of the data; Figures 3.2a and 3.2b are compilations of all foliation and lineation measurements.

Figure 3.5 summarizes the variation of lineation direction with geographic location. The data are divided into separate domains bounded by high angle faults. The average lineation direction may be quite disparate between two adjacent domains. Implicit in this observation is a potential kinematic complexity: individual blocks of the tectonic stack may have rotated significantly along vertical axes during movement on Neogene faults.

Figure 3.6 shows the distribution of shear sense indicators in the southern Rand Mountains. These kinematic indicators vary systematically with structural position and appear to preserve a progressive history of shear zone interactions. Several conclusions may be drawn from the available data:

(1) The latest ductile movement on Fault III was directed toward the north-northeast. This activity postdated the development of mylonitic fabrics at lower structural levels.

(2) Penetrative southwest noncoaxial fabrics within Plate II are overprinted by a variety of folds and localized shear zones which dominantly

Figure 3.5: Map showing the fluctuation of average lineation direction between domains bounded by high angle faults in the southern Rand Mountains. The lineation data of Figure 3.1 are plotted here as rose diagrams.

Figure 3.6: Geographic, structural, and temporal distribution of kinematic indicators observed in mylonites of the southern Rand Mountains. See also discussion in text.

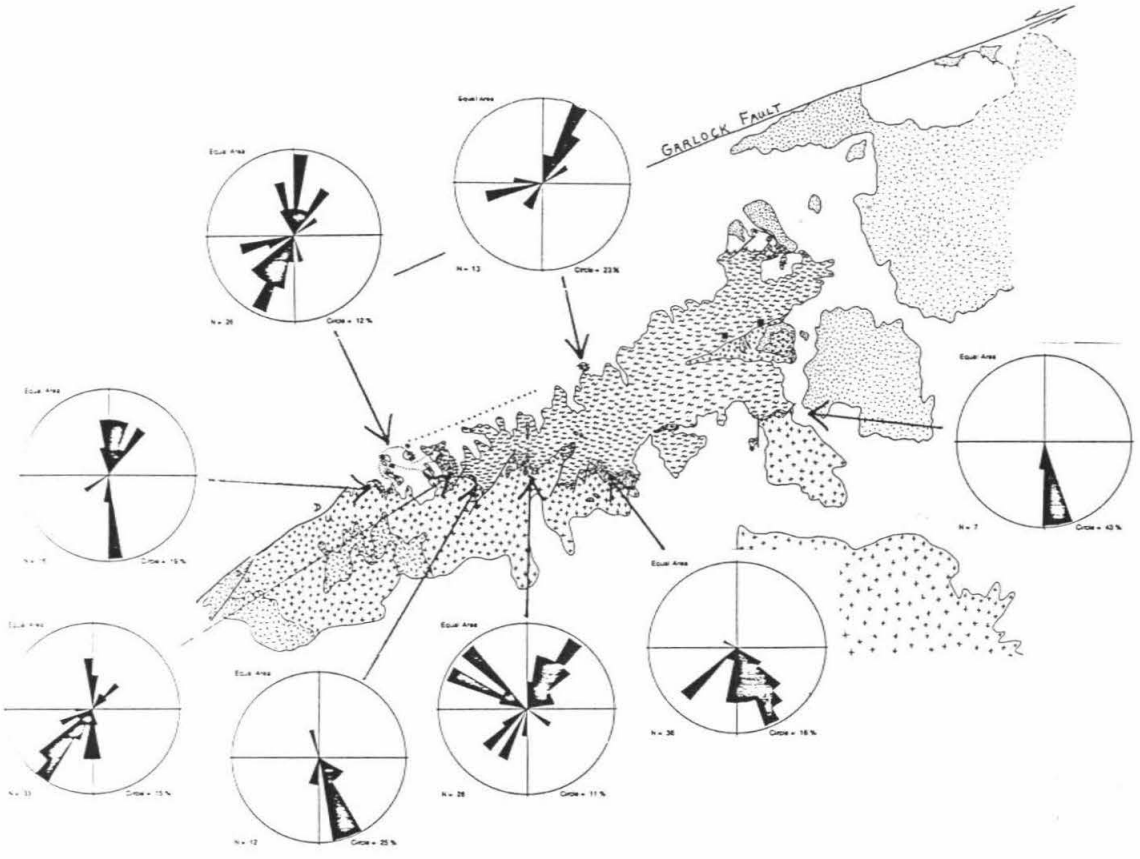

Figure 3.5

DISTRIBUT EMATIC INDICATORS
(S and Thrust)

EXPLANATION:

	Early Phase	Late Phase
Shear Sense Along Fault I		
Shear Sense Within Plate II		
Shear Sense Near Fault III		

Direction of dominant shear

Two opposed directions of shear

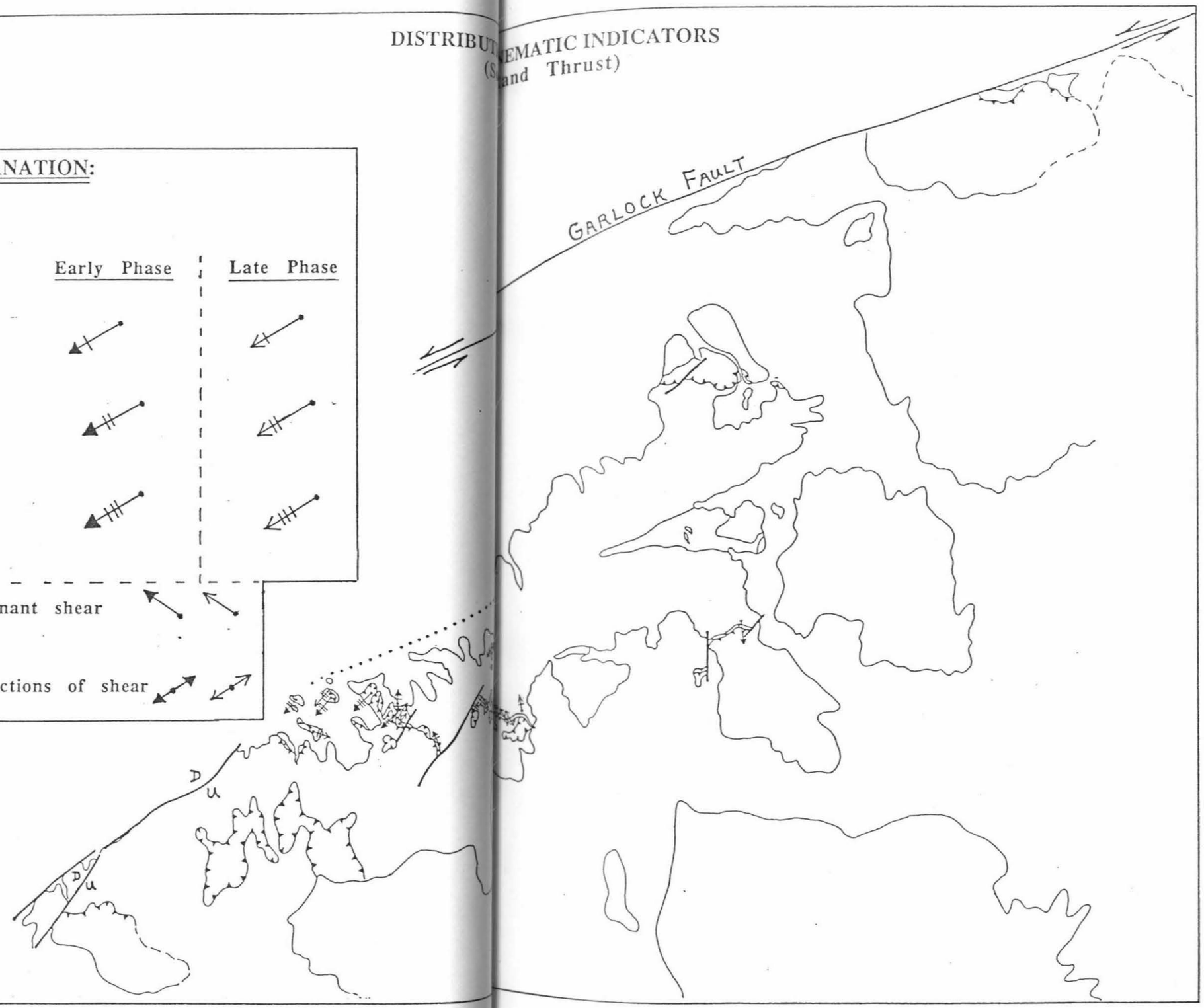

Figure 3.6

verge northward. Plate II was therefore emplaced in a southwest directed shear regime prior to its local reactivation along opposed trajectories.

(3) Shear sense indicators near Fault I yield conflicting results. Asymmetric fabrics from closely spaced mylonite samples may display opposite directions of rotation. There is some indication that the north vergent fabrics are later in the sequence. Many samples, although highly strained, show no dominant sense of asymmetry. The presence of conjugate shear bands and crossed girdle quartz c-axis patterns suggests that coaxial strain may have been important in partitioning deformation at this structural level.

CHAPTER 4

INTERPRETATION AND DISCUSSION

Tectonic development of the Rand Thrust Complex involved a complicated sequence of Mesozoic and Cenozoic plutonic, metamorphic, and deformational events. Geological observations described in the preceding two chapters place the following constraints on the tectonic evolution of this region:

(1) The four plates of the tectonic stack record separate geologic histories which predate their involvement in the Rand Thrust Complex. Plate I represents an immature marine sedimentary sequence and part of its oceanic basement which were regionally metamorphosed to greenschist (and locally, albite-epidote-amphibolite) facies prior to emplacement of the Randsburg Granodiorite in Late Cretaceous time. Schistosity and most of the folds in the Rand Schist developed during prograde metamorphism, perhaps in a subduction zone environment. Mobilization and emplacement of the bull quartz veins was late or post metamorphic. Plate II represents an assemblage of granitic to dioritic plutons with associated calcareous and quartzitic country rocks which were deformed under much higher temperature (garnet-amphipolite grade) conditions. Accepting a tentative correlation with the gneisses of the Tehachapi Mountains, this regional metamorphic event probably culminated at about 100 Ma. Plates III and IV represent two separate calc-alkaline plutons which were probably emplaced into the Sierra Nevada batholith. Plate III locally appears to intrude Plate IV; hence, the low angle contact between these two plates may be a tectonically modified intrusive

contact.

(2) The four plates are presently juxtaposed along three discrete low angle faults of regional extent. Primary mineralogies and textures of each plate are overprinted by new assemblages and fabrics which indicate that faulting occurred under greenschist facies or lower metamorphic conditions. Retrograde fluids were important in the development of mylonitic fabrics at deep structural levels. Cataclasites associated with Faults II and III represent drier and/or shallower deformational conditions.

(3) Stacking of the plates involved significant movements along all three faults. One or more of these structures were reactivated during development of the complex. The timing of fault movements may be constrained as follows:

(a) All movements postdate the separate prograde metamorphism of Plates I and II, as well as the igneous cystallization of Plates III and IV.

(b) In the southern Rand Mountains, Plates I, II, and III were juxtaposed during the same movement event. Persistence of a narrow, continuous slice of Johannesburg Gneiss between Plates I and III implies that Plate II was imbricated and attenuated when Plate III overthrust Plates I and II. The marble layers preserved at the top and bottom of this tectonic slice may have played an important role in lubricating the shear zone and in localizing ductile strain within a narrow interval.

(c) Plate IV may have ridden "piggyback" on Plate III during the overthrusting event of (b). It is clear from the distribution of fabrics that Fault III has not accommodated nearly as much ductile shear strain as Faults I and II.

(d) The Randsburg Granodiorite intrudes the lower structural levels of the Rand Thrust complex. Hence, the timing of event (b) is constrained between

84 Ma (the interpreted age of the Plate III granodiorite) and 79 Ma (the interpreted age of the Randsburg Granodiorite). Discrete ductile shear zones within the Randsburg Granodiorite represent younger tectonic disturbances of minor significance.

(e) Two or more reactivations of Plate III along Fault II (and possibly along Fault I) are suspected. Asymmetric folds which deform Plate II mylonites are highly variable in vergence direction, implying late complicated relative motions between Plates I and III while still in the ductile regime. All Plate II and Fault I mylonites are overprinted by brittle fabrics, suggesting that deformation continued (or resumed) at shallower crustal levels. Cataclastic textures within the granodiorite just above Fault II are in marked contrast to mylonitic fabrics preserved at deeper structural levels, indicating that the PlateIII/Plate II contact has been reworked as a brittle fault. Finally, in the southern Sierra Nevada, Fault II is highly discordant to steeply dipping foliations in the gneisses of Plate II. The latest movement of Plate III in that region therefore postdated ductile deformation and tilting of Plate II.

(f) Fault III truncates Faults I and II in the southeastern Rand Mountains. Thus, final displacement of Plate IV postdated the tectonic juxtaposition of Plates I, II, and III. The movement of Plate IV may have been kinematically coordinated with late reactivations of Plate III and Plate II.

(4) Kinematic information derived from field and microstructural measurements places constraints on the directions of motion along the various faults. In general, the shear sense indicators show that deep levels of the Rand Thrust Complex were dominated by transport of the upper plates along south or southwestward trajectories, while shallower levels moved in a north or northeastward direction. A complimentary **temporal** sequence of intense south vergent noncoaxial strain followed by less penetrative northward

reactivation is also preserved. The most straightforward interpretation of available kinematic evidence therefore requires that south or southwest directed imbrication of the four plates was succeeded by local northward displacements of the upper two plates. The early overthrusting event corresponds broadly to a late Cretaceous episode of crustal shortening recognized throughout the southwestern Cordillera (see G. H. Davis, 1979; Drewes, 1980; Simpson, 1984; Haxel et al., 1984; Reynolds et al., 1986b; Tosdal, 1986; Bykerk-Kauffman and Janecke, 1987; Smith and Gehrels, 1987; Hoisch et al., 1988; Richard and Sutter, 1988). The younger north directed events may represent a response of the Rand Mountains region to Early Miocene extension documented in nearby parts of the Mojave desert (see Howard and John, 1987; Dokka et al., 1988; Glazner et al., 1988; G. A. Davis, 1988). It is conceivable that certain levels of the complex were reactivated as detachment faults.

(5) Ambiguities in shear sense which occur along Fault I are problematic. South vergent noncoaxial fabrics are common along the southern Rand thrust, but many samples display evidence for a late northward component of simple shear, and coaxial fabrics are frequently preserved. The apparently conflicting data from this structural interval are interpreted to be the result of one or more of the following deformational mechanisms:

(a) coaxial flattening with local development of simple shear domains during tectonic stacking of three massive plates onto the Rand Schist,

(b) overprinting of south vergent mylonitic fabrics during the northward reactivations of Plates III and IV, or

(c) northward overprinting of the Fault I mylonites during flexural slip folding and uplift of the Rand Mountains Antiform.

(6) The total amount of shortening related to movement along the Rand Thrust Complex can be estimated from regional outcrop patterns. Given that

Plate II was imbricated between Plates I and III, the minimum displacement equals the outcrop width of Faults I and II in the direction of transport. Assuming a south-southwestward trajectory, a minimum displacement of 20 km may be measured from the map after 60 km of sinistral slip is removed from the Garlock Fault. The total north-northeastward displacement of Plate IV along Fault III is uncertain, however, it was significant enough to develop a two meter thick mylonite zone.

(7) Wide dispersion in the lineation data (ranging from NW-SE to NE-SW) could be the result of complicated relative motions between various levels of the tectonic stack. However, the average lineation trends appear to fluctuate somewhat systematically between geographic domains bounded by high angle faults (see Figure 3.5). It is possible that part of this variation is due to vertical axis rotation of large crustal blocks along these Neogene faults. Significant strike slip movements would be necessary to cause such rotations. In any event, it should be borne in mind that the present day lineation directions may not record the the original movement trajectories.

(8) The Neogene history of the Rand Thrust Complex is constrained by crosscutting and overlapping hypabyssal, sedimentary, and volcanic rocks. A thick section of middle to upper Tertiary conglomerates, arkose, tuffs, and andesites unconformably overlies the Rand Schist and the Randsburg Granodiorite, indicating that Plate I had been uplifted and unroofed by this time. The age of the overlap sequence is constrained by an 18 Ma? rhyolite porphyry plug which intrudes into the base of the section. Dikes related to this porphyry crosscut Plates I, II, and III in the Rand Mountains, while dikes related to a porphyry of similar age intrude all levels of the complex in the southern Sierra Nevada. All four plates were therefore in place by Middle Miocene time. The clastic section has been syndepositionally folded about east-

northeast axes coincident with the general trend of the Rand Mountains antiform (see Hulin, 1925, Smith, 1964, and Dibblee, 1967). Folding has affected strata as young as Middle Pliocene age. Finally, all lithologies and structures are displaced by Basin and Range style block faults, and the complex has been offset approximately 60 km along the Garlock Fault.

SUMMARY OF TECTONIC SEQUENCE

Integration of all available lithologic, structural, and geochronologic data from the Rand Thrust Complex permits the following interpretation of the tectonic sequence:

(1) Formation of the protoliths of Plates I through IV in separate geologic environments,

(2) Separate metamorphism and deformation of Plates I and II under dissimilar conditions, and probably at different times,

(3) Late Cretaceous tectonic juxtaposition of Plates I, II, and III along low angle faults, initially during one overthrusting event. The transport direction was dominantly south-southwest,

(4) Emplacement of the Randsburg Granodiorite (79±1 Ma) into the lower two plates of the complex,

(5) Multiple reactivation of various structural levels, culminating in the movement of Plate IV along a north-northeast trajectory,

(6) Uplift of the complex and erosion to the level of Plate I, accompanied by early accumulation of a Middle Tertiary overlap sequence ,

(7) Early Miocene emplacement of shallow level felsic intrusive centers accompanied by locally intense hydrothermal alteration,

(8) Continued Miocene-Pliocene subaerial accumulation of sedimentary and volcanic strata, with syndepositional folding about east-northeast axes,

(9) Displacement of the complex along high angle faults, including the Garlock Fault,

(10) Erosion to the present levels of exposure.

PART II:

THE MAGDALENA METAMORPHIC CORE COMPLEX

CHAPTER 5

INTRODUCTION

The crystalline and supracrustal rocks of northwestern Mexico offer exciting opportunities to study the evolution of regional low angle fault systems. Thrust faults and detachment faults of suspected Late Mesozoic to middle Cenozoic age abound in the desert ranges of Sonora and Baja California. Only recently have some of these shear zones been mapped in detail. Their significant role in the Mesozoic-Cenozoic tectonic evolution of the southwestern Cordillera is rapidly becoming apparent. It is now clear that this structurally complex region of Mexico has experienced the same general pattern of Late Mesozoic-Early Cenozoic crustal shortening followed by Middle Cenozoic extension that one observes north of the international border. The precise timing of events may differ slightly, but the overall tectonic history is consistent and compelling. The following study focuses on one area of north central Sonora where essential elements of this tectonic evolution are well preserved.

The Magdalena metamorphic core complex (named for its location near the small city of Magdalena de Kino, Sonora) reveals a system of low angle shear zones which developed in response to Middle Tertiary regional northeast-southwest extension of the continental crust. Deformed strata of the complex preserve the intense deformational imprint of these extensional shear zones as well as structures and fabrics related to earlier tectonic events.

It can be demonstrated that the main phase of extension followed emplacement of late leucogranites into a previously strained crustal section, the deep levels of which had been inflated by two earlier generations of granitoids. Syntectonic sedimentary deposits and contractional structures which occur at shallower stratigraphic levels constrain important episodes of regional uplift and crustal shortening that predate the main extensional event.

Lithological components of the Magdalena metamorphic core complex were mapped during an intensive study of the area between 1985 and 1989. In the following chapters, a Middle Mesozoic through Middle Cenozoic tectonostratigraphy is defined. Geological structures and rock fabrics are analyzed, and their deformational and kinematic sequence is established. The magnitude and geometry of regional deformations are constrained by systematic variations in finite strain and fabric intensity. The timing of deformational events is bracketed by a variety of intrusive units which were emplaced before, during, or after the accumulation of strain in their respective country rocks. Tectonic reconstruction of the original stratigraphy is facilitated by comparison of undeformed strata to highly deformed correlative rock assemblages. Total displacements across the important fault zones are estimated from finite strain data and from stratigraphic piercing points. Finally, the tectonic history of the study area is interpreted in a more regional context.

GEOGRAPHIC LOCATION AND ACCESS

The study area (shown in Figures 0.1 and 5.1) is located in north central Sonora within a transition zone between low hills of the Sonoran desert to the west and high ranges of the Sierra Madre Occidental to the east. The area is

divided roughly in half by the Rio Magdalena drainage system. The rocks described below are exposed mainly in mountain ranges on either side of this perennial stream. Maximum topographic relief is on the order of 1000 meters. Additional exposures (often covered by thick growths of cactus) are found in the foothills and in topographically subdued portions of the drainage basin. Limited paved road access is afforded by Mexican federal highways 2 and 15. A diversity of unpaved ranch roads and connecting routes provide access to other more isolated regions (see Figure 5.2).

PREVIOUS STUDIES

Rocks of the Magdalena area were first mapped in reconnaissance during the 1920's by a Mexican geologist named Teodoro Flores. In his pioneering treatise of 1929, Flores describes the geology and known mineral deposits exposed in a 20 kilometer strip on either side of the Southern Pacific Railroad between Guaymas and Nogales, Sonora (see Figure 5.1). The accuracy of Flore's mapping is quite remarkable, considering that most of the ground was covered on horseback and the map was constructed without a base, utilizing only a compass (for triangulation) and a barometer (for elevation). I found Flore's detailed field observations illuminating and immensely useful in planning my geological traverses.

Several of the lithologic units originally described by Flores make up important components of the tectonostratigraphy defined in Chapter 6. These rock assemblages include:

(1) a thick sequence of rhyolite porphyries associated with porphyritic granites which occur in a wide belt between Nogales and Imuris,

(2) a group of metamorphic rocks exposed north of Magdalena and west of

Figure 5.1: Location map showing area of this study (8), relative to areas of previous or concurrent studies. (1) Flores, 1929, (2) Valentine, 1936, (3) Salas, 1968, (4) Gilmont, 1978, (5) Stephens and Anderson, 1986, (6) Segerstrom, 1987, (7), Kitz and Anderson, 1988, in progress.

Figur 5.2: Geography of the study area, showing locations of physiographic features referenced in text.

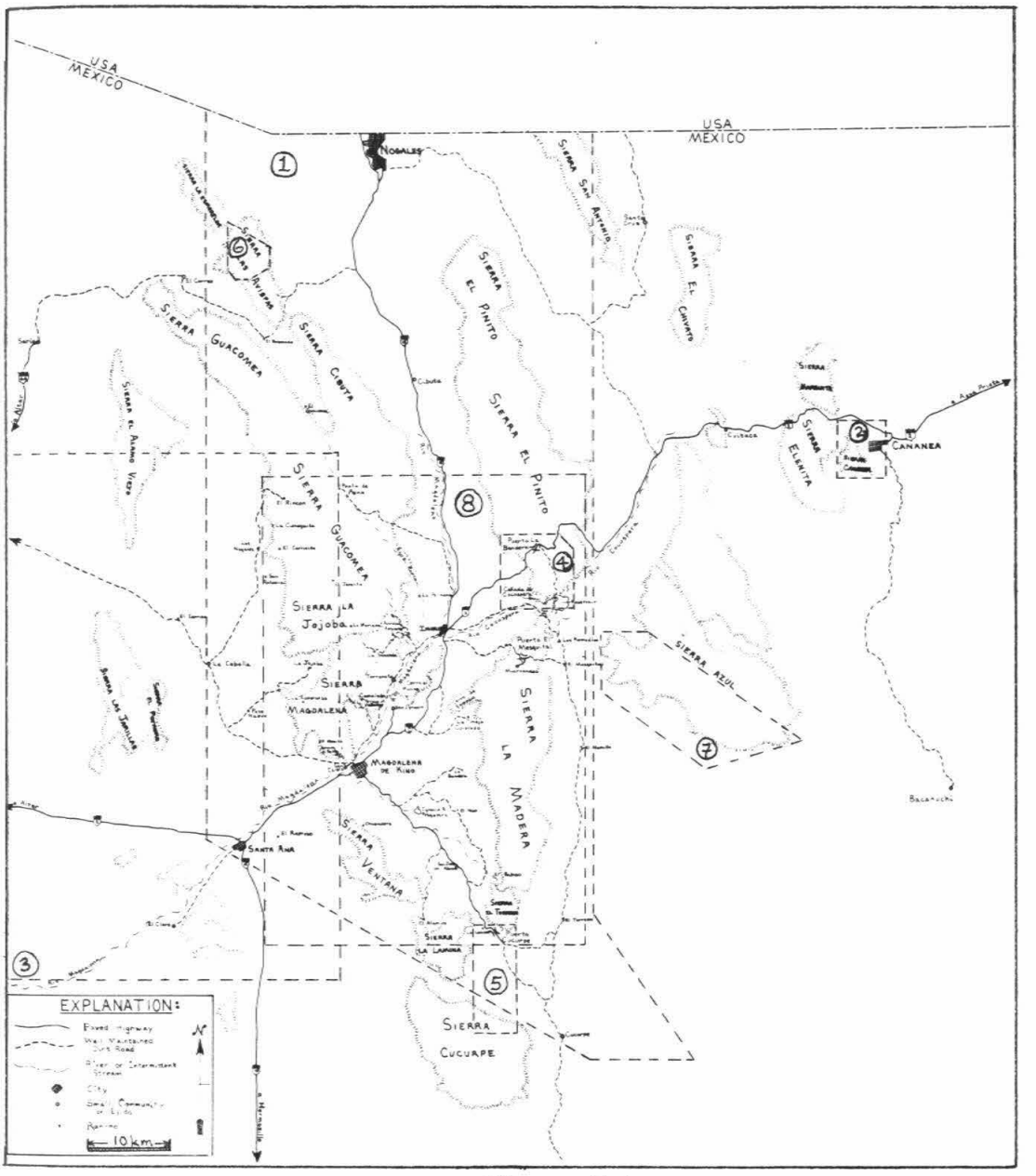
USA
MEXICO
USA
MEXICO
NOGALES
SIERRA SAN ANTONIO
SIERRA EL PINITO
SIERRA EL CARMITO
SIERRA LOS IBERRA
SIERRA GUACOMEA
SIERRA CIBUTA
SIERRA EL ALAMO VERDE
SIERRA
SIERRA ELENITA
CANANEA
SIERRA GUACOMEA
SIERRA EL PINITO
SIERRA LA Jojoba
SIERRA AZUL
SIERRA MAGDALENA
SIERRA LA MADERA
MAGDALENA DE KINO
SANTA ANA
SIERRA VENTANA
SIERRA LA LAMPARA
SIERRA CUCURPE
EXPLANATION:
10 km

Figure 5.1

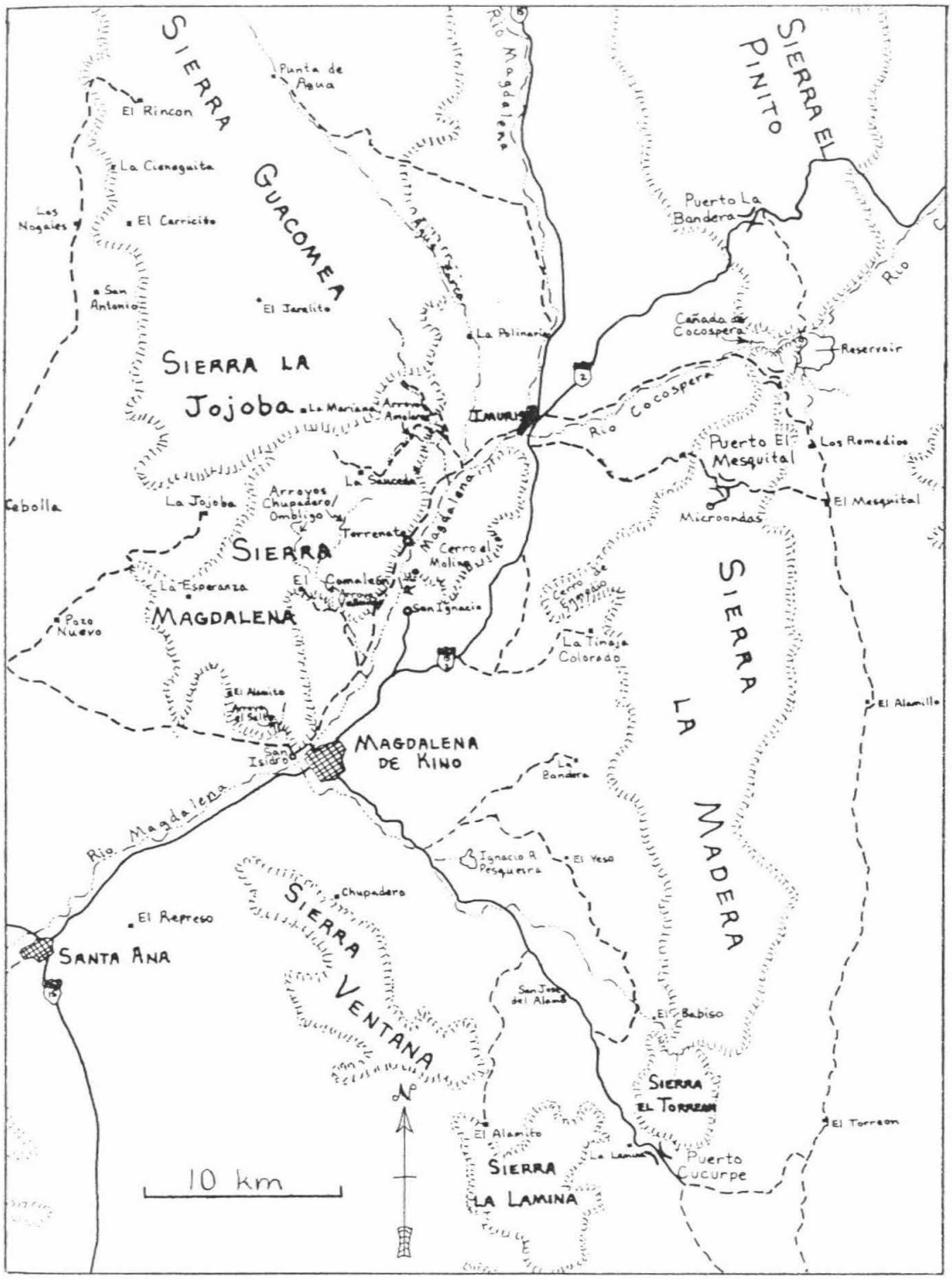
SIERRA GUACOMEA
Punta de Agua
El Rincon
La Cienaguita
Los Nogales
El Carricito
San Antonio
El Jarelito
Rio Magdalena
SIERRA EL PINITO
Puerto La Bandera
Rio
Cañada de Cocospera
Reservoir
SIERRA LA Jojoba
La Mariana
Arroyo Amaloya
IMURIS
La Polinaria
Cocospera
Rio
Puerto El Mesquital
Los Remedios
El Mesquital
Microondas
Cebolla
La Jojoba
Arroyos Chupadero/ Ombligo
La Saucedita
Magdalena
Torrenate
SIERRA MAGDALENA
Cerro el Molino
El Comalito
Arroyo Valencia
La Esperanza
San Ignacio
Pozo Nuevo
Cerro Empedo
La Tinaja Colorado
SIERRA LA MADERA
El Alamillo
El Alamito
Arroyo el Saltito
MAGDALENA DE KINO
San Isidro
La Bandera
Rio Magdalena
Ignacio R Pesqueira
El Yeso
Chupadero
SIERRA VENTANA
El Represo
SANTA ANA
San José del Alamo
El Babiso
SIERRA EL TORREON
El Torreon
El Alamito
SIERRA LA LAMINA
La Lamina
Puerto Cucurpe
10 km
N

Figure 5.2

Imuris that include granite gneisses, mica schists, and a variety of metasedimentary rocks with marble interlayers,

(3) a large mass of granite intruded by fine grained dikes, exposed in the Sierra Madera east of Magdalena and Imuris,

(4) a folded section of fine grained clastic strata with Lower Cretaceous fossiliferous limestone beds, exposed east of Santa Ana,

(5) an extensive andesitic volcanic field which makes up the high ridge (Sierra Ventana) south of Magdalena, and

(6) a diversity of tilted conglomerate beds preserved in topographically low portions of the Rio Magdalena basin.

Salas (1968) mapped at reconnaissance scale the metamorphic, sedimentary, and volcanic rocks exposed in the Santa Ana quadrangle (see Figure 5.1). His study area included the western portions of the Sierras Magdalena and Guacomea, the southern part of the Sierra el Alamo Viejo, and all of the Sierras las Jarillas and Potrero to the west. In the course of sampling metasedimentary strata , exposed throughout these ranges, Salas noted systematic trends in metamorphic grade (from greenschist to "granulite" facies), which he attributed to the spatial association of numerous deformed granitic intrusions. He also concluded that the metamorphic strata were Precambrian in age.

Regional studies by Anderson and Silver have established a geochronologic framework for much of central and northern Sonora. Elements of their work which are important to my analysis of the geology near Magdalena include:

(1) the regional distribution of Precambrian basement rocks (Silver and Anderson, 1974; Anderson and Silver, 1977, 1979, 1983),

(2) definition of a west-northwest trending Jurassic magmatic arc across the north central part of Sonora (Anderson et al., 1969; Anderson and Silver, 1978),

(3) documentation of a group of Late Cretaceous plutons which display an eastward younging trend (Anderson and Silver, 1974, 1977; Anderson et al., 1969, 1980; Silver and Chappell, 1988),

(4) Recognition of an extensive belt of metamorphic strata with regionally consistent NE-SW lineations (Anderson, et al., 1977, 1980),

(5) extension of a belt of Cordilleran metamorphic core complexes with associated detachment faults into central Sonora (Anderson et al., 1977, 1980), and

(6) documentation of early Tertiary ages for a suite of deformed two mica granites exposed in the lower plates of these core complexes (Anderson et al., 1980, Silver and Anderson, 1984).

A Masters thesis by Gilmont (1978) addresses the stratigraphy of an important section exposed in the Puerto la Bandera area northeast of Imuris (see Figure 5.1). Although I disagree with some of this author's age assignments, his documentation of the sedimentology was invaluable in helping me develop stratigraphic correlations to highly deformed and metamorphosed strata preserved in the ranges west of Imuris. In particular, Gilmont's Cocospera Formation serves as a key tectonostratigraphic and strain marker in my reconstructions of the region.

Many other geological studies of nearby areas were drawn upon in my efforts to understand the regional stratigraphy and tectonics. These include a description of Jurassic? and Cretaceous? strata southwest of Nogales (Segerstrom, 1987), an interpretation of the Jurassic-Cretaceous boundary in

the Cucurpe-Tuape area (Rodriguez-Casteneda, 1986), a detailed stratigraphic analysis of Lower Cretaceous marine strata exposed northeast of Cucurpe (Kitz and Anderson, 1988), a study of Aptian-Albian limestones and associated Cretaceous beds north of Altar (Jacques-Ayala, 1986; Jacques-Ayala and Potter, 1987), descriptions of the stratigraphy and structure of the Agua Prieta region (Taliaferro, 1933; Rangin, 1977b), and a documentation of the stratigraphy and structure of the El Tigre mining district in northeastern Sonora (Montano-Jimenez, 1988). Also of interest were an analysis of Mesozoic-Cenozoic low angle structures near Caborca and Altar (de Jong, 1988), and a description of Precambrian and Jurassic? thrust sheets exposed between Magdalena and Cucurpe (Anderson et al., 1984; Stephens and Anderson, 1986). Discussions with Tom Anderson and Lee Silver over the years have been important factors in my research. Finally, the observations of countless other workers on the geology of southern and western Arizona and northern Sonora were helpful in developing a regional geologic perspective.

GENERAL GEOLOGICAL SETTING

The Magdalena metamorphic core complex developed within an evolving portion of the southern Basin and Range Province. Throughout this province, bedrock geology is typically exposed in isolated, north or northwest trending mountain ranges separated by broad alluviated valleys. The present day topography and geomorphology are the result of horst and graben development in an extensional tectonic environment. High angle normal faults that bound most of the ranges are believed to be relatively young structures, probably active only during the past 10 million years (Stewart, 1978). Their recent domination of the Basin and Range structure has been

important in exposing a wide spectrum of profiles through the middle and upper crust.

The more extensively studied Arizona segment of the Basin and Range Province provides a relevant data base for comparing my observations from Mexico. Many common geologic and tectonic links exist between the two regions. Widespread portions of southern and western Arizona have experienced a remarkably consistent two stage history of Late Mesozoic-Early Cenozoic thrust faulting, magmatism and metamorphism followed by Middle Tertiary extension along shallowly dipping brittle-ductile normal sense shear zones (detachment faults). I believe the same pattern is represented near Magdalena, but with a unique assemblage of rocks. The transition from crustal shortening to crustal extension in this area is depicted in Figure 7.16.

Strata of the Magdalena metamorphic core complex are preserved in two plates of the Magdalena detachment fault system. These rocks owe their present level of exposure to Late Cenozoic uplift along a network of northeast and northwest trending high angle normal faults, and to minor late reactivation of certain segments of the detachment fault. A succession of stream terraces preserved at various levels along the length of the Rio Magdalena drainage basin attest to relatively recent tectonic uplift of the region.

The Magdalena detachment fault is well expressed geomorphically as a shallow dipping, broadly folded surface which flanks the southern Sierra Magdalena, the southeastern part of Cerro de Enmedio, and the western and southern portions of the Sierra Madera. Southwestward movement along this high strain interface has effectively unroofed a ductilely deformed plutonic and metamorphic substrate from structurally and stratigraphically higher

unmetamorphosed sedimentary and volcanic rocks. Together these two plates comprise a once continuous Jurassic through Middle Tertiary crustal section.

Rocks of the Magdalena core complex record a pre-detachment tectonic history in addition to deformational fabrics directly related to Middle Tertiary displacement on the detachment fault. Late Cretaceous-Early Tertiary depositional, magmatic, and structural events in the upper plate correspond broadly to deeper seated plutonic and metamorphic episodes in the lower plate. A transition from regional crustal contraction to localized crustal extension is implicit in the crosscutting field relationships. Observations developed in the next three chapters place constraints on the timing, geometry, and mechanics of this evolutionary process. The geology and tectonostratigraphy are outlined in Chapter 6. Local and regional structures and fabrics are described in Chapter 7. The geometry of strain associated with two ductile deformational events is analyzed in Chapter 8. Finally, the tectonic sequence is summarized in Chapter 9.

CHAPTER 6

GEOLOGY AND TECTONOSTRATIGRAPHY

Diverse lithologies in the Magdalena area record the Mesozoic and Cenozoic tectonostratigraphic development of part of an important orogenic belt. Across a 50 kilometer wide corridor, a distinctive Jurassic through Lower Cretaceous stratigraphy preserves the cumulative effects of multiple superimposed deformational events. The deeper parts of this Jura-Cretaceous section serve as a convenient stratigraphic and strain markers in tracking the structural evolution of the middle crust through a time interval that overlapped the emplacement of three generations of Late Cretaceous-Middle Tertiary granitoids. Fossiliferous Lower Cretaceous limestone beds present at higher stratigraphic levels provide a key reference horizon useful for constraining the sedimentary, volcanic, and deformational history of the upper crust during the same time interval. The resulting composite Jurassic through middle Tertiary tectonostratigraphy is presently exposed in two structural plates separated by a regional low angle fault (the Magdalena detachment fault). The lower plate and the upper plate represent highly evolved portions of the middle crust and upper crust, respectively.

The geology and structure of the study area are compiled on a 1:50,000 scale topographic base map with a contour interval of 20 meters (see Plate 2). The locations of all samples used for strain analysis are plotted on Plate 4. Petrographic analyses of representative samples are tabulated in Appendix B. All mineralogical modes are based on volumetric estimates.

Several regions of the lower plate were mapped at more detailed scales of 1:20,000 or 1:30,000. These areas serve as "type localities" useful for evaluating stratigraphic correlations and applying quantitative structural and strain analysis. Large portions of the Sierra Guacomea, the Sierra la Jojoba, and the Sierra el Pinito were not mapped due to accessibility problems. Mapping in the upper plate is also incomplete. The data shown there include a compilation of mapping by Flores (1929), Salas (1968), and Stephens and Anderson (1986) as well as observations made by myself during reconnaissance traverses through various sedimentary and volcanic sequences.

Specific sites described in the text are keyed to locations of the ranches, roads, and physiographic features shown in Figure 5.2. The geology of the study area is summarized in Figure 6.1. A generalized northeast-southwest cross section is shown in Figure 6.2. To facilitate description and correlation of the tectonostratigraphy, I have divided the mapped area into three geographic domains: In the **Northeast Low Strain Belt,** a well preserved Jurassic through Lower Cretaceous type section is described. The section is compared to similar strata exposed outside the study area, and the basis for regional stratigraphic correlation is established. Next, a layered metamorphic sequence exposed in the **Central High Strain Belt** is described. Age relationships between deformed supracrustal rocks and multiple generations of granite are documented, and the supracrustal rocks are interpreted to be metamorphosed equivalents of the northeastern type section. Finally, after a brief description of the **Magdalena detachment fault**, the **Upper Plate Stratigraphy** is addressed, with a focus on two well exposed areas. A transition from marine deposition to active intracontinental clastic sedimentation and volcanism is established, and evidence for a regional Late

Cretaceous?-Early Tertiary unconformity is discussed.

The last portion of this chapter briefly describes the widespread occurrences of alluvium and colluvium in the study area. While these young deposits were not studied in detail, their general distribution provides indirect insight into Late Cenozoic structural modifications of the pre-Middle Tertiary tectonostratigraphy.

Figure 6.1a: Generalized geologic map of the Magdalena Metamorphic core complex.

Figure 6.1b: Explanation for geologic map and cross section.

Figure 6.2: Northeast-southwest cross section through the Magdalena metamorphic core complex, along a line connecting Santa Ana and Puerto la Bandera. Vertical exaggeration = 2. Geology is projected in from 10 to 15 kilometers on either side.

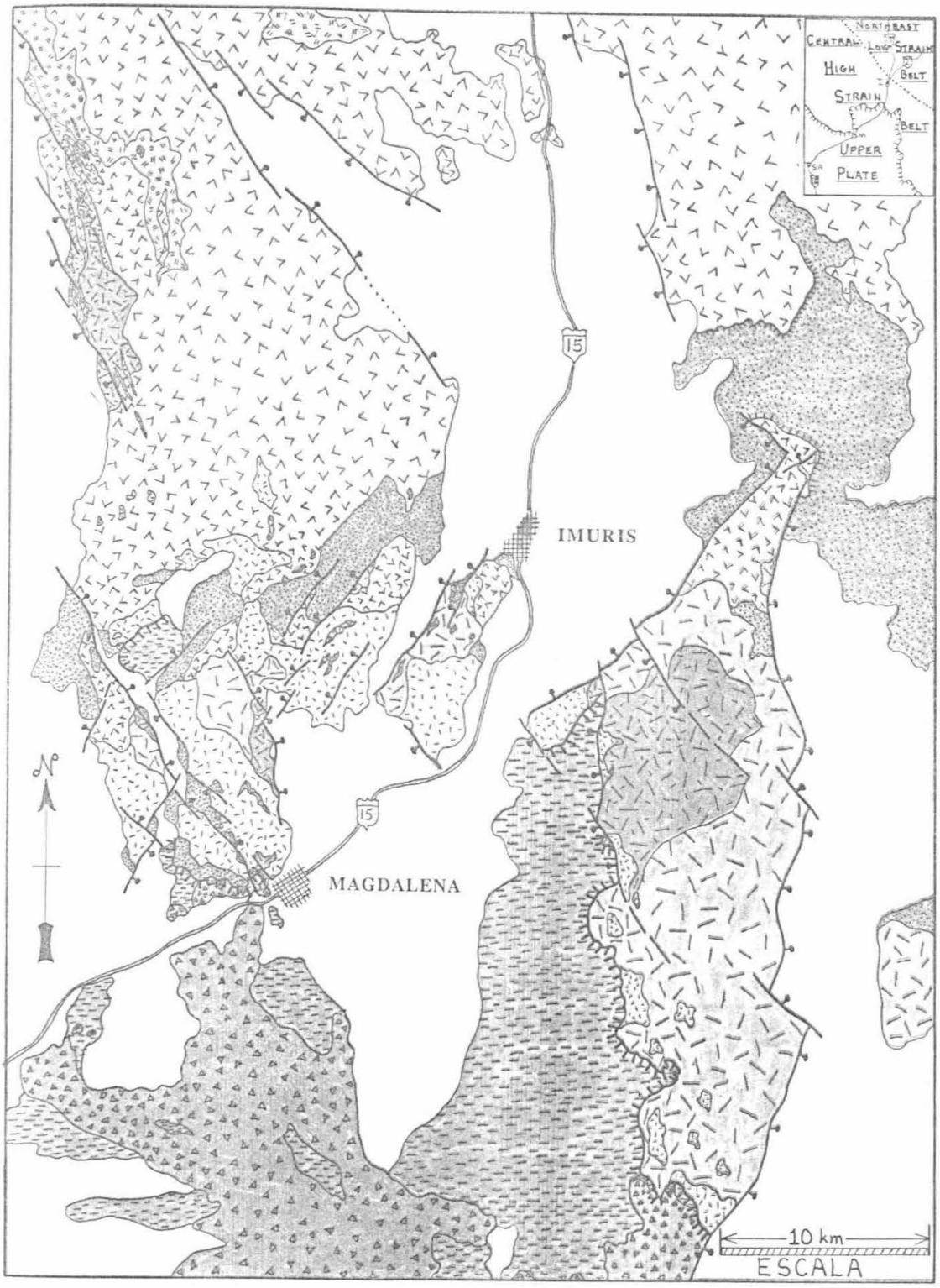
NORTHEAST
CENTRAL
LOW STRAIN
BELT
HIGH
STRAIN
BELT
UPPER
PLATE
15
IMURIS
15
MAGDALENA
N
10 km
ESCALA

Figure 6.1a

EXPLANATION

UPPER PLATE:

CRETACEOUS-TERTIARY SEDIMENTARY ROCKS

CRETACEOUS-TERTIARY VOLCANIC ROCKS

MAGDALENA DETACHMENT FAULT

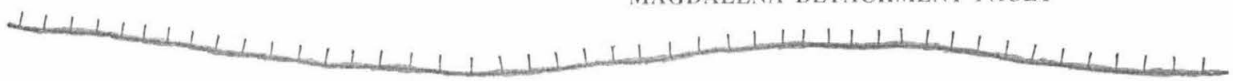

LOWER PLATE:

LATE CRETACEOUS– MID TERTIARY GRANITOIDS

OLIGOCENE?

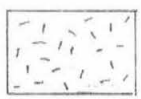

LEUCOGRANITE (Two mica, garnet bearing granite, aplite, and pegmatite

EARLY TERTIARY?

TWO MICA GRANITE-GRANODIORITE (with garnet)

LATE CRETACEOUS

BIOTITE GRANODIORITE-GRANITE (no garnet)

MESOZOIC COUNTRY ROCKS

UPPER JURASSIC?-LOWER CRETACEOUS SEDIMENTARY ROCKS (Quartz pebble conglomerate, sandstone, siltstone, shale, and limestone

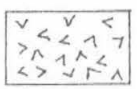

JURASSIC SUPRACRUSTAL ROCKS (Rhyolite porphyry, rhyolite clast conglomerate, quartz arenite)

JURASSIC? PLUTONIC ROCKS

Figure 6.1b

CROSS SECTION THROUGH THE MAGDALENA METAMORPHIC CORE COMPLEX

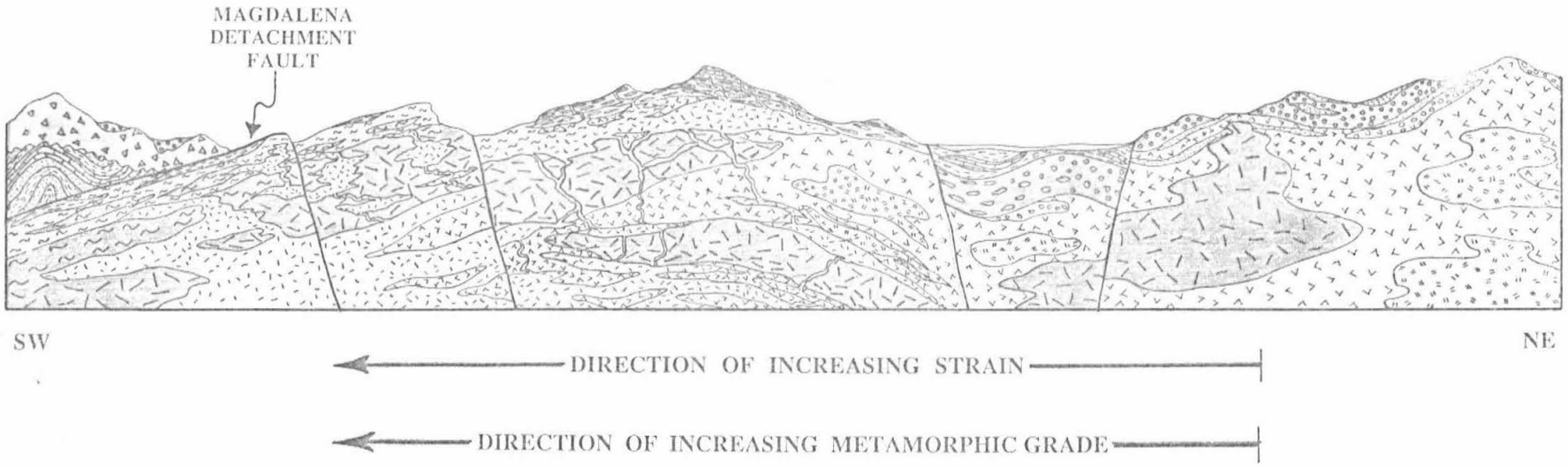

VERTICAL EXAGGERATION ABOUT 2X

Figure 62

LOWER PLATE TYPE STRATIGRAPHY: THE NORTHEAST LOW STRAIN BELT

Unmetamorphosed to weakly metamorphosed rocks that make up the type Jurassic-Lower Cretaceous stratigraphy occur to the north, northeast, and east of Imuris. The type section (shown in Figure 6.3) consists of a layered series of interstratified rhyolite and quartz arenite, volcanic conglomerate, and intrusive granite porphyry, overlain in faulted unconformity by well bedded deposits of fluvial conglomerate, sandstone, and siltstone. The base of the type section is not exposed. The volcanic strata become progressively more recrystallized and strained in a transition zone between the Rio Cocospera and Puerto el Mesquital, where they are intruded by two distinctive two mica granite plutons.

FELSIC VOLCANIC SERIES (AND ASSOCIATED ROCKS):

A diverse assemblage of felsic volcanic arc related rocks covers a large portion of the northeastern map area. Excellent exposures occur in new roadcuts along recently upgraded Highway 15 north of Imuris, in roadcuts along Highway 2 near Puerto la Bandera, in the walls of the Rio Cocospera canyon, and along the crest of the northern Sierra Madera.

Rhyolite Porphyry (rhy) makes up the bulk of the felsic series. Part of this unit was mapped by Gilmont (1978), who named it "El Pinito Rhyolite" for its occurrence in the Sierra el Pinito. The rock varies in composition from rhyolite to rhyodacite or quarz latite. The texture is porphyritic-aphanitic, with phenocrysts of subrounded quartz and euhedral to fragmented feldspar in a white to light gray felsic groundmass. Phenocryst

Figure 6.3: Stratigraphy of the type section, Northeast Low Strain Belt. Rock symbols as in Figure 6.1b.

RIO COCOSPERA/PUERTO LA BANDERA SECTION

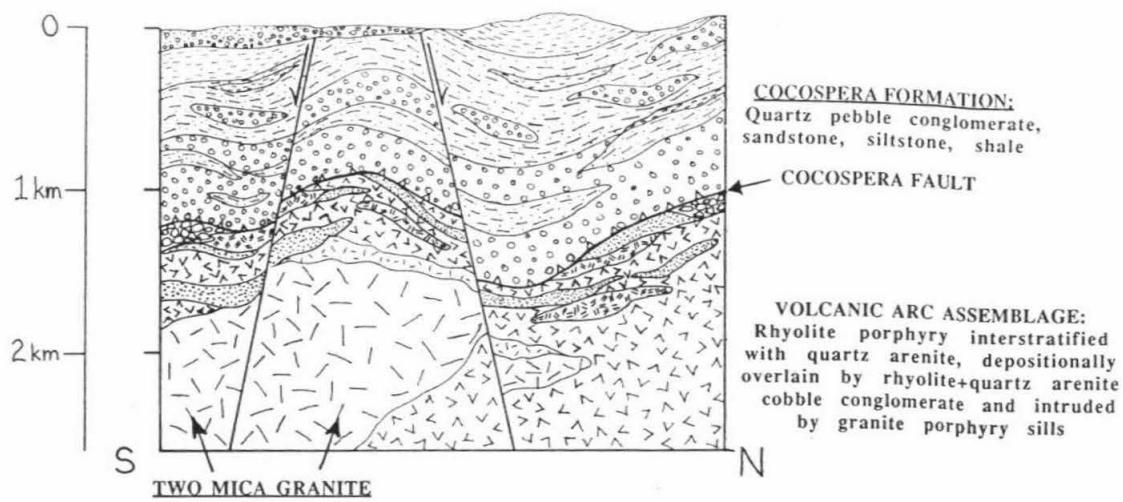

Figure 6.3

content varies from 10% to 50%, and crystals as large as 6 millimeters in diameter are common. The rhyolite frequently exhibits a primary flow banding which is invariably subparallel to the orientation of interstratified quartz arenite lenses. Outcrops of rhyolite porphyry near Highway 2 are essentially unmetamorphosed, however, farther south in the contact aureole of the two mica granites, the groundmass and feldspar phenocrysts are thoroughly recrystallized. There the rock is characterized by residual quartz eyes in a sugary felsic matrix.

In thin section, both microcline and sodic plagioclase are observed as phenocrysts. The microcline may be partially replaced with sericite. Anhedral quartz phenocrysts are generally subequent and sometimes almost spherical in shape. Zircon, sphene, and magnetite? occur as accessory phenocrysts. The groundmass is composed of extremely fine grained feldspar, quartz, devitrified glass?, white mica, and biotite. Contacts between phenocrysts and groundmass are sharply defined. In recrystallized samples, the groundmass is coarser grained, and boundaries with recrystallized phenocrysts tend to be diffuse.

The widespread geographic distribution of the rhyolite porphyry as well as its lithologic continuity and lack of textural variability suggest that the volcanic unit was extruded as thick, laterally extensive flows or sheets. Additional mapping of the rhyolite would be helpful in subdividing individual flow units and in correlating specific stratigraphic intervals over large areas.

Rhyolite Breccia (rbr) occurs as irregular masses within the rhyolite porphyry. The rock is comprised of angular, centimeter to decimeter sized fragments of fine grained rhyolitic material in a highly silicified felsic matrix. Outcrops form resistant, uneven surfaces, and tend to be stained dark

reddish purple (due to hydrothermal Mn? alteration). Quartz filled fractures pervade the rock. The breccia may represent a pyroclastic deposit, but its proximity to large fault zones suggests a tectonic origin. I have interpreted this unit as a fault breccia derived from a rhyolitic protolith.

Quartz Arenite (qss) is present as layers up to 50 meters thick within the upper portion of the felsic series. One of these layers, the "Bandera Sandstone," was mapped by Gilmont (1978) in the area just south of Highway 2 near Puerto la Bandera. Several other slightly recrystallized quartz arenite lenses are interlayered with rhyolite on both sides of the Rio Cocospera canyon, and in the Sierra Madera north of Puerto el Mesquital.

The quartz arenites are fine to very fine grained, moderately sorted, and well indurated. Outcrops are highly resistant and typically form prominent ledges. Bedding is defined by thin bands of dark minerals (zircon and magnetite), and decimeter and meter scale cross bedding is present in places. Fresh surfaces are white or light gray. Weathered surfaces tend to be stained dark purple. Where unfaulted, contacts with the rhyolite porphyry are sharp and conformable. The sandstones are clearly interstratified with the rhyolite and are therefore coeval with at least the upper part of the rhyolitic sequence.

Gilmont (1978) studied the petrography of the Bandera Sandstone in detail. The four thin sections I examined from the qss unit are consistent with his results. In general, the rock is made up of 60% to 70% well rounded detrital grains cemented by authogenic sericite and silica. At least 80% of the grains are quartz; the remainder are feldspars or volcanic rock fragments probably derived from the rhyolite porphyry.

Rhyolite Cobble Conglomerate (vcg) is the highest stratigraphic unit of the felsic series. One small mass is exposed in roadcuts immediately east of Puerto la Bandera. Here a pristine depositional contact between the conglomerate and underlying rhyolite porphyry is preserved (see Figure 8.6a). The conglomerate is composed of well rounded cobbles of white and gray rhyolite porphyry in a poorly sorted, weakly indurated lithic sand matrix. Rare pebbles of light gray quartzite and quartz arenite are present as accessory clasts. Both the rhyolite cobbles and their matrix appear to have been locally derived from the rhyolite porphyry unit.

A larger mass of rhyolite cobble conglomerate occurs along the crest of the northern Sierra Madera. Here the conglomerate also contains locally abundant cobbles of quartz arenite and rare pebbles of fine grained dark gray biotite-feldspar schist. The volcanic and sandstone clasts are lithologically identical to the stratigraphically deeper rhy and qss units, respectively. A systematic metamorphic/strain gradient is well displayed by this conglomerate mass. In the northernmost exposures the matrix minerals are recrystallized and a weak schistosity is apparent. Farther south the entire rock is recrystallized and the conglomerate clasts are noticeably elongate. Where the conglomerate is intruded by the Mesquital Granodiorite (see below) it is more accurately classified as a stretched cobble conglomerate.

The top of the rhyolite cobble conglomerate unit was observed in one place on the northern Sierra Madera ridge crest. There a small mass of quartzite-volcanic cobble conglomerate similar to part of the Cocospera Formation (see next section) rests in apparent depositional contact upon the rhyolitic conglomerate. The contact is marked by an abrupt color change from white-light gray in the older unit to green-orange in the younger. Also, the percentage of quartzite and quartz arenite clasts increases significantly.

Field relationships indicate that the rhyolite cobble conglomerate is younger than the interbedded rhyolite/quartz arenite sequence, but older than an intrusive sill of granite porphyry (see below). The conglomerate is also older than the Cocospera Formation, and older than the crosscutting Mesquital Granodiorite.

Granite Porphyry (grp) intrudes all components of the felsic series described above. Sills of granite up to 100 meters thick occur in at least two stratigraphic positions in the northern Sierra Madera. The granite porphyry becomes more metamorphosed toward the south. Exposures 1/2 kilometer north of the microondas road are quite foliated and recrystallized.

Compositionally the porphyry is a biotite-sphene granite. Texturally it varies from granite porphyry to coarse grained porphyritic granite. Euhedral microcline megacrysts up to 2 centimeters long are common, as are coarse (5 to 10 millimeter diameter) subspherical quartz phenocrysts. The medium to fine grained groundmass is composed of plagioclase, alkali feldspar, biotite, and sphene. The extreme porphyritic character of the granite implies that it was emplaced at shallow crustal levels.

The intrusive nature of the granite porphyry is best displayed on the crest of the northern Sierra Madera, where it forms a concordant sheet between the interlayered rhyolite/quartz arenite sequence and the stratigraphically higher rhyolite cobble conglomerate. The granite sill becomes abruptly finer grained within 1 to 2 meters of its upper contact with the conglomerate. Both the percentage of phenocrysts and their average size decrease markedly. In some places this border phase may exhibit a flow foliation.

Where granite porphyry intrudes the rhyolite porphyry the contacts

appear gradational, for the finer grained phase of the granite is similar in composition and texture to the rhyolite. The age relationships between these units thus tend to be equivical, particularly where a deformational fabric has been superimposed. However, an independent line of reasoning argues that the granite is younger than the rhyolite: no granite porphyry clasts are present in the vcg unit, but rhyolite and quartz arenite cobbles are ubiquitous. Had the rhyolite and granite porphyry been a coeval suite one would expect to see a contribution from both of these units in the conglomerate.

Counterparts to the granite porphyry are known in many areas of northern Sonora (Anderson and Silver, 1978; Corona, 1979) and southern and western Arizona (Tosdal et al., 1988). Typically the granites are intruded as sills into well stratified sections of rhyolite, conglomerate, and sandstone. Specific occurrences of granite porphyry north of the mapped area include exposures in the Sierra las Avispas, in the western Sierra el Pinito, and in a group of hills west of Nogales. These granite outcrops were first described and mapped by Flores (1929). All appear to have been emplaced into thick rhyolitic sequences.

COCOSPERA FORMATION (csp):

The felsic volcanic strata are stratigraphically and structurally overlain by a fining upward quartz rich clastic sequence. Sedimentological features of this conglomeratic section were studied in detail by Gilmont (1978), who named it the "Cocospera Formation" for its geographic association with the Rio Cocospera drainage. Excellent exposures of this unit are preserved in the canyon of the Rio Cocospera, in Highway 2 roadcuts, and along bulldozer tracks near the power lines south of Puerto la Bandera.

The Cocospera Formation is made up of layers and lenses of cobble-

pebble conglomerate interbedded on a decameter and meter scale with green sandstone, siltstone, and mudstone. Gilmont interpreted the assemblage as a fluvial sequence, based on: (1) the ubiquitous occurrence of asymmetric channel deposits, cut and fill structures, and normally graded beds, and (2) the statistical shape of conglomerate clasts. Sediment transport direction (determined from crossbed orientations) was dominantly toward the south or southwest. In general, the size of conglomerate clasts decreases up section, as does the ratio of conglomerate to finer grained sedimentary rock.

In the canyons of the Rios Cocospera and Los Remedios the conglomerate beds are clast supported and well indurated. Sandstone and siltstone comprise less than 30% of the section. The conglomerates are composed of well rounded, subelliptical pebbles and cobbles set in a poorly sorted matrix of sand and gravel. A typical clast population from this area is: 25% quartzite, 10% quartz arenite, 10% rhyolite porphyry and aphanitic felsite, 12% green lithic sandstone, 15% green siltstone or shale, 5% green andesite? porphyry or black mafic volcanic with white feldspars, 1% black chert, 1% nonfossiliferous, light gray to brown limestone, rare coarse grained granite porphyry, and 20% matrix. Gilmont (1978) reports the presence of limestone cobbles with Oxfordian fossils, but none were encountered during my traverses. The stratigraphically deeper felsic series was certainly an important source terrane, for the rhyolite, quartz sandstone, and granite porphyry clasts are lithologically identical to the rhy, qss, and grp units, respectively. The rest of the clasts originated from sources outside the study area.

Cocospera conglomerate exposures just south of Puerto la Bandera represent either stratigraphically higher or more distal deposits. Here, sandstone, siltstone, and shale make up about 75% of the section. The

conglomerates are matrix supported and the clasts are dominantly of pebble size. In comparison to the clast population described above, quartzite, quartz arenite, and chert are significantly more abundant, andesite is rare, and the green sandstone and siltstone clasts are absent. Also quite common are moderately indurated, light brown sandstone and siltstone pebbles which were probably reworked from slightly deeper intraformational beds.

Sandstone, siltstone, and mudstone layers within the Cocospera Formation were analysed petrographically by Gilmont (1978). The three thin sections I studied agree with his conclusions. These immature beds have an average composition of lithic wacke or feldspathic wacke. In sandstone layers, subangular, moderately sorted grains with a clay rich matrix are cemented by authogenic sericite and calcite. In finer grained siltstone or mudstone horizons the grains are matrix supported, and the clay is commonly altered to chlorite, imparting a distinctive green color to these sediments. The sand grains typically include a representative population of quartz, sodic plagioclase, microcline, rhyolite, andesite, quartz arenite, and rare perthite. Most components of this population could realistically have been derived from the stratigraphically deeper felsic series.

The contact between the Cocospera Formation and locally underlying Bandera Sandstone and El Pinito Rhyolite was interpreted by Gilmont (1978) to be depositional. However, after reexamining this relationship in Gilmont's type area and walking many more kilometers of the basal conglomerate throughout the region, I have concluded that the contact, while originally depositional, is now almost everywhere a fault (the exception is an exposure on the crest of the northern Sierra Madera, described above). The fault is a low angle surface, generally concordant with bedding in the superjacent conglomerate. Deformation appears to have been localized within a narrow (1

to 5 meter) zone. The presence of fault gouge, silicified breccias, and slickensided shear surfaces implies that movement took place at shallow crustal levels. Total displacement along this faulted unconformity is uncertain (see Chapter 7).

The top of the Cocospera Formation is not exposed in the mapped area. However, the conglomerate can be traced along strike to the southeast, where it is stratigraphically and structurally overlain by a thick (greater than 2 kilometers) Lower Cretaceous marine sequence (Kitz and Anderson, 1988; Kitz, personal communication, 1988). These marine beds are dominantly composed of siltstones and shales, with at least two prominent fossiliferous limestone horizons. Distinctive Aptian-Albian fauna collected from the limestones permit correlation of the marine sequence to the Bisbee Group of southeastern Arizona and northeastern Sonora (Kitz and Anderson, 1988). These strata thus place an upper bound on the age of the Cocospera Formation.

INTRUSIVE UNITS:

A variety of dikes, veins, and plutons intrude the type stratigraphy described above. Their distribution and crosscutting relationships place constraints on an important post Early Cretaceous metamorphic and deformational event.

Porphyritic two mica granite occurs as two separate masses intrusive into different stratigraphic levels of the type section. The top of one small granite pluton is well exposed in the lower part of Arroyo los Remedios, immediately downstream from the diversion dam. This intrusion was named "**Presa Granite**" by Gilmont (1978). The main mass of the granite is a medium grained porphyritic bio+muscovite granite with euhedral microcline

and large, subspherical quartz phenocrysts. Its average mineralogy (from point count data of Gilmont) is 45% microcline, 32% quartz, 18% albite, 3% biotite, 1% muscovite, with trace quantities of zircon, apatite, and magnetite. Xenoliths of recrystallized felsic volcanic schists are common. The flat roof of the pluton is delimited by a sheetlike mass of fine grained aplite, about 50 meters thick. Several pegmatite dikes (4 centimeters to 2 meters wide) eminate from the granite into recrystallized rhyolite porphyry country rocks.

Along the eastern base of the northern Sierra Madera a slightly finer grained porphyritic granodiorite (hereafter referred to as the **Mesquital Granodiorite**) intrudes a ridge forming mass of recrystallized and moderately strained rhyolite cobble conglomerate. The contact dips moderately to the northwest, and crosses the crest of the range just north of Puerto el Mesquital. In the drainage immediately west of the pass the granodiorite sharply crosscuts deformational fabrics in both the rhyolite conglomerate and the rhyolite porphyry. Inclusions of these felsic schists are common within the pluton. East of Puerto el Mesquital, an elongate mass of highly deformed marble and fine grained metasedimentary rock is intruded by the granodiorite. These metamorphic rocks are somewhat enigmatic, but their composition and location imply a correlation to the Lower Cretaceous marine strata exposed just outside the study area to the southeast. Available data thus indicate that the Mesquital Granodiorite was emplaced after a deformation that involved rocks as young as Early Cretaceous.

The Mesquital Granodiorite is medium grained and porphyritic, with an average mineralogy of 50% plagioclase, 25% quartz, 20% K feldspar, 4% to 5% biotite, and less than 1% muscovite. Red garnet occurs frequently at deeper structural levels where the rock approaches a composition of monzogranite. Euhedral phenocrysts of K feldspar up to 1 cm long give the pluton its

porphyritic texture; this mineral also is present as a groundmass constituent. Shallow structural levels of the granodiorite are commonly cut by discrete ductile shear zones (see Chapter 7), but for the most part the pluton is undeformed. Fine grained biotite bearing aplite and coarse muscovite-garnet pegmatite occur as veins, dikes, and sills within the granodiorite. Where the host pluton is locally affected by a ductile deformation, the aplites and pegmatites share at least part of the fabric.

Porphyritic Dacite Dikes intrude rhyolite porphyry, rhyolite cobble conglomerate, and the Cocospera Formation, but were not observed within the two mica granites. These dikes are porphyritic-aphanitic, and contain about 35% phenocrysts of hornblende and plagioclase in subequal amounts. The dacites occur as steep northwest trending dikes 1/2 to 3 meters wide. They crosscut a recrystallized and locally schistose fabric in the felsic series.

Post-Two Mica Granite Intrusions include a group of 1/2 to 3 meter wide fine grained mafic dikes (which range in composition from andesite to basalt) and a set of quartz veins. These dikes and veins are steeply dipping and share a common northwest strike. They crosscut the fabric of all the units described above.

INTERPRETATION OF TYPE STRATIGRAPHY

The volcanic and sedimentary strata described above record an interval of volcanic arc activity and sedimentary basin formation that spanned the Jurassic period and the first half of the Cretaceous. A Jurassic age is inferred for the felsic volcanic series on the basis of lithologic similarities with strata

in southern Arizona and northwestern Sonora which have been well dated by U/Pb methods. These Jurassic strata include:

(1) the Fresnal Canyon Sequence of the Baboquavari Mountains (Wright, et al., 1981; Tosdal et al., 1988),

(2) the Mount Wrightson Formation of the Santa Rita Mountains (Riggs, et al., 1986, 1987), and

(3) a suite of felsic volcanic porphyries and associated volcaniclastic rocks exposed in a west northwest trending belt between Cananea and San Luis, Sonora (Anderson and Silver, 1978, 1979). The supracrustal assemblages of areas (1) through (3) are characterized by porphyritic rhyolite to rhyodacite flows interstratified with quartz arenites, and volcaniclastic conglomerate and sandstone. Shallow granitic intrusions are common locally. Interpreted U/Pb ages reported by the above workers range between 205 Ma and 170 Ma.

The Cocospera Formation occupies the stratigraphic interval between the Jurassic volcanic series and the Lower Cretaceous marine strata. Its age is thus interpreted to be Late Jurassic to earliest Cretaceous. The rhyolite, quartz arenite, and granite porphyry clasts were derived from the underlying Jurassic felsic series. The immature sandstone, siltstone, and shale clasts and the rare limestone cobbles may have originated from Upper Jurassic clastic/carbonate sequences known farther south (see Rangin, 1977a; Rodriguez-Castaneda, 1986; Anderson et al., 1988). These strata are the most probable source for the Oxfordian fossil bearing limestone clasts. Paleozoic beds exposed intermittently throughout northern and central Sonora are likely sources for the quartzite and chert pebbles. Those sources must have been quite distal, for none of the fossiliferous limestones that characterize the Upper Paleozoic have been recognized in the Cocospera clast assemblage. Finally, the dark volcanic porphyry clasts with white feldspar phenocrysts

could have been eroded from Jurassic? andesites and dacites presently exposed near Cananea (Valentine, 1936), or Jurassic flows, breccias, and agglomerates reported west of the Rio San Miguel de Horcasitas (Rangin, 1977a; Anderson et al., 1988).

On the basis of lithologic similarity and stratigraphic position, the Cocospera Formation correlates with a quartzite-volcanic-limestone-granite-metamorphic clast conglomerate exposed within an Upper Jurassic section between Tuape and La Lamina (Rodriguez-Castaneda, 1986; Anderson et al., 1988), and to a fining upward conglomerate that forms the base of an Upper Barremian through Lower Albian marine sequence near Cerro de Oro (Gonzales-Leon and Jacques-Ayala, 1988). Also a likely correlative of the Cocospera conglomerate is a section of quartzite-rhyolite porphyry clast conglomerate, lithic sandstone, and siltstone exposed northeast of Altar. This unit, the El Amol Formation, appears to be in thrust contact with underlying Lower Cretaceous beds (Garcia Y Barragan et al., 1988; de Jong, personal communication, 1988).

A Late Jurassic-Early Cretaceous age interpretation for the Cocospera Formation is in conflict with the Early Miocene age assignment proposed by Gilmont (1978) on the basis of pollen found in one of the mudstone layers. I believe the older age interpretation is more consistent with the local and regional geology. Specifically:

(1) The Cocospera Formation and its equivalents in northern Sonora are stratigraphically constrained by underlying Jurasssic rocks and overlying Lower Cretaceous beds.

(2) Within the Central High Strain Belt the Cocospera Formation has been metamorphosed to amphibolite grade, ductilely deformed, uplifted, and eroded to its present level of exposure. It seems unlikely that these events could have

happened since Early Miocene time.

(3) A great variety of post-Lower Cretaceous conglomerates have been mapped during the course of this study. Without exception, all of these conglomerates contain gray limestone clasts with distinctive Aptian-Albian fossils. The Cocospera conglomerate does not.

The paleogeography implied by the Jurassic-Lower Cretaceous type stratigraphy is consistent with the regional tectonic framework. The Jurassic volcanic series is an important component of a 150+ kilometer wide continental margin magmatic arc that evolved during oblique subduction of the Farallon (or Kula?) Plate under the North American Plate (Anderson and Silver, 1978; Coney, 1979; Tosdal et al., 1988). The rhyolites and granite porphyries represent volcanic extrusions and subvolcanic intrusions, respectively. The volcaniclastic conglomerates and sandstones were probably deposited in local extensional basins (possibly collapsed calderas) and the interbedded quartz arenites may represent influxes of mature sand from large intracontinental dune fields (see Busby-Spera, 1988).

The Upper Jurassic-Lower Cretaceous Cocospera Formation is correlative to the Glance Conglomerate, a regionally distinctive time stratigraphic unit exposed in southeastern Arizona and northeastern Sonora. Occurences of Glance Conglomerate are interpreted as syntectonic deposits related to a Late Jurassic-earliest Cretaceous disturbance (Bilodeau, 1978; Bilodeau et al., 1987). The Glance Conglomerate appears to have been deposited in alluvial fans along the margins of northwest striking fault bounded basins. Clast populations vary in accordance with the geology of local block uplifts.

The fine grained strata that overlie the Cocospera Formation east of the study area were deposited during an Early Cretaceous marine incursion (Kitz and Anderson, 1988). Accumulation of these sediments apparently took place

in an isolated arm of the Bisbee Basin (a regional depocenter believed to have developed during back arc rifting; see Dickenson, 1981).

An important post-Early Cretaceous orogenic event has affected the type stratigraphy in the northern Sierra Madera. This event is represented by the southward increase in fabric intensity (schistosity and pebble elongation) within the felsic series. An associated thermal metamorphism has caused recrystallization of the volcanogenic section and growth of chlorite in the Cocospera Formation. Field relationships in this area demonstrate that the Presa Granite and the Mesquital Granodiorite are younger than most of the deformation and metamorphism, and therefore place a lower limit on the age of the orogenic event. K/Ar ages of 33.2±0.7 and 26.3±0.6 have been reported for biotite separated from the Presa and the Mesquital plutons, respectively (Gilmont, 1978; Damon et al., unpublished data). However, these ages may record the waning stages of a regional thermal event rather than true emplacement ages (see discussion in Chapter 7).

LOWER PLATE DEFORMED STRATIGRAPHY: THE CENTRAL HIGH STRAIN BELT

In the Sierras Magdalena, Jojoba, Guacomea, and Madera, a diverse assemblage of greenschist to lower amphibolite grade metamorphosed supracrustal rocks is intimately associated with at least three generations of deformed granite. Mapping of the layered rocks reveals highly strained remnants of a consistent stratigraphy that can be correlated protolith by protolith to the undeformed Jura-Cretaceous rocks in the northeast. All components of the type section occur in the Central High Strain Belt in the

appropriate stratigraphic positions.

An increase in deformational intensity (as measured by gradients in finite strain and rock fabric) is displayed in northeast to southwest traverses through the Central Belt. Fabric relationships between the supracrustal assemblage and the younger granites imply a two stage deformational sequence. Specifically, a regional fabric in the country rocks that developed during emplacement of the older granites is overprinted by a second, locally intense mylonitic fabric that affects all three generations of granites as well as their country rocks.

Various structural levels of the deformed stratigraphy are well preserved in three areas that were mapped at more detailed scales of 1:30,000 or 1:20,000. Representative stratigraphic columns for these three areas are shown in Figures 6.4-6.6. In general, supracrustal rocks of successively higher structural and stratigraphic position are exposed in traverses from the north to the south. Also, the ratio of granite to supracrustal rock increases toward the south. The central and southern portions of the Sierra Madera are completely underlain by granite and granite gneiss.

Figure 6.4: Stratigraphy of the central Sierra Magdalena.

Figure 6.5: Stratigraphy of the southern Sierra Magdalena.

Figure 6.6: Stratigraphy of the west central Sierra Guacomea.

LA SAUCEDA SECTION

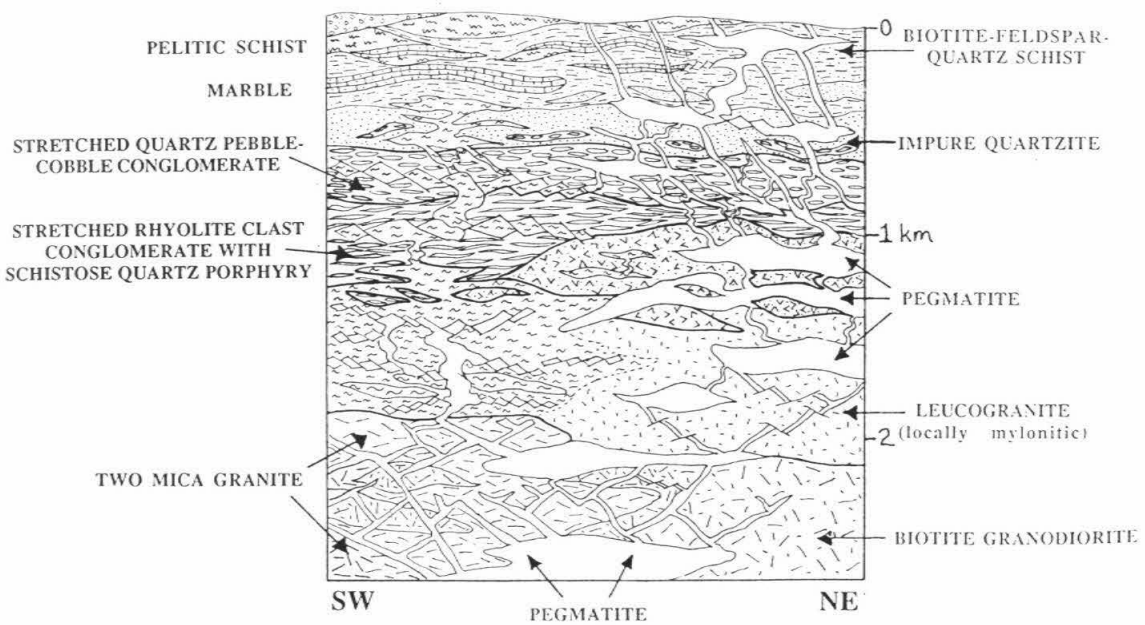

Figure 6.4

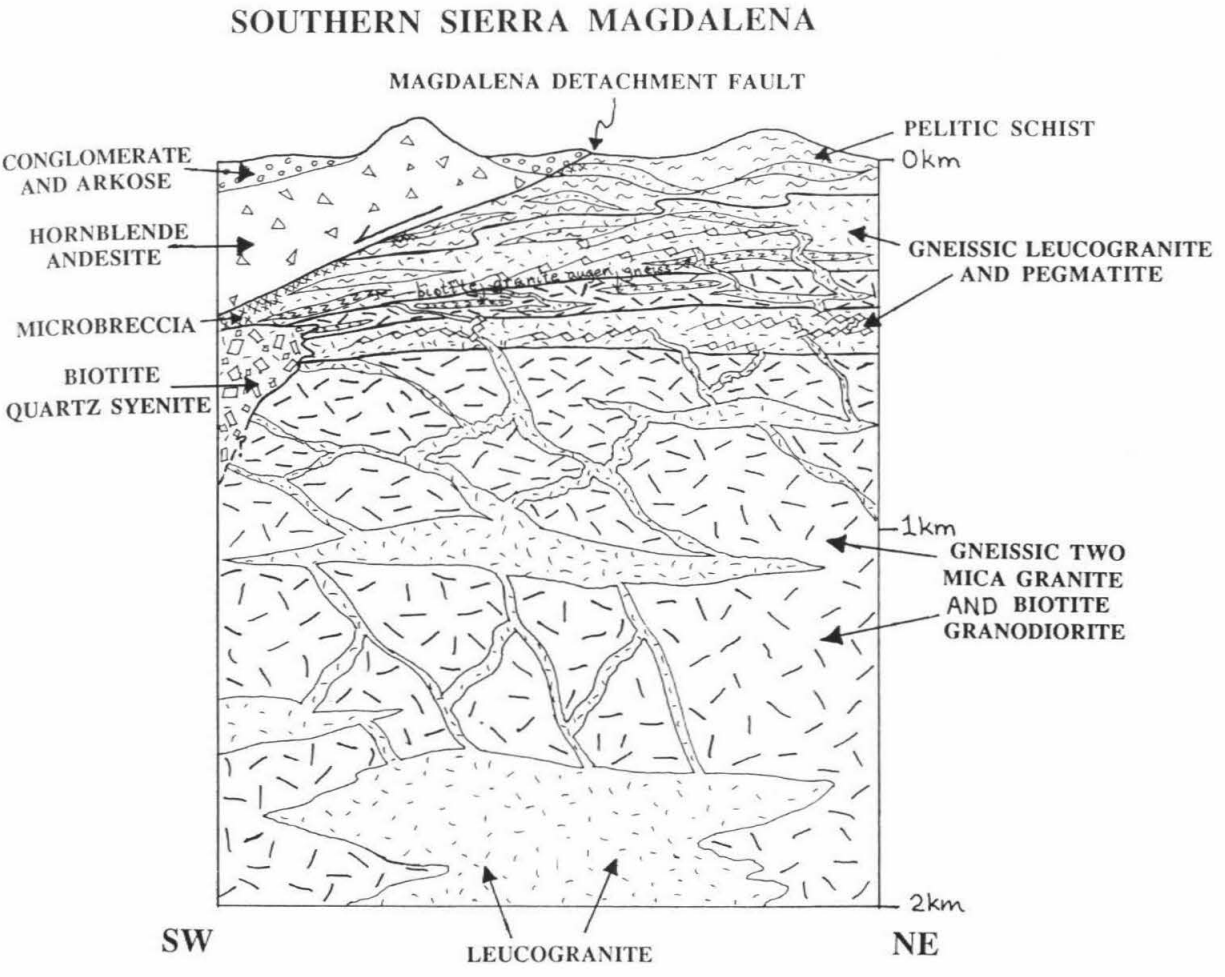
SOUTHERN SIERRA MAGDALENA
MAGDALENA DETACHMENT FAULT
PELITIC SCHIST
0km
CONGLOMERATE AND ARKOSE
HORNBLENDE ANDESITE
MICROBRECCIA
BIOTITE QUARTZ SYENITE
GNEISSIC LEUCOGRANITE AND PEGMATITE
1km
GNEISSIC TWO MICA GRANITE AND BIOTITE GRANODIORITE
2km
SW
LEUCOGRANITE
NE

Figure 6.5

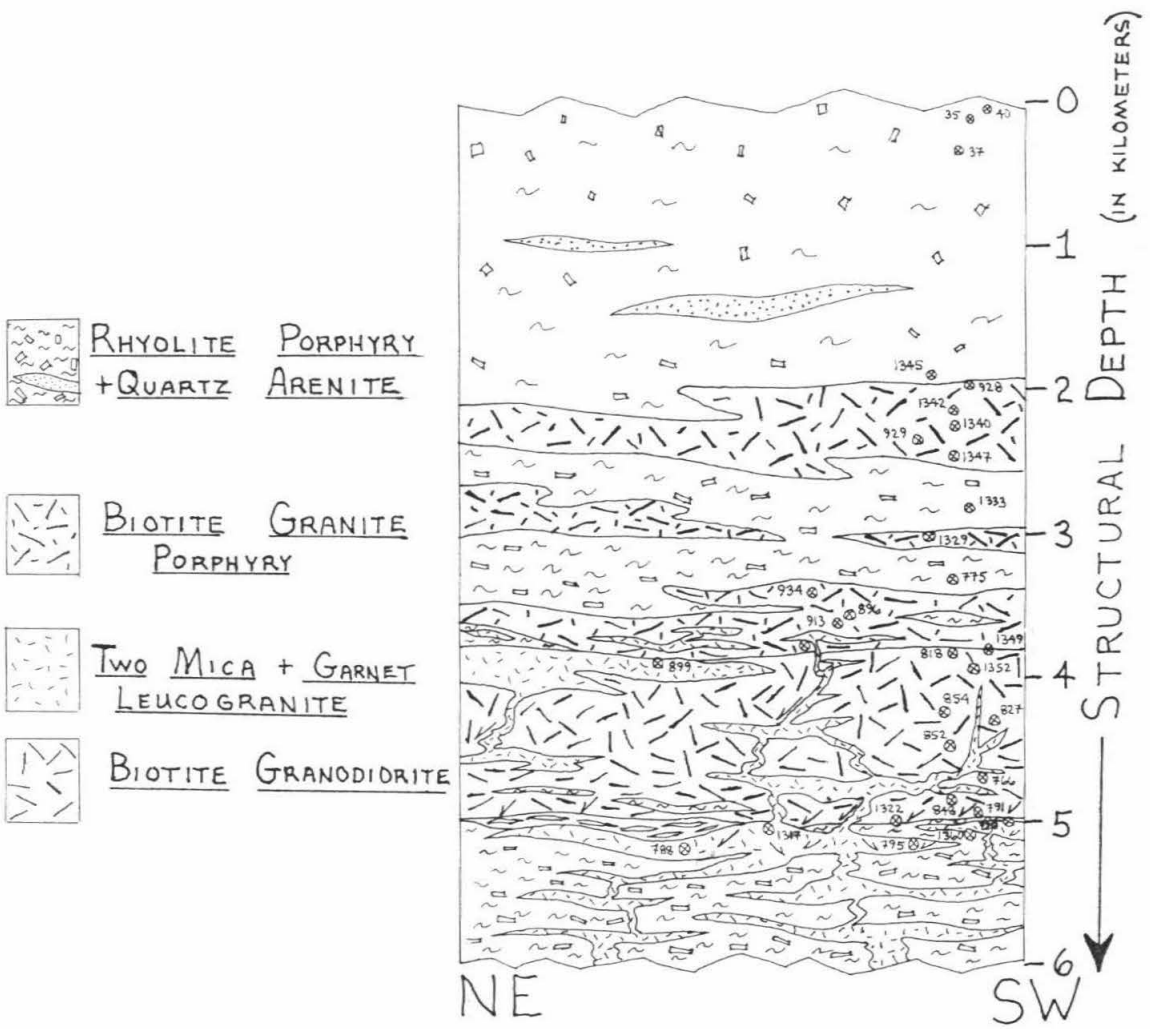
WEST CENTRAL SIERRA GUACOMEA
RHYOLITE PORPHYRY
+QUARTZ ARENITE
BIOTITE GRANITE
PORPHYRY
TWO MICA + GARNET
LEUCOGRANITE
BIOTITE GRANODIORITE
0
1
2
3
4
5
6
STRUCTURAL DEPTH (IN KILOMETERS)
NE
SW

Figure 6.6

For purposes of the following discussion, the crystalline rocks of the Central High Strain Belt are divided into two groups: a **Metamorphosed Supracrustal Assemblage**, and a **Granitic Plutonic/Orthogneiss Complex**.

METAMORPHOSED SUPRACRUSTAL ASSEMBLAGE:

FELSIC SCHISTS AND GNEISSES

A thick series of quartzofeldspathic schists and gneisses exposed in the Sierra Guacomea, the Sierra la Jojoba, and the northern Sierra Magdalena represent the deepest known stratigraphic levels of the Magdalena core complex. These rocks are light gray in color, and typically weather beige, tan, or sometimes rust red. The schists form flaggy outcrops, while the gneisses are more massive.

Schistose Quartz Porphyry (mqp) is the most common lithology of the felsic series. In the northern Sierra Magdalena this unit forms the substrate to a laterally extensive stretched rhyolite clast conglomerate member. In the central Sierra Guacomea, quartz porphyry is interlayered with sill like masses of deformed granite porphyry and lenses of recrystallized quartz arenite. About 6 kilometers of metamorphosed strata are exposed as a northeast dipping homocline in this latter area. The lower portion of the layered sequence is intruded by a large (up to 1 km thick) sill of biotite granodiorite and smaller sills and dikes of leucogranite (both to be described later). Metamorphic grade and foliation intensity increase with depth in the quartz porphyry dominated country rocks.

The schistose quartz porphyry is characterized by a relict porphyritic-

aphanitic texture: conspicuous phenocrysyts of subrounded quartz and recrystallized feldspar are isolated in a fine grained sugary matrix of feldspar, quartz, and mica. The rock displays a weak to moderate schistosity, defined by the subparallel alignment of micas and elongate phenocrysts. Two distinctive compositions were observed: (1) plag-microcline-qtz-musc-mgt schist, and (2) plag-microcline-qtz-hbld-ep-sph±bio±chl schist. The latter variety is commonly associated with the granite porphyry sills. A downward increase in metamorphic grade is apparent in this rock, as hornblende and epidote (and sometimes chlorite) give way to biotite and sphene.

The schistose quartz porphyry was clearly derived from a porphyritic volcanic protolith. In the northern part of Arroyo Agua Zarca, quartz porphyry grades transitionally into a lithology that looks identical to the rhyolite porphyry unit of the Northeast Low Strain Belt. The geographic extent and thickness of individual mappable units suggest that the quartz porphyry originally accumulated as widespread lava flows. The variability in mineral assemblages probably reflects primary compositional variations between rhyolite and hornblende bearing rhyodacite.

Metamorphosed Granite Porphyry (mgrp) is interlayered with schistose quartz porphyry in the central Sierra Guacomea. The rock is texturally and compositionally heterogeneous; protoliths vary between medium grained porphyritic biotite- sphene granite and fine to medium grained K-feldspar-plag-qtz-hbld-bio porphyry. Large (1/2 to 1 centimeter) subspherical quartz phenocrysts and 1 to 3 centimeter long augen shaped microcline megacrysts are common features. Contacts with the finer grained schistose quartz porphyry layers tend to be gradational and concordant.

Granite porphyry at shallow structural levels is slightly to moderately

recrystallized and only weakly deformed. Structurally deeper exposures of the granite (near the contact with the biotite granodiorite sill) are thoroughly recrystallized and strongly foliated. Here an almost schistose fabric is defined by elongate recrystallized quartz and microcline phenocrysts and an alignment of recrystallized biotite domains. Metamorphic assemblages in the granite suggest an increase in grade with depth. Chlorite, epidote, and hornblende are present at shallow levels while biotite is the only mafic mineral in the deepest exposures.

Massive Quartzofeldspathic Gneiss (mav) is a common rock type in the Sierra la Jojoba and in nearby areas. The gneiss is white to light gray, and forms resistant, massive outcrops. It appears to be stratigraphically and structurally deeper than the schistose quartz porphyry and the stretched volcaniclastic strata. Lineations and foliations are much more poorly developed in the gneiss than in the mqp and mgrp units.

The gneiss is fine to very fine grained, and is dominantly composed of recrystallized feldspar and quartz. Biotite, white mica, and opaques are common accessory minerals. A very weak centimeter scale compositional foliation is defined by layers rich in biotite and opaques. Because larger crystals are virtually absent, the protolith was certainly not a porphyry. Also the lack of primary compositional banding or regular textural variations indicates that the protolith was probably not a well layered sedimentary sequence. My best guess for a protolith would be a fine grained crystal poor silicic ash flow tuff. Such a lithology was not observed in undeformed state within the mapped area. However, thick deposits of ash flow tuff do occur farther north in the Sierra las Avispas (see Segerstrom, 1987) and immediately north of the international border in the Pajarito Mountains (Riggs, 1987). In

both of these areas, the tuffs are associated with rhyolite porphyry. More work is necessary to better define the geographic extent and stratigraphic position of the quartzofeldspathic gneiss unit, and its relationship to other metavolcanic units.

Stretched Volcanic Conglomerate (mvcg) comprises the highest stratigraphic and structural unit of the metamorphosed felsic series. In many places this schistose lithology clearly was derived from a rhyolite clast conglomerate protolith. In other areas, extreme strain and recrystallization have obscured most primary textural relations, and it is uncertain whether the volcaniclastic protolith was originally pyroclastic (i.e., agglomeratic) or sedimentary (conglomeratic). When relatively large, isolated quartz and feldspar grains are visible it can be argued that the original clasts were porphyritic felsic volcanic or hypabyssal rocks.

The deformed volcaniclastic unit is typically composed of elongate clasts of fine grained recrystallized felsic material aligned in a fine grained schistose matrix of feldspar, muscovite, quartz, and biotite. A strong mineral lineation coincides with the mesoscopic stretching direction of the clasts. The clasts and the matrix are frequently of similar composition and texture, making it easy to miss the clastic nature of the rock upon first glance. However, the definition of clast margins is often enhanced by local concentrations of biotite and muscovite. Also, the felsic clasts tend to be poorer in mica than their matrix.

Mapping of the stretched volcaniclastic unit demonstrates that it overlies a thick sequence of schistose quartz porphyry. The contact between the two units can usually be defined within a couple of meters. The volcaniclastic rocks are generally richer in muscovite and more schistose

than the quartz porphyry unit. The contact relations are well exposed in the vicinity of Arroyo Agua Zarca. Here the strain is fairly moderate, and it can be seen that the stretched clasts were once well rounded conglomerate cobbles composed of rhyolite porphyry, aphanitic silicic volcanic rock, minor quartz arenite, and rare medium gray quartzite. The schistose conglomerates are frequently interlayered with finer grained feldspar-sericite-quartz schist. A weak fabric in the underlying mqp unit is concordant with the schistosity in the conglomerate. Recrystallized quartz arenites occur commonly as 3 to 20 meter thick layers within the upper portion of the quartz porphyry, but do not persist at deeper stratigraphic levels.

Muscovite-Feldspar-Quartz Schist (mfs) is interlayered with the stretched volcaniclastic rocks. This well lineated, fine grained schist may be very quartz rich, and may contain isolated stretched rhyolite or quartzite pebbles. The mineralogy is plagioclase-microcline-quartz-muscovite (or sericite), with accessory biotite, zircon, and opaque minerals. Garnet occurs in the highest grade schists. The protolith was likely a fine grained felsic volcanogenic sediment. Finer grained sericitic schists and phyllites were probably derived from mudstones or siltstones; coarser grained muscovite-feldspar-quartz schists may represent metamorphosed arenites.

Quartzite (qss) derived from fine grained quartz arenite is commonly interlayered with metamorphosed rhyolite in the Sierra Guacomea. The quartzite is also interleaved with metamorphosed granite porphyry north of El Rincon. In several areas the quartzite contains significant amounts of garnet and white mica. Mapping of this lithology is incomplete, hence stratigraphic correlations between the scattered locations shown on the map are tenuous.

However, in general the quartzite appears to be restricted to the shallower stratigraphic levels of the felsic schist and gneiss series.

Biotite Schist occurs as discordant, tabular masses within various metavolcanic units. The rock is characterized by 1 to 2 centimeter long recystallized feldspars in a matrix of biotite and feldspar. The schist shares a common foliation with the adjacent lighter colored felsic volcanic rocks, but on a larger scale its outcrop pattern frequently is discordant to the local metamorphic layering. The biotite schists were not studied in detail; however, I suspect that they represent porphyritic mafic dikes metamorphosed and rotated during the deformation of their volcanic host rocks.

QUARTZITIC, CALCAREOUS, AND PELITIC METASEDIMENTARY ROCKS

The felsic schists and gneisses are regionally overlain by a highly deformed, fining upward metasedimentary series. In contrast to the characteristic light gray color of the stratigraphically and structurally deeper felsic series, the metasedimentary rocks are distinctively green, orange, dark gray, or dark brown. A variety of quartzitic, calcareous, and pelitic bulk compositions provide opportunities to place constraints on the metamorphic paragenesis.

Lithologic components of the metasedimentary series are described below in stratigraphic succession from the quartz rich metaconglomerates at the base to the pelitic schists and marbles at the top. A fairly complete section is exposed in the vicinity of La Sauceda and Arroyo Amolares. The pelitic schists and marbles are better represented farther to the southwest in exposures between Magdalena and Rancho la Esperanza.

Stretched Quartz-Volcanic-Sandstone Clast Conglomerate (**qcg**) marks the base of the metasedimentary series. This highly resistant quartz rich conglomeratic unit achieves a thickness of 150 meters in places. Its boundary with underlying stretched volcaniclastic strata or muscovite-feldspar-quartz schist is concordant with the local schistosity and can everywhere be located to within 1 meter. The contact is sharply delineated in the field by the first appearance of abundant stretched quartzite clasts and a coincident sudden appearance of epidote and green amphibole. A general change from felsic/muscovitic to quartzitic/calcareous bulk composition is also quite striking. These contact relationships are best displayed in the spectacular exposures of Arroyo Amolares.

The metaconglomerate occurs as sheetlike masses 5 to 15 meters thick with finer grained interlayers of quartz rich semischist and biotite feldspar schist. The relative proportion of conglomerate decreases up section, but isolated lenses of metaconglomerate are common within the finer grained strata well into the middle part of the section. Conglomerate clasts have been stretched and flattened parallel to a well developed schistosity in the matrix material. A strong mineral lineation displayed on foliation surfaces corresonds to the maximum elongation direction of the stretched clasts (see pebble shape analysis in Chapter 8).

The protolith conglomerate was clast supported and comprised of well rounded pebbles and cobbles of highly variable initial shape (see Chapter 8). Identifiable clasts in the deformed La Sauceda/Arroyo Amolares section include quartzite, fine grained quartz arenite, rhyolite porphyry, quartz-feldspar-hornblende porphyry, and black chert. Many other clasts have been recrystallized to such an extent that their original fine grained textures are obliterated. Those composed mainly of feldspar and quartz were perhaps

derived from an aphanitic silicic volcanic source; others composed of fine grained feldspar, hornblende, biotite, and quartz may once have been mudstone or siltstone clasts.

The characteristic green color of this portion of the section is largely due to its upper greenschist-lower amphibolite metamorphic mineral assemblage. Epidote, green amphibole, and quartz are ubiquitous, and biotite and grossular garnet are abundant. Plagioclase, microcline, and white mica round out the prograde mineral assemblage. Chlorite is rarely encountered except in the vicinity of post-metamorphic shear zones and fractures. As will be described in Chapters 7 and 8, a significant amount of dynamic strain was superimposed on the conglomerate during and after equilibration of the metamorphic minerals.

Impure Quartzite (q) is intimately associated with the stretched quartz-volcanic-sandstone clast conglomerate, and also tends to grade in and out of biotite-feldspar schist layers. This lithology weathers orange, primarily due to oxidation of epidote. The "quartzite" is composed of at least 50% quartz, with varying proportions of plagioclase, microcline, epidote, hornblende, biotite, grossular garnet, zircon, tourmaline, and opaque minerals. In some samples, a relict clastic texture allows one to infer that the protolith was a moderately sorted medium to fine grained sandstone. An abundance of zircon also suggests a detrital origin.

The quartzite is highly resistant and strongly lineated compared to the finer grained biotite-feldspar schists. Varieties with significant proportions of hornblende and biotite display semi schistose textures. Boundaries with adjacent units of the metasedimentary series are typically gradational. The quartzite unit was differentiated in the field by its abundance of quartz, lack of

schistosity, and characteristic orange weathering appearance.

Biotite-Feldspar Schist (bfs) is interlayered with metaconglomerate and impure quartzite, and dominates the middle portion of the metasedimentary section. This dark gray to dark green-gray rock is fine to very fine grained, with a weakly lineated schistose to semi schistose fabric. The mineralogy is plagioclase-microcline-biotite-quartz-zircon-epidote-opaque. Well formed pyrite cubes are locally present. Some samples preserve primary sedimentary textures suggestive of a siltstone protolith. An abundance of biotite and lack of quartz relative to the impure quartzite unit make the bfs unit easy to distinguish in the field.

Marble (m) forms fairly continuous and conspicuous marker horizons in the upper portion of the metasedimentary section. The thickest exposures occur along the western slope of the Sierra Magdalena between El Alamito and La Esperanza. Other exposures are interlayered with biotite-feldspar schist in the upper part of the La Sauceda section. The marble is extremely fine grained, thoroughly recrystallized, and often quite impure. Important mineral phases in addition to calcite include quartz, plagioclase, epidote, sericite, and opaques. Grossular garnet is abundant in some samples. The color of this lithology varies from light gray to pink-orange to white. A submillimeter scale layering tends to be concordant with the local foliation, but may be folded disharmonically.

Considerable effort was expended (without success) searching for fossils in the marble. Sheared renmants of probable fossils are encountered in many places, but any diagnostic features have been destroyed during metamorphism. I was unable to relocate the site of an Oxfordian fossil

reportedly found in the marbles south of La Esperanza (M. Montano, personal communication, 1986)

Pelitic Schist and Phyllite (pe, ph) are preserved in the highest exposed stratigraphic levels of the metasedimentary series. These rocks were mapped as a distinctive unit in the field on the basis of their pelitic metamorphic mineral assemblage and their brown or reddish brown color. The mineralogy is dominated by muscovite (or sericite), quartz, biotite, and feldspar. Staurolite, andalusite, and cordierite? form abundant porphyroblasts in the medium or fine grained pelitic schists. Garnet was observed in three samples. Very fine grained brown metasedimentary rocks lacking in porphyroblasts were mapped as phyllite. The schists tend to be richer in quartz and better lineated than the phyllites.

The prograde mineral assemblages and metamorphic textures in the pelitic schists are significantly overprinted by a noncoaxial retrograde shear fabric. Asymmetric shear bands disturb an earlier schistosity, and biotite in the neighborhood of the shear bands may be replaced by chlorite. Chlorite also fills spaces in garnets which have been fractured and rotated during the deformation. Large quartz grains are drawn out into dynamically recrystallized ribbons, indicating that they were deformed in a greenschist facies environment (see Chapter 7).

GRANITIC PLUTONIC/ORTHOGNEISS COMPLEX:

The metamorphosed supracrustal assemblage described above has been deformed with at least three generations of granite. The granites were emplaced at various times during a long lived period of regional

metamorphism and deformation. Crosscutting relationships indicate that an early ductile strain event associated with greenschist to amphibolite grade metamorphism occurred after crystallization of the oldest granite but prior to emplacement of the youngest granitic suite. Deformational fabrics and primary intrusive relationships that developed during the early strain event have generally been overprinted or completely obscured by a younger mylonitic fabric. Networks of leucogranite dikes and veins associated with the last phase of plutonism make convenient markers for gauging the intensity of this late deformation. In regions of the metamorphic core not much affected by the ductile shear fabric, pegmatite veins are discordant to the local schistosity and display only minor amounts of rotation or internal strain. In regions of higher shear strain the pegmatites are noticeably deformed (boudinaged or buckled), significantly rotated, and may be completely transposed into the mylonitic foliation.

The granites were subdivided into map units on the basis of their mineralogies and inferred protolith textures (even with the most deformed granite orthogneisses it was usually possible to decide whether the protolith was coarse or fine grained). Contacts between individual map units are often gradational. Some of the regions mapped as leucogranite or leucogneiss in the Sierra Magdalena are actually masses of older granitic host rock that have been flooded by significant proportions (greater than 50%) of leucogranite in the form of interconnected sheets and sills. The areas mapped as bgd or 2gr contain lesser amounts of the younger leucogranite.

Granites of the Central High Strain Belt are described below in order of their field sequence. The Streckeisen classification scheme for plutonic rocks (1967) was used wherever applicable

Porphyritic Biotite Granodiorite (pbgd) represents the oldest known phase of the plutonic sequence. This lithology was emplaced as a large sill into a layered series of rhyolite porphyry, quartz arenite, volcaniclastic conglomerate, and granite porphyry in the west central Sierra Guacomea. A lithologically similar granodiorite reappears in the deepest structural levels of the central Sierra Magdalena, where it is overlain by sill like masses of gneissic two mica granite and leucogranite. Elongate pendants of biotite granodiorite occur within two mica granite in the lower part of the tilted fault block east of Terrenate. At structurally shallow levels of the lower plate in the southern Sierra Magdalena, sheets strongly mylonitic gneiss derived from a porphyritic biotite granodiorite protolith are interlayered with highly deformed leucogranite and coarse grained biotite granite augen gneiss.

The best preserved mass of porphyritic biotite granodiorite forms the steep escarpment along the western front of the Sierra Guacomea. This rock was studied by Anderson et al. (1980), in a regional geochronological survey of deformed granites. These authors determined a U/Pb zircon age of 78±3 Ma for a sample (referred to as "Guacomea Gneiss") representative of the moderately strained, structurally deep portion of this pluton.

My mapping in the Sierra Guacomea indicates that the granodiorite is a sill at least 12 kilometers in length and up to 700 meters thick. The lower boundary of the pluton is marked almost everywhere by a narrow belt of highly recrystallized felsic schists. The upper boundary is partly obscured by a younger, finer grained leucogranite sill. Leucogranite sills that invade the layered "floor rocks" are apparently connected by a series of dikes to the shallower sill. A fabric developed in the lower part of the granodiorite appears to have been superimposed on the leucogranites as well. Vertical traverses through the granodiorite sill show that foliation intensity decreases

upward, the fabric becomes less recrystallized, and the proportion of alkali feldspar increases. The upper contact with schistose quartz porphyry is frequently obscured by sheets of leucogranite localized along this interface.

The main mass of the bgd unit may be classified as a medium to coarse grained well foliated porphyritic biotite granodiorite. Its average mineralogy is similar to that reported for the Guacomea Gneiss by Anderson et al. (1980): about 32% plagioclase, 21% K-feldspar, 37% quartz, and 8% to 10% biotite. Accessory minerals include sphene, zircon, chlorite and opaque. Isolated K-feldspar crystals as long as 2 centimeters give the rock a porphyritic appearance. Foliation in the deeper part of the intrusion is defined by the alignment of biotite and flattened, recrystallized coarse quartz and feldspar crystals. Lineations are poorly to moderately developed. At shallower structural levels the granodiorite is unlineated and barely foliated. Large, weakly undulose, subequant quartz grains show only traces of recrystallization. This lithology is slightly finer grained and less porphyritic than the Guacomea Gneiss. It has less biotite and more K-feldspar, and commonly contains large (up to 6 millimeters diameter) red garnet and mesoscopically visible muscovite. The contact between the two phases of the granodiorite appears to be transitional and gradational.

Porphyryitic biotite granodiorites of the Sierra Magdalena are generally similar in mineralogy and texture to the Guacomea Gneiss. However, some varieties are significantly poorer in quartz and richer in biotite (up to 15% or 20%), and contain isolated porphyroclasts of plagioclase that give the rock a distinctive spotted appearance. The granodiorite may be interlayered on a meter scale with less mafic porphyritic two mica granites, or may occur as inclusions within structurally higher granites. Moderately foliated masses granodiorite are crisscrossed by veins of pegmatite that share a common

fabric with their host. The deepest known exposures of granodiorite can be unfoliated or strongly foliated; in the latter case the fabric shows evidence for being statically annealed.

Porphyritic biotite granodiorites in high shear strain regions of the southern Sierra Magdalena are better classified as mylonites. Quartz rich granodiorites are strongly lineated and display classic S-C fabrics typical of noncoaxially deformed granitic orthogneisses. The more mafic varieties (biotite quartz diorites?) behave quite differently: these rocks are characterized by rounded porphyroclasts of plagioclase in a black aphanitic matrix of finely comminuted biotite, feldspar, and quartz. Typically, the black mylonites are interlayered with sheared leucogranite and boudinaged pegmatite on a centimeter and decimeter scale. Isolated sheets of mylonitic coarse grained biotite granite augen gneiss occur at one particular structural level. Exposures of this variable lithologic assemblage were mapped collectively as **mixed gneiss (mgn)**.

Porphyritic Biotite Monzogranite (pbgr) is the oldest known intrusive unit in the Sierra Madera. This pluton is exposed in the high part of the range beginning one kilometer south of Puerto el Mesquital, where it forms the roof of the Mesquital Granodiorite. Farther to the south in an area affected by the regional mylonitic fabric, the monzogranite is intimately interlayered with gneissic two mica granite and highly deformed leucogranite. The transition between these two regions has not been mapped out in detail, but it appears that the young leucogranites were important in modifying an original contact between the monzogranite and the two mica granite, and also in locallizing the ductile strain. Traverses from the northeast to the southwest through the monzogranite indicate a gradational

increase in the intensity of mylonitic fabric.

The monzogranite in its undeformed state is medium to coarse grained and porphyritic, with euhedral megacrysts of pink-orange microcline (1 to 4 centimeters in the longest dimension) set in a groundmass of quartz, plagioclase, microcline, and biotite. Quartz grains are quite large (up to 8 millimeters diameter) and subequent. The average mineralogy of the monzogranite is 35% microcline, 30% quartz, 27% plagioclase, and 8% biotite. Accessory minerals include sphene and zircon. In highly deformed areas the granite is recognizable as an augen gneiss, with coarse, pink, oval shaped K feldspars aligned in a sheared matrix subparallel to attenuated quartz grains. An abundance of biotite and quartz cause this rock to appear quite dark compared to the younger leucogranites with which it is deformed.

Porphyritic monzogranite overlies the Mesquital Granodiorite along a south dipping contact that can be traced for several kilometers across the main ridge of the northern Sierra Madera. This contact may be somewhat gradational: in one traverse up a western spur of the main ridge the contact was defined as the place where K feldspar phenocrysts in the porphyritic rock became somewhat larger (greater than 1 cm) and more abundant (both units in this area have a medium grained groundmass with large quartz grains). Further uphill along strike the boundary between the granodiorite and the monzogranite is marked by a 10 meter thick interval of gneissic biotite rich granodiorite. This granodiorite has a porphyritic texture similar to the monzogranite, and may be a finer grained mafic phase of that pluton. It displays a strong mylonitic foliation concordant with the main contact. Also intimately associated with the contact (here and in several other places) are deformed sills and dikes of pegmatite and biotite aplite. The boundary between the two plutons appears to have localized a fair amount of noncoaxial strain,

and may also have been a zone of weakness that favored emplacement of the younger intrusives.

Porphyritic Two Mica Granite (2gr) is volumetrically the most important of the exposed post Early Cretaceous intrusive units. This lithology underlies most of the central and southern Sierra Madera and occurs as large sill shaped masses in the Sierra Magdalena and in the hills south of Imuris. The Mesquital Granodiorite and Presa Granite of the northeastern belt should also be included in this group, as should a small pluton near El Alamillo (west of the Sierra Madera). Significant portions of these granites have been involved in subsolidus mylonitic deformation. In most cases it is possible to trace an undeformed pluton into regions of progressively greater shear strain. Gradients in the rock fabric along such traverses are useful in constraining the magnitude and geometry of the finite strain in granite dominated areas of a regional ductile shear zone (see Chapter 8).

The most continuous exposures of two mica granite with the greatest structural relief are found in the Sierra Madera. Although partly deformed, these granites are relatively homogeneous compared with those to the west that have hosted significant volumes of leucogranite prior to their involvement in the shear zone. The Sierra Madera lithology varies in composition from monzogranite to granodiorite. It is typically medium grained, with a slightly porphyritic texture enhanced by relatively large K feldspar crystals. Quartz grains range from 2 to 8 millimeters in diameter, and are subequent in undeformed samples. A characteristic mineralogy is: 35% to 40% plagioclase, 25% to 30% quartz, 25% to 30% K feldspar, 4% to 5% biotite, and 1% muscovite. Euhedral red garnet up to 5 millimeters in diameter is quite conspicuous in some outcrops. The granite is leucocratic compared to the

porphyritic biotite monzogranite with which it is interlayered in highly deformed areas of the west central Sierra Madera.

In general the two mica granites of the Sierra Madera become more deformed to the west and southwest. A gradational boundary between granite and orthogneiss is defined on the basis of finite strain measurements and the distribution of fabric intensity (see Figure 8.44). West of this boundary the granites have experienced significant noncoaxial strain, and display classic S-C structures (see Chapters 7 and 8). The highest structural levels of these mylonitic orthogneisses are bounded by the Magdalena detachment fault along the western base of the range. Here a significant proportion of the rock volume is comprised of leucogranite sills. At deeper structural levels leucogranite occurs less abundantly as sheared interlayers within mylonitic porphyritic two mica granite.

Extensive exposures of porphyritic two mica granite also occur in the central and southern Sierra Magdalena, where they are invaded by and ductilely deformed with swarms of leucogranite. Here the two mica granites underlie a regionally extensive sheet of leucogranite. Inclusions of metamorphic rock recognizable as pelitic schist, stretched volcaniclastic schist, schistose quartz porphyry, impure quartzite, and biotite feldspar schist are locally preserved. Where the base of the granites are exposed they overlie biotite granodiorite. Contacts are usually gradational, with interfingering of the two units on a meter or decimeter scale. The texture may not change across the boundary, hence, one might be tempted to explain the compositional differences as a differentiation phenomenon within a single pluton. However, granodiorite often occurs as elongate, isolated masses higher up in the granite, implying that these more mafic rocks are xenoliths within a younger intrusion.

Like the two mica granites of the Sierra Madera, the Sierra Magdalena granites are medium grained porphyritic garnet bearing monzogranites and granodiorites, with 3% to 6% biotite and visible muscovite. Virtually all exposures are deformed to some extent. An upward increase in strain can be demonstrated in many areas. This gradient is reflected qualitatively by the intensity of fabric and the degree of transposition of younger leucogranite intrusives (pegmatite dikes and veins are discordant to the foliation in deep levels of the granites but are almost parallel to layering at shallow levels).

Leucogranite and Leucogneiss (lgr, bgr, lgn) are terms used to lump the diverse assemblage of weakly to strongly deformed biotite poor felsic intrusions associated with the last phase of granitic plutonism. These late granites appear to be related to a regional thermal reactivation of the Central High Strain Belt that followed an early strain event and crystallization of the granodiorite and granite plutons. They are older than most of the deformation associated with the Magdalena detachment fault. The leucogranites are characteristically white or light pink in color. Common lithologies include pegmatite, fine grained biotite-garnet monzogranite, muscovite-garnet aplite, biotite aplite, and muscovite-biotite-garnet granite. They occur at all exposed structural levels of the lower plate as interconnected networks of veins, dikes, sills, and sheets. At map scale the leucogranites appear to have "ponded" at various stratigraphically and/or structurally controlled horizons. Presumably they are derived from an important region of melting at depth. Specific occurrences of leucogranite (and leucogneiss) are described below, from the deepest known exposures to the shallowest.

Along the base of the west central Sierra Guacomea, a group of leucogranite sills 1 meter to 50 meters thick are exposed within an eastward

dipping sequence of felsic schists. The sills make up a large volume (up to 50%) of the section in this area. The dominant lithologies are fine grained, equigranular, leucocratic muscovite-biotite granites and biotite-muscovite monzogranites. Both varieties contain abundant (1% to 2%) red garnet. Biotite content rarely exceeds 2%. A representative mineralogy (petrographically determined by Salas, 1968) is: 35% plagioclase (An 14), 30% microcline, 26% quartz, 1% biotite, 1% opaque, and 2% garnet. Very fine grained muscovite-garnet aplite and coarse pegmatite occur frequently as veins and dikes a few centimeters to a few meters thick. These crisscross the granites and the schistose country rocks, and appear to connect individual leucogranite sills.

A weak fabric in the above leucogranite sills is expressed by a mesoscopic quartz grain shape foliation and the alignment of whatever biotite is present. This foliation is concordant with a preexisting layering in the country rocks. It seems to have developed at the same time as a set of normal sense ductile shear zones which affect all lithologies at this structural level (see Chapter 7).

Some of the leucogranites stop abruptly at the basal contact of the porphyritic biotite granodiorite sill, almost as if this older pluton had acted as an impermeable barrier. However, many veins and dikes of pegmatite, aplite, and biotite monzogranite do intrude the granodiorite. East of San Antonio the leucogranite dikes comprise about 25% of the rock volume. Close examination reveals that the dikes have been rotated, internally strained, and sheared during penetrative deformation of the deeper levels of their host granodiorite. Two important points are borne out by the field relations: (1) the leucogranites are younger than the porphyritic biotite granodiorite, and (2) a significant amount of ductile strain has been superimposed on both units.

West of Rancho El Rincon, the porphyritic granodiorite pinches out,

and its upper (northeastern) boundary is marked by a large leucogranite sill. This lithology is a fine to medium grained leucocratic biotite-muscovite-garnet monzogranite with subordinate amounts of pegmatite and muscovite-garnet aplite. It forms resistant outcrops that cap the ridge crest for several kilometers. The granite apparently was intruded along a previously existing contact between the granodiorite and schistose quartz porphyry/granite porphyry. Smaller sills and dikes of a similar leucogranite have been injected into the first 200 meters of these superjacent metamorphic rocks.

Farther to the south, in the Sierra la Jojoba, fine grained leucocratic monzogranites with associated pegmatite and aplite occur as isolated masses within the metavolcanic strata. The geometries of these intrusives have not been mapped out in detail, hence their boundaries shown on Plate III are highly generalized.

Leucogranites are abundant in the Sierra Magdalena, where they form a regionally continuous sill (up to 500 meters thick) localized between coarser grained porphyritic two mica granites or biotite granodiorites and structurally higher metamorphosed supracrustal rocks. Smaller sills and dikes of similar composition and texture are very common at higher levels within the supracrustal section. The main sill is apparently fed by the ubiquitous dikes and veins that crisscross the underlying plutons. Xenoliths of older schists and orthogneisses are locally prevalent. In the southern Sierra Magdalena the leucogranite sill contains an interval rich in sheared out sheets of biotite granodiorite and coarse grained biotite granite augen gneiss. This interval, mapped as **mixed gneiss (mgn)**, is sandwiched between mylonitic gneisses composed almost exclusively of leucogranite.

Most of the leucogranites in the Sierra Magdalena are moderately to strongly deformed, and were mapped as **leucogneiss (lgn)**. The most

common lithologies are fine grained equigranular muscovite-biotite-garnet monzogranite and fine grained biotite monzogranite. These gneisic leucogranites are pervaded by veins of pegmatite 1 to 5 centimeters thick that have acted as almost passive planar markers during deformation. The effects of rotation and boudinage have broken the veins into strings of interconnected diamond shaped K feldspar crystals. These extended veins tend to parallel a mylonitic foliation in the granite, giving the rock a characteristic layered appearance. Bulk strain in the leucogneisses may be calculated by determining the amount of rotation and finite elongation of the veins in various directions (see Chapter 8).

Structural relationships between the leucogranites and their country rocks in the Sierra Magdalena indicate that the granites postdate an early deformational event, but are pre-kinematic relative to development of a penetrative mylonitic fabric. Near La Sauceda, crosscutting dikes and veins of leucogranite have been buckled, rotated, and boudinaged during progressive deformation of their supracrustal host rocks. However, the total strain recorded by the leucogranites is but a fraction of the bulk strain preserved in the country rocks. Destraining of the section to a pre-leucogranite configuration confirms the existence of an older deformational episode (see Chapter 8). 10 kilometers farther to the southwest almost all lithologies are transposed into the late mylonitic foliation, and the earlier deformational fabric cannot be differentiated.

Deformed leucogranites also occur in the central and southern Sierra Madera, where they tend to be concentrated at preferred structural horizons within coarser grained porphyritic granite orthogneisses. The roof of one small fine grained biotite monzogranite pluton is exposed in the lower portion of Canada el Oso. This sill shaped intrusion is extremely mylonitized where it

interfingers with porphyritic biotite monzogranite. Dikes of pink biotite aplite that appear to emanate from the sill also carry a strong mylonitic fabric. To the south, pegmatite, aplite, and fine grained biotite granite are interlayered with their mylonitic granite host rocks on a variety of scales. Southeast of Mina San Miguel, fine grained leucogranites concordant with the foliation in their host porphyritic monzogranite make up approximately 10% of the total rock volume. The locations and highly generalized boundaries of some of the larger leucogneiss masses in the Sierra Madera are shown on Plate 2.

Coarse Grained Biotite Granite Augen Gneiss (bgagn) occurs in the southern Sierra Magdalena as highly attenuated and sheared lenses interlayered with mylonitic biotite granodiorite and leucogranite. Known exposures are restricted to a 50 meter wide structural interval within a larger sill shaped mass of fine grained biotite monzogranite, pegmatite, and aplite. The augen gneiss of Arroyo el Salto was first mapped and described in the late 1970s by Anderson and Silver, who proposed its correlation to one of the regional suites of Proterozoic basement granites known in southwestern North America.

The gneiss is easily distinguished by its extremely coarse grained texture: pink augen shaped microcline crystals up to 10 centimeters long are deformed with a sheared matrix of coarse quartz, shredded biotite, and comminuted plagioclase. The rock is strongly foliated and lineated, and displays a well developed S-C structure. Its protolith was undoubtedly a very coarse grained porphyritic biotite granite. The augen gneiss is preserved as discontinuous 8 to 50 centimeter wide sheets concordant to the local mylonitic foliation. This unit is mapped as a component of the **mixed gneiss (mgn)**.

Porphyritic Biotite Quartz Syenite (qsy) is the youngest known granitic intrusive unit in the lower plate. Three small masses of this lithology were encountered in the southern Sierra Magdalena. The best exposed of these is a small pluton that intrudes mixed gneiss in the west wall of the lower Arroyo el Salto. Here the quartz syenite interfingers with the gneiss along a contact which is generally discordant to the mylonitic foliation in the host. The margin of the quartz syenite is somewhat sheared, but the main mass of the pluton is only incipiently deformed. A rotated xenolith of strongly foliated mixed gneiss has been incorporated into unfoliated quartz syenite. Clearly, most of the mylonitic fabric in the gneissic wall rocks developed prior to emplacement of this pluton.

The quartz syenite is coarse grained and porphyritic. Euhedral white K feldspar crystals 1 to 3 centimeters in the longest dimension are intergrown with randomly oriented books of coarse biotite. Interstitial quartz grains are undulose and commonly recrystallized along grain boundaries. Plagioclase is rare, and the red garnet that tends to characterize the leucogranites is absent.

INTERPRETATION OF THE LOWER PLATE DEFORMED STRATIGRAPHY

The crystalline rocks of the Central High Strain Belt are of critical importance in evaluating the tectonic evolution of the Magdalena core complex, for they represent the portion of the lower plate that experienced the most intense metamorphism, plutonism, and ductile strain. Geological field observations (supported by available geochronological data and the structural and strain analyses of Chapters 7 and 8) permit the following interpretations:

(1) The metamorphosed supracrustal assemblage is generally correlative with the Jurassic through Lower Cretaceous type stratigraphy of the Northeast

Belt.

(2) The supracrustal rocks were intruded by at least three generations of granites during a long lived (Late Cretaceous through Oligocene?), perhaps episodic regional thermal disturbance.

(3) Two important ductile strain events are resolvable; one prior to and one subsequent to emplacement of the leucogranites. Supporting arguments for these interpretations are presented below.

My proposed stratigraphic correlation between the Central High Strain Belt and the Northeast Low Strain Belt is based on striking similarities in rock type, composition, texture, and lithologic sequence. Although the strata in the Central Belt are metamorphosed to grades as high as middle amphibolite facies, in all cases it can be argued that the metamorphic mineral assemblage was derived from a rock of suitable composition and texture (and suitable stratigraphic position) in the Northeast Belt. In my model the felsic schist/gneiss series and the quartzitic/calcareous/pelitic metasedimentary rocks are correlative to the northeastern volcanic series and the Cocospera Formation, respectively. A variety of observational data support this interpretation:

(a) The schistose quartz porphyry grades laterally into rhyolite porphyry similar to that of the Northeast Belt.

(b) Clean, fine grained quartzites and quartzose sandstones are interlayered with rhyolite porphyry in both areas.

(c) Some of the stretched volcaniclastic rocks are clearly derived from a conglomerate with a clast population similar to that of the rhyolite cobble conglomerate unit.

(d) Volcanoclastic conglomerate forms the highest stratigraphic unit of the felsic series in both areas.

(e) Biotite-sphene granite porphyry occurs as sill shaped masses within the felsic series in both areas.

(f) An unconformity between a felsic volcanogenic series and a quartz rich sedimentary section is mappable as a continuous, low angle surface in both areas.

(g) The clast population of the stretched quartz-volcanic-sandstone pebble conglomerate matches that of the Cocospera conglomerate, as does the mesoscale interlayering of conglomeratic and fine grained metasedimentary material, and the general fining upward character of the section.

(h) The metasedimentary section is rich in quartz and ferromagnesian/calcsilicate minerals while the underlying metavolcanic series is dominated by feldspar, quartz, and white mica. An analogous contrast in bulk composition is evident in the Northeast Belt.

(i) Pelitic schists and marbles in the upper part of the metasedimentary sequence indicate that the conglomerate member was originally overlain by fine grained, clay rich marine? sediments and limestones. These metamorphic strata of the southern and central Sierra Magdalena are of uncertain correlation. They may represent an extension of the Lower Cretaceous marine sequence which overlies a quartz-volcanic-sandstone pebble conglomerate in the Sierra Azul (Kitz, personal communication, 1988). Alternatively, they may be metamorphosed equivalents of the Upper Jurassic beds exposed intermittently between Tuape and La Lamina. There, a section of red mudstones and volcaniclastic sandstones with Late Oxfordian ammonites (Rangin, 1977a; Anderson et al., 1988) is overlain by andesitic flows and breccias, which in turn are overlain by a quartz and volcanic pebble conglomerate that fines upward into a group of siliciclastic mudstones interbedded with lithic arenites and limestones. These strata underlie a

marine section with characteristic Lower Cretaceous fossils (T. Anderson, personal communication, 1988). The pelites and marbles of the Central High Strain Belt thus have a loosely constrained Oxfordian to Albian age.

The intrusive units in the lower plate track the thermal evolution of the metamorphic core and place constraints on the timing of metamorphism and deformation. These rocks are known to be younger than the Jurassic and Lower Cretaceous strata they intrude. The oldest pluton in the field sequence (porphyritic biotite granodiorite) has a well constrained U/Pb age of 78±3 Ma (Anderson et al., 1980). It was emplaced into the felsic series along a stratigraphic (or possibly structural) discontinuity (see Chapter 7). The porphyritic two mica granites that comprise the second plutonic phase have not been dated radiometrically. However, by analogy to a group of lithologically similar granites dated in nearby areas (namely the 58±3 Ma Sierra Mazatan granodiorite and the 57±3 Ma Puerto del Sol granite of Anderson et al., 1980, and the 58±2 Ma Pan Tak granite of Wright and Haxel, 1984), these granites were probably emplaced during the Early Tertiary. One component of the second plutonic suite (the Mesquital Granodiorite) is clearly younger than deformational fabrics developed in the felsic series.

The leucogranite suite represents a third magmatic pulse of uncertain age. These granites have not been dated directly, but some insight can be gained from available K/Ar data on older two mica granite plutons. Biotites from the two granites of the northern Sierra Madera and muscovite from a crosscutting pegmatite yield ages between 26 and 33 Ma (Gilmont, 1978; Damon et al., unpublished data, 1988). These numbers should be conservatively interpreted as minimum ages. Given the geometry and geographic distribution of the leucogranite suite, it is likely that the K/Ar ages cited above reflect an uplift and/or cooling of the crust subsequent to a regional thermal

reactivation associated with leucogranite emplacement. Similar models have been proposed to explain Middle Tertiary K/Ar ages in other Cordilleran metamorphic core complexes (see also discussion in Chapter 7). In any event, the leucogranites are younger than the two mica granites, but probably no younger than Late Oligocene. Their involvement in the Magdalena shear zone implies a Middle Tertiary age for the development of the superimposed mylonitic fabrics.

GEOLOGICAL CHARACTER OF THE MAGDALENA DETACHMENT FAULT ZONE

The lower and upper plates of the Magdalena core complex are separated by an abrupt discontinuity of regional extent: the **Magdalena detachment fault**. The fault maps out as a shallow (less than 30° dip), broadly warped surface that defines the southwestern margin of the Central High Strain Belt. This surface marks a fundamental discontinuity in lithology, metamorphic grade, style of deformation, and finite strain. The detachment fault evolved as a consequence of shear strain concentration within a particular stratigraphic interval of a previously deformed and layered crust. Southwest directed normal sense movement along the fault has translated the upper plate to its present position. A significant amount of displacement is implied by the juxtaposition of two very different rock assemblages.

The Magdalena detachment fault is best defined in the field as a zone of cataclasis and hydrothermal alteration superimposed upon the lower plate metamorphic rocks. This brittle deformation zone commonly forms a resistant ledge approximately 5 to 50 meters thick that caps the structurally highest portions of the lower plate. Where not excised by younger faults, the

cataclastic zone dips directly beneath unmetamorphosed upper plate rocks. Preferential preservation of the detachment surface during erosion has resulted in a classic geomorphic expression that one tends to associate with metamorphic core complexes throughout the Cordillera (see Figures 6.7a-b).

Cataclastic rocks that characterize the detachment fault are derived either from mylonitic granites or mylonitic schist/phyllite. The granites have been transformed into silicic breccias and microbreccias. Randomly oriented, pervasive fracture networks are filled with quartz, and feldspar fragments are heavily sericitized. Biotite bearing granites in the Sierra Madera form classic green chloritic microbreccias in the vicinity of the detachment fault. Bleached white cataclasites derived from leucogranites are more common. Unlike the granites, the schists and phyllites do not form extensive exposures of cataclasite. However, breccias and microbreccias composed mainly of quartz and chlorite occur sporadically where the metamorphic rocks are in contact with andesites of the upper plate.

The intensity of the brittle fabric decreases gradationally with distance beneath the detachment fault. Zones of cataclasite occur within the mylonitic host rocks, and blocks of ductilely sheared granite are commonly entrained in microbreccia. In general, the mylonites appear to have been progressively reworked by brittle deformational processes (see Chapter 7). The effects of retrograde alteration (sericitized feldspars and chlorite filled shear bands) are restricted to the upper 50 meters of the lower plate mylonites.

Timing of movement along the Magdalena detachment fault is constrained by a variety of criteria. The brittle fabrics and chloritic/sericitic alteration are clearly younger than the ductile mylonitic fabrics in the lower plate, and are younger than the late leucogranite suite. Microbreccias in the western Sierra Madera are sharply intruded along northwest trends by near

Figure 6.7a: Photograph looking southwest from the north central Sierra Madera. The Magdalena detachment fault dips gently southwest beneath the city of Magdalena de Kino.

Figure 6.7b: Photograph looking southeast toward the southern Sierra Madera and the Magdalena detachment fault.

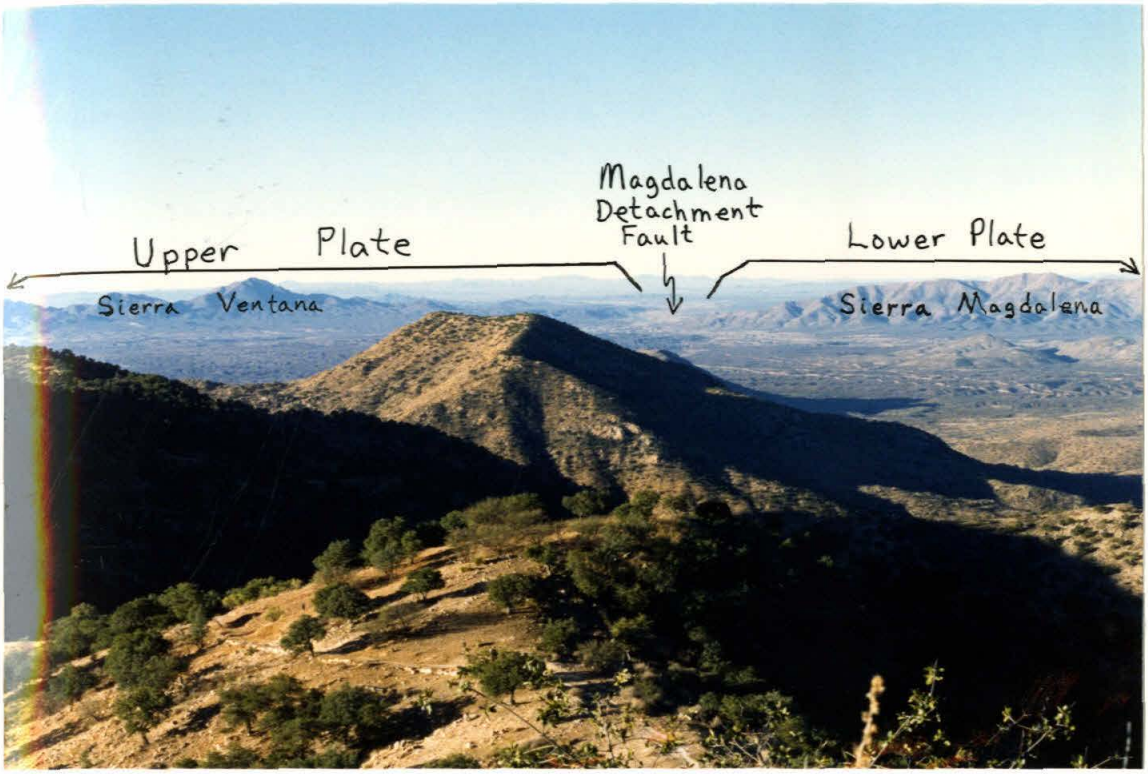

Figure 6.7a

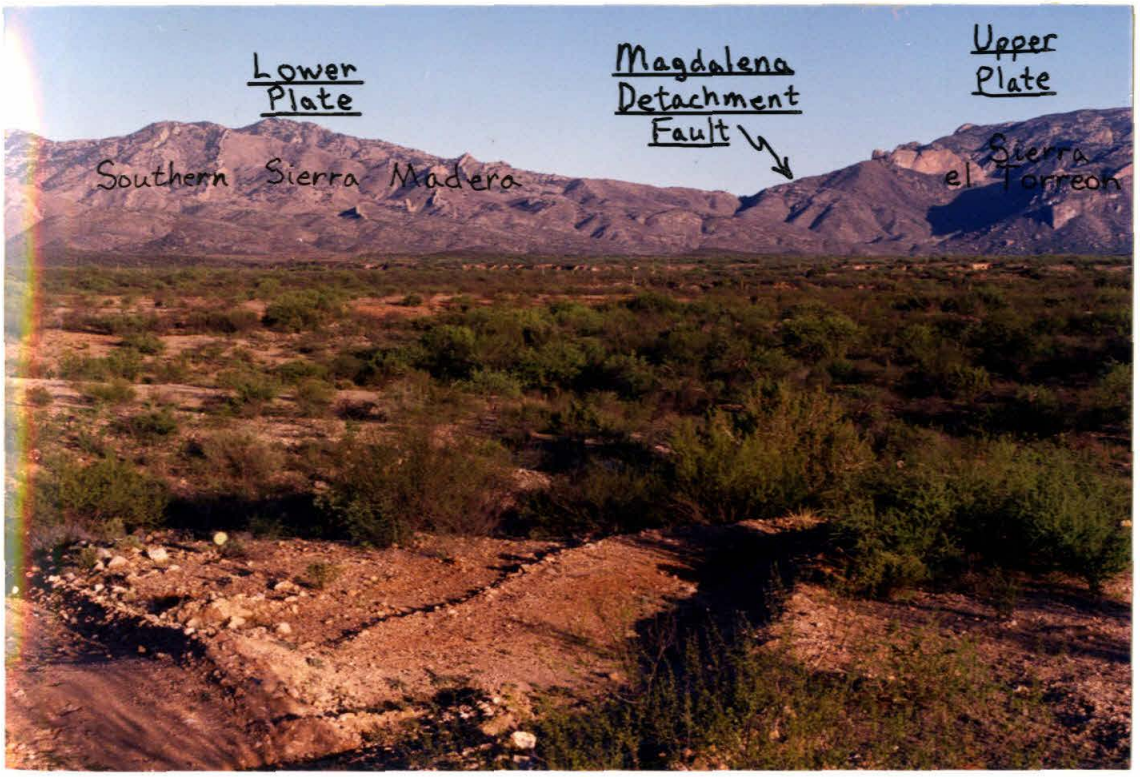

Figure 6.7b

vertical fine grained biotite-feldspar quartz latite dikes. These dikes also cut sediments of the upper plate in similar orientations, suggesting that transport of the upper plate and development of the brittle fabrics took place prior to emplacement of the dikes. However, close inspection reveals that dikes within the upper plate have been sheared off by the detachment fault. None were observed to cut cleanly across the lower plate/upper plate contact. Thus, there has been some additional slip along the detachment fault (without much rotation) subsequent to the main microbreccia forming event. Similar relationships were observed northwest of Magdalena, where andesitic dikes that crosscut mylonitic fabrics in the lower plate appear to be truncated by the detachment fault. Further evidence for renewed movement on the detachment fault is indicated by a conglomeratic sequence exposed west northwest of Magdalena. This conglomerate contains mylonitic lower plate clasts (and is therefore younger than the uplift of the metamorphic core), but its contact with lower plate schists is clearly a low angle fault which coincides with the mapped detachment fault.

UPPER PLATE STRATIGRAPHY

The upper plate of the Magdalena metamorphic core complex is comprised of a diverse assemblage of unmetamorphosed, structurally complicated sedimentary and volcanic rocks. These strata range in age from Early Cretaceous to Middle Miocene. They attain an aggregate structural thickness of 6 to 8 kilometers. The upper plate has been displaced southwestward relative to the lower plate; removal of an acceptable amount of slip on the Magdalena detachment fault would restore these rocks to a position

stratigraphically and structurally above the Central High Strain Belt (see Chapters 8 and 9).

The stratigraphy outlined below is a preliminary synthesis based on field observations recorded during reconnaissance traverses through various exposed sections. Stratigraphic relationships are summarized in two schematic columns (Figures 6.8 and 6.9) which correspond to the regions best studied. It should be emphasized that the rocks have been classified according to their mesoscopic field appearance. Mineralogies and textures have not been verified microscopically. Many of the intermediate and mafic volcanic rocks are extensively altered, hence some dacites or basaltic andesites may have been mistaken for andesites. The stratigraphy and structure of many areas of the upper plate have yet to be worked out in detail. Local unconformities, thickness variations, and lateral facies changes make it difficult to draw time-stratigraphic correlations. The effects of young deformation (folding, thrusting, and normal faulting) have introduced additional complexities. Nevertheless, an internally consistent sedimentary and volcanic succession is preserved throughout the region.

Overall tectonostratigraphic patterns record the evolution of a large intermontane basin during a protracted period of episodic tectonic activity and volcanism. Systematic variations in conglomerate clast populations track the sequential uplift and erosion of distinctive source areas. As it filled the basin was inundated by a variety of volcanic flows and tuffs which display an upward transition in composition from andesite/dacite to bimodal rhyolite/basalt. This volcanic sequence can be matched with the stratigraphy of a volcanic complex that bounds the basin on the south and west.

Figure 6.8: Generalized stratigraphy of the upper plate, based on observations from the region between Santa Ana and Rancho el Alamito.

Figure 6.9: Generalized stratigraphy of the upper plate, based on observations from the region between La Tinaja Colorado and El Babiso.

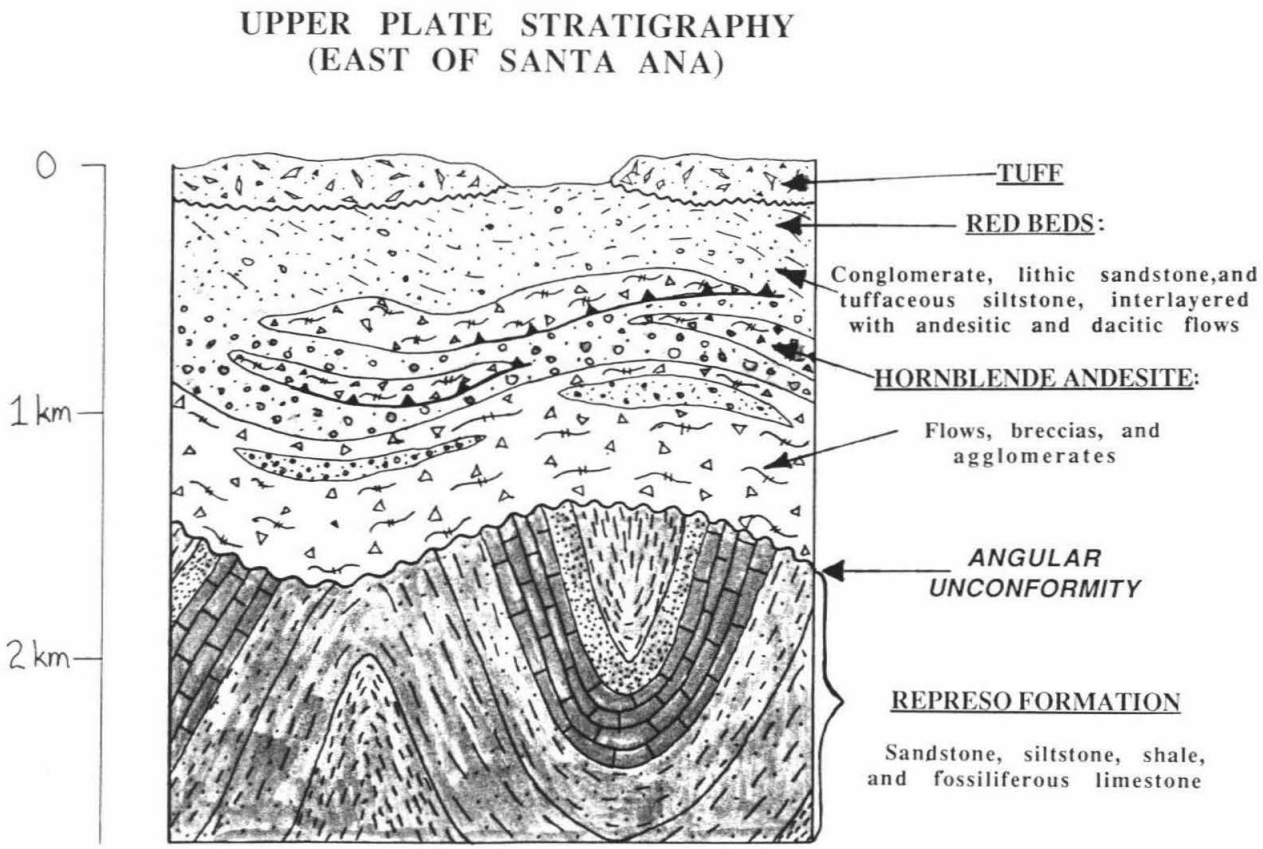
UPPER PLATE STRATIGRAPHY
(EAST OF SANTA ANA)
0
1 km
2 km
TUFF
RED BEDS:
Conglomerate, lithic sandstone,and tuffaceous siltstone, interlayered with andesitic and dacitic flows
HORNBLENDE ANDESITE:
Flows, breccias, and agglomerates
ANGULAR UNCONFORMITY
REPRESO FORMATION
Sandstone, siltstone, shale, and fossiliferous limestone

Figure 6.8

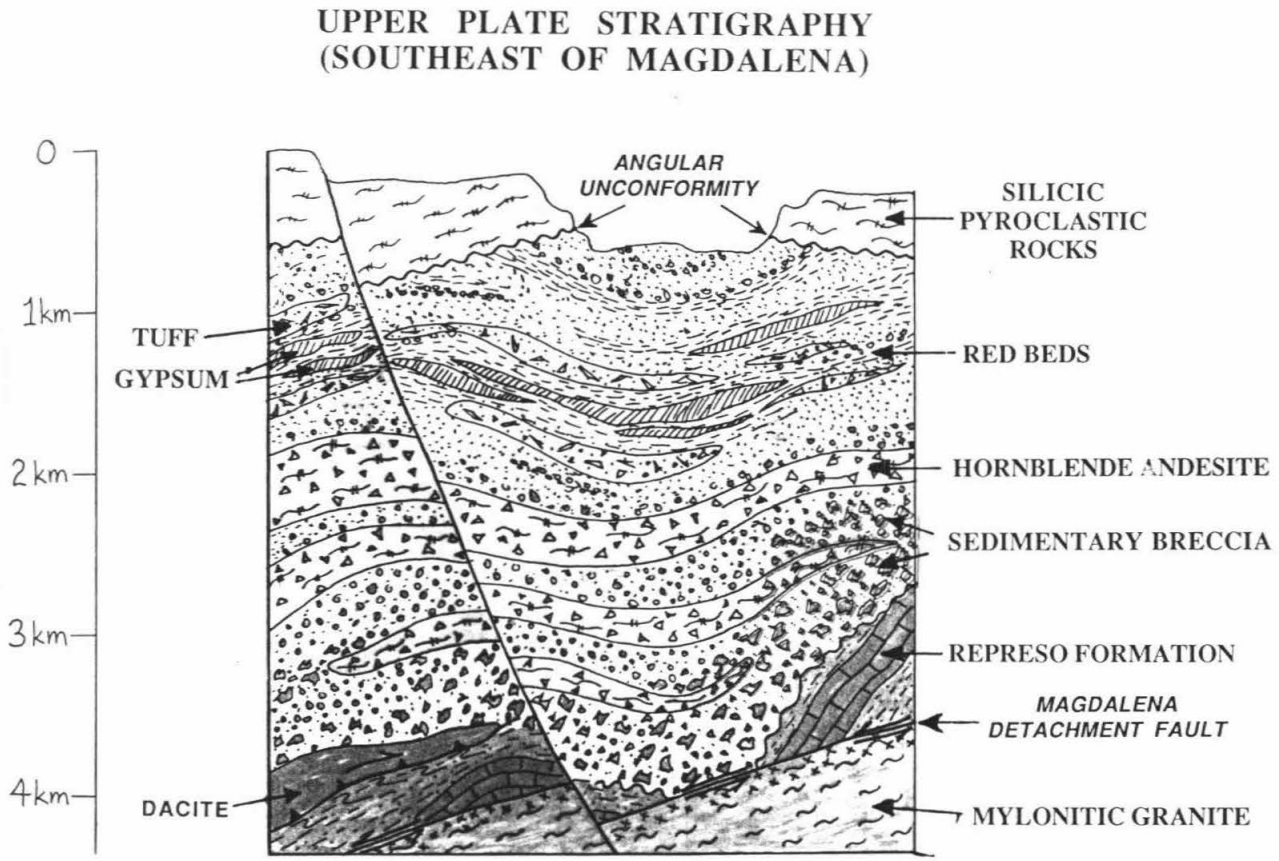
UPPER PLATE STRATIGRAPHY
(SOUTHEAST OF MAGDALENA)
0
1km
2km
3km
4km
ANGULAR
UNCONFORMITY
SILICIC
PYROCLASTIC
ROCKS
TUFF
GYPSUM
RED BEDS
HORNBLENDE ANDESITE
SEDIMENTARY BRECCIA
REPRESO FORMATION
MAGDALENA
DETACHMENT FAULT
DACITE
MYLONITIC GRANITE

Figure 6.9

The upper plate stratigraphy evolved during the same general time interval that the lower plate was experiencing extensive plutonism and ductile deformation. Possibilities for causative relationships between metamorphic/plutonic events in the lower plate and sedimentary/volcanic events in the upper plate are intriguing.

In the descriptions below, rocks of the upper plate are divided into three lithologic assemblages: (1) a **Lower Cretaceous Marine Sequence**, (2) an **Upper Cretaceous? Through Middle Miocene Intermontane Group**, and (3) a **Middle Tertiary Volcanic Complex.**

LOWER CRETACEOUS MARINE SEQUENCE (Kr, ls)

Lower Cretaceous sedimentary rocks are preserved intermittently throughout the area in the cores of Tertiary anticlines and in windows through younger volcanic rocks. Occurrences of Lower Cretaceous fossils near Santa Ana were first reported by Flores (1929). A limestone rich section was measured near Rancho el Represo by Salas (1968), who collected a representative suite of Aptian-Albian index fossils.

The Lower Cretaceous strata are dominantly composed of shale, siltstone, lithic graywacke, and rare granule conglomerate. These sediments were deposited in fining upward sequences in a mixed fluvial/coastal marine environment (Navarro-Fuentes and Tellez-Duarte, 1988). The middle part of the section contains abundant fossiliferous limestones, calcareous sandstone or siltstone, and shale representative of a marine platform or lagunal environment. This limestone horizon forms a prominent marker bed in the vicinity of Santa Ana. Its peculiar outcrop pattern suggests that the section has been folded, as do the frequent reversals in dip observed throughout the

section. Post-Early Cretaceous deformation has certainly been significant (note for example the near vertical beds northeast and southeast of Santa Ana), but the geometry and kinematics of the deformation have not been documented. The detailed structure of these sedimentary rocks thus remains an important target for future research.

A 485 meter thick section north of El Represo was described by Salas (1968), who named it the "Represo Formation." This sequence is dominated by light gray to brown fossiliferous limestone, light brown calcareous siltstone, and dark red brown shale. One bed of granule conglomerate with clasts of quartzite, chert, shale, andesite porphyry, basalt, and phyllite is present. Four kilometers southeast of Santa Ana, Salas described a section of red brown shale, gray green granule conglomerate, and coarse to fine grained lithic graywacke which he proposed to be representative of the bulk of the Lower Cretaceous section. The graywackes contain up to 35% subrounded to angular lithic grains. The constituency of these grains is similar to that of the associated conglomerate beds: quartzite, chert, shale, volcanics, and metamorphic rocks.

Salas (1968) also mapped a sequence of limestone, siltstone, and shale exposed as a window beneath andesitic volcanic rocks of the Sierra la Lumbrera. These tilted beds probably correlate with fossiliferous Lower Cretaceous strata that occur along strike to the west.

Along the western base of the central and southern Sierra Madera, large blocks of fossiliferous, light to medium gray Lower Cretaceous limestone are preserved immediately above the Magdalena detachment fault. These limestone beds are locally underlain by light brown calcareous siltstone and then by green, dark red, and purple shales. The sequence looks identical to part of the Represo Formation. Farther south along strike (in the pass southeast of El Babiso), correlative strata? have experienced the effects of the

detachment fault to a greater degree. Here, a tectonic slice of marble mylonite and sheared argillite is trapped between lower plate granitic microbreccias and an overlying sequence of silicic ignimbrites.

North of El Alamito, steeply dipping beds of purple or maroon siltstone and shale, white to light purple lithic sandstone, and rare granule conglomerate are exposed beneath an overlap assemblage of andesite, dacite, and conglomerate. Systematic variations in dip across this window indicate that the section has been tightly folded about east-west axes. Unfortunately, no fold hinges were observed in the field. The section is at least 2 kilometers thick in this area. Based on lithologic similarities to parts of the Represo Formation, to strata in the Sierra Azul (Kitz and Anderson, 1988), and to clastic beds south of La Lamina (Anderson et al., 1988), the El Alamito section is tentatively assigned an Early Cretaceous age.

Lastly, exposures of red shale, brown siltsone, and rare gray brown lime mudstone occur as an isolted klippe in the Sierra Magdalena north of La Esperanza. Salas (1968) correlated these beds with the Represo Formation. The sedimentary rocks are locally truncated at their base by the Magdalena detachment fault, and are elsewhere bounded by high angle normal faults. Most primary sedimentary features have been destroyed by a dense, penetrative fracture network.

UPPER CRETACEOUS? THROUGH MIDDLE MIOCENE INTERMONTANE GROUP

The Intermontane Group preserves a record of continental sedimentation that began with uplift and erosion of the Lower Cretaceous marine strata. Coarse sedimentary breccias and conglomerates, lithic

graywackes, and immature mudstones reflect a rapid accumulation of debris from proximal source regions. Clast populations from different stratigraphic horizons can often be related to distinctive sources. Variations throughout the section provide indirect evidence for a systematic sequence of tectonic uplift and/or erosion. Fine grained well laminated shales, gypsum beds, and lacustrine limestones in the upper part of the section indicate the presence of a large mudflat. These low energy beds are in turn overlain by poorly indurated fluvial conglomerates, tuffaceous arenites, and mudstones.

A variety of volcanic flows and tuffs are interlayered with the intermontane deposits. In general one observes that dacites and andesites occur in the middle part of the section, whereas a bimodal suite of rhyolitic tuff and basalt is interlayered with the clastic sediments at higher levels.

Sedimentary units of the Intermontane Group are described below, from the oldest deposits to the youngest. Then the succession of interstratified volcanic rocks is described. Except where specified, my observations were taken from exposures between the Sierra Madera and the main road connecting Magdalena and Cucurpe. The area west of the road is currently being mapped in more detail.

SEDIMENTARY UNITS:

Sedimentary Breccia (sbr) and associated high energy fluvial deposits comprise the basal member of the Intermontane group. These sediments were deposited in a tectonically active basin bounded by blocks of uplifted Lower Cretaceous marine strata and older? granitic basement. The breccia rests unconformably on the Lower Cretaceous beds in a few places. More typically, however, its lower contact is faulted. West of El Babiso the breccia has been thrust over younger conglomerates. North of El Babiso the

Magdalena detachment fault appears to truncate a large antiformal structure in the breccia.

The sedimentary breccia unit is characterized by an extremely immature texture and a relative paucity of andesitic clasts compared with younger conglomerates. The breccia is usually clast supported and well indurated. Highly angular clasts ranging in size from pebbles to boulders are bound in a poorly sorted gravelly matrix. Weathered exposures may be green or red. Bedding is crudely defined by layers of gravel and coarse lithic sandstone. Monolithologic breccias composed of fine sandstone or limestone (**lbr**) are frequently encountered. These may represent large masses or blocks of the Lower Cretaceous section which have been brecciated in situ during a younger deformation. At least two periods of relative quiescence are recorded by finer grained intervals of lithic sandstone, siltstone, and pebble-granule conglomerate. The upper portion of the sedimentary breccia unit contains a gray andesite/dacite flow which is locally repeated along thrust faults.

Analysis of the breccia clasts reveals a predominance of lithologies readily correlative with the Lower Cretaceous marine sequence. A typical clast population includes 30% fine grained, well indurated purple quartz-feldspar-lithic sandstone, 50% green, purple, or red siltstone and shale, 1% to 4% Represo type limestone, 5% light purple quartz porphyry, 1% black chert, 2% white or light purple quartzite, and 1% white bull quartz. The limestone clasts are distinctively light gray or yellow brown, and highly fossiliferous. They generally occur as isolated cobbles or boulders. In one place, blocks of limestone as large as cars were observed.

The sedimentary breccia contains local concentrations of other distinctive clasts. These include cobbles of rhyolite porphyry similar to the

rhyolites of the Northeast Belt, and green andesite or diorite porphyries with hornblende, biotite, and white feldspar phenocrysts. A very conspicuous foreign clast type is medium grained biotite granite or syenite. Boulders and cobbles of this lithology were shed northward from an uplifted granite mass now preserved as a window beneath younger, volcanic rich conglomerate near La Cinta de Plata. The absence of the entire lower portion of the Intermontane Group south of La Cinta de Plata demonstrates that this region was a paleohigh during deposition of the sedimentary breccia unit. The biotite granite has no counterpart anywhere else in the study area. Its distinctive quartz poor, K feldspar rich mineralogy suggests a possible correlation to a regional suite of Jurassic granites (L.T. Silver, personal communication, 1988).

The top of the sedimentary breccia unit is difficult to define precisely. Southeast of El Babiso, the upper part of the breccia interfingers laterally with the red conglomerate unit. North of there the contact is approximately located between the first and second andesite flows. The younger conglomerate is noticeably richer in volcanic clasts. East of El Yeso the sedimentary breccia is overlain by fine grained beds of calcareous siltstone and shale with thick intervals of gypsum. The red conglomerate unit is missing in this area.

The sedimentary breccia and associated finer grained strata represent near source deposits that accumulated through a combination of fluvial and colluvial mechanisms. Source regions included the Lower Cretaceous marine sequence, Jurassic rhyolite porphyry, Jurassic? or Cretaceous? andesite/diorite porphyry, and Jurassic? granite. The breccia is younger than Albian and older than the second andesite flow. The breccia is also older than a pronounced influx of andesitic debris into the basin. Its probable correlation with similar conglomeratic units throughout Sonora and southern Arizona implies a genetic link to a regional Late Cretaceous-Early Tertiary tectonic

disturbance (see Interpretation of Upper Plate Stratigraphy).

Red Conglomerate (rcg) can be distinguished from the sedimentary breccia by its color, mesoscopic texture, and clast content. The conglomerate weathers either red or dark reddish purple. It forms well indurated beds that are clearly fluvial in origin. Fining upward cycles are ubiquitous. The clasts are more rounded than those in the sedimentary breccia, and finer grained clastic layers are much more common. The upper part of the unit is dominated by lithic sandstone **(rss)** and granule conglomerate. Volcanic flows and tuffs of variable composition are interstratified with the conglomerate. They illustrate a transition from andesitic to rhyolitic/basaltic volcanism.

The red conglomerate contains all of the clasts observed in the sedimentary breccia. New clasts which make this unit distinctive include: (1) highly altered dark reddish purple aphyric andesite or basaltic andesite, (2) light purple to medium gray oxyhornblende andesite, and 3) light gray to purple flow banded dacite porphyry. The andesites and dacites often make up more than 50% of the population. Some of the sand and gravel layers are derived exclusively from andesite (these beds are characteristically dark purple or maroon). Cobbles and boulders of Represo limestone, rhyolite porphyry, and biotite granite (possibly reworked from older deposits) are locally conspicuous. South of La Cinta de Plata, the biotite granite clasts are noticeably absent in what appears to be a lateral facies equivalent of the red conglomerate. These deposits rest directly on biotite granite basement, with no intervening sedimentary breccia. Apparently this basement source for the sedimentary breccia had subsided by the time the volcanogenic conglomerate was deposited.

Several other isolated conglomeratic sequences probably correlate with

the red conglomerate unit. These include: (1) reddish-purple conglomerates that overlie hornblende andesite northeast of Cerro Ventana, (2) purple conglomerates and red lithic sandstones exposed west of La Tinaja de Colorado, and (3) steeply tilted beds of red sandstone and conglomerate that overlie hornblende andesite just above the Magdalena detachment fault northwest of Magdalena. These conglomerates all contain abundant Lower Cretaceous clasts and a diversity of volcanic clasts. Biotite granite cobbles are present in (2) and (3). The conglomerates of (3) contain highly indurated clasts of a quartz-volcanic-sandstone conglomerate very similar to the Cocospera conglomerate.

The red conglomerates were probably deposited in alluvial fans and braided streams within a tectonically active basin. Sedimentation rate and transport energy fluctuated significantly, and various bedrock sources contributed material at different times. Stratigraphic relations along the southern margin of the basin imply that a granitic source was succeeded by multiple andesitic/dacitic sources as the conglomerate accumulated.

Monolithologic Siltstone Breccia (sb) is interbedded with the upper part of the red conglomerate unit south of La Cinta de Plata. Two discrete layers can be separated in places. The breccia is overlain by pink or yellow tuff and laminated lake beds in the Sierra el Torreon. The younger volcanic beds abruptly pinch out to the northwest, where the breccia is overlain by a shallower, volcanic rich facies of the red conglomerate unit.

The breccia is dark red brown and highly indurated. It is comprised of angular pebble and cobble sized fragments of very fine grained quartz-feldspar-lithic sandstone and silicic siltstone cemented together with very little matrix. This unit represents coarse debris shed from a proximal source. Deposition took place after accumulation of a thick conglomeratic sequence

derived in part from a dacite/andesite terrane. A convenient source for the breccia clasts is provided by a large mass of purple-red sandstone/siltstone which is thrust northward over andesite near La Lamina. The volcanic tuffs that overlie the breccia unit also overlap this imbricated thrust terrane (which includes a structurally higher klippe of Precambrian granite and gneiss; see Anderson, et al., 1984; Stephens and Anderson, 1986). Thus it appears that the monolithologic breccia is a syntectonic deposit related to a significant disturbance that predated the onset of voluminous silicic volcanism.

Lake Beds (lb)are preserved basin wide in the middle or upper part of the Intermontane Group. These low energy sediments record a temporary change in depositional conditions to a mud flat/lacustrine environment. Representative lithologies include gypsum, calcareous siltstone, shale, water lain tuff, lacustrine limestone, and laminated siliceous siltstone. Sedimentation took place during the early phases of silicic volcanism. The first felsic tuffs to appear in the section occur just beneath the lake bed sediments, where the underlying red conglomerate unit makes an abrupt tranition to sandstone. Several additional felsic tuffs or reworked tuffs are present within lake bed interval and at higher stratigraphic levels. A continuous vesicular basalt flow occurs within the upper part of the lake bed unit. This in turn is overlain by a thin interval of calcareous siltstone and lacustrine limestone.

Gypsum (yeso, **y**) is presently being mined from outcrops 3 kilometers east of El Yeso. Correlative beds are exposed in the core of an anticline southwest of El Yeso. Individual gypsum layers range in thickness from 1 to 5 centimeters. They are interlayered with pink or light brown siltstones and shales, and occasionally, stromatolitic limestones and white water lain tuffs.

Lacustrine limestone **(lls)** was encountered southeast of San Jose del Alamo, where it forms one and sometimes two continuous marker horizons within a fine grained interval of light brown calcareous siltstone and light green to light purple shale. The limestone varies from a fine grained calcarenite to a laminated (stromatolitic) lime mudstone. Red jasper or chert sometimes occurs in layers less than 1 centimeter thick. No fossils were observed. The main limestone horizon occurs just above a vesicular basalt flow, which in turn overlies tuffaceous sandstones, water lain tuffs, and siltstones.

Northeast of La Lamina, beds of finely laminated siliceous siltstones are openly folded with depositionally overlying silicic pyroclastic breccias. This distinctive lithology is characterized by a submillimeter scale interlayering of red and light gray siltstone with clear, amorphous silica. These rocks were clearly deposited in a low energy environment. Angular fragments of the laminated siltstone are commonly entrained in the younger volcanic flows, and also are found in some of the younger conglomerates.

Upper Continental Deposits (ucd) include a variety of poorly sorted, weakly indurated clastic beds that comprise the upper part of the Intermontane Group. These sediments are interstratified with at least two basalt flows and one felsic tuff. They overlie the lake bed unit and/or the first basalt flow in several places between El Yeso and La Lamina. Folding of the section in this area demonstrates a relatively young tectonic episode.

Cobble and boulder conglomerate **(cg)** are abundant within the lower part of this unit east of the Magdalena-Cucurpe road. The conglomerates may weather red or white. New clast types not observed in the stratigraphically deeper conglomerates include: (1) medium to fine grained dark green to black

hornblende-biotite quartz diorite or tonalite, (2) dark purple or black basalt, (3) felsic tuff, and (4) coarse grained biotite granite with large (1 to 2 centimeter) euhedral alkali feldspar and quartz grains as coarse as 1 centimeter. This latter lithology is similar to the porphyritic biotite monzogranite of the central Sierra Madera. An isolated exposure of red conglomerate in the Rio Sasabe wash 2 kilometers southwest of Magdalena may correlate with the upper continental deposits. This conglomerates contains clasts of laminated siltstone known to outcrop only in the Sierra el Torreon.

Sandstone, siltstone, and mudstone (ss) occur abundantly within the upper continental clastic unit. These strata are moderately to poorly indurated and compositionally immature. The sandstones are poorly sorted and composed mostly of lithic grains. Those derived from andesitic sources tend to weather dark red-purple. Others associated with felsic tuffs weather to a cream or white color. The siltsones and mudstones may be white, light brown, light green, or pink.

Excellent exposures of the sandstone and associated finer grained facies are preserved along the Magdalena-Cucurpe road between the reservoir Ignacio Pesquerira and San Jose del Alamo. These sandstones contain abundant tuffaceous grains reworked from slightly deeper felsic volcanic layers. The most continuous sandstone sequence occurs immediately beneath the silicic pyroclastic flows of the Sierra el Torreon. Other well exposed sandstone beds occur 5 kilometers west of San Jose del Alamo and 1 to 5 kilometers southwest of El Yeso. At the present stage of mapping it is not feasible to correlate individual members over long distances.

VOLCANIC UNITS:

Andesite Flows (a, ab) are interstratified with the upper part of the sedimentary breccia unit and the lower part of the red conglomerate unit west of El Babiso. The andesites are the oldest known extrusive units in the Intermontane Group. Two (or three?) flows were deposited over an extended period of time during which the associated coarse clastic beds became significantly richer in andesitic fragments. The oldest flow is fine grained, pinkish gray andesite (or dacite?), with hornblende and feldspar phenocrysts. Many outcrops display a mesoscopic dark and light purple flow banding. Northwest of El Babiso this 30 meter thick flow has been repeated by a thrust fault. Along its base in one place, underlying beds of siltstone and sandstone are tightly folded and overturned toward the northeast. The andesite may be moderately cleaved and slightly metamorphosed (sericite and epidote are abundant).

Higher up in the section, andesite flow breccia and agglomerate are interstratified with red conglomerate. Two separate flow units are locally present. The flows attain a maximum thickness of 15 meters. Some areas have been reworked by sedimentary processes to produce andesite clast conglomerates. This lithology may be extremely altered to a dark purple red color, and usually the mineralogy is hard to determine. The most common rock type is an agglomerate with cobble sized subrounded fragments of hornblende andesite in a dark purple aphyric flow matrix. These rocks are often associated with dark, locally vesicular aphanitic flows which may be basaltic andesites.

A large mass of green and purple propylitized andesite and andesite breccia overlies Lower Cretaceous limestone north of El Babiso. Here the contact between the two units appears to be a faulted unconformity. The

andesite is depositionally overlain by a succession of andesite clast conglomerate, red or gray siltstones and shales, maroon lithic sandstone, and finally by a thick sequence of red conglomerate with abundant andesite clasts. In this particular area, the sedimentary breccia unit is not present between the Lower Cretaceous beds and the andesite. This highly altered andesite flow probably correlates with one of the upper andesite flows described in the previous paragraph.

Northwest of Magdalena a possible correlative andesite agglomerate is juxtaposed against mylonitic granite and schist along the Magdalena detachment fault. These resistant volcanic flows and breccias are composed mostly of medium grayish-purple hornblende andesite. Oxyhornblende is present in some samples. Hematite alteration and calcite veining are common features. The agglomerate is often reworked into monolithologic conglomerate. As described earlier, the andesite is overlain by beds of red conglomerate, lithic sandstone, and mudstone that characterize the shallower levels of the intermontane group.

Felsic Tuffs (tu) are interbedded with the clastic sediments in the upper portion of the Intermontane Group. These volcanic rocks were deposited intermittently over an extended period of time during which the depositional environment evolved from high energy fluvial to quiescent lacustrine back to fluvial. Many of the tuffs have been reworked into tuffaceous sandstones or volcanic wackes. Fragments of tuff occur abundantly in younger conglomerates.

The tuffs are best exposed in a southwest facing section east of San Jose del Alamo. The lowest unit is interbedded with red conglomerate and is stratigraphically higher than a series of andesitic flows. This 3 meter thick

tuff is light yellow and highly vesicular. It contains about 30% lithic volcanic fragments (rhyolites and felsites) in a chalky matrix. A thinner (1/2 to 1 meter) yellow-white tuff is interstratified with conglomerates and sandstones 20 meters up section. This tuff is also vesicular, but it is richer in feldspar and quartz crystals than the older unit. Partially reworked equivalents of this crystophyric tuff occur along strike to the south. Farther up section are several coarse sandstone layers that appear to have been derived largely from tuffaceous material. Overlying the tuffaceous sandstones are lake beds (described above). Capping these strata is a ridge forming unit of interbedded crystal-lithic tuff and feldspar-lithic-quartz sandstone. Along strike to the south this tuff contains abundant purple silicic volcanic fragments, and also a few foreign clasts, including: (1) medium grained biotite granite with euhedral pink K feldspar crystals, and (2) coarse grained Sierra Madera type biotite monzogranite with large rounded quartz phenocrysts. Finally, within the upper part of this sequence close to the Magdalena-Cucurpe road, white tuffs and felsic volcanic wackes are interlayered with conglomerates that contain a relatively "late" clast population (fine grained mafic and intermediate volcanics, immature sandstone, siltstone, felsic tuff, rhyolite porphyry, and biotite granite).

Additional exposures of felsic tuff were mapped in other parts of the Magdalena basin. All tend to occur high within the intermontane section. Salas (1968) mapped a series of tuffs and basalts in the Sierra la Lumbrera. These volcanic rocks apparently overlie a thick sequence of hornblende andesite and andesite breccia.

Vesicular Basalts (vb) are interstratified with the upper part of the Intermontane Group. At least two flows are present. The oldest flow overlies

siltstones, shales, and water lain tuffs southeast of San Jose del Alamo. This 10 to 20 meter thick flow contains abundant zeolites. Another flow occurs higher up in the continental clastic section, where it helps define the ridge southwest of San Jose. A younger? olivine bearing basalt flow with near vertical columnar joints caps two prominent peaks west of La Cinta de Plata. This flow overlies the oldest basalt flow (and associated siltstones) in pronounced angular unconformity. The olivine basalt thus places an upper bound on the timing of folding (or tilting) within the Intermontane Group.

TERTIARY VOLCANIC COMPLEX

Clastic sediments of the Intermontane Group interfinger to the south and west with a thick pile of volcanic rocks that dominate both the geology and the landscape. Mapping in this region has just recently been initiated, so the stratigraphy proposed below is based on only a few preliminary observations. K/Ar ages for various portions of the volcanic complex have been reported by Miranda and Quiroz (1988). Their age determinations seem to be consistent with the field sequence (see Interpretation section below).

Andesite and Dacite (ha. ab) are the oldest known components of the volcanic complex. West of El Alamito beds of red-purple andesite agglomerate, andesite breccia, and andesite conglomerate overlie steeply tilted Lower Cretaceous? shales and siltstones in sharp angular unconformity. Locally these andesites are cut by fine grained dacite dikes. 2 1/2 kilometers north of El Alamito, massive flows of fine grained light purple-pink dacite? with broken feldspar phenos appear to overlie the steeply dipping Lower Cretaceous? beds. These volcanic rocks may be fed by dikes of altered biotite-

feldspar dacite porphyry which intrude the marine sediments nearby. An associated sequence of interlayered andesite breccias, vesicular andesite flows, and lithic sandstones occurs 1 kilometer farther north. Stratigraphic relationships between the andesites and dacites are not yet worked out in this area.

In the vicinity of Rancho el Represo, less altered andesite flows and agglomerates unconformably overlie the type Represo Formation of Salas (1968). These andesites are characterized by abundant hornblende and plagioclase phenocrysts in a dense, light purple to medium gray aphanitic matrix. Their stratigraphic relationship to the the andesitic flows to the southeast is uncertain, but it is likely that they correlate with a mass of hornblende andesite that comprises most of the Sierra Ventana (see Flores, 1929).

Silicic Pyroclastic Rocks and Basalt Flows (sig, b) comprise a cogenetic volcanic suite that unconformably overlies the andesites and dacites, and also part of the Intermontane Group. These strata form prominent cliffs that cap the ridges on either side of Puerto Cucurpe. The sequence contains a distinctive yellow tuff bed **(yt)** that serves as an important stratigraphic marker. Inspection of this horizon from the proper vantage point indicates that the pyroclastic beds of the western mass (Sierra la Lamina) are subhorizontal, but those in the eastern mass (Sierra el Torreon) have been folded and locally faulted.

In the Sierra el Torreon early basaltic phases of the bimodal suite are not present. Here a thick sequence of felsic pyroclastic rocks rests upon the siltstone breccia unit and overlaps an imbricated stack of thrust sheets. The pyroclastic strata are mapped collectively as one unit **(sig)**, with the

exception of the yellow tuff (**yt**) and a pink tuff (**pt**) which are delineated separately. The ignimbrites are at least 350 meters thick. They appear to pinch out abruptly toward the west.

Lithologies encountered while traversing the lower parts of the Sierra el Torreon include: massive pink-red crystal-lithic tuff breccia, rhyolitic agglomerate with felsic volcanic clasts, quartz latite tuff with pumice fragments and abundant silicic volcanic clasts, andesite/basalt pebble conglomerate and lithic sandstone, and clast supported silicic volcanic breccia. Angular fragments of laminated siliceous siltstone, andesite, basalt, and red sandstone are commonly entrained in the lower parts of the pyroclastic sequence. Rhyolites, rhyodacites, and felsic tuffs are more abundant as breccia clasts in the upper horizons. The distinctive marker bed is a yellow-white vesicular quartz latite tuff with abundant pumice fragments and variable amounts of foreign volcanic clasts. Holes resulting from the weathering out of pebble and cobble sized clasts cause this unit to appear more vesicular than it really is. The yellow tuff occurs within the middle part of the ignimbrite sequence. It locally splits into two layers.

In the Sierra la Lamina, basalt flows dominate the subhorizontal volcanic section. The lowermost unit is a medium purple-gray aphanitic, flow banded basalt or basaltic andesite. It overlies a red or purple andesite-dacite clast conglomerate. Above the basalt flow is the following conformable sequence: (1) pink-orange fine grained rhyolite or quartz latite tuff with abundant tuffaceous sandstone layers (25 meters thick), (2) purple-gray aphanitic basalt similar to first basalt flow (20 meters), (3) yellow to cream colored lithic-pumice lapilli tuff with lots of holes (60 meters), and (4) another basalt flow (30 meters). Two or more additional flows which cap Mesa el Potrero were only observed from a distance. The yellow tuff is lithologically

identical to that in the Sierra el Torreon, and therefore provides a stratigraphic tie between the two mountains.

INTERPRETATION OF THE UPPER PLATE STRATIGRAPHY

The upper plate rocks preserve an important transition from quiescent marine sedimentation to active continental clastic deposition and volcanism. This transition is marked by an unconformity between deformed Lower Cretaceous marine strata and overlying intermontane sediments and/or volcanic rocks. The unconformity is of considerable interest, for it reflects an uplift and period of rapid erosion that occurred sometime during the metamorphism, granitic plutonism, and ductile deformation associated with the development of the Magdalena core complex. The precise age and duration of the unconformity are debatable, however the local and regional geology provide important constraints. Data which bear on the chronology and regional tectonic significance of the upper plate stratigraphy are discussed below.

(1) The fossiliferous limestones of the type Represo Formation are regionally correlative with the Aptian-Albian Mural Limestone of southeastern Arizona and northeastern Sonora. Marine sandstones, siltstones and shales above and below the Represo Formation are probably equivalent to the clastic portion of the Bisbee Group (Navarro-Fuentes and Tellez-Duarte, 1988). On a more local scale, these Lower Cretaceous beds correlate with the marine strata mapped by Kitz and Anderson (1988) near the Sierra Azul, and perhaps with the upper part of a section exposed south of La Lamina (Anderson et al., 1988). The Arroyo Sasabe and El Chanate Formations north of Altar (see Jacques-Ayala and Garcia Y Barragan, 1988) represent a more

volcanogenic western facies of the Lower Cretaceous. That section is dominated by fluvial and shoreline deposits, with abundant conglomerates and rare flows derived from an andesitic source (perhaps the Alisitos volcanic arc of Baja California?; see Silver and Chappell, 1988).

(2) Between El Represo and El Alamito, steeply tilted Lower Cretaceous beds are unconformably overlain by andesites and dacites that make up the bulk of the Sierra Ventana. Miranda and Quiroz (1988) report K/Ar ages of 27.3±0.6 Ma and 26.9±0.6 for basalt and "alkaline latite", respectively, from the same sierra. Their sample localities were not specified. In this area, then, the marine strata were deformed sometime between Aptian and Late Oligocene time.

(3) Continental clastic deposits of the Intermontane Group accumulated during much of the Tertiary, and perhaps during the Late Cretaceous. The upper part of the section has been radiometrically dated; the lower part is constrained only to be younger than its Lower Cretaceous substrate. The age of the upper portion of the Intermontane Group is Early Miocene or younger, based on K/Ar ages of 21.4±1.0 Ma and 19.6±0.9 Ma for "alkaline basalt" and "alkaline andesite" interstratified with rhyolitic tuffs and fluvial sediments (see Miranda and Quiroz, 1988). These samples were apparently collected from the section exposed near San Jose del Alamo. The upper beds of the Intermontane Group probably correlate with a sequence of Miocene conglomerates, sandstones, siltstones, and limestones exposed near Tubutama (Roldan-Quintana, 1986). A basalt flow within the lower part of that section has yielded a K/Ar age of 22.3±0.56 Ma (Carillo, 1985).

The age of the lower part of the section depends in part on the ages of the associated andesitic flows and breccias. The andesites are known to be older than the Early Miocene basalts and younger than the sedimentary

breccia unit. One likely source for these flows is the Late Oligocene andesite complex of the Sierra Ventana (Miranda and Quiroz, 1988). However, comparison of the Magdalena andesite/conglomerate assemblage to similar sequences in other areas suggests that the andesites could be as old as Late Cretaceous. In a survey of relevant literature I have investigated all possible regional sources for the andesites of the lower Intermontane Group. In summary:

(a) Late Cretaceous andesites and dacites with associated rhyolitic tuffs have been well documented in southern Arizona. These include exposures in the Silver Bell Mountains (Sawyer, 1986), in the Galiuro Mountains (Mark and Goodlin, 1987), and in the Santa Rita Mountains, the Empire Mountains, and the western Canelo Hills (P. T. Hayes, 1970; M. J. Hayes, 1987).

(b) In the Sierra Madre Occidental of Sonora, highly altered andesites and dacites with subordinate rhyolitic tuffs (known as the "lower volcanic complex") occur between folded Lower Cretaceous marine strata and unconformably overlying Oligocene through Early Miocene rhyolitic ignimbrites (King, 1939; Clark et al., 1979; McDowell and Clabaugh, 1979). The older volcanics are commonly associated with hypabyssal intrusives and small granitic stocks. Andesites and tuffs of the lower volcanic complex that have been radiometrically dated exhibit a spectrum of K/Ar ages ranging from 52 Ma to 30 Ma (Clarke et al., 1979; McDowell and Clabaugh, 1979; Roldan-Quintana, 1986).

(c) Many of the Sonoran andesites rest directly on or are interstratified with post-Lower Cretaceous conglomerates. Specific examples of these include exposures in the Sierra El Tigre (Montano-Jimenez, 1988), in the Cananea mining district (Valentine, 1936), north of the Sierra las Avispas (Segerstrom, 1987), north of Altar (Jacques-Ayala and Garcia Y Barragan, 1988; Garcia Y

Barragan et al., 1988), near Aconchi (Amaya-Martinez et al., 1988), and near Arivechi and in the Sierra San Javier (King, 1939).

(d) A Middle Tertiary generation of andesites and dacites is also widespread in southern Arizona and Sonora. These volcanic rocks are an important constituent of the "upper volcanic supergroup" of the Sierra Madre Occidental (McDowell and Clabaugh, 1979). Only in a few places have they been differentiated from associated silicic ash flow tuffs.

(4) The sedimentary breccia unit may be appreciably older than the rest of the overlying Intermontane Group. Geologic relations in the Magdalena area indicate that this unit was deposited proximal to an uplifted Lower Cretaceous source prior to the onset of andesitic volcanism. Comparison with numerous other sections in Sonora and southern Arizona suggests that the sedimentary breccia may be a syntectonic deposit related to a regional Late Cretaceous disturbance. Possible correlative sequences include the Fort Crittendon Formation of southern Arizona (P. T. Hayes, 1970; M. J. Hayes, 1987), the Claflin Ranch Formation of the Silver Bell Mountains, Arizona (Sawyer, 1986), and the Snake Ridge Formation of the Cabullona Basin, northeastern Sonora (Taliaferro, 1933). These conglomeratic units have well constrained Late Cretaceous ages. All contain abundant Lower Cretaceous clasts. The first two formations underlie Latest Cretaceous andesite/rhyolite sequences. Other conglomerates which may correlate with the sedimentary breccia include the Palomitas Conglomerate of the Sierra El Tigre (Montano-Jimenez, 1988), polymictite breccias near Rayon (Gonzales-Leon, personal communication, 1988) and near Arivechi (Almazan-Vasquez, 1988), the Navosaigame Conglomerate of the El Campo mining district, western Chihuahua (Hovey, 1905), and the lower member of the Liebres Formation in northeastern Chihuahua (Keller et al., 1982). All of these conglomerates rest on erosional

surfaces cut into Lower Cretaceous and older rocks. All are discordantly overlain by Tertiary volcanic strata. Clearly these coarse clastic deposits represent a tectonic disturbance or uplift of regional significance. However, the pre-volcanic conglomerates in Mexico have not been dated directly by radiometric means, so the age, duration, and regional contemporaneity of the implied unconformity are uncertain. In the Magdalena area the sedimentary breccia unit has a loosely constrained Late Cretaceous or Early Tertiary age.

(5) Systematic variations in clast population within the Intermontane Group record a history of erosion genetically related to discrete Late Cretaceous through Middle Tertiary mountain building episodes. The sedimentary breccia unit and the lower part of the red conglomerate unit were deposited north and west of uplifted Jurassic and Lower Cretaceous sources. Perhaps the tight folding of the Lower Cretaceous beds was associated with this event. The Jurassic? biotite granite source was buried at about the time the basin was flooded with andesitic debris derived from sources to the south and west. Then (prior to the onset of silicic volcanism) a late pulse of siltstone breccia was apparently shed northward from a tectonically emplaced thrust sheet.

(6) Early phases of a bimodal rhyolite/basalt suite were extruded at about the same time that part of the basin evolved to a lacustrine environment. The bulk of these volcanic rocks accumulated in the Sierras La Lamina and El Torreon; however, representative flows and tuffs made it part of the way into the intermontane basin.

(7) The upper plate was detached from the lower plate along the Magdalena detachment fault. Major movements on this fault predated post-Early Miocene shortening of the upper plate.

(8) The basin was significantly shortened prior to extrusion of the

youngest basalt flow. This deformational event is reflected by:

(a) north-northwest trending folds in the Intermontane Group,

(b) east-northeast directed thrust faults and overturned folds west of El Babiso,

(c) folding of the silicic ignimbrites in the Sierra El Torreon, and

(d) an angular unconformity between the oldest and youngest? basalt flows.

NEOGENE FLUVIAL AND COLLUVIAL DEPOSITS

Poorly consolidated and poorly sorted fluvial and colluvial sediments underlie large portions of the study area. These deposits are alike in that they all contain clasts of lower plate mylonitic granite, hence they are younger than the uplift and exposure of the metamorphic core. All are probably younger than Early Miocene. A more detailed analysis of the sediments would undoubtedly be helpful in working out the younger tectonic history of the region.

Red Conglomerate (Tcg) is the oldest known post mylonitic sedimentary unit. This lithology is distinguished from the similar appearing conglomerate of the Intermontane Group by its abundant granitic mylonite clasts. Well bedded, tilted and block faulted exposures were encountered 6 kilometers northwest of La Bandera and 5 kilometers west-northwest of Magdalena. In this latter area the conglomerate appears to have been truncated at the base during renewed activity along the Magdalena detachment fault.

Terrace Deposits (Qt) occur on gently sloping bedrock surfaces that flank both sides of the Rio Magdalena between Magdalena and Imuris. Two distinctive horizons were mapped locally. Several more apparently define elevated surfaces farther up the valley. The deposits are typically composed of rounded cobbles of granite, rhyolite porphyry, or metamorphic rock. The terraces were probably incised during periods of rapid uplift of the Magdalena drainage basin.

A 200 to 300 meter thick section of poorly consolidated fluvial deposits with abundant terrace cobbles is downfaulted against the northwestern Sierra Madera and the southwestern Sierra el Pinito. Excellent exposures are afforded by the microondas road and Highway 2, respectively. These coarse sediments probably represent alluvial fan deposits that were reworked by the Rio Magdalena as the basin was uplifted. The clast poulation contains most local lower plate lithologies as well as abundant basalt cobbles.

Alluvial Fan Deposits are preserved along the downdropped sides of lower plate horst blocks. These sediments are poorly sorted and indurated, and may be hundreds of meters thick. Inverted sequences of mixed rhyolite/felsic schist/metasedimentary/granitic conglomerate or sedimentary breccia (**TQmx, Qmx**) overlain by granite cobble-boulder conglomerate (**TQgr, Qgr**) are typical. Frequently there is some angular discordance between the two units. These alluvial fan and fault scarp deposits record the uplift and erosion of progressively deeper structural levels of the lower plate. Most have been deeply incised by modern streams. Occasionally the fans were observed in direct fault contact with uplifted bedrock.

Valley Fill (TQvf) is a term used to lump the poorly indurated and

poorly sorted fluvial gravels that obscure bedrock in the topographically low parts of the Magdalena drainage basin. The gravels may be tilted as much as 15°. Good exposures are preserved in roadcuts along Highway 15. Clasts are angular, and range in size from sand to small cobbles. Clast populations are highly variable and dependent on the local bedrock geology. Valley fill deposits north of Imuris tend to be dominated by rhyolite porphyry. Those exposed between Imuris and Magdalena are rich in mylonitic granite. The valley fill along the Magdalena-Cucurpe road is comprised mostly of andesite, basalt, sandstone, and silicic ignimbrite clasts.

CHAPTER 7

STRUCTURE AND TECTONICS

Rocks of the Magdalena metamorphic core complex provide a three dimensional transect through a structurally dismembered section of crust at least 15 kilometers thick. The fortuitous exposures of this region allow one to study, at a variety of scales, rocks deformed under a range of metamorphic conditions since Middle Cretaceous time. Distinctive structures and fabrics record the imprint of specific deformational events, and crosscutting or superposed stuctural features constrain the tectonic sequence of this highly extended region.

While mapping and correlating the geology in the Magdalena area I was able to sort out several generations of geological structure. Orientations of bedding, foliations, lineations, dikes, folds, veins, faults, and fractures were measured systematically, and rock fabrics were closely analyzed. In addition to providing geometric control (thicknesses of units, projections of surfaces, orientations of strain components, etc.), these data are useful in deducing the deformational sequence relative to emplacement of various intrusive units. Local and regional structural patterns may be interpreted as follows:

(1) The Magdalena core complex developed within a region of Lower Cretaceous and older crust. Localization of metamorphism, plutonism, and deformation was apparently controlled by a pre-existing northwest trending regional structural grain.

(2) Early phases of core complex evolution involved regional metamorphism and deformation of the pre-Middle Cretaceous supracrustal

rocks. Metamorphism was accompanied by at least two pulses of granitic plutonism. This long lived? event is broadly correlative to a regionally recognized Late Cretaceous-Early Tertiary orogeny.

(3) Timing of the early metamorphic/deformational event is constrained by crosscutting plutons. The Late Cretaceous (78±3 Ma) Guacomea Granodiorite is apparently pre-kinematic; however, local stratigraphic relationships suggest that this granodiorite sill may have been emplaced along an older (now obscured) thrust fault. The Early Tertiary? Mesquital Granodiorite is clearly younger than fabrics associated with the early event.

(4) Deep seated metamorphism and plutonism were accompanied at the surface by structural disturbances that resulted in development of a regional unconformity and subsequent accumulation of thick continental deposits and volcanic rocks.

(5) Swarms of Middle Tertiary? leucocratic two mica granites represent either the culmination of regional metamorphism or a thermal reactivation of the plutonic/metamorphic belt. The leucogranites were emplaced in a regime of northeast-southwest extension, and they may have played an important role in weakening the middle and upper crust.

(6) Extensional strain in the middle crust was initially accommodated by leucogranite emplacement and associated thermal expansion about a northwest trending axis. As extension progressed shear strains became concentrated near the margins of large leucogranite sills.

(7) A runaway mechanical situation soon prevailed whereby the bulk of the strain was localized within a 2 to 4 kilometer thick southwest vergent ductile shear zone. This shear zone evolved into a brittle fault (the Magdalena detachment fault), which ultimately resulted in juxtaposition of the two very different lithologic assemblages that comprise the upper and lower plates.

(8) Folds within the upper and lower plates record a modest amount of northeast-southwest directed shortening subsequent to the main detachment event.

(9) Late Cenozoic movements along NE and NW striking high angle normal faults have exposed various structural levels of the complex.

Observational data bearing on the above interpretations are documented in this chapter. Structural and fabric elements are discussed sequentially in the order of their chronological development. For ease of explanation the tectonic sequence is divided into seven phases or time slices: (a) **Pre-Middle Cretaceous Paleogeographic and Structural Development**, (b) **Late Cretaceous-Early Tertiary Plutonism, Metamorphism, and Deformation,** (c) **Middle? Tertiary Emplacement of Leucogranites**, (d) **Post-Leucogranite Ductile Deformation**, (e) **Early Miocene? Detachment Faulting**, (f) **Miocene? Folding**, and (g) **Late Cenozoic Block Faulting.** Each phase is addressed separately from a multiscale perspective. First, structural features specific to the Magdalena area are described and analyzed. These features are then compared to structures of similar age and character in northern Sonora and southern Arizona. A basis for regional correlation is established and the large scale geologic context for each tectonic phase is interpreted.

PRE-MIDDLE CRETACEOUS PALEOGEOGRAPHIC AND STRUCTURAL DEVELOPMENT

LOCAL CONSIDERATIONS

Within the study area evolution of the pre-Middle Cretaceous paleogeography can be inferred from the distribution of the Lower Plate Type

Stratigraphy and its deformed equivalents. Primary stratigraphic relationships are preserved in the Northeast Low Strain Belt; correlative features are overprinted by core complex related fabrics in the Central High Strain Belt.

Jurassic Volcanic Arc Evolution: The Lower? Jurassic rhyolite porphyries and quartz arenite beds accumulated within a volcanic arc environment, probably on Precambrian basement. Although the base of the felsic series is not exposed in the Magdalena area, Precambrian granites are known to underlie Jurassic? volcanic rocks at Cananea and near the international border northeast of Nogales (Anderson and Silver, 1977). The rhyolite-quartzite-quartz arenite clast conglomerate was deposited in an intra-arc basin of considerable size. This unit is presently distributed in a broad west-northwest trending belt. Its locus of deposition was probably controlled by large faults now largely obscured by superposed structures. The Middle? Jurassic granite porphyries were emplaced into the felsic series as hypabyssal sills. These do not appear to be associated with metamorphism or deformation.

Late Jurassic-Early Cretaceous Basin Evolution: A highly conspicuous feature of the lower plate stratigraphy is an unconformity between the Jurassic felsic series and the Upper Jurassic-Lower Cretaceous Cocospera Formation. The unconformity marks a regional transition from a volcanic arc environment to a fluvial/shallow marine environment.

The Cocospera Formation forms the base of a south or southwest facing fining upward clastic section. This section is overlain by fine grained marine sediments and limestones of Lower Cretaceous age (Kitz, personal communication, 1988). Most of the Cocospera clasts were derived from a

northeastern source region; however, some may have been eroded from Upper Jurassic beds in the south. The general stratigraphic succession in the study area implies that a large basin was abruptly formed, rapidly filled with clastic debris, and then inundated by an Early Cretaceous sea.

REGIONAL CONSIDERATIONS

On a larger scale, several independent criteria indicate that the southwestern Cordillera had acquired a strong regional northwest trending structural grain by Early Cretaceous time:

(1) The Jurassic arc of the southwestern Cordillera as outlined by numerous workers (Anderson and Silver, 1969, 1978; Wright, et al., 1984; Tosdal, et al., 1988; Busby-Spera, 1988), follows a west-northwest trend across northern Sonora, southern Arizona, and southern California (see Figure 7.1). In some areas caldera complexes have been mapped, and syntectonic volcanic conglomerates have been documented. Intra-arc Jurassic structures, where well preserved, tend to strike northwest. A Jurassic metamorphic event observed in other areas does not appear to be present near Magdalena.

(2) Conglomerates of the same generation as the Cocospera conglomerate have been reported over widespread areas of the southwest Cordillera. The best studied of these is the Glance Conglomerate of southeastern Arizona, which apparently represents the accumulation of alluvial fan deposits in northwest trending basins of Late Jurassic or Earliest Cretaceous age (Bilodeau, 1978, 1987). In addition to the conglomeratic formations cited in Chapter 6, likely correlative sequences include a group of conglomerates in northeastern Sonora (Taliaferro, 1933; Imlay, 1939; Montano-Jimenez, 1988), the Summit Conglomerate of the Pajarito Mountains, Arizona (Riggs, 1987), the La Jareta Formation of the Sierra las Avispas (Segerstrom,

Figure 7.1: Late Jurassic-Earliest Cretaceous paleogeography of northern Sonora and southern Arizona. Known and suspected occurrences of Jurassic volcanic/plutonic rocks and Upper Jurassic-Lowermost Cretaceous sedimentary rocks are shown relative to Precambrian basement and Paleozoic platform sediments. Y = Yuma; P, Phoenix; A, Ajo; S, Sonoyta; Ca, Caborca; M, Magdalena; N, Nogales; C, Cananea; T, Tucson; AP, Agua Prieta. Sources of data: King, 1939; Imlay, 1939; Cooper and Silver, 1964; Anderson, et al., 1969; Anderson and Silver, 1977; Anderson and Silver, 1979; Wright et al., 1981; Haxel et al., 1984; Rodriguez-Castaneda, 1986; Bilodeau, et al., 1987, Reynolds, 1987; Riggs, 1987; Segerstrom, 1987; Tosdal, 1988; de Jong, 1988; Montano-Jimenez, 1988.

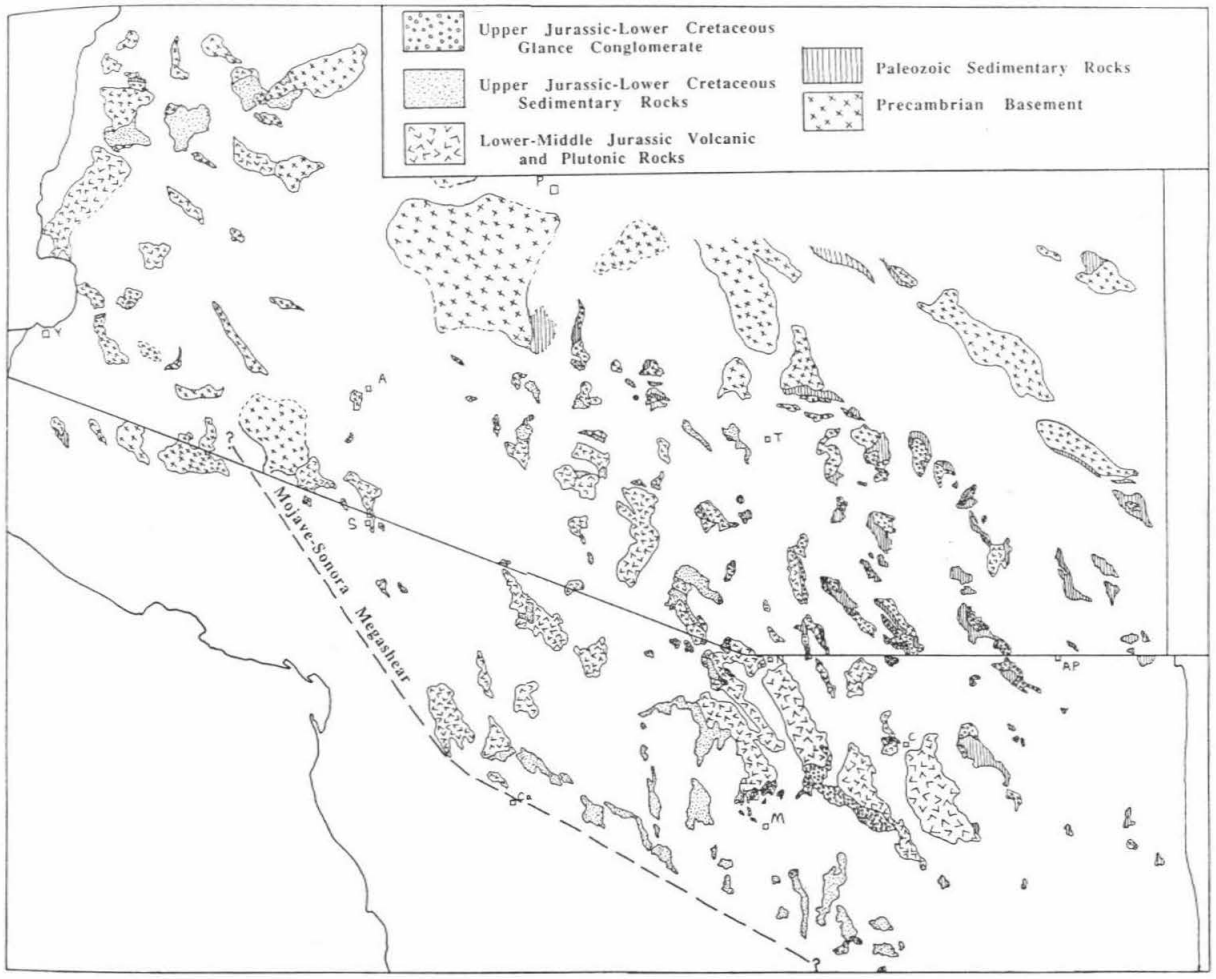
Upper Jurassic-Lower Cretaceous Glance Conglomerate
Upper Jurassic-Lower Cretaceous Sedimentary Rocks
Lower-Middle Jurassic Volcanic and Plutonic Rocks
Paleozoic Sedimentary Rocks
Precambrian Basement
Mojave-Sonora Megashear
P
A
T
S
M
AP

Figure 7.1

1987), and the lower part of the McCoy Mountains Formation in southwestern Arizona (Tosdal, 1986; Richard, et al., 1987). All of these conglomerates are derived from pre-Cretaceous sources. Their regional distribution is shown in Figure 7.1. While a direct spatial relationship to uplifted Late Jurassic fault blocks has not been established in Sonora, the conglomerates do tend to occur in isolated northwest trending belts. Paleogeographic reconstructions are unfortunately inhibited by the affects of younger deformation.

(3) Stratigraphic hiatuses representing either non-deposition of Lower Cretaceous rocks or erosional stripping of said strata are preserved in many areas of Sonora and southern Arizona that are immediately adjacent to Lower Cretaceous depocenters. A section near Cananea reveals an angular unconformity between a Jurassic? rhyolite/trachyte series and an Upper Cretaceous?-Early Tertiary? andesitic-conglomeratic section. Near Rayon, Upper Cretaceous conglomerates are deposited directly upon Late Precambrian shelf sediments (Gonzales-Leon and Jacques-Ayala, 1988) Likewise, several ranges in southern Arizona display depositional gaps between Late Cretaceous conglomerates and pre-Cretaceous rocks (Titley, 1976; Hayes and Drewes, 1978). Figure 7.2 shows the regional distribution of Lower to Middle Cretaceous strata in contrast to areas where rocks of this age are known to be missing. A simplistic interpretation of the data would treat the former areas as sedimentary basins and the latter areas as paleo highs. While some of the apparent paleo highs may actually represent areas of younger (i.e. Late Cretaceous) uplift and erosion, the facies patterns strongly suggest that Early Cretaceous deposition occurred on the down side of northwest trending block faults.

(4) Northwest trending high angle faults played an important role in shaping the structural architecture of the southwestern Cordillera prior to

Figure 7.2: Early to Middle Cretaceous paleogeography of northeastern Sonora and southeastern Arizona, showing regions of marine inundation. Also shown is a region of Early through Middle Cretaceous nondeposition (or nonpreservation). Sources of data: Flores, 1929; Taliaferro, 1933; King, 1939; Imlay, 1939; Salas, 1968; Rodriguez-Castaneda, 1986; Jacques-Ayala, 1986; Dickinson and Klute, 1987 (articles therein); Kitz and Anderson, 1988; Anderson, et al., 1988.

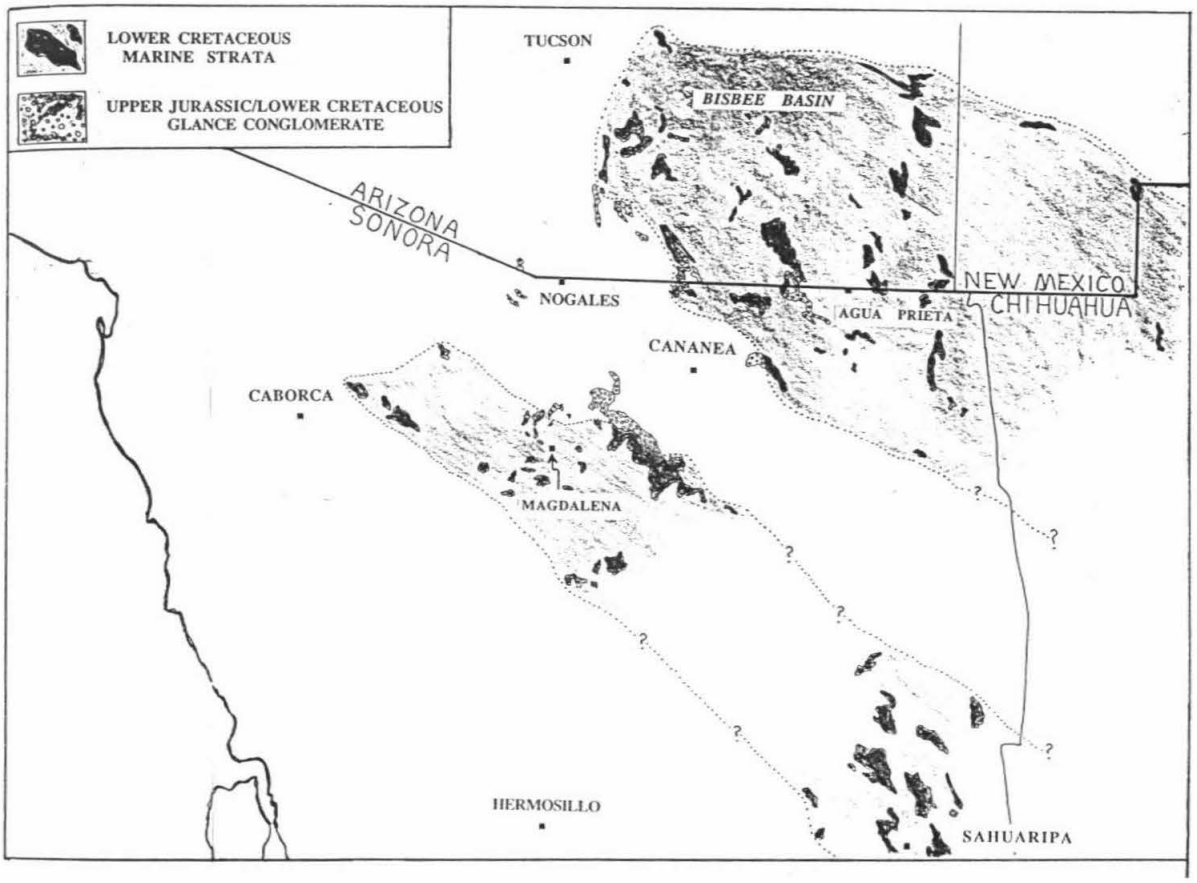
LOWER CRETACEOUS
MARINE STRATA
UPPER JURASSIC/LOWER CRETACEOUS
GLANCE CONGLOMERATE
TUCSON
BISBEE BASIN
ARIZONA
SONORA
NOGALES
NEW MEXICO
CHIHUAHUA
AGUA PRIETA
CANANEA
CABORCA
MAGDALENA
HERMOSILLO
SAHUARIPA

Figure 7.2

Cretaceous time. A pair of subparallel northwest striking sinistral strike slip faults have been proposed to explain large scale offsets in the Precambrian baasement, and truncation of the continental margin during the Late Jurassic (Silver and Anderson, 1974, 1983; Anderson and Silver, 1979). The trace of one of these faults (Mojave-Sonora Megashear I) occurs southwest of my study area. Initial formation of the localized Late Jurassic-Early Cretaceous basins is quite possibly related to regional stresses associated with development of the megashear system. Alternatively, the northwest trending half graben basins of southeastern Arizona have been related to Late Jurassic-Early Cretaceous back arc rifting (Dickinson, 1981).

(5) Finally, the localization of Late Mesozoic through Middle Tertiary metamorphic core complexes along northwesterly trends in Arizona and northern Sonora suggests the influence of a pre-existing, similarly oriented structural grain. My regional tectonic model (see Chapter 9) uses the alignment of core complexes to argue that the complexes developed as a direct consequence of thermal upwelling within weak linear regions of the continental lithosphere.

LATE CRETACEOUS-EARLY TERTIARY PLUTONISM, METAMORPHISM, AND DEFORMATION

The marine basin that occupied the Magdalena-Cucurpe-Santa Ana-Altar region in Early Cretaceous time became the locus of intense orogenic activity during the Late Cretaceous and Early Tertiary. Within the lower plate of the Magdalena core complex this time period is characterized by regional metamorphism and ductile deformation interspersed with at least two generations of granitic plutonism. At shallower structural levels the orogeny

is recorded by a significant disruption of the Lower Cretaceous marine sequence, formation of a large intermontane basin, and preservation of a significant unconformity.

EMPLACEMENT OF THE GUACOMEA GRANODIORITE

The Late Cretaceous porphyritic biotite granodiorite of the Sierra Guacomea was emplaced as a sill into a layered series of Lower? Jurassic rhyolite porphyries, quartz arenites, volcanic conglomerates, and granite porphyries. No associated dike phases are known. Elongate xenoliths of felsic schist within the upper portion of the sill represent either foundered roof pendants or residual layers of country rock. Original contact relationships between the granodiorite and its host rocks are overprinted by a younger deformational fabric, and are locally obscured by a younger leucogranite sill. However, two independent lines of evidence suggest that the granodiorite was emplaced into a previously disturbed section, possibly along a thrust fault:

(1) Comparison of the Sierra Guacomea volcanic sequence to that in the northern Sierra Madera reveals an apparent repetition of strata in the Guacomea sequence. The rhyolite cobble conglomerate unit, which regionally occupies the highest stratigraphic position in the felsic series, occurs at deep structural levels west of El Rincon. Here rhyolitic conglomerate and associated muscovite-feldspar-quartz schists are preserved between an underlying rhyolite/quartz arenite sequence and an overlying quartz porphyry/granite porphyry/quartzite sequence. The biotite granodiorite sill occurs along strike immediately to the south at the same horizon as the conglomerate. Where the granodiorite pinches out the upper part of the conglomerate unit is intruded out by a younger leucogranite. Two alternative models might explain this peculiar stratigraphic configuration: (a) the Jurassic section was duplicated

via thrusting prior to the Late Cretaceous, and the granodiorite was emplaced along the resulting structural discontinuity, or (b) the conglomerate of the Sierra Guacomea represents an early episode of volcaniclastic deposition within a normal stratigraphic succession, and the granodiorite was simply emplaced along bedding planes.

(2) Strain gradients within the granodiorite and its overlying country rocks reveal that while the upper part of the granodiorite sill is barely deformed, most of the superjacent porphyries are significantly strained (see Figure 8.17). The strain data can be rationalized in two ways: (a) the granodiorite was emplaced into previously deformed country rocks, or (b) a younger deformation (marked by a conformable foliation in both units) was superimposed in such a way that most of the strain accumulated in the roof rocks of the sill.

So, there is some evidence for a pre 78 Ma deformational event, but at the present stage of research this evidence is circumstantial and equivocal.

REGIONAL METAMORPHISM AND DUCTILE DEFORMATION

Structural evidence for a significant episode (or episodes?) of Late Cretaceous-Early Tertiary metamorphism and ductile strain is preserved in the fabrics of the lower plate schists. These fabrics are in part younger than the Guacomea Granodiorite, and older than the leucogranite suite. In the northern Sierra Madera the early fabrics are intruded by the Early Tertiary? Mesquital Granodiorite. Differentiation of the older regional fabric is hampered by the fact that in most places a post-leucogranite ductile deformation has been superimposed. However, structures preserved in areas not severely affected by the late strain provide constraints on the geometry and mechanics of an important regional orogenic event.

Prograde Metamorphic Fabrics and Mineral Assemblages: Dynamothermal metamorphism of the lower plate supracrustal rocks has resulted in development of crystalloblastic schistose fabrics and growth of prograde mineral assemblages over a large region. A southwestward increasing gradient in fabric intensity coincides with an increase in metamorphic grade from sub-greenschist to garnet amphibolite facies. Within the rhyolite porphyry and granite porphyry units the transition from unmetamorphosed protolith to schist is marked by the following features (listed in order of increasing metamorphism and strain): (1) recrystallization of the felsic groundmass, (2) development of a weak mica foliation, (3) recrystallization and elongation of the phenocrysts, and (4) development of a penetrative schistosity and lineation. The rhyolite cobble conglomerate unit exhibits a similar set of fabric intensity criteria: first the matrix recrystallizes and takes on a weak schistosity, then the cobbles become progressively more stretched and recrystallized as the whole rock develops a strong lineation and schistosity. Fabric gradients within the Cocospera conglomerate and stratigraphically higher units are defined by: (a) growth and alignment of chlorite, biotite, and amphibole, (b) recrystallization and elongation of pebbles and quartz or feldspar grains, and (c) transposition of primary bedding into schistosity.

Microscopic analysis of the schistose supracrustal rocks demonstrates that they were strained under prograde metamorphic conditions. Deformational mechanisms were entirely crystal-plastic, with the bulk of the strain accommodated by recrystallization. Where relatively large grains (i.e., phenocrysts or pebbles) are isolated within a finer grained matrix, a significantly higher proportion of the strain is absorbed in the matrix (see

Chapter 8). In the porphyries, feldspar and quartz phenocrysts recrystallized under stress typically form highly elongate aggragates of recrystallized subgrains aligned parallel to the mica foliation. Those samples collected away from the Middle Tertiary mylonite zone show no signs of noncoaxial deformation: long axes of recrystallized phenocrysts are symmetric relative to the mica foliation, and their subgrain constituents are subequent and randomly oriented. Virtually all effects of dynamic strain (i.e., grain boundary sliding, shear band development, intragrain fracturing, quartz subgrain elongation, and porphyroclast rotation) have been annealed by the recrystallization process.

Metamorphic isograds are qualitatively defined by prograde mineral assemblages identified in the field and in thin section. The pelitic schists preserve a Barrovian type mineral paragenesis. Within the more calcareous and psammitic portions of the metasedimentary sequence, relative abundances of calcic amphibole, biotite, grossular garnet, chlorite, and epidote were diagnostic. The metavolcanic rocks generally display a monotonous quartz-two feldspar-muscovite-biotite assemblage, with an occasional appearance of garnet in lower amphibolite grade schists. In general, metamorphic grade increases toward the southwest, from sub-greenschist facies near Puerto la Bandera to lower amphibolite facies in the Sierra Magdalena. Coincidence of the regions of highest grade with areas underlain by significant volumes of granite implies that metamorphism was related to emplacement of the granites. In the west central Sierra Guacomea an increase in metamorphic grade with depth can be demonstrated.

The duration of metamorphism is uncertain. In the west central Sierra Guacomea the schistosity appears to postdate emplacement of the Guacomea Granodiorite. In the northern Sierra Madera the prograde fabrics are older

than the Mesquital Granodiorite. Elsewhere, in the Sierras Magdalena and Jojoba, the supracrustal section is flooded with leucogranite. In these regions an associated thermal anomaly may have kept local areas hot until Middle Tertiary time.

Structural Elements: Structures which developed in the lower plate supracrustal rocks during the Late Cretaceous-Early Tertiary orogeny include macroscopic foliation and lineation, and map scale folds. These structures are overprinted by a locally penetrative mylonitic fabric, and by post-mylonitic folds. The resulting interference patterns are complex (see Figure 7.3). In areas of strong overprint the geometry of the early strain field cannot be interpreted until the effects of the two younger deformational events are removed. However, the Magdalena area provides a fortunate set of exposures in that one can walk continuously through the Middle? Tertiary mylonite zone into areas where the older fabrics are well preserved. It is thus possible to elucidate kinematic information about Late Cretaceous-Early Tertiary ductile deformation within the lower plate.

Orientations of bedding and/or schistosity were measured from outcrops at various stratigraphic and structural levels of the supracrustal series. The schistosity is generally expressed by a preferred planar orientation of micas and a flattening of feldspar and quartz. Lineations, where present, are defined by an alignment of mica or amphibole, and an elongation of quartz and feldspar within the foliation plane. These schistosities and lineations reflect the geometry of the bulk cumulative strain in the supracrustal series. The schistosity marks the orientation of the XY plane of the finite strain ellipsoid, and the lineation gives the maximum elongation direction. Where sandstone, conglomerates, or porphyries are involved in the deformation, a measure of

the magnitude and geometry of strain is provided by the shape and orientation of stretched grains, clasts, or phenocrysts.

Figure 7.3 summarizes structural elements of the lower plate. Shown in the stippled pattern are regions affected by Middle? Tertiary noncoaxial mylonitic deformation and post-mylonitic northwest or north-northwest trending folds. Away from these areas the foliation patterns reveal a series of west, west-northwest, or east-northeast trending map scale folds. The fold axes appear to plunge bidirectionally away from a linear structural culmination. This effect has been created by superposition of the younger folds and the resulting exposure of deep structural levels of the lower plate.

Figure 7.3 also shows the distribution of lineations in the lower plate. The overall lineation pattern represents an interference between at least two ductile strain events. In regions strongly affected by the mylonitic deformation lineations are shallow and directions cluster tightly between N30E and N50E. This trend coincides with the average lineation of N45E observed in the mylonitic granites. Other regions of the lower plate exhibit anomalous lineation directions which reflect an earlier, pre-mylonitic ductile strain episode. Several geographic domains with N60E to S85E lineations were observed in the central portion of the lower plate. Farther northwest (near El Rincon), lineations trend N5W to N25E. The mechanism for formation of these anomalous lineations is poorly understood, but presumably they are kinematically related to development of the east-west trending folds.

In two regions, systematic variations in lineation direction with depth imply that older fabrics have been rotated by the younger deformation. Between Imuris and La Sauceda, lineations measured in volcanogenic schists strike about N65E while those measured in the structurally higher metasedimentary series strike N45E. Apparently the southwest directed

Figure 7.3a: Generalized structural and fabric map of the Magdalena metamorphic core complex.

Figure 7.3b: Explanation for Figure 7.3a.

STRUCTURES AND FABRICS IN THE MAGDALENA CORE COMPLEX

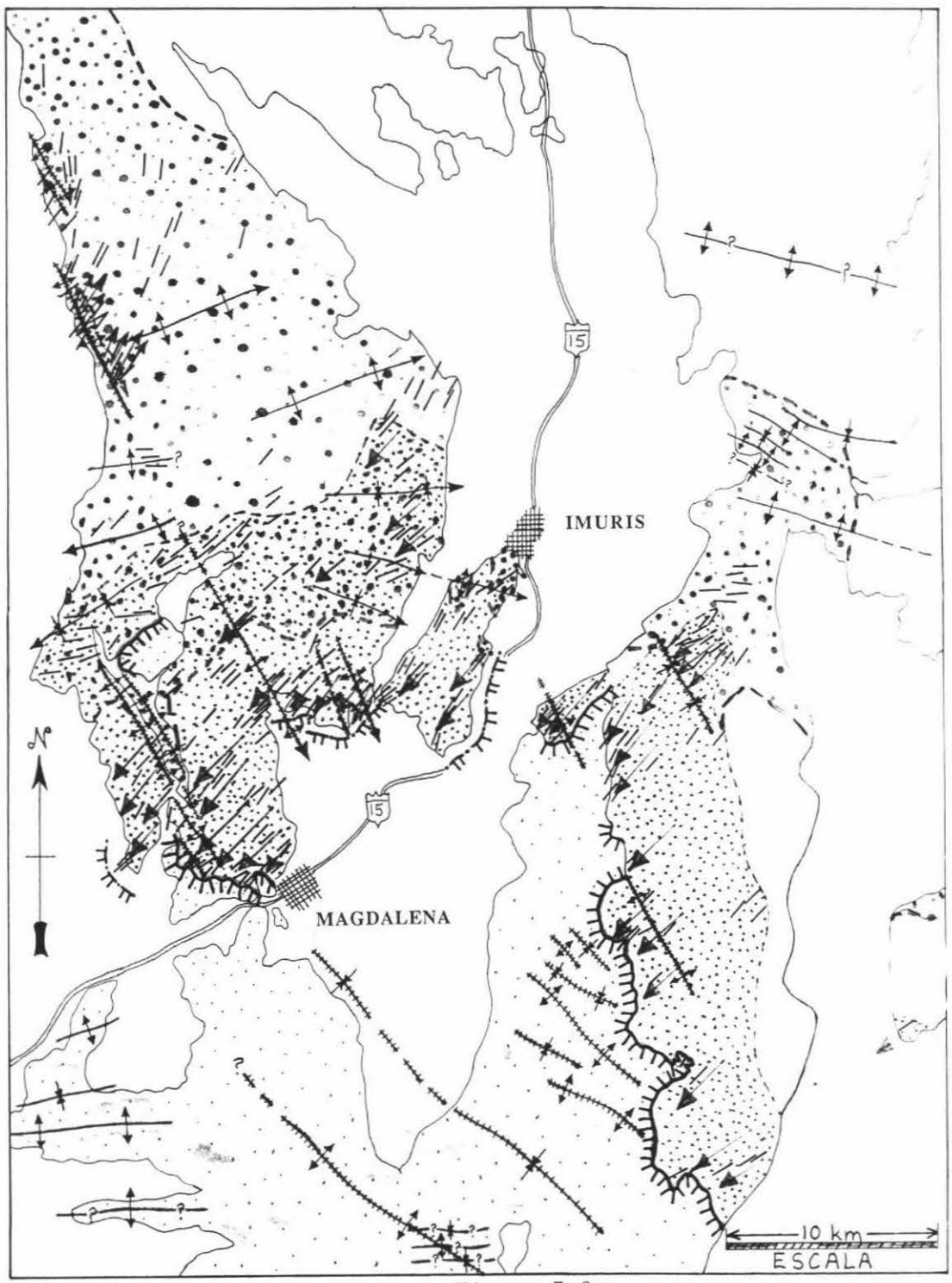

Figure 7.3a

EXPLANATION

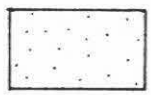

UPPER PLATE ROCKS

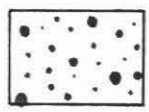

REGIONAL METAMORPHIC FABRIC
(Late Cretaceous-Early Tertiary)

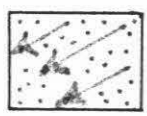

MYLONITIC FABRIC
(Middle Tertiary)

MAGDALENA
DETACHMENT FAULT

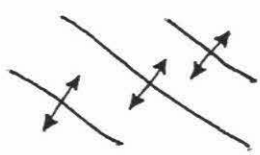

AXES OF EARLY FOLDS
(post-Albian pre-Middle Tertiary)

AXES OF LATE FOLDS
(Miocene)

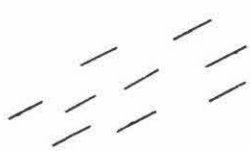

LINEATIONS

Figure 7.3b

mylonitic fabric has more strongly overprinted the metasedimentary rocks. A contrasting situation exists near El Rincon, where lineations measured at deeper structural levels strike N30E to N40E, and those farther up section strike N5W to N25E. The effects of noncoaxial deformation are noticeably stronger at the deeper levels, where leucogranites are involved.

EMPLACEMENT OF THE PORPHYRITIC TWO MICA GRANITES

Porphyritic two mica granites were emplaced during late phases of the Late Cretaceous-Early Tertiary orogeny. Only one of these granites (the Mesquital Granodiorite) is demonstrably post-kinematic. This pluton has intruded fairly shallow levels of the felsic series (i.e., it crosscuts the stratigraphically high rhyolite cobble conglomerate unit in the northern Sierra Madera).

In the Sierra Magdalena porphyritic two mica granite forms a tabular mass between structurally deeper biotite granodiorite and overlying leucogranites and metamorphic strata. This two mica granite also appears to have been emplaced at shallow levels. Unfortunately the superimposed mylonitic deformation has obscured any possibility of differentiating an older fabric in the country rocks.

In the southern Sierra Madera structural relationships of the porphyritic two mica granite to earlier fabrics cannot be determined due to the absence of country rock exposure. However, the granite does appear to have a gradational subhorizontal contact (now highly sheared) with structurally overlying porphyritic biotite monzogranite.

An independent measure of the emplacement depth of these granites is provided by prograde mineral assemblages in the metamorphosed supracrustal series. Certainly the granites were not emplaced any deeper than the depths

indicated by their highest grade country rocks. The most common high grade assemblage in the pelitic schist is garnet-staurolite-biotite-muscovite-quartz-plagioclase±andelusite. This assemblage is diagnostic of the lower-middle amphibolite facies, corresponding to a pressure of about 4 kilobars and a depth of about 12 kilometers.

UPPER PLATE DISTURBANCES

Late Cretaceous-Early Tertiary plutonism and metamorphism were accompanied at shallower crustal levels by active mountain building and basin development, with associated folding, thrust faulting, syntectonic sedimentation, and volcanism. Structural and facies relationships preserved in the upper plate sedimentary and volcanic record provide insight into the geometry and timing of these tectonic disturbances. The tectonic sequence may be modeled as follows:

(1) disruption and probable tight folding of the Lower Cretaceous marine sequence,

(2) development of a pronounced unconformity on "up" blocks of the Lower Cretaceous strata and Jurassic? granites, with syntectonic deposition on "down" blocks to the north and northwest,

(3) north directed emplacement of the La Lamina thrust complex, with a contribution of debris to the north onto now subsided "up" blocks, and

(4) extrusion of andesite flows from a western source late during event (3). The absolute timing and duration of these events is uncertain. Event (1) is younger than Middle Cretaceous; event (4) may be Oligocene.

Tight? Folding of Lower Cretaceous Strata: Steeply dipping beds of the Lower Cretaceous marine sequence record the oldest known structural

disturbance in the upper plate. The strata exposed near El Represo and El Alamito strike east-northeast and west-northwest, respectively. Several dip reversals observed in both areas suggest that the sequence is tightly folded. Plate 2 includes a compilation of known Lower Cretaceous exposures in the Magdalena-Santa Ana region. Structural data near Santa Ana are borrowed from King (1939) and Salas (1968). Although the exposures are intermittent, the data define a consistent pattern of east-west trending, upright folds. Axes may plunge gently in either direction. However, as emphasized previously, the detailed structure and stratigraphy have yet to be worked out in this region. The kinematics of folding and the fundamental driving mechanism behind this disturbance are uncertain.

The Great Unconformity: An important post Middle Cretaceous-pre Middle Tertiary tectonic disturbance is indirectly recorded by a major unconformity within the upper plate sedimentary and volcanic sequence. Stratigraphic and paleogeographic relationships shown in Figure 7.4 indicate that a large region was uplifted and eroded while syntectonic debris accumulated in a proximal basin. Stratigraphic columns from the inferred paleo highs display pronounced unconformities between tilted Lower Cretaceous beds or Jurassic? granite and overlying Oligocene? andesite and/or red conglomerate. The location of the basin is marked by the sedimentary breccia unit. Where exposed, the base of this unit rests conformably? upon Lower Cretaceous limestone and siltstone. The original geometry of the basin has been obscured by Miocene detachment faulting, folding, and thrust faulting. However, abrupt changes in stratigraphy near the inferred basin margins suggest that deposition of the sedimentary breccia was controlled by major faults.

Figure 7.4: Paleogeography of the upper plate during deposition of the sedimentary breccia unit.

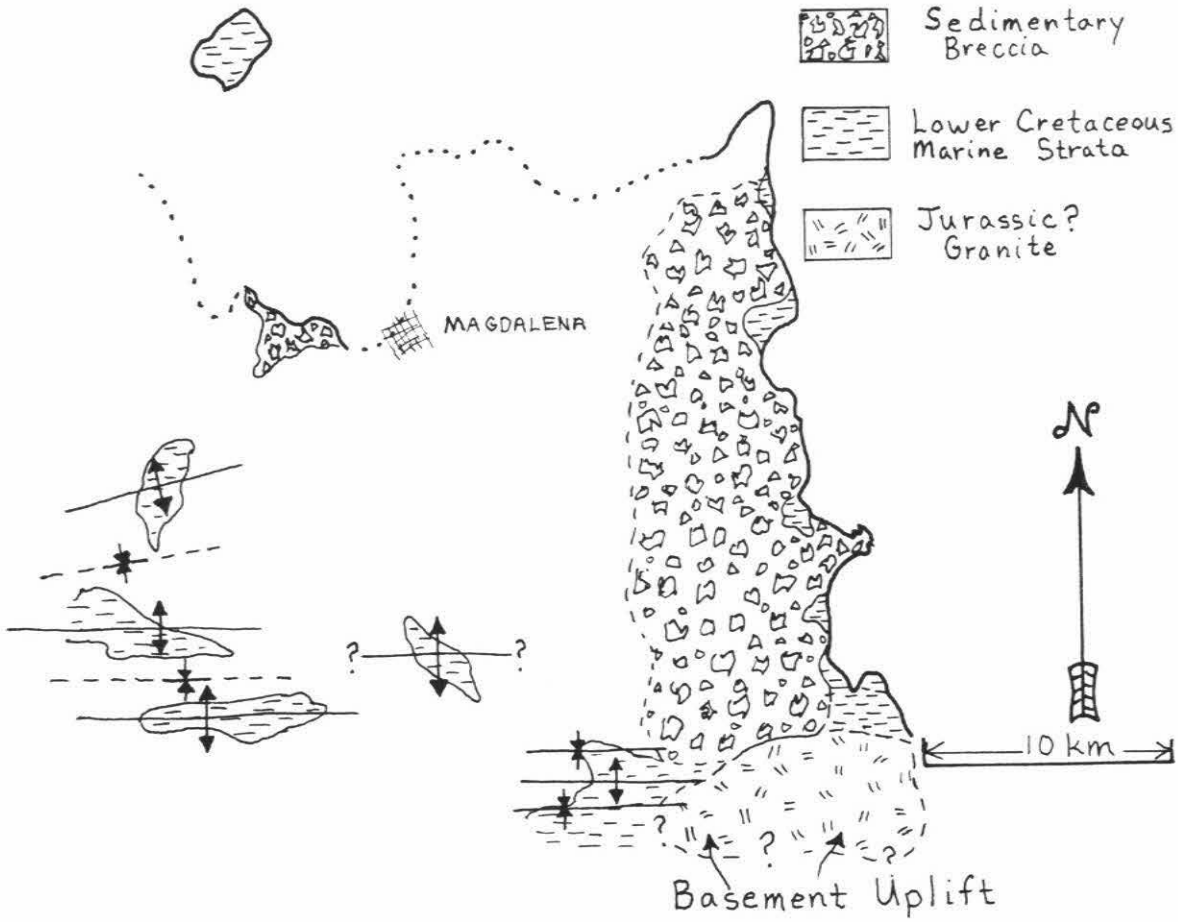
Sedimentary Breccia
Lower Cretaceous Marine Strata
Jurassic? Granite
MAGDALENA
N
10 km
Basement Uplift

Figure 7.4

The composition and distribution of clasts in the red conglomerate unit preserve a transition to a different sedimentary environment with new and more diverse provenances. Figure 7.5 shows the inferred paleogeography during deposition of the upper part of the red conglomerate unit. By this time the granite basement source for the sedimentary breccia had subsided. Overlapping fluvial deposits contain an abundance of andesite clasts derived from newly exposed source regions. These sources probably included: (1) the andesite complex of the Sierra Ventana, (2) intraformational andesite flows, and (3) the lowermost plate of the La Lamina thrust complex (see below).

Tectonic Emplacement of the La Lamina Thrust Sheets: Stratigraphic evolution of the upper plate was influenced by north vergent emplacement of exotic thrust sheets prior to the Middle Tertiary. The La Lamina thrust complex, as mapped by Stephens and Anderson (1986), comprises a dismembered upper plate of Precambrian micrographic granite and gneiss, and a lower plate of mixed sedimentary rocks. Excellent three dimensional exposures are afforded by a series of recently excavated roadcuts between Puerto Cucurpe and La Lamina. Along this transect the crystalline rocks overlie red and purple lithic sandstone and siltstone along a gently south dipping fault. At deeper structural levels the sediments are imbricated with dark purple-red andesite. Then, immediately south of La Lamina the sandstones are thrust over a large mass of purple andesite along a shallow south-southwest dipping fault.

Timing for emplacement of these thrust sheets is loosely constrained. The ages of the sedimentary rocks and the andesites are uncertain, but these rocks probably correlate with an upper Jurassic marine graywacke/andesite assemblage exposed farther south near La Colgada (see Rangin, 1977a;

Figure 7.5: Paleogeography of the upper plate during deposition of the red conglomerate unit.

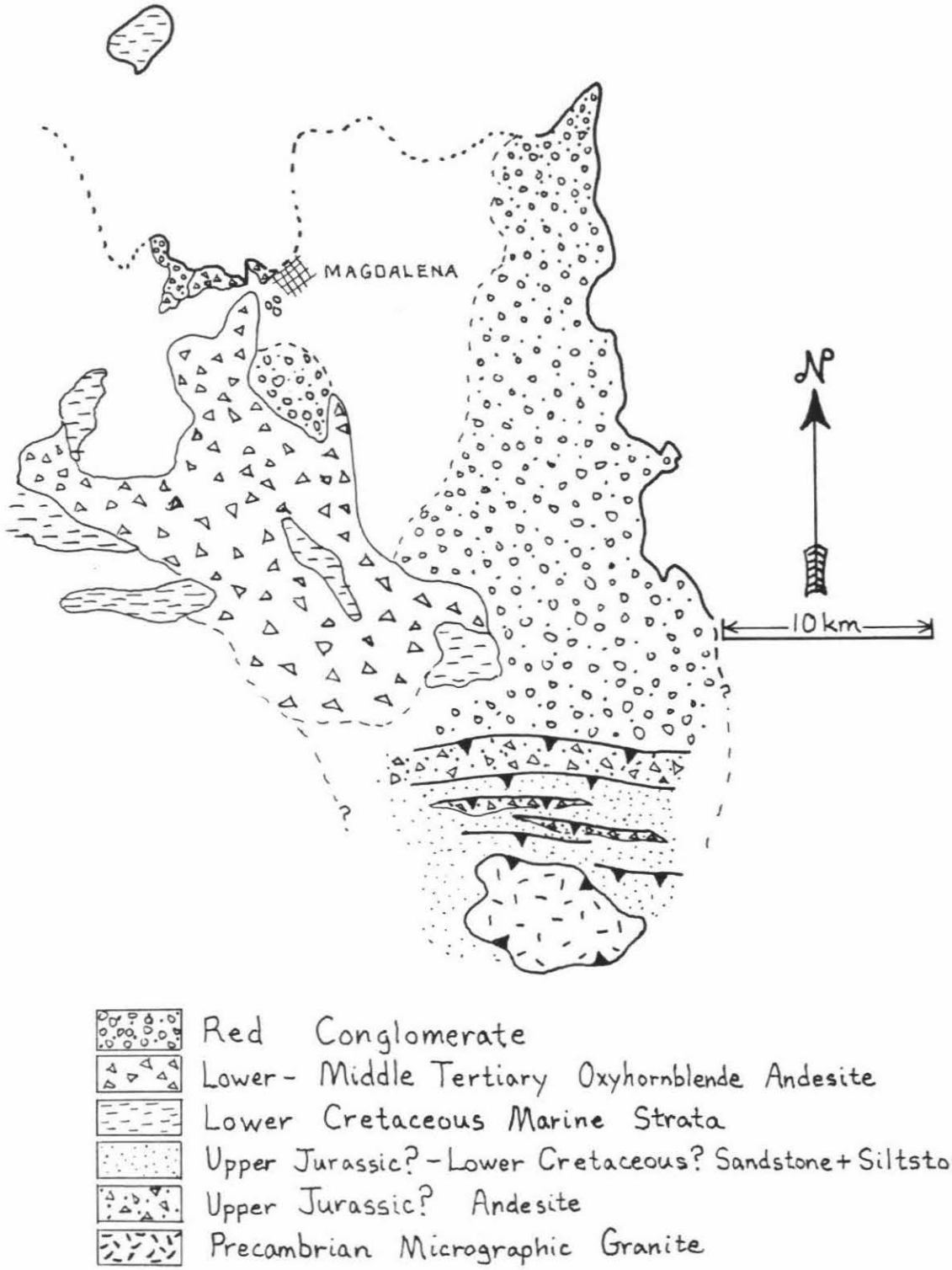
MAGDALENA
N
10 km
Red Conglomerate
Lower - Middle Tertiary Oxyhornblende Andesite
Lower Cretaceous Marine Strata
Upper Jurassic? - Lower Cretaceous? Sandstone + Siltstone
Upper Jurassic? Andesite
Precambrian Micrographic Granite

Figure 7.5

Anderson, et al., 1988). Alternatively, the sediments may be part of the Lower Cretaceous marine sequence. Early Miocene? silicic pyroclastic rocks overlap the thrust complex. Indirect evidence for the age of thrusting is preserved in the sedimentary record of the Intermontane Group. A sudden influx of dark purple-red andesite clasts in the upper part of the red conglomerate unit reflects the emergence of an andesitic source lithologically similar to the lowest plate of the La Lamina complex. The stratigraphically higher siltstone breccia unit was derived from a nearby southerly source, possibly the middle plate of the thrust complex. The La Lamina thrust sheets thus appear to have been unroofed subsequent to the tectonic event that resulted in deposition of the sedimentary breccia unit, but prior to the onset of silicic volcanism. However, available data do not preclude the possibility that the thrust sheets were initially emplaced long before their exposure to surface erosion (i.e., thrusting could be as old as Late Jurassic).

Interpretation of the Kinematic Sequence: Geographic coincidence of the east trending folds in the Lower Cretaceous sequence and the north directed thrusts of the La Lamina complex implies that these structures may be genetically related. Although unroofing of the thrust shets clearly occurred after uplift and erosion of the Lower Cretaceous beds, the general evolution of structures can be explained by a progressive deformational sequence. Figure 7.6 illustrates my preferred model for the Late Cretaceous-Early Tertiary development of the upper plate stratigraphy. Essentially, the Lower Cretaceous strata and their granitic basement were folded, uplifted, and eroded during north-south compression; then the La Lamina thrust sheets encroached from the south and shed debris into a foreland basin. This model has additional appeal in that folds of similar

Figure 7.6: Tectonic model for the Late Cretaceous-Early Tertiary stratigraphic development of the upper plate.

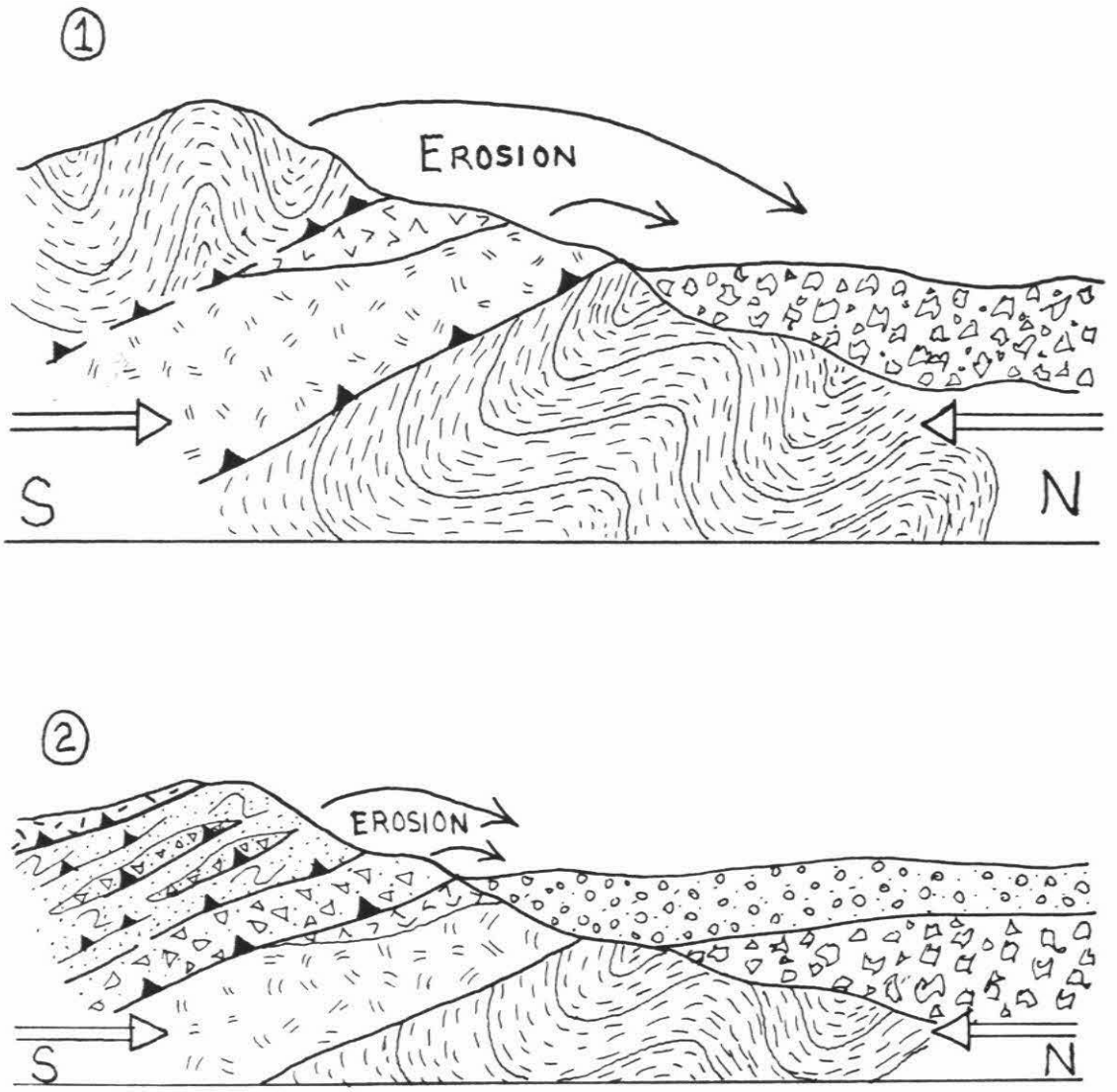

Figure 7.6

orientation and age are preserved within the lower plate of the Magdalena core complex. Also, east trending tight folds have been reported in Upper Jurassic and Lower Cretaceous beds exposed beneath the crystalline thrust klippen south of Puerto Cucurpe (Anderson, et al., 1988).

REGIONAL CORRELATION

The Late Cretaceous-Early Tertiary tectonic history preserved in the Magdalena area places new constraints on our understanding of a long lived regional orogeny. Throughout the southwestern Cordillera this time period is characterized by deep seated metamorphism and plutonism, localized andesitic volcanism, and the development of local and regional unconformities. Several generations of associated thrust faults involve both basement and supracrustal rocks. Regional tectonic features relevent to large scale interpretation of the Magdalena structures are described below:

Eastward Migration of the Cretaceous Batholith: The earliest phases of post-Jurassic plutonism in northern Mexico and southern Arizona record eastward migration of a Cretaceous magmatic arc from a position presently marked by the axis of the Sierra Nevada/Peninsular Ranges batholith. Silver and Anderson (1974) have demonstrated an eastward younging trend in Late Cretaceous plutonism of northern Sonora, from 80-97 Ma near the Gulf of California to 60-70 Ma near the Chihuahua border (see also Clark, et al., 1982; Silver and Chappell, 1988). A similar younging trend across the Basin and Range province of the southern United States has been reported (Coney and Reynolds, 1977,). Within this broad belt a slightly younger suite of Late Cretaceous-Early Tertiary peraluminous two mica granites appears to be confined to areas of regional metamorphism and basement involved thrusting

(see below). In southern Arizona the older granitoids are distinguished from the younger by a variety of petrologic and geochemical characteristics (Haxel et al., 1983). Also, the older granites tend to be involved in thrust faulting, while the two mica granites are generally post-kinematic.

Representative Late Cretaceous-earliest Tertiary calc-alkaline plutons in north central Sonora include the 74±2 Ma Rancho los Alamos granodiorite (Anderson, et al., 1980), and the 69±1 Ma Chivato monzodiorite and 64±3 Ma Cuitaca granodiorite (Anderson and Silver, 1978). In the Magdalena area the oldest post-Middle Cretaceous pluton is the 78±3 Ma Guacomea Granodiorite. This lithology is compositionally different from all younger granites in the study area. In most ways it compares with the Late Cretaceous metaluminous granitoid suite of Haxel et al. (1983). However Guacomea Granodiorite does not contain the hornblende seen in the three nearby granitoids of this generation.

Basement Involved Thrusting With Associated Regional Metamorphism: The Late Cretaceous-Early Tertiary was a time of profound crustal shortening throughout the southwestern Cordillera. At middle crustal levels this period is characterized by basement involved thrusting and spatially associated regional metamorphic gradients. Figure 7.7 shows the regional distribution of known Late Cretaceous-Early Tertiary thrusts of this type. In addition to their apparent contemporaneity, these thrust complexes are similar in that: (1) the youngest rocks involved in thrusting are Late Cretaceous calc-alkaline granitoids, (2) dynamic strain features (i.e., mylonite zones and noncoaxial fabrics) are usually overprinted by schistose, prograde metamorphic fabrics, and (3) the regional metamorphic fabrics are intruded by peraluminous two mica±garnet granites. However, the thrust complexes

Figure 7.7: Late Cretaceous-Early Tertiary tectonic map of northern Sonora and southern Arizona (see text for discussion). Sources of data: Taliaferro, 1933; King, 1939; Cooper and Silver, 1964; Rangin, 1977b; Shakel, et al., 1977; G. H. Davis, 1979; Anderson and Silver, 1979; Anderson, et al., 1980; Drewes, 1980; Hardy, 1981; Haxel, et al., 1984; Tosdal, 1986, 1988; Rodriguez-Castaneda, 1986; Stephens and Anderson, 1986; Reynolds, 1987; de Jong, 1988; Kitz and Anderson, 1988.

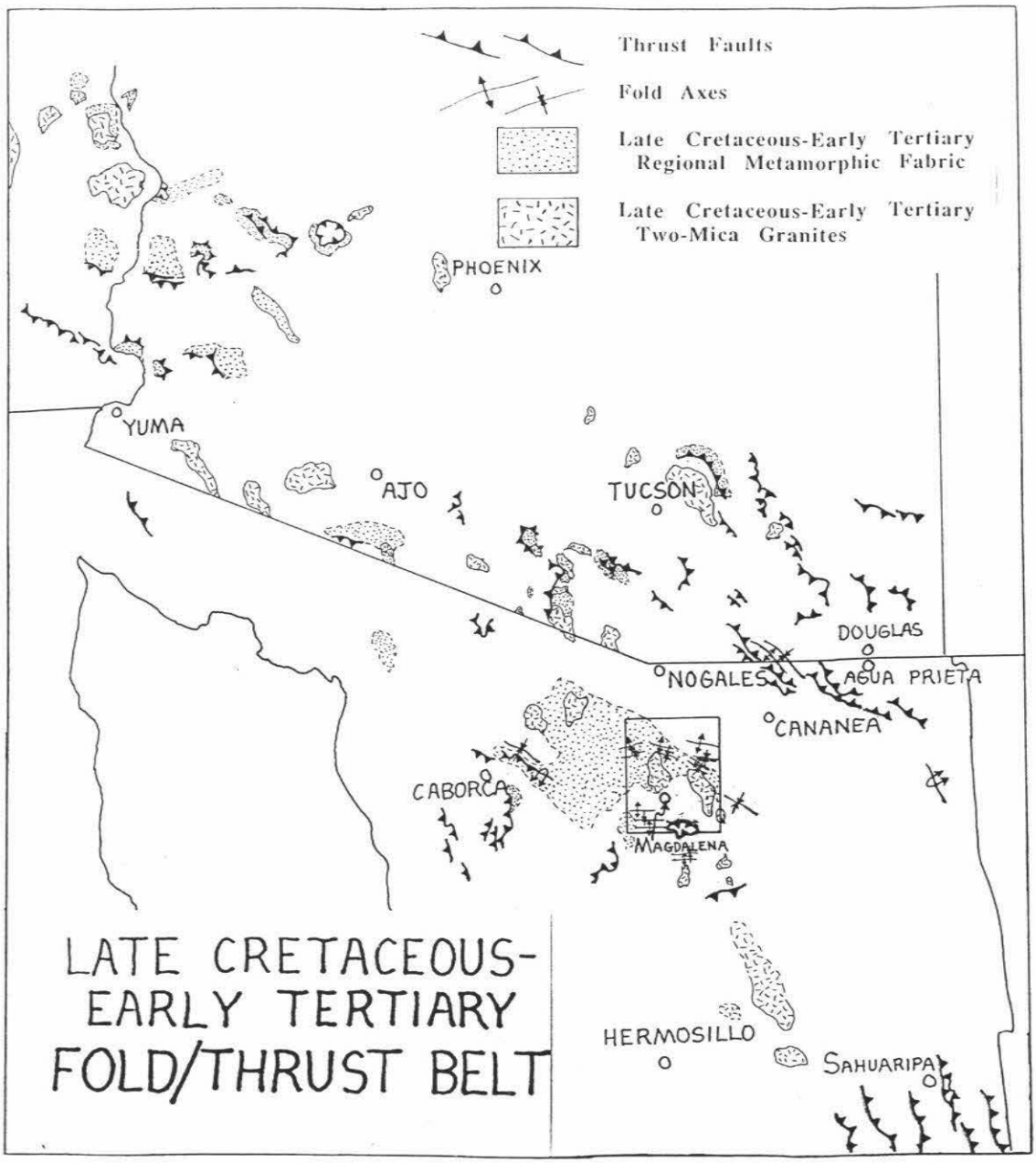
Thrust Faults
Fold Axes
Late Cretaceous-Early Tertiary Regional Metamorphic Fabric
Late Cretaceous-Early Tertiary Two-Mica Granites
PHOENIX
YUMA
AJO
TUCSON
DOUGLAS
NOGALES
AGUA PRIETA
CANANEA
CABORCA
MAGDALENA
HERMOSILLO
SAHUARIPA
LATE CRETACEOUS-EARLY TERTIARY FOLD/THRUST BELT

Figure 7.7

differ in one significant way: transport directions as demonstrated by asymmetric folds, kinematic indicators, and elongation lineations are nonsystematic between separate thrust domains. Whether these variations are due to original variability in local stress fields or to subsequent tectonic rotations is not known. Some of the better studied areas are briefly described below.

In northwestern Sonora, basement involved thrust faults have only recently been mapped in enough detail to discern a Late Mesozoic age of deformation. South of Caborca a family of thrust faults places Precambrian crystalline basement and overlying late Proterozoic through Paleozoic platform sediments over Mesozoic sedimentary and volcanic rocks (de Jong, et al., 1988) Near Quitovac a thrust klippe of Jurassic? granite overlies Mesozoic metavolcanic and metasedimentary rocks (George Smith, personal communication, 1986). The lower plates of both thrust complexes display synkinematic metamorphic fabrics. The west vergent thrust in the Sierra La Vibora was active between 95 and 80 Ma (de Jong, et al., 1988).

Several thrust faults in north central Sonora juxtapose Precambrian rocks against strata as young as Lower Cretaceous (Anderson et al., 1984; Rodriguez-Castaneda, 1986; Stephens and Anderson, 1986). However, these faults do not appear to be associated with regional metamorphism. They were probably active at fairly shallow crustal levels.

In southeastern Arizona, blocks of Proterozoic granite and schist are thrust in various directions over sedimentary rocks as young as Upper Cretaceous (Cooper and Silver, 1964; G. H. Davis, 1979; Drewes, 1980). Synkinematic prograde metamorphic fabrics are strongly developed in two areas: In the Little Rincon Mountains, Proterozoic granodiorite is thrust northeastward over Paleozoic sediments and Proterozoic Pinal Schist (Smith

and Gehrels, 1987). In the northeastern Catalina Mountains, Paleozoic strata are thrust eastward over Late Cretaceous granodiorite and Proterozoic granite (Janecke, 1987; Bykerk-Kaufmann and Janecke, 1987). Thrust related fabrics in the upper and lower plates of both complexes are intruded by two mica granite plutons.

In south central Arizona, the Baboquavari thrust system places Jurassic granitic, volcanic, and sedimentary rocks over a diverse assemblage of Jurassic and Lower Cretaceous? lithologies (Haxel, et al., 1984). The nearby Quitobaquito Thrust places Precambrian? gneiss and Late Cretaceous granodiorite over Jurassic volcanic and granitic rocks (Haxel, et al., 1984). In both regions prograde metamorphic fabrics within the lower plates intensify as the thrusts are approached, and similarly oriented fabrics are present in the basal part of the upper plates. Two mica garnet bearing granites locally intrude these fabrics. Occasionally, margins of the post-kinematic granites display a younger fabric which is apparently related to local reorientation of the regional schistosity and lineation.

In western Arizona and southeastern California, a record of Late Mesozoic basement involved crustal shortening and metamorphism is preserved in the Maria fold and thrust belt and the Mule Mountains thrust. Movement on a number of thrusts is associated with Late Cretaceous regional metamorphism. In the Harquahala Mountains, a south vergent thrust system that juxtaposes Proterozoic and Jurassic granites and gneisses with an overturned Paleozoic/Mesozoic section is overprinted by a pre-72 Ma schistosity (Richard and Sutter, 1988). In the Granite Wash Mountains, the southwest vergent Hercules Thrust also places Proterozoic and Jurassic crystalline rocks over Paleozoic and Mesozoic supracrustal strata (Reynolds et al., 1980, 1986b, 1988). An associated prograde metamorphic fabric is intruded

by two post-kinematic Late Cretaceous plutons. In the Dome Rock Mountains, Cretaceous metamorphic fabrics are cut by the latest Cretaceous Mule Mountains Thrust (Tosdal, 1986). Finally, in the Old Woman, Big Maria, and Piute Mountains, Paleozoic cratonal sediments involved in ductile nappes display syntectonic metamorphic fabrics that developed at about 80 Ma (Hoisch et al., 1988).

Late Cretaceous-Early Tertiary thrust faults involving crystalline rocks have been recognized in other parts of southern California. The west vergent Peninsular Ranges mylonite zone (Simpson, 1984) is developed within Late Cretaceous granites. Also active during this time interval was the Vincent-Orocopia-Chocolate Mountains-Rand thrust system (for related discussion see Part I of this thesis).

In the Magdalena region, definitive evidence for basement involved thrusting with metamorphism is lacking, perhaps due to the severe overprint of core complex related plutonism and mylonitization. However, the schistose fabrics and metamorphic gradients preserved in the lower plate are analogous to regional metamorphic fabrics associated with basement thrusting elsewhere. These early fabrics, known to be younger than the 78 Ma Guacomea Granodiorite are similarly intruded by an Early Tertiary? two mica granite pluton.

Emplacement of Post-Kinematic Two Mica Granites: Throughout the Late Cretaceous-Early Tertiary orogenic belt a suite of peraluminous granites intrudes structures and fabrics related to basement involved thrusting and regional metamorphism. Typical characteristics of two mica garnet bearing monzogranites in southern Arizona are summarized by Haxel et al., (1983). Compared to the slightly older suite of metaluminous calc-

alkaline granitoids described earlier, these granites are compositionally restricted, more leucocratic, and lacking in hornblende. U/Pb geochronology on the Pan Tak Granite of the Baboquavari Mountains indicates an emplacement age of 58±2 Ma, and demonstrates a significant inherited Middle Proterozoic zircon component (Wright and Haxel, 1982). In a model proposed by Haxel et al., (1984), the peraluminous granites are products of crustal anatexis, apparently a consequence of crustal thickening near basement involved thrusts and related thermal perturbations.

In Sonora, analagous? granites in the Sierra Mazatan and near Puerto del Sol were studied by Anderson, et al., (1980). These authors obtained U/Pb ages of 57±3 Ma and 58±3 Ma, respectively, for the two granites. In the Magdalena area, Eocene U/Pb ages are reported for granites from unspecified locations (Silver and Anderson, 1984). Many of the Sonoran granites are significantly overprinted by mylonitic fabrics related to core complex development.

Figure 7.7 also shows the regional distribution of known or suspected Late Cretaceous-Early Tertiary peraluminous two mica+garnet granites. Without exception the granites are intrusive into older metamorphic rocks. Primary ages of the granites in western Arizona and southeastern California tend to be somewhat older than those in southern Arizona and Sonora; however, reliable geochronological control is limited. Many of the granites have experienced a significant Middle Tertiary thermal disturbance subsequent to their emplacement (Reynolds et al., 1988;).

The porphyritic two mica+garnet granites of the Magdalena core complex are probably part of the regional post-kinematic peraluminous granite suite. Only one of these (the Mesquital Granodiorite) is unequivocally younger than the regional metamorphism and deformation. The remainder

are too strongly overprinted by younger fabrics to determine age relationships to the metamorphic fabric.

Upper Crustal Folding and Thrusting: Significant post Middle Cretaceous-pre Middle Tertiary shortening at shallow crustal levels is recorded by folds and thrusts that involve Lower Cretaceous sedimentary rocks, and sometimes Upper Cretaceous-Lower Tertiary andesites and conglomerates. Some of these structures are shown in Figure 7.7. As with the deeper seated basement involved thrusts, directions of convergence implied by these structures are highly variable.

In Sonora, locally preserved sections of Lower Cretaceous marine sediments provide a convenient marker for post-Middle Cretaceous deformation(s). King (1939) mapped a series of west vergent thrusts in the central Sonora portion of the Sierra Madre Occidental. These structures involve Aptian-Albian limestones and stratigraphically higher andesites. Near Sahuaripa, Lower Cretaceous beds are thrust over Tertiary conglomerates. Generally, the folds and thrusts are discordantly overlain by Middle Tertiary silicic ignimbrites. Taliferro (1933), Imlay (1939), and Rangin (1977b) mapped portions of a southwest vergent fold/thrust belt in the Agua Prieta region of northeastern Sonora. In this area, two upper crustal deformational phases can be distinguished: (1) an Aptian-Cennomanian phase, corresponding to the basal conglomerate of the Upper Cretaceous Snake Ridge Formation, and (2) a Late Cretaceous-Early Tertiary phase, represented by the thrusting of Paleozoic and Lower Cretaceous beds over the Upper Cretaceous. Northeast of Cucurpe, Lower Cretaceos marine strata are involved in a southwest vergent nappe structure (Kitz and Anderson, 1988). North and northeast of Altar, Lower Cretaceous beds and younger andesites are folded

along west and northwest trends, and are locally overlain by Upper Jurassic? sandstones and conglomerates along northeast vergent thrusts (Jacques-Ayala et al., 1986; Garcia y Barragan et al., 1988; de Jong, 1988). Southwest of Altar, a Middle or Late Cretaceous basement involved thrust is folded and locally overturned about northwest trending axes (de Jong, 1988).

A variety of shallow thrust faults in north central Sonora involve Precambrian rocks. These structures are believed to be shallow because they are not directly associated with regional metamorphism or the post-kinematic two mica granites. East and north of Tuape, Precambrian micrographic granite and overlying Paleozoic quartzite are thrust over Upper Jurassic and Lower Cretaceous volcanic and sedimentary rocks (Anderson, et al., 1984; Rodriguez-Castaneda, 1986; Stephens and Anderson, 1986; Rodriguez-Castaneda et al., 1988). Near Rayon, Upper Proterozoic carbonates and quartzites structurally overlie a Lower Cretaceous marine section (Amaya-Martinez et al., 1988). An analogous? family of thrust faults in southeastern Arizona place Precambrian granites and schists with Paleozoic cover over Cretaceous sedimentary rocks (Cooper and Silver, 1964; G. H. Davis, 1979; Drewes, 1981).

Farther east, a major fold/thrust belt is developed in Phanerozoic sedimentary rocks of southern New Mexico, west Texas, Chihuahua, and Cohuila. Shortening in this region began in the latest Cretaceous and continued through the Early Tertiary.

In south central and western Arizona and southern California, a diversity of Late Cretaceous-Early Tertiary shallow level folds and thrusts are known. However, for the sake of brevity, these are not discussed.

Representative shallow crustal fold/thrust structures are preserved in the upper plate of the Magdalena core complex. These include the east-west folds in the Lower Cretaceous, and the north vergent thrusts of the La Lamina

complex.

Local and Regional Unconformities: The Late Cretaceous-Early Tertiary stratigraphic record of the southwestern Cordillera displays unconformities of variable duration which indirectly reflect local and/or regional tectonic disturbances. In general the unconformities are marked by conglomerates of Late Cretaceous or Early Tertiary age which rest upon Lower Cretaceous and older rocks. The conglomerates occur along the margins of larger regions that lack Late Cretaceous or Early Tertiary supracrustal rocks. In Arizona, a vast area of Late Cretaceous-Early Tertiary nondeposition (or nonpreservation) corresponds to the "Mogollon Highlands" of Cooley and Davidson (1963), who used the term "to denote a positive area in central and southern Arizona and nearby regions that furnished sediments to the Colorado Plateau and the Basin and Range provinces throughout Mesozoic and Cenozoic time." A similar "depositional gap" occurs in a broad northwest trending belt across north central Sonora (see Figure 7.2).

Geographic coincidence of these depositional gaps with the belt of regional metamorphism and basement involved thrusting is striking. The regional stratigraphic patterns may be interpreted as follows: (1) The depositional gaps represent Late Cretaceous-Early Tertiary paleohighs, or (and?) (2) strata originally present in these areas have been removed, either by erosion or by tectonic processes (i.e., Middle Tertiary detachment faulting). In the upper plate of the Magdalena core complex, the unconformity preserved above the deformed Lower Cretaceous section is a newly recognized component of this large scale scenario.

MIDDLE TERTIARY EMPLACEMENT OF LEUCOGRANITES

GENERAL DESCRIPTION AND AGE RELATIONSHIPS

Texturally diverse leucogranites of probable Middle Tertiary age flood the lower plate of the Magdalena core complex. These granites may be late phases of the more porphyritic and texturally uniform Early Tertiary two mica+garnet granite plutons. In this interpretation the leucogranites date the culmination of dynamothermal metamorphism seen in the country rocks of the porphyritic plutons. Alternatively, the leucogranites may represent a separate (Middle Tertiary?) thermal reactivation of the lower plate plutonic and metamorphic rocks. The absolute emplacement age of the leucogranite suite has yet to be established. However, the geometry of these granites, and their occurence at many structural levels above, below, and within the porphyritic plutons suggests that they are indeed products of a separate magmatic episode.

Field criteria demonstrate that the leucogranites are late in the plutonic sequence. Sills of various dimensions are injected into previously metamorphosed and layered rocks. Leucogranite dikes and veins clearly intrude across older metamorphic fabrics, and crisscross the porphyritic two mica±garnet granites. A predominence of dikes with northwest trends suggest that the leucogranites were emplaced during a period of northeast-southwest extension.

All of the leucogranites are deformed to some extent. Deformation has been accommodated by internal strain, rotation and shear of primary intrusive contacts, buckling, and boudinage. This superimposed ductile fabric intensifies toward the southwest, where most leucogranite dikes, veins, and sills are transposed into a mylonitic foliation (see next section). In Arroyo El

Salto, a young leucogranite phase (the biotite quartz syenite) discordantly intrudes the mylonitic leucogranites, but is itself slightly sheared, demonstrating that granitic plutonism continued locally during mylonitization.

GEOMETRY OF EMPLACEMENT

Figure 6.1 shows the geographic distribution of leucogranites in the Magdalena area. The largest masses of leucogranite form sills which can be followed continuously for many kilometers (see Figure 7.8). In general the leucogranite sills are localized along three structural and stratigraphic horizons:

(1) The deepest exposed granites pervade the metamorphosed rhyolite/quartz arenite series directly beneath the Guacomea Granodiorite.

(2) 300 to 700 meters up section, another sill forms the roof of the granodiorite.

(3) Farther south in the Sierra Magdalena, the largest and most extensive sill (or group of sills) occupies a higher stratigraphic horizon between underlying older granites and overlying metavolcanic and metasedimentary rocks. This sill has been mapped over an area of 300 km^2.

The leucogranite sills are interconnected by a network of pegmatite and aplite dikes and veins. Two or more dike sets can be differentiated in the west central Sierra Guacomea and in Arroyo Amolares (see Figures 7.9, 8.26 and 8.28). These leucogranite dikes have been variably deformed and rotated during southwest directed noncoaxial strain of the lower plate. The amount of shear strain associated with this ductile deformation may be quantified by restoring the dikes to their initial configuration (see Chapter 8).

Figure 7.8: Photograph showing the sill like character of the leucogranites in the west central Sierra Guacomea. View is to the south along the range front, from a vantage point due east of Rancho el Rincon. Rock symbols: pbgd = porphyritic biotite granodiorite, mqp = metamorphosed quartz porphyry, qss = quartz arenite, lgr = fine grained leucogranite and leucocratic biotite monzogranite.

Figure 7.9: Photograph of leucogranite dikes cutting stretched quartz pebble conglomerate in Arroyo Amolares. View is to the southeast. The two dominant dike sets in this area dip north and northeast (see also structural data, Figure 8.27).

Figure 7.8

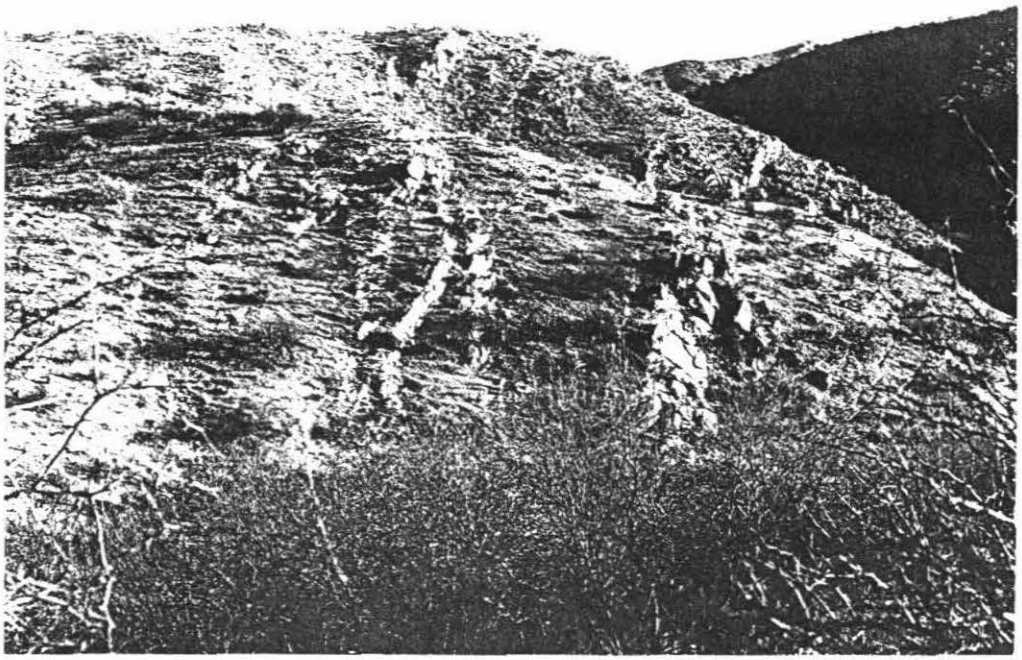

Figure 7.9

In map view the leucogranites are distributed throughout a broad northwest trending belt. The overall geometry of the leucogranite suite implies that magmas derived from a region of melting at depth "ponded" at structurally controlled levels of the middle and upper crust during their ascent. Regional extensional stresses that prevailed during plutonism facilitated the migration of magma along northwest striking cracks. The northwest trend of the leucogranite belt at map scale is probably a reflection of these regional stresses.

REGIONAL CORRELATION

Throughout the Basin and Range province the lower plates of known metamorphic core complexes contain late suites of leucogranite that predate at least some of the characteristic mylonitic deformation. The leucogranites range in composition and texture from fine or medium grained biotite monzogranite or granodiorite to fine grained muscovite-garnet granite to pegmatite to muscovite-garnet aplite. Very few have been well dated, but available data suggest Middle Tertiary emplacement ages. In the Ruby Mountains of Nevada, leucocratic biotite monzogranites, biotite granodiorites, and two mica+garnet granites have yielded U/Pb ages between 29 and 39 Ma (Wright and Snoke, 1986). In the South Mountains of Arizona, highly differentiated alaskite and two mica granite occur as late phases of a Miocene (22±4.1 Ma, U/Pb) biotite granodiorite pluton (Reynolds et al., 1986). In the Catalina Mountains, a biotite-hornblende granodiorite associated with the latest known phase of granitic plutonism has been dated at 27±2 Ma (U/Pb, Shakel et al., 1977). Other Middle Tertiary granites have been identified in southern Arizona, but are not associated with metamorphic core complexes.

These include the Cardigan Peak pluton near Ajo (about 30 Ma, U/Pb, Tosdal, unpublished data, cited in Hagstrum et al., 1987), and several small granite stocks in southeastern Arizona (Drewes; 1980, Reynolds, 1988).

In northern Sonora, young leucogranites of uncertain age are intrusive into regionally metamorphosed rocks, and are locally involved in mylonitization. These include occurrences in the Sierras Santa Teresa, Camponado, El Alamo Viejo, and Pozo Verde. In the Sierra Las Jarillas, dikes and sills of garnet bearing leucogranite intrude a group of tight to isoclinal southwest vergent overturned folds developed in greenschist to amphibolite grade metasedimentary rocks. In Cerro Carnero, leucocratic biotite granodiorite and pegmatite intrude metasedimentary rocks and are involved in a west vergent mylonite zone (de Jong, personal communication, 1988). The granodiorite has yielded a K/Ar age of 14.8±0.5 Ma on biotite. Metamorphic muscovite and biotite from the country rocks have yielded K/Ar ages between 16 and 17 Ma. Hornblende from a nearby amphibolite has a K/Ar age of 54.7±3.1 Ma. (all age determinations by Hayama et al., 1984).

The spatial coincidence of leucogranite with the lower plate mylonite zones of metamorphic core complexes throughout the Basin and Range province is striking (see Figure 7.10). In Arizona and northern Sonora, deformed leucogranites exposed in the lower plates of metamorphic core complexes define two (or perhaps three) northwest trending belts. K/Ar ages from the axial regions of the northern core complex belt have been reset to values between 30 and 18 Ma (Reynolds, et al., 1988). Similarly, K/Ar ages from pre-Middle Tertiary granites in southwestern Arizona display an eastward younging trend, from 53 to 38 Ma, as the southern belt of core complexes is approached (Tosdal and Miller, 1987). A general causative relationship between leucogranite emplacement, thermal perturbation, and mylonitization

Figure 7.10: Regional distribution of Middle Tertiary mylonite zones in the lower plates of metamorphic core complexes, Arizona and southern Sonora. Stippled regions denote mylonites; barbed lines are Late Cretaceous-Early Tertiary thrust faults; hachured lines are Middle Tertiary detachment faults; x's mark known or suspected Middle Tertiary granites. Letters mark cities listed in Figure 0.1. See text for discussion and sources of data.

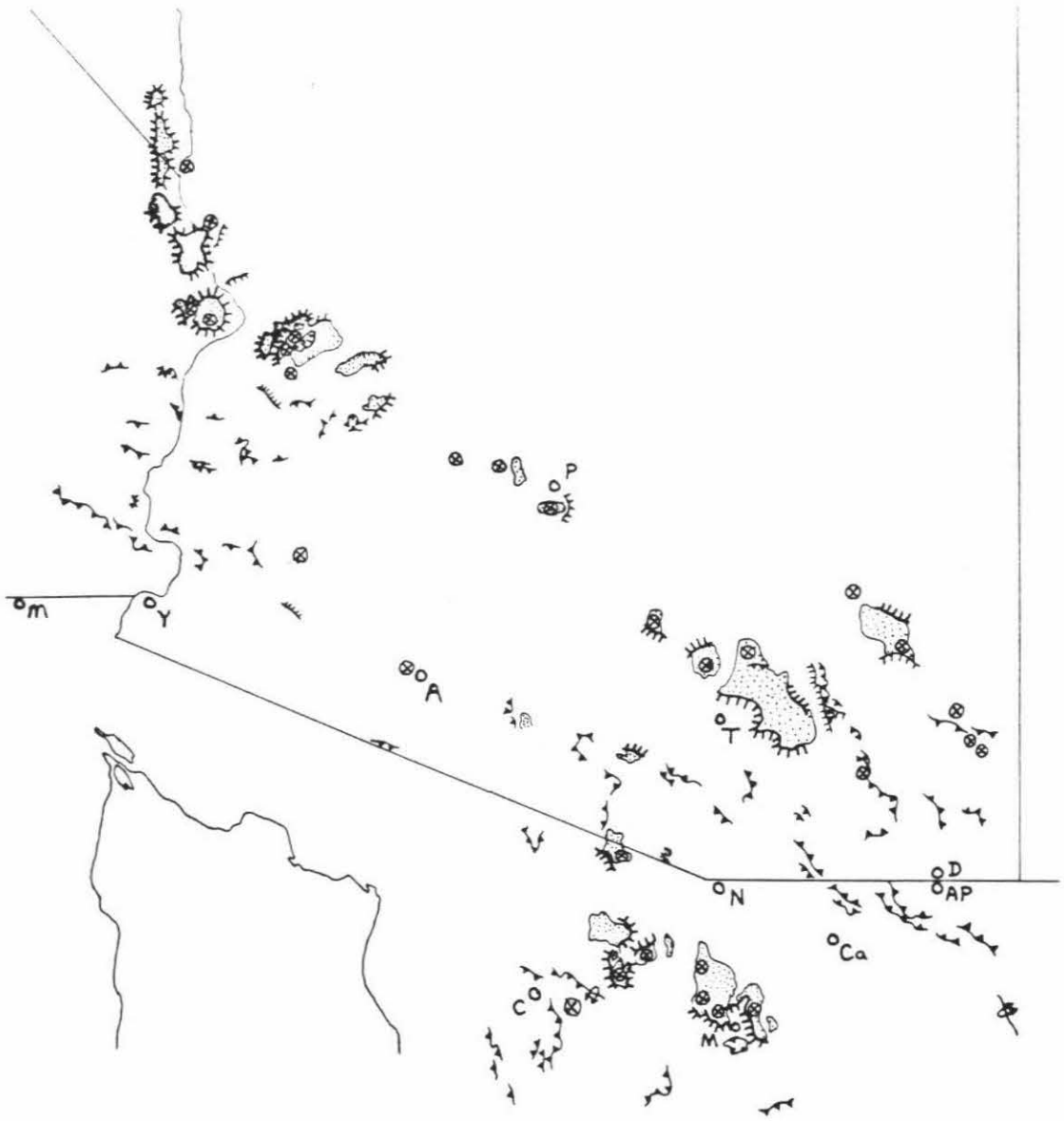

Figure 7.10

is implied. In a simplistic model, the leucogranites represent products of a Middle Tertiary thermal reactivation of the crust along localized, linear trends. Thermally driven uplift of the structurally overlying crust provided a driving mechanism for the development of regional normal sense ductile shear zones (see next section; see also Chapter 9)

POST-LEUCOGRANITE DUCTILE DEFORMATION

A significant portion of the lower plate has been affected by ductile strain subsequent to emplacement of the leucogranite suite. Structures and fabrics related to this period of deformation are described from two separate regions. Strain in both regions is localized within and near large leucogranite sills. In the **northern region**, an increasing downward deformational gradient can be demonstrated (see Figure 8.17). Crosscutting relationships indicate that an early phase of foliation development with southwestward rotation of dikes was succeeeded by slip along discrete, northeast vergent normal sense shear zones. In the **southern region** the effects of ductile strain are more extreme, and a diversity of rocks have been converted to true mylonites. An increasing upward deformational gradient is mapped over an area of 500+ square kilometers in the Sierras Magdalena and Madera (see Figures 8.2 and 8.23). This deformational zone has a structural thickness of 2 to 4 kilometers. Consistent kinematic indicators and lineations demonstrate that the rocks of the southern region were deformed in a southwest vergent noncoaxial shear zone.

NORTHERN REGION

Along the western front of the central Sierra Guacomea, leucogranite sills are exposed in the core of a north-northwest striking antiform. These

leucogranites (with their schistose volcanic/quartz arenite country rocks) are the structurally deepest known exposures of the Magdalena core complex. The leucogranite/schist assemblage shares a common deformational fabric with the overlying Guacomea Granodiorite. The shallowly east dipping basal contact of the granodiorite is well exposed for 8 kilometers along the range front (see Figure 7.8).

Mesoscopic structures: Leucogranite sills throughout the northern region display a weak to moderate foliation and sometimes a weak lineation. These fabrics are subtle due to the paucity of biotite in the granites. The foliation is expressed by a flattening of individual medium quartz grains parallel to muscovite and/or rare biotite. This quartz grain shape foliation is parallel to schistosity in the metavolcanic country rocks and is generally concordant with the sill boundaries. Near the basal contact of the Guacomea Granodiorite, the foliation in the leucogranites is more pronounced. Here the grain shape fabric is cut at angles of 30° to 40° by 1 to 4 centimeter wide, discontinuous normal sense shear zones. The shear zones verge both northeast and southwest, but the northeast directed set dominates.

Within the Guacomea Granodiorite, fabric intensity decreases from the basal contact upward. In its lower part, the granodiorite exhibits a strong foliation marked by a preferred orientation of biotite and a coincident flattening of coarse feldspar and quartz grains. This foliation is concordant to the schistosity observed in metarhyolite pendants. Weakly developed lineations trend N30-40E. The gently (10° to 20°) east dipping fabric is transected by a group of northeast dipping leucogranite dikes (see Figure 8.26). Many of the dikes display a foliation parallel to that in the granodiorite. Shear strain concentrations along dike margins indicate that they have been

rotated toward the southwest during formation of the foliation in their granodiorite host.

Structurally higher parts of the granodiorite are nonlineated and only weakly foliated. Large dikes of leucogranite within the older rock are oriented at steeper angles (50° to 70°) relative to the foliation. Post-leucogranite strain appears to be minimal. However, within the schistose roof rocks of the granodiorite, intrusive masses of leucogranite are buckled and boudinaged (see Figures 8.19-8.22). A significant amount of strain has thus been accommodated in that part of the metavolcanic series subsequent to leucogranite emplacement.

A family of discrete 1 to 50 centimeter wide ductile shear zones crosscut the strong fabrics developed in the vicinity of the basal granodiorite contact (see Figure 7.11a). Most of these shear zones dip 40° to 60° northeast and display consistent normal sense displacements. Foliated leucogranite dikes and metavolcanic schists marker units are offset distances of 5 centimeters to 3 meters along subparallel shear planes spaced anywhere from 10 centimeters to 10 meters apart. Quartz, and (locally) epidote and chlorite are concentrated along the shear surfaces. The angle between the shear zones and foliation in the host rocks is typically 30° to 40°. The shear zones clearly developed after the foliation forming event in the schists, the leucogranites, and the Guacomea Granodiorite, and by definition, after southwestward rotation of the dikes. The total displacement integrated across this late deformational zone is relatively minor (i.e., average shear strain is less than 0.5). The discrete shear zones probably reflect local readjustments of stresses near the basal granodiorite contact following the main foliation forming episode.

Figure 7.11a: Orientations of late discrete ductile shear zones, west central Sierra Guacomea.

Figure 7.11b: Orientations of discrete ductile shear zones in the Mesquital Granodiorite, north central Sierra Madera.

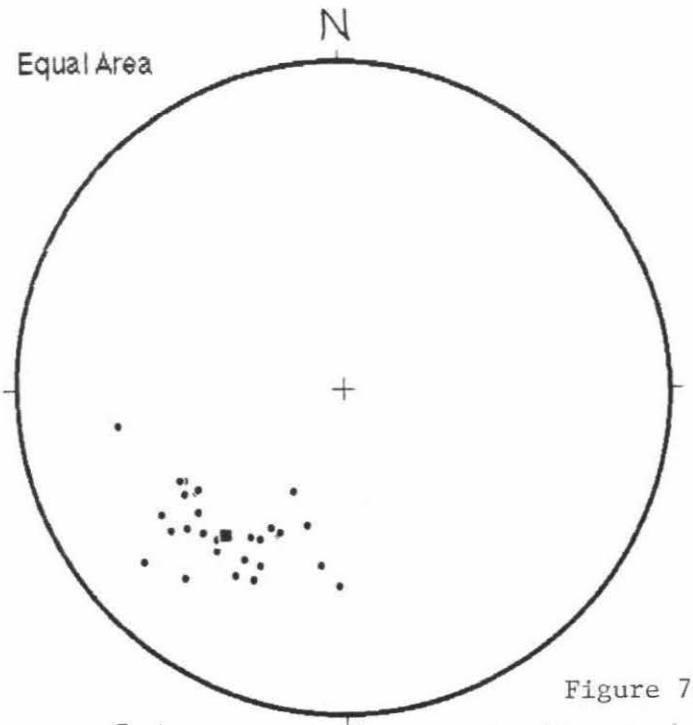

Figure 7.11a

Poles to Discrete Ductile Shear Zones, West-Central Sierra Guacomea

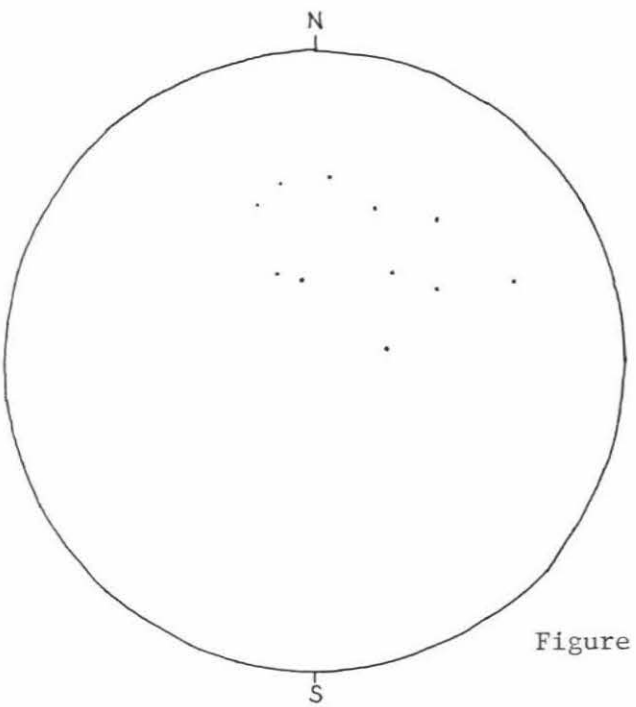

Figure 7.11b

Poles to Discrete Ductile Shear Zones, Puerto el Mesquital

Microstructures: Samples of deformed leucogranite, granodiorite, and schist were studied petrographically to determine the mechanisms and conditions of deformation, and to search for microscopic kinematic indicators. All thin sections were sliced perpendicular to foliation and parallel to lineation (if present).

The fabric in the fine to medium grained leucogranites is characterized by elongation of discrete quartz grains and partial recrystallization of the feldspars. At low strains the quartz grains are undulose and noticeably elongate, but only recrystallized near their margins. Local concentrations of shear strain are recorded by incipient recrystallization along specially oriented feldspar-quartz or feldspar-feldspar grain boundaries. Typically these recrystallized zones define two sets of planes arranged symmetrically about the quartz grain shape foliation (see Chapter 8). At higher strains the quartz grains may be completely recrystallized into highly elongate aggragates of strain free subgrains, and feldspars may be internally recrystallized. Two discrete directions of high shear strain are commonly marked by planar zones of finely recrystallized, mechanically comminuted feldspar and quartz. Normal sense displacement along these shear planes is demonstrated by the deflection of quartz grain aggregates and micas. In one leucogranite sample (MX795), a southwest dipping set of shear planes is offset by a northeast dipping shear plane, which in turn is displaced by a separate southwest vergent plane. The micro shears thus developed as conjugate sets during coaxial flattening of the leucogranite. Other samples collected closer to the basal granodiorite contact display noncoaxial fabrics. Here a northeast dipping set of shear planes dominates the structure. Quartz grains caught up in the discrete 1 to 30 centimeter wide mylonite zones may be stretched as

much as 50:1.

Microfabrics within the porphyritic Guacomea Granodiorite intensify gradationally from the top of the pluton to the bottom. Strain has been accommodated by progressive elongation of large quartz grains, partial or complete rerystallization of feldspar, and mechanical disaggregation and alignment of biotite. In the stretched quartz grains, strain is partially recovered by recrystallization along grain boundaries, however, the highly undulose cores retain their coherence at elongations as great as 8:1. Large alkali feldspar crystals have absorbed the deformation via production of smaller, strain free plagioclase and orthoclase, and the matrix feldspars are likewise recrystallized near grain boundaries. Biotite has been shredded along cleavage planes and rotated into the foliation without any apparent recrystallization. Away from the discrete shear zones, evidence for dynamic, noncoaxial strain is lacking. Biotite is symmetrically disposed about the quartz/feldspar grain shape foliation. Disequilibrium features such as shear bands, intragrain fractures, and quartz subgrain foliations are absent.

The discrete shear zones in the granodiorite preserve noncoaxial S-C microstructures. Highly elongate, dynamically recrystallized quartz ribbons and feldspar porphyroclasts with comminuted tails define an S foliation; fine grained shreds of biotite are concentrated along a unidirectional set of normal sense shear planes (C-planes). Chlorite and white mica are intergrown with the biotite, and feldspar porphyroclasts are partially seicitized. The margins of large feldspars are often recrystallized, and intragrain fractures are healed by smaller strain free feldspar grains. Within the quartz ribbons, recrystallized subgrains are usually polygonal and equiaxial, with sharply defined grain boundaries. In a few cases, elongate subgrains with serrate grain boundaries define a secondary oblique grain shape foliation. This

foliation marks the orientation of the instantaneous finite strain ellipsoid relative to the larger scale S and C planes. The overall fabric geometry of these mylonites is indicative of deformation within a northeast vergent noncoaxial shear environment (a conclusion consistent with observed offsets along the shear zones).

Conditions of Deformation: The microstructures described above permit estimation of the prevailing metamorphic conditions during the post-leucogranite ductile strain event. Early fabric development within the Guacomea Granodiorite and the leucogranite sills involved plastic strain via recrystallization. However, the presence of significantly strained, nonrecrystallized quartz grains and nonrecrystallized biotite suggests that temperatures were not high enough to anneal these minerals. The fabric probably developed in a sub-amphibolite facies environment. The absence of chlorite indicates deformational conditions above greenschsit grade and/or a lack of water. Overall fabric symmetry implies that deformation involved a significant component of coaxial shortening.

In the discrete shear zones, recovery of strain in the quartz ribbons via dynamic recrystallization and the relatively small subgrain size indicates deformation at upper greenschist facies, as does the preservation of healed microcracks in the feldspars (Simpson, 1985). The presence of chlorite and white mica in the shear bands and sericite within the feldspar porphyroclasts suggests that fluids were abundant. These shear zones thus developed in a retrograde environment at temperatures near 350^{o} C and pressures of 3-4 kilobars. They represent regions of highly localized noncoaxial deformation.

SOUTHERN REGION

Crystalline rocks of the southern region are pervaded by a mylonitic fabric that can be mapped continuously from an area of incipient development (i.e., from a line connecting Puerto el Mesquital and Picacho el Tompiate) toward the southwest, where it is most strongly developed. The most intensely deformed rocks occur at the highest structural positions, where they are bounded by the Magdalena detachment fault. Foliations throughout the upper 100-200 meters of the mylonitic sequence are subparallel to the detachment fault, but tend to dip at slightly shallower angles.

The mylonites are characterized by shallow foliations and lineations that developed as a consequence of noncoaxial strain within a southwest vergent ductile shear regime. Considering the Magdalena detachment fault to be the upper boundary of this shear zone, one finds that the structural thicknes of underlying rocks affected by mylonitization varies between 2 and 4 kilometers (see Chapter 8). Subsequent folding of the mylonitic gneisses along north-northwest trends has exposed deep levels of the shear zone in the cores of antiforms. It is thus possible to study the degree of fabric development, the prevailing deformational mechanisms, and the metamorphic environment at different positions within the shear zone. Observations described below demonstrate systematic spatial and temporal variations in these parameters.

Mesoscopic Structures: Structural elements measured throughout the southern region include mylonitic foliation, stretching lineations, shear bands, dike and vein orientations, asymmetric folds, and discrete shear zones. Some of these structures are summarized in Figure 7.3. Various lithologies have responded to the strain in different ways. Fabric transitions are

described below for three compositionally and texturally diverse rock types.

Medium to Coarse Porphyritic Granitoid Protoliths

The porphyritic biotite granodiorites and two mica±garnet granites originally had relatively uniform textures, and therefore serve as strain gauges for measuring the intensity of the superimposed mylonitic fabric. At the deepest structural levels, these plutonic rocks are unfoliated and unlineated, and may appear to be recrystallized. Dikes and sills of leucogranite crosscut the porphyritic host at many angles. The first signs of strain are reflected by a weak biotite foliation which corresponds to a slight elongation of quartz grains. At these levels a weak lineation is developed, and leucogranite veins and dikes within the granitoid are generally oriented at angles of 20^{o} to 30^{o} to the foliation.

Structurally higher exposures display convincing mylonitic fabrics. A strong compositional foliation defined by layers rich and poor in biotite is enhanced by a subparallel arrangement of flazered quartz grains and flattened feldspar. This S foliation is transected at angles of 15^{o} to 25^{o} by a set of southwest dipping normal sense shear planes (C planes). Frequently, a less penetrative antithetic set of shear planes dips 30^{o} to 50^{o} northeastward relative to S. Sheared leucogranite veins at these levels tend to be subparallel to the mylonitic foliation. The most deformed medium to coarse grained granitoids occur as highly attenuated sheets within mylonitic leucogranite less than 100 meters below a projection of the Magdalena detachment fault. These mylonites are pervaded by a unidirectional set of closely spaced, southwest vergent shear planes. The foliation is defined by extremely elongate quartz ribbons and thin lamellae of finely crushed feldspar. Angles between S and C are typically less than 10

Leucogranite Protoliths

The deepest exposures of leucogranite in the southern region intrude porphyritic biotite granodiorite or two mica granite. Where a foliation is apparent in the host rock, leucogranite dikes and veins are slightly deformed and show evidence of rotation and incipient boudinage. East of La Mesa, tabular masses of leucogranite dip 20° to 40° northeastward relative to the foliation in their host biotite granodiorite. This geometry is consistent with a model in which the leucogranite dikes have rotated southwestward during deformation of the granodiorite.

Mylonitic fabrics in the structurally higher fine grained leucogranite sills are subtle due to the paucity of biotite. However, ubiquitous crosscutting pegmatite dikes and veins record the relative importance of the superposed strain through rotation and internal deformation. An upward and southwestward increase in noncoaxial fabric intensity is demonstrated by a comparison of structures in two well exposed areas.

In Arroyo Vallecito, 1 to 5 centimeter wide pegmatite veins have been rotated and boudinaged during deformation of their fine grained biotite-muscovite-garnet monzogranite host. The veins display a significant preferred orientation relative to foliation in the granite. Figure 7.12 shows that the vein attitudes scatter symmetrically about a great circle defined by the biotite foliation. Most of the veins have rotated toward the southwest in a sense that decreases their angular discordance to the foliation. The elongation associated with rotation is generally accommodated by southwestward slip along discrete shear planes that transect the veins at angles of 20° to 30°. The net effect is to produce subparallel sheets of diamond shaped boudins. Some pegmatite veins exhibit back rotation accommodated by slip along northeast dipping shear planes. Also, most of the highly extended boudins contain

Figure 7.12: Orientations of boudinaged pegmatite veins in Arroyo Vallecito. Data points are apparent dips of the veins along various outcrop faces. The best fit plane corresponds to the foliation in the deformed fine grained biotite monzogranite host.

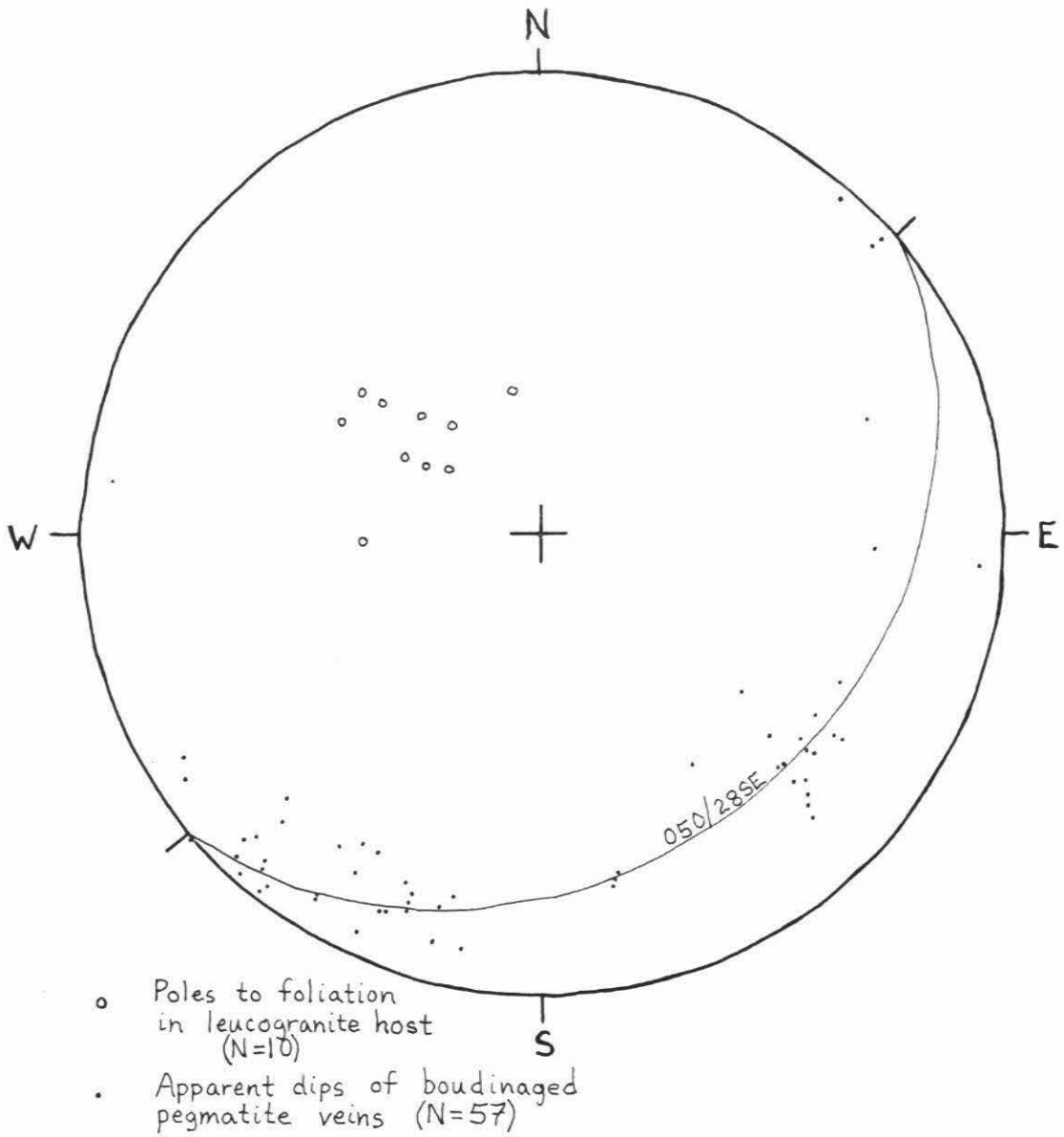
N
W
E
S
050/28SE
o Poles to foliation in leucogranite host (N=10)
. Apparent dips of boudinaged pegmatite veins (N=57)

Figure 7.12

similarly oriented fractures with relatively minor amounts of northeast slip. Clearly, deformation of these rocks involved a component of coaxial shortening strain. However, the southwest directed shear planes are dominant in this area. The simple shear strain component associated with southwestward vein rotation is quantified in Chapter 8.

In the structurally higher southern Sierra Magdalena, pegmatite veins within fine grained leucogranites or coarser porphyritic granitoids display extreme preferred orientations. The veins have been completely transposed into the penetrative mylonitic foliation of their host gneisses. Widely separated, diamond shaped boudins record elongations in excess of 500% in this plane. Southwest vergent shear planes typically truncate the boudins at angles of 20° to 30°, then rapidly shallow out into near concordance with the prevailing foliation. Frequently, elongate K-feldspar crystals within boudinaged pegmatites display antithetic (northeastward) displacement along shear planes oriented 25° to 50° to the elongation direction. These features probably represent the partitioning of strain near local textural heterogeneities within a regime of bulk southwest vergent simple shear.

Supracrustal Schist Protoliths

Rocks of the metamorphosed supracrustal series have been affected to varying degrees by post-leucogranite ductile deformation. In general their mesoscopic structures reflect the cumulative strain resulting from two or more deformational episodes. In Arroyo Amolares and in Arroyos Chupadero/Ombligo, leucogranite dikes that crosscut a pre-existing fabric have been rotated to the southwest during a later noncoaxial deformation. Both strain events can be quantified in these area (see Chapter 8). In the southern Sierra Magdalena, a strong southwest directed mesoscopic S-C fabric

pervades most of the metasedimentary schists. Interlayered sheets of highly deformed leucogranite display the same fabric orientation. Marble layers are converted into fine grained calc mylonites. Occasionally these laminated marbles display southwest vergent asymmetric folds.

Discrete Ductile Shear Zones

Figures 7.11b and 8.31 show the distribution of discrete normal sense ductile shear zones that crosscut mylonites derived from all three of the above protoliths. These 1 to 5 centimeter wide shear zones form quartz rich, curviplanar surfaces with strong S45W lineations. They are characteristically late in the deformational sequence. Offsets of marker units are measurable in decimeters or meters.

In the north central Sierra Madera, a group of south and southwest dipping discrete shear zones cut weak fabrics in the Mesquital granodiorite (see Figure 7.11b). Some were observed to displace younger aplitic phases. These ductile shear zones apparently form the lower boundary of the southwest vergent mylonite zone that dominates the structure of the range to the south.

In the southern Sierra Magdalena, discrete shear surfaces often bound large (truck sized) tabular or lozenge shaped masses of mylonitic granite gneiss. They typically dip southwestward at angles steeper than either S or C.

In the stretched quartz-sandstone-volcanic conglomerate unit near La Sauceda, the discrete shear zones dip moderately south, southwest, and northeast (see Figure 8.31). Steep northeast dipping normal shears were observed in two places. Quartz, epidote, and chlorite are commonly associated with these zones, but chlorite is not present in the adjacent metamorphic rocks.

Microstructures: The fabric transitions suggested by outcrop scale observations are further demonstrated by petrographic analysis. Microstructural traverses through the mylonite zone are described below. The three protolith types are treated separately. All samples were cut perpendicular to foliation and parallel to lineation. Statistical measurements bearing on the geometry and distribution of the planar features observed in thin section (and in oriented hand specimens) are discussed at length in Chapter 8.

Medium to Coarse Porphyritic Granitoid Protoliths

The least deformed porphyritic granodiorites and granites occur at the structurally deepest levels of the lower plate. Biotite is randomly oriented, and slightly undulose quartz grains show no obvious change in shape although they may be recrystallized near their margins. Feldspar-quartz or feldspar-feldspar grain boundaries are often disrupted by recrystallization, but the feldspars themselves display little sign of internal deformation. In one place, a steeply west dipping mesoscopic shear zone observed in biotite granodiorite proved to have a statically annealed texture in thin section.

At higher structural levels (and slightly higher strains), quartz grains are noticeably elongate and may be completely recrystallized. Feldspars are often fractured internally, and grain boundary sliding has induced the incipient development of angular porphyroclasts. Biotite, which defines the foliation at larger scales, is seen to be distorted and rotated into alignment with two conjugate sets of normal sense shear bands. The shear bands are enhanced by narrow zones of recrystallization along appropriately oriented feldspar grain boundaries. Typically, the shear bands bisect the quartz grain

shape foliation at angles of 30° to 35°. Often the southwest directed set dominates the northeast set (see Chapter 8).

True noncoaxial S-C microfabrics are developed at shallower levels and greater strains. Quartz grains are drawn out into dynamically recrystallized ribbons, and an oblique quartz subgrain foliation may be developed. Feldspars form subangular to subrounded porphyroclasts isolated in a matrix of finely comminuted feldspar and quartz. Tails of dynamically recrystallized and/or mechanically disaggregated feldspar extend from the porphyroclasts to define an S foliation parallel to the long dimension of the quartz ribbons. Shreds of biotite are localized along narrow deformation bands (C planes), which displace the S planes in a normal sense, and dip southwestward 15° to 25° relative to S. A subordinate set of antithetic shear bands may dip northeastward 30° to 50° relative to the mylonitic foliation. These antithetic shears apparently accommodate a rotation of S planes induced by the more penetrative southwest directed shear planes (see Figure 8.42).

Porphyritic granitoids sampled from the highest possible structural levels are extremely deformed. Dynamically recrystallized quartz ribbons have aspect ratios as great as 150:1. An oblique quartz subgrain foliation within the ribbons indicates rotation in a sense consistent with observed displacement along the closely spaced unidirectional shear planes. Subrounded residual feldspar porphyroclasts are completely isolated within an extremely fine grained matrix of feldspar, biotite, and quartz. The larger feldspars comprise only 10% to 50% of the rock volume. Delta type porphyroclasts (Simpson, 1986), display a consistent southwestward sense of rotation. These delta grains indicate that the strain rate has outpaced the rate of dynamic recrystallization (Ramsey and Huber, 1987). The angle between S and C is generally less than 10°; however, more precise quantification of this

angle at such high strains must be done statistically (see Chapter 8).

Leucogranite Protoliths

The fine grained leucogranites exhibit an analogous microfabric transition from deep to shallow levels of the mylonite zone. At low strains the shear bands are poorly expressed due to the fine grain size and limited abundance of biotite. However, subplanar regions of localized strain are marked by the recrystallization of grain boundaries along preferred directions. These deformation bands are symmetrically disposed about a weak quartz grain shape foliation.

At moderate to high strains the leucogranite fabrics are generally noncoaxial. Dynamically recrystallized quartz ribbons usually exhibit an oblique subgrain foliation. Southwest vergent shear bands are ubiquitous, and transect the foliation at angles between 20° and 5°. Sigma shaped feldspar porphyroclasts (Simpson, 1986), display a common orientation consistent with "asymmetric drag" of the porphyroclast tails between subparallel shear bands. In muscovite bearing lithologies, white mica porphyroclasts are back rotated relative to the foliation in a manner analogous to the "mica fish" of Lister and Snoke (1984). All of these features demonstrate that the strain was dominantly noncoaxial, with a consistent southwestward sense of rotation.

Supracrustal Schist Protoliths

Microstructures in a variety of lithologies from the supracrustal series reflect heterogeneous responses to the late ductile strain. Diverse mineral assemblages provide control on the metamorphic conditions during deformation. Fine grained metasedimentary and metavolcanic rocks preserved as xenoliths within the deepest exposed levels of the porphyritic

granitoids display moderately well foliated crystalloblastic fabrics in thin section. except for weakly undulose quartz grains, most dynamic strain has been recovered. The equilibrium mineral assemblage in these rocks is quartz-muscovite-biotite-plagioclase-magnetite.

At shallower structural levels near La Sauceda the effects of dynamic, noncoaxial strain have generally outpaced recovery via static recrystrallization. Most of the metamorphosed quartz porphyries and stretched volcanic conglomerates display crystalloblastic textures, but abundant recrystallized quartz and feldspar phenocrysts are backtilted toward the northeast relative to a foliation defined by recrystallized micas. Tails of recrystallized material that extend from the phenocrysts are consistently asymmetric in a sense indicative of southwestward rotation. In the stretched quartz-sandstone-volcanic conglomerate unite, clast elongation is dominantly accommodated by recrystallization. Noncoaxial fabrics are most conspicuous in highly attenuated quartzite pebbles and near clast boundaries. Dynamically recrystallized quartz subgrains define an oblique subgrain foliation that dips northeastward 10^{o} to 30^{o} relative to the boundary of the stretched pebble. In one sample, micro boudins of green amphibole are displaced along low angle, southwest directed normal sense shear bands. Stable mineral assemblages during noncoaxial deformation in this region include quartz-green amphibole-epidote-biotite-plagioclase-white mica-magnetite.

Pelitic schists from structurally high parts of the central and southern Sierra Magdalena record a two or three stage deformational sequence in their microstructures. An early prograde metamorphism and deformation was associated with the growth of andelosite, staurolite, and garnet porphyroblasts in a foliate matrix of biotite, muscovite, quartz, and plagioclase. A younger noncoaxial fabric is superimposed on this crystalloblastic fabric. Dynamically

recrystallized quartz ribbons are sheared in a normal sense by southwest directed C planes. An oblique subgrain foliation in the ribbons is subparallel to backtilted muscovite fish (Lister and Snoke, 1984). All of these features indicate a top-to-the-southwest sense of shear. In a few samples, late phases of noncoaxial deformation were accompanied by retrograde alteration of the primary lower amphibolite facies mineral assemblage. Chlorite has replaced biotite along shear bands, and has also filled fractures in garnet and/or staurolite. Rotation and shear of the new chlorite minerals indicates that deformation continued at these lower temperature conditions. The retrograde fabrics occur only at very high structural levels, within 50 meters of the present day projection of the Magdalena detachment fault. Samples of sheared pelitic schist from deeper structural horizons do not contain chlorite.

Conditions of Deformation: The structures described from the southern region above indicate that deformational conditions during the post-leucogranite strain event varied systematically with geographic location, structural position, and time. An upward and southwestward increase in fabric intensity is clearly demonstrated. Transition from low strain coaxial fabrics to moderate or high strain noncoaxial fabrics is accompanied by a gradual change from slip along conjugate shear planes to preferred slip along the southwest directed set. The progressive elongation of quartz grains and associated development of S foliation planes across this strain gradient shows that the S and C planes evolved **synchronously** (a similar conclusion was reached by Naruk et al., 1986, for the S-C mylonites in Arizona's Catalina Mountains). The noncoaxial strain gradient is tracked independently by the progressive southwestward rotation of pegmatite veins, and their corresponding increasing degree of preferred orientation. The overall

distribution of strain in the southern region can be modeled as the lower part of a crustal scale simple shear zone (see Chapter 8).

Mineral assemblages and microstructures show modest variations in metamorphic conditions during deformation. The deepest structural levels of the shear zone preserve prograde biotite-quartz-feldspar-muscovite assemblages. Local deformation zones marked by recrystallization of strain free quartz and feldspar are suggestive of deformation at albite-epidote-amphibolite facies (Simpson, 1985). At intermediate and shallow levels away from the Magdalena detachment fault, green amphibole, epidote, biotite, and muscovite were chemically stable during deformation. Disequilibrium features like dynamically recrystallized quartz ribbons with oblique subgrain foliations, and mechanically disaggregated feldspars (only partially annealed) indicate deformation at upper greenschist facies. These fabrics are crosscut by lower grade quartz-chlorite-epidote bearing shear zones. The mylonitic schists and orthogneisses very close to the Magdalena detachment fault are pervaded with chlorite and sericite. The localized distribution of this retrograde asemblage suggests that greenschist grade deformation was late in the sequence, and was confined to the structurally shallowest levels.

In summary, most of the mylonites formed in a regime of southwest vergent simple shear under conditions between upper greenschist and albite-epidote-amphibolite facies. The uppermost parts of the mylonitic sequence were overprinted by greenschist grade noncoaxial fabrics late in the deformational history. Spatial coincidence of the retrograde fabrics with greenschist and sub-greenschist grade brittle structures preserved along the Magdalena detachment fault suggests a causal relationship.

AGE OF MYLONITIZATION

The age of mylonitic deformation within the lower plate of the Magdalena core complex is constrained to be younger than the youngest involved leucogranite phase. In Arroyo El Salto, the bulk of the mylonitic fabric is older than the biotite quartz syenite pluton, which has intreuded very late during deformation. Radiometric age control on the leucogranites is not available, however, mica K/Ar ages from the northern Sierra Madera provide some constraints. Discrete southwest vergent shear zones that croscut weak fabrics in the Mesquital granodiorite were active at metamorphic conditions of middle to upper greenschist facies; i.e., they developed at temperatures near the blocking temperatures for argon loss in muscovite and biotite (350^{o} C and 300^{o} C, respectively). K/Ar ages of 26.3±0.6 (from biotite in the Mesquital Granodiorite) and 29.4±0.7 (from muscovite in metavolcanic wall rocks) have been obtained by Damon et al. (unpublished data). These ages suggest that the region cooled from 350^{o} C to 300^{o} C during the Late Oligocene, approximately synchronous with activity on the discrete shear zones.

Considering the northern Sierra Madera shear zones to be of the same generation as the late shears in the Sierra Magdalena, the regional, more penetrative mylonitic fabric is interpreted to be older than Late Oligocene. Leucogranites involved in the mylonitic deformation are younger than their Early Tertiary? porphyritic two mica+garnet country rocks. Hence, the age of the main mylonitic event is probably Early-Middle Oligocene.

REGIONAL CORRELATION

Mylonitic fabrics in the Magdalena area are very similar to the late penetrative shear zone fabrics preserved in the lower plates of metamorphic core complexes throughout the Basin and Range province. In most

comparable regions, the mylonites define shallow dipping noncoaxial shear zones with consistently oriented stretching lineations. The structurally highest exposed portions of the mylonitic sequences are separated from overlying unmetamorphosed upper crustal rocks by low angle, brittle detachment faults. Kinematic indicators in the mylonites display a sense of shear consistent with normal slip on the detachment faults. In many cases, the mylonites (and associated detachment faults) have been folded into doubly plunging antiforms and synforms. The intimate interlayering of sheared leucogranite with older orthogneiss, paragneiss, or schist is a common characteristic of the highly deformed regions of most Cordilleran metamorphic core complexes.

Figure 7.13 shows the regional distribution of areas affected by penetrative mylonitic deformation of known or suspected Middle Tertiary age. Occurrences are restricted to the lower plates of metamorphic core complexes. The direction of shear determined from lower plate fabrics is indicated for each area. Three striking features are apparent in the data set:

(1) the sheared rocks are aligned within narrow, northwest trending en echelon belts that roughly coincide with the locus of Middle Tertiary granitic plutonism (compare Figures 7.10 and 7.13),

(2) regional domains of consistent shear sense may be carried for distances of 500 kilometers or more, and

(3) oppositely directed shear sense domains appear to be symmetrically disposed about two northwest trending axes.

One way to model the data is to treat each shear sense domain as a regional noncoaxial shear zone. It is my opinion that the divergent shear zones were driven by instabilities resulting from thermal expansion of the crust during localized Middle Tertiary plutonism. In this model, regional

Figure 7.13: Regional distribution of Middle Tertiary core complex mylonite zones, showing sense of shear in the lower plates determined from various kinematic indicators. Directions in Arizona were compiled by Wust, 1986.

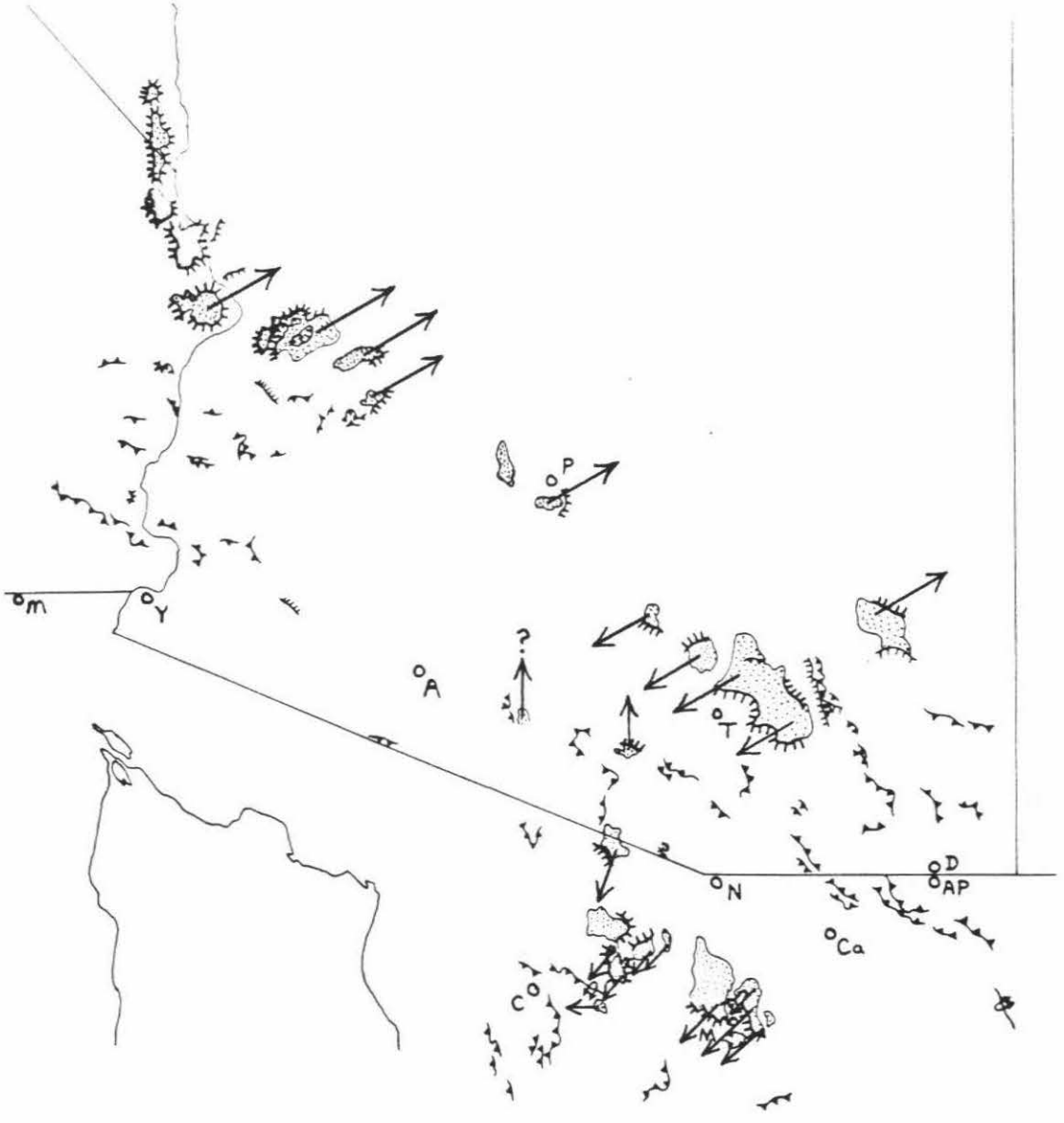

Figure 7.13

extensional strain is accommodated by crustal scale boudinage, with concentration of noncoaxial deformation on the flanks of Middle Tertiary plutonic "welts". Each of the shear sense domains in Figure 7.13 would correspond to a separate regional shear zone. The model requires that displacement in a given direction be essentially synchronous over distances of 500+ kilometers. Movements along regional shear zones with opposed vergence directions may or may not have been contemporaneous. In most areas, the absolute timing of shear zone activity awaits more precise and complete geochronological research.

EARLY MIOCENE? DETACHMENT FAULTING

Two extensive low angle fault systems mark important zones of upper crustal decoupling (or detachment) that developed in response to heterogeneous extension of the Magdalena region during Middle Tertiary time. These faults record normal sense displacements along shallow dipping surfaces. Both are associated with brittle deformation. Contemporaneity of movement has not been established, but available geological data suggest that the two faults may have acted together as a system during the same general time interval.

THE MAGDALENA DETACHMENT FAULT

As described in Chapter 6, the Magdalena detachment fault separates the structurally highest levels of the lower plate mylonitic sequence from unmetamorphosed strata of the upper plate. The fault defines the sinuous southwestern boundary of the Central High Strain Belt. It's orientation is generally concordant with shallowly dipping (less than 35°) foliations in the

subjacent mylonitic gneisses. The detachment has been broadly folded with the mylonites about north-northwest trending axes. Late Cenozoic horst blocks preserve various segments of the folded surface.

A diversity of structural criteria indicate that: (1) movement on the Magdalena detachment fault was kinematically coordinated with normal sense displacement on the subjacent mylonitic shear zone, and (2) the detachment fault acted as a strain guide along which ductilely deformed lower plate rocks were transported to shallow crustal levels. Regarding assertion (1), shear bands (C-planes) in the lower plate mylonites are parallel to the projected trace of the detachment fault, and southwest vergent kinematic indicators are consistent with normal sense displacement of the upper plate. Shear strain variations within the mylonitic sequence are the result of noncoaxial deformation in a crustal scale shear zone, with an upper boundary of similar orientation to that of the detachment fault (see Chapter 8). Assertion (2) is supported by the fact that shear strain in the lower plate increases dramatically in close proximity to the detachment fault. Also, upper greenschist-lower amphibolite grade mylonites immediately beneath the detachment fault are progressively overprinted by retrograde mineral assemblages and cataclastic fabrics indicative of deformation in a shallower, more fluid rich environment. Microbreccias exposed along the detachment surface record complex, multistage histories of ductile deformation followed by brecciation, silicification, and chloritization, then rebrecciation with additional fluid infiltration. The ultra-fine grain size of the microbreccia matrix and the abundance of hydrous minerals suggest a possible role of strain softening, or even superplasticity. Overall spatial and temporal fabric relations demonstrate that the area affected by low angle normal faulting evolved from a diffuse zone of ductile strain to a localized zone of brittle strain.

Cataclastic deformation apparently became focused along the high strain portion of a mylonite zone as it was uplifted to shallower crustal levels.

THE COCOSPERA FAULT

The low angle fault that marks the base of the Cocospera Formation in the Northeastern Low Strain Belt is informally referred to as the **Cocospera fault.** Two separate segments of this fault were mapped. Near Puerto la Bandera and Highway 2, the gently south dipping surface wraps around the southern end of the Sierra El Pinito. In the vicinity of the Rio Cocospera canyon, the fault bounds the northern Sierra Madera on three sides. High angle normal faults cut the Cocospera fault in both areas.

The Cocospera fault may have tectonically excised significant portions of the lower plate type stratigraphy. It juxtaposes various facies and stratigraphic horizons of the Cocospera Formation with rhyolite, quartz arenite, or granite porphyry. The rhyolite cobble conglomerate unit (representative of the upper part of the felsic volcanic series) is notably missing. In the Rio Cocospera canyon, the fault cuts deeply into the rhyolite/sandstone sequence, and truncates the northeastern part of the Presa Granite.

Brittle fabrics preserved near the Cocospera fault indicate activity at shallow crustal levels. Along its northern segment, the fault is marked by a narrow (1/3 to 2 meter wide) gouge zone in rhyolite porphyry. Farther south, structurally underlying quartz arenites, rhyolite, and granite porphyry are brecciated and silicified. However, this zone of brittle deformation is not as pervasively developed as that associated with the Magdalena detachment fault.

Normal sense displacement along the Cocospera fault is inferred from younger over older structural relationships, and from the apparent omission

of strata. Directions and magnitude of displacement are uncertain due to an absence of kinematic indicators and piercing points. It is not known whether the Cocospera fault was active as one continuous surface or if displacement was accommodated along various segments at different times.

TIMING OF DETACHMENT FAULTING

The age of displacement along the two low angle faults is at present only loosely constrained by sparse geochronological data. Brittle fabrics of the Magdalena detachment fault are older than the crosscutting biotite quartz latite dikes of the Sierra Madera, but are no older than the mylonites they overprint and retrograde. The microbreccias formed at temperatures below 300° C (the temperature above which quartz behaves ductilely), hence they are probably younger than the Late Oligocene mica cooling ages of the northern Sierra Madera (Damon et al., unpublished data, 1988). The Cocospera fault cuts the Presa Granite, and by a similar argument, must be younger than the granite's 33±0.6 Ma biotite K/Ar age (Gilmont, 1978). Detachment faulting occurred prior to Middle? Miocene folding of the lower plate. Finally, clasts of Sierra Madera type coarse grained biotite monzogranite in folded conglomerate beds of the upper Intermontane Group show that the lower plate was exposed to erosion prior to post-Early Miocene folding of the upper plate (these conglomerates are believed to be stratigraphically younger than Early Miocene rhyolites and basalts reported farther south; see Miranda and Quiroz, 1988). The detachment faults were therefore probably active between Late Oligocene and Early Miocene time.

INTERPRETATION AND REGIONAL CORRELATION

The Magdalena detachment fault and the Cocospera fault belong to a

family of Middle Tertiary low angle normal faults exposed throughout the Basin and Range province. These faults are generally characterized by brittle deformational fabrics and localized hydrothermal alteration. Various crystalline and supracrustal lithologies may be juxtaposed, sometimes as imbricate slices bounded by subparallel or splaying normal faults. The most widely studied detachment faults occur in Cordilleran metamorphic core complexes, where low angle fault surfaces of great areal extent (1000 to 15000 square kilometers) separate diverse upper crustal rocks from mylonitic crystalline rocks representative of middle crustal depths. Geologists agree that the core complexes represent regions of pronounced intracontinental extension, and that detachment faults and mylonite zones were instrumental in their development. However, many questions have been raised regarding the role that the detachment faults and mylonites played in partitioning extensional strain at a crustal scale. Hotly debated topics include:

(1) the absolute age and duration of detachment faulting compared to mylonitic deformation,

(2) the amount of displacement along the detachment surface,

(3) the original dip of the detachment faults and/or mylonite zones, and

(4) the thermal and mechanical evolution of the crust in regions of core complex development.

Over the past 10 or 12 years, efforts to model detachment faults in a context of regional continental extension have produced the two alternative schools of thought summarized below. In **"evolving simple shear zone"** models (see G. H. Davis, 1980, 1983; G. A. Davis, et al., 1986; Wernicke, 1985), the upper and middle crust is extended by normal sense displacement along discrete, upward tapering simple shear zones (see Figure 7.14a). Detachment faults represent surfaces of localized slip along the upper crustal, brittle

Figure 7.14a: Shear zone model for metamorphic core complex development. Reproduced from G. A. Davis, et al., 1986.

Figure 7.14b: "Megaboudinage" model for extension of the continental crust. Reproduced and modified from G. H. Davis, 1980.

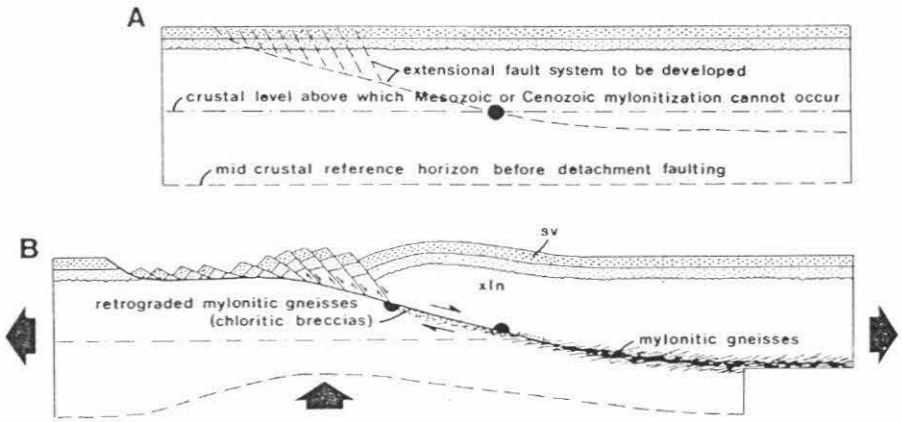

Diagram illustrating development of evolving shear zone during lithospheric extension. A: Configuration of crust prior to onset of extension of crystalline basement and overlying sedimentary and volcanic cover. Depth of section is about 20 km with no vertical exaggeration. B: Configuration of distended crust after about 20% extension (from A) and isostatic uplift. Section is balanced. Lower-plate rocks are drawn upward and out from beneath upper-plate rocks. Mylonitic gneisses formed below crustal levels indicated by dash-dot line are transported to higher structural levels where they are retrograded and cataclastically deformed.

GEOLOGY, January 1986 (G.A. Davis, et al.)

Figure 7.14a

Boudinage characteristics (from Ramsay, 1967). Stippling added to denote regions of likely cataclastic deformation. Decollement zones would preferentially develop at corners of blocks in upper diagram and within necked ends of lensoids in lower diagram.

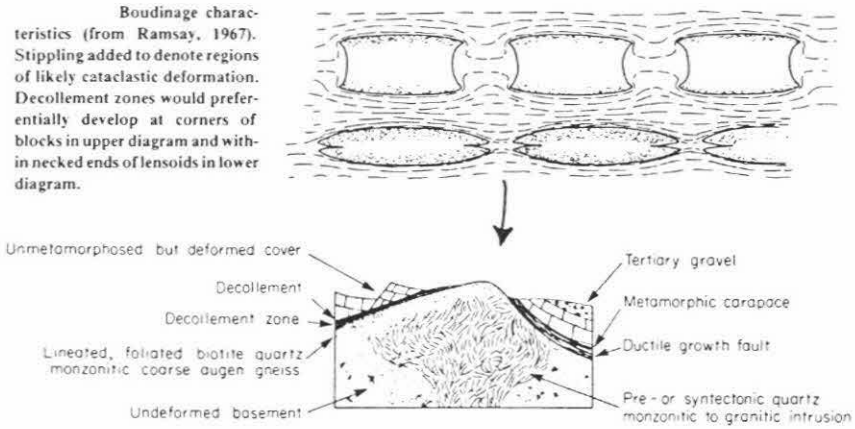

(from G.H. Davis, 1980)

Figure 7.14b

segments of these shear zones, while coeval mylonites record more distributed ductile deformation accumulated near the shear zones at depth. During shear zone activity, the mylonites are dragged upward into regions of progressively more brittle deformation, where displacement is concentrated at the top of the mylonite zone. Thus the mylonites presently exposed at the surface are slightly older than the cataclasites that mark the detachment fault.

Evolving shear zone models are compatable with the upward transition from ductile mylonitic fabrics to cataclastic fabrics observed in transects through most core complexes. Lower plate fabrics approach a simple shear geometry, with displacement in the same direction as that indicated by the rotation of upper plate fault blocks. The models provide a mechanism for the uplift of middle crustal plutonic and metamorphic rocks. Considering normal slip along the shear zone to be the only means of uplift, total displacement along the detachment fault can be estimated from simple trigonometry. The amount of displacement depends upon: (1) the depth of the lower plate rocks (now at the surface) at the inception of normal faulting, (2) the original dip of the shear zone, and (3) the amount of shear zone rotation during displacement. Figure 7.14a illustrates the geometrical constraints on displacement provided by various evolving shear zone models. Such models have been integrated into regional syntheses of Middle Tertiary extension across the Cordilleran hinterland (see G. H. Davis, 1980, 1983; Wernicke, 1985). An essential feature of these crustal scale syntheses is that most of the extensional strain is partitioned into narrow deformation zones which penetrate to at least middle crustal levels. The shallow dipping, subplanar zones are generally oriented at right angles to the regional extension direction. While the hanging walls may extend somewhat along subsiduary normal faults, the footwalls are treated as rigid blocks. At this scale the crust

can be viewed as being pulled apart into "megaboudins" (G.H. Davis, 1980; see also Figure 7.14b).

In contrast, **"uniform stretching"** models (Rehrig and Reynolds, 1980; Miller et al., 1983; Hamilton, 1987; Gans, 1987) require that extensional strain be distributed more evenly throughout the crustal column (see Figure 7.15). Detachment faults are thought to represent "exhumed" portions of the Middle Tertiary brittle-ductile transition. Above these sharply defined interfaces, upper crustal rocks extend in a brittle fashion via imbricate normal faulting and block rotation. Below the detachment faults, middle and lower crustal lithologies extend via ductile mechanisms. Strain is accommodated by displacement along anastomosing shear zones and/or pervasive flattening, and thinned areas of the lower plate are rejuvenated by influxes of synextensional magma (Gans, 1987; Hamilton, 1987). Thermal effects of these magmas may elevate the brittle-ductile transition (Gans, 1987).

Uniform stretching models differ from evolving shear zone models in at least five fundamental ways:

(1) extension is relatively uniform throughout a given vertical crustal profile,

(2) magmatism is important in the extensional process,

(3) uplift of the lower plate is driven by vertical forces (bouyancy and isostacy) associated with thermal input from the magmas and distension of the upper crust,

(4) only late in the extensional history do upper crustal detachment faults become kinematically coordinated with normal sense mylonite zones of the lower plate, and

(5) estimated displacements across the detachment faults are on the order of 5 to 15 kilometers rather than 40 to 60 kilometers.

Figure 7.15: Two uniform stretching models for metamorphic core complex development. Reproduced from Rehrig and Reynolds (1980), and Gans (1987).

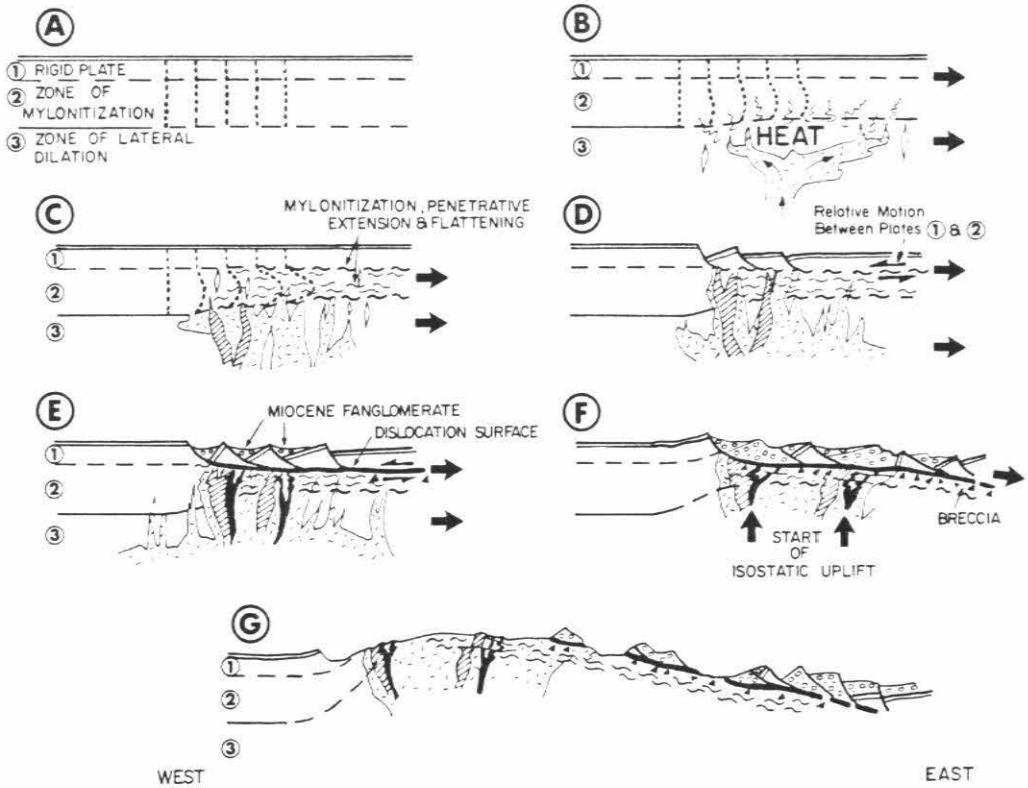

Model for Tertiary evolution of metamorphic core complexes. (A) Concept of three crustal layers, each responding distinctly to Tertiary heating and tensional stress. (B) Magma emplacement and east-northeast-directed extension initiate necking (stretching) in zone 2. (C) Continued extension in zone 3 leads to tensional separation and intrusive dilation; mylonitization develops in more ductile zone 2. (D) Differences in response to crustal extension between zones 1 and 2 create differential strain and fragmentation of rigid plate. (E) Continued differential strain between zones 1 and 2 and dissipation of heat creates the dislocation of surface and further rotational faulting of upper-plate blocks; rapid fanglomerate-breccia accumulation within fault-bounded troughs; clasts mainly from nonmylonitic plate 1, but exposure and erosion of mylonite zone may occur locally. (F) As tectonic denudation proceeds, area of maximum thinning responds to removal of zone 1 by isostatic uplift and deformational thinning in zone 2. (G) Present configuration of complex. (Rehrig + Reynolds, 1980)

Figure 15

Gans: Crustal Stretching Model for the Eastern Great Basin (1987)

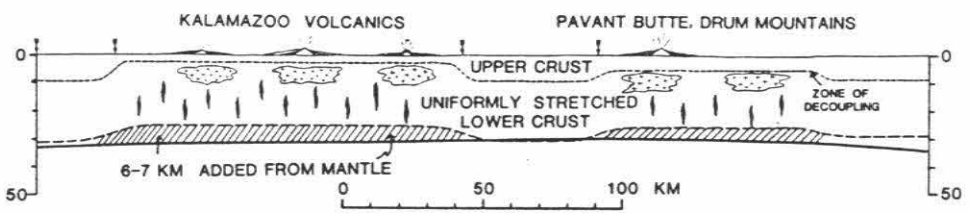

A highly generalized present-day cross section of the eastern Great Basin that illustrates the two-layer, open-system model for crustal stretching. See text for discussion.

Detachment fault/mylonite relationships preserved in the Magdalena core complex shed fresh light on some of the controversies surrounding intracontinental extension. In my opinion, evolution of the Magdalena detachment fault involved a combination of the two models described above. Figure 7.16 illustrates the probable sequential history of crustal extension in the Magdalena area. The following points are emphasized:

(1) The Early Tertiary? porphyritic two mica granites record a transition from regional metamorphism and deformation (via thrust faulting?) to more localized magmatism. These plutons were emplaced at relatively shallow crustal levels (12 to 15 kilometers depth) within a northwest trending belt of finite width. Their role in the extension process is unclear, but it seems that thermal effects of the plutonic suite may have weakened this particular region of crust.

(2) Temporal association of magmatism with the early phases of extension is demonstrated by the ubiquitous occurrence of northwest trending leucogranite dikes along the axis of the two mica granite belt. Contemporaneous leucogranite sills were emplaced at various depths into a subhorizontally layered medium (this layering may have been produced by an earlier episode of coaxial flattening). Further evidence for synextensional magmatism is provided by some of the upper plate volcanic rocks, which have yielded Late Oligocene to Early Miocene K/Ar ages.

(3) The leucogranites are products of Middle Tertiary crustal melting induced by an influx of basaltic? magma at depth. Melting occurred along a northwest trending axis. An associated linear thermal anomaly resulted in bouyant uplift of the crust, and probably northeast-southwest stretching of strata situated above the leucogranites. Upper crustal normal faults such as the Cocospera fault may have developed at this time. A normal fault (or

Figure 7.16: Preferred model for tectonic development of the Magdalena metamorphic core complex. True scale: one inch = 5.9 kilometers. This model incorporates the geologic, structural, and strain data of Chapters 6-8. The sections are not completely balanced, but they do depict the geometrical features of the deformational sequence more accurately than the schematic profiles of Figures 9.1-9.6. In this model, a crustal section comprised Precambrian basement (pC) overlain by Jurassic volcanic/plutonic rocks (J), Upper Jurassic-Lower Cretaceous quartz pebble conglomnerate (J_U-K_L), and Lower Cretaceous marine strata (K_L) is shortened (barbed lines = thrust faults) and metamorphosed during Late Cretaceous and early Tertiary time. This deformed stratigraphy is intruded by (and inflated by?) post-kinematic two mica granite plutons (T_E) during the Early Tertiary. The onset of Middle Tertiary extension is marked by emplacement of leucogranite dikes and sills into the middle and lower upper crust, and extrusion of volcanic rocks at the surface (Tm). Thermal bouyancy of the region pervaded by leucogranite causes the upper crustal section to become gravitationally unstable. A southwest vergent normal sense ductile shear zone nucleates near the most extensive leucogranite sill, while extensional strain is relieved at shallower crustal levels by brittle slip along normal faults (hachured lines). As extension proceeds, one of the upper crustal normal faults merges with the ductile shear zone, facilitating the uplift of mylonites to the surface. See text for further discussion.

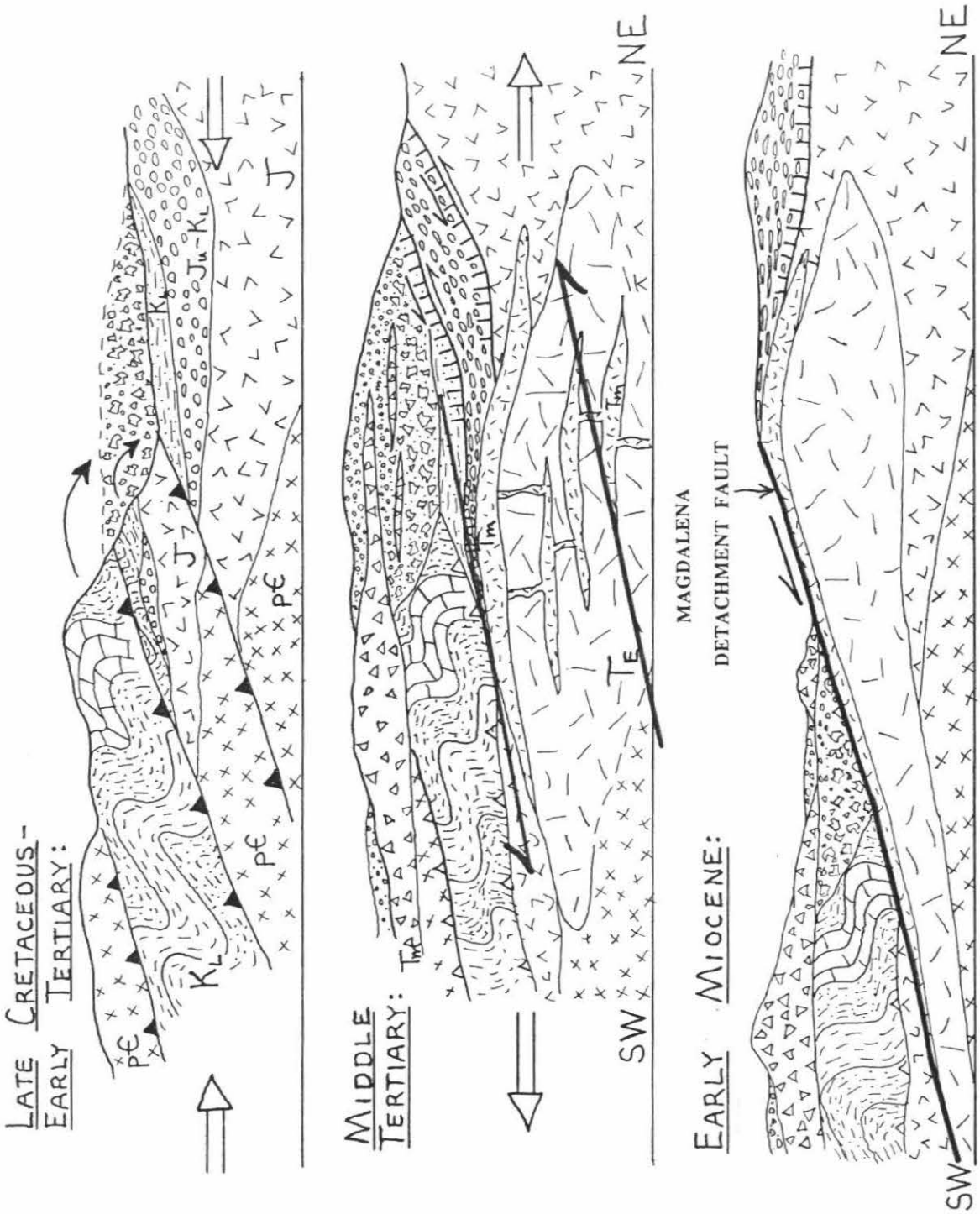
LATE CRETACEOUS-
EARLY TERTIARY:
pC
pC
pC
K
K
J
J
Ju-K
MIDDLE
TERTIARY:
Tma
Tm
Tm
Te
SW
NE
MAGDALENA
DETACHMENT FAULT
EARLY MIOCENE:
SW
NE

FIGURE 7.16

normally reactivated thrust fault) at the base of the Lower Cretaceous marine sequence is postulated.

(4) Thermal upwelling produced gravitational instabilities along preferred structural horizons, particularly near the contact between the leucogranite sill of the Sierra Magdalena and the overlying supracrustal section. Displacement at this level was directed southwestward away from the axis of the leucogranite belt. The region affected by noncoaxial deformation eventually became a broad zone of distributed shear strain. Constraints imposed by pre-extensional leucogranite/supracrustal contact relationships indicate that the shear zone nucleated at a shallow dip (30° or less).

(5) As displacement accumulated on the shear zone, mylonitic rocks were translated closer to the surface, and shear strain was localized within a narrow interval. Sometime during this movement phase, an upper crustal normal fault (the proto Magdalena detachment fault) "captured" the mylonite zone and facilitated its uplift and transport through the brittle regime. One consequence of this process was the excisement of sheared rocks corresponding to the upper half of the mylonite zone (see Chapter 8). In addition, large portions of the supracrustal section were cut out by the Magdalena detachment fault.

(6) The magnitude of displacement along the Magdalena detachment fault is constrained by the fact that rocks presently exposed beneath the fault originated at depths between 10 and 15 kilometers. Displacement calculations depend on whether uplift was due solely to normal slip on the detachment fault, or if a certain amount of thermally or isostatically driven vertical uplift preceded or accompanied early phases of extension. In the first case, uplift of the 10 or 15 kilometer deep rocks along a 30° southwest dipping shear zone yields displacements of 20 or 30 kilometers, respectively. In the second case, a

superimposed component of 5 kilometers vertical uplift would reduce displacement estimates by 10 kilometers. Finite strain measurements across the mylonite zone demonstrate that a minimum of 10 kilometers displacement was accommodated by ductile deformation in the lower plate (see Chapter 8).

MIOCENE? FOLDING

A significant Late Cenozoic shortening event is recorded by north-northwest trending folds in both the lower and upper plates of the Magdalena core complex. These folds developed subsequent to detachment faulting but prior to the onset of Basin and Range style block faulting. The detachment surface itself is broadly folded along similar northwesterly trends, and has been locally reactivated.

LOWER PLATE FOLDS

Middle Tertiary mylonites of the lower plate have been broadly folded about north-northwest trending axes. These folds are evident in the map patterns as well as the foliation distributions. The cores of antiforms are generally occupied by porphyritic granitoids and associated deep level rocks, while the axes of synforms are marked by thick exposures of the deformed supracrustal section.

Figure 7.3 shows folds derived exclusively from measurements of mylonitic foliation in granitic rocks. Representative fold axes are shallow and may be doubly plunging. The average fold trend is north-northwest. Wavelengths range from 3 to 6 kilometers. Some fold axes appear to be offset slightly between various block faulted domains. These offsets are useful in reconstructing the distribution of horst blocks prior to Basin and Range extension (see next section).

UPPER PLATE FOLDS AND THRUSTS

Contractional structures in the upper plate include a fold/thrust belt developed in the low hills between the Sierra Madera and the Magdalena-Cucurpe road. These north-northwest structures involve Early Miocene basalts and tuffs, and stratigraphically higher conglomerates that contain lower plate clasts. Hence, the folding is younger than uplift of the lower plate along the Magdalena detachment fault. One anticlinal fold axis is well exposed in gypsum beds, siltstones, and conglomerates southwest of El Yeso. A deeper portion of the folded section is broken by thrust faults within a 6 to 8 kilometer long zone east of El Babiso (see Plate 2). In one location, the sedimentary breccia unit is thrust east-northeastward over purple-maroon conglomerates of the middle Intermontane Group. Farther up section, the first andesite flow unit has been structurally repeated at least once. Siltstones beneath this flow locally exhibit tight, overturned folds indicative of east-northeast vergence (see 7.17a-b).

The Magdalena detachment fault was probably reactivated as a slip surface during the Miocene shortening event. East of El Yeso, dikes which cut microbreccias of the detachment surface and sedimentary rocks of the upper plate have been truncated by renewed movement on the fault. The direction and magnitude of this late displacement are not constrained, but the general consistency of dike orientations in both the upper and lower plates suggests that associated rotational effects were minimal.

Figure 7.17a: Photograph showing thrust contact (arrows) between andesite (and) and underlying folded lithic sandstone, siltstone, and shale beds (ss) of the sedimentary breccia unit. View is toward the northwest from a location 3 km west-northwest of El Babiso. Hammer is 18 inches long.

Figure 7.17b: Photograph from same outcrop as Figure 7.17a, showing overturned folds in the sandstone/siltstone/shale sequence immediately beneath thrust fault. View is toward the northwest. Hammer is 18 inches long.

Figure 7.17a

Figure 7.17b

LATE CENOZOIC BLOCK FAULTING

The Late Cenozoic tectonic evolution of the Magdalena region is characterized by block faulting in a regime of modest extension. This young deformational phase is responsible for the present day distribution of mountains and valleys. Block faults have been mapped throughout the lower plate, where they displace the folded mylonitic sequence and offset various segments of the Magdalena detachment fault (and also the Cocospera fault). High angle faults in the upper plate have not been mapped completely, but appear to follow similar trends.

The block faults typically separate uplifted bedrock exposures from old alluvium. Where clearly exposed they display a normal fault geometry, with dips ranging between 75° and 50°. Projections of offset marker units demonstrate displacements of tens of meters to more than 2500 meters. Fault trends show two preferred directions of high angle faulting: N30E±10 and N20W±10. The northwest set may dominate; however, conflicting crosscutting relationships indicate that late movements of the two fault sets were contemporaneous.

The Late Cenozoic block faults are interpreted to be dip slip normal faults of "Basin and Range" style (Stewart, 1978). These faults developed in response to extensional stresses in the upper crust. Bulk extension due to block faulting can be roughly determined by reconstructing the various horst blocks of the lower plate. A simplistic comparison of the horst shapes indicates that many of the block margins can be fit together like pieces of a jigsaw puzzle. Generally the region has extended in an east-west direction. Overall Basin and Range extension is estimated to be on the order of 10% to 15%, compatable with values calculated by Stewart (1978) for the Great Basin

in Nevada and Utah.

CHAPTER 8:

STRAIN ANALYSIS

The structures and fabrics described in Chapter 7 reveal in a qualitative way the sequence of deformation leading to development of the Magdalena metamorphic core complex. **Quantitative** constraints on the geometry, mechanics, and history of strain are presented below. Specifically, finite strain gradients associated with two separate ductile deformation events are mapped across the lower plate. The effects of the Middle Tertiary? noncoaxial mylonitic deformation are separated from an earlier (Late Cretaceous to Early Tertiary?) regional fabric, and the associated deformed plutono-stratigraphic sequences are "destrained" to their initial configuration. Only then can early geometry of the Magdalena core complex and its subsequent tectonic evolution be properly modeled in three dimensions. At the close of this chapter, the finite strain data are integrated into a series of balanced cross sections that demonstrate quantitatively how extensional strain was partitioned within this particular region of continental crust.

The methods of strain analysis described below involve measurement of the shape and orientation of deformed lithological markers and comparison with undeformed shapes and orientations of the same markers. Fortunately, the Magdalena area preserves a diversity of strain markers that can be correlated with confidence between deformed and undeformed settings. Strain measurements were accomplished on outcrops in the field, and on oriented hand samples, thin sections, and photographs in the laboratory. Sample locations are plotted on Plate 4.

Finite strain data from the lower plate are subdivided below into two groups: (1) strains measured from the lower plate supracrustal assemblage, and (2) strains measured from the granitic plutonic/orthogneiss complex. The reduced data are contoured as separate gradients in Figures 8.1 and 8.2. The gradient of (2) represents a locally intense deformational event, mostly of noncoaxial geometry, that postdates Middle Tertiary emplacement of the leucogranites. The degree of noncoaxiality in a given area is measured by the amount of rotation of late leucogranite dikes relative to their host rocks, and the intensity of S-C fabric. The gradient of (1) represents the total accumulation of strain in the supracrustal rocks since Middle Cretaceous time. In most places the strain pattern is dominated by the younger (Late Oligocene-Early Miocene?) deformation. However, in special areas it is possible to partition strains between the young granites and their country rocks, and hence deduce the relative importance of the pre-leucogranite and post-leucogranite deformations.

In all of the following strain analyses, measurement errors associated with the determination of angles, axial ratios, or separation distances are assumed to be random and only on the order of a few percent. These sources of error are ignored, but in some cases they may contribute significantly to the overall scatter in the data. In addition, it is assumed that any volume change associated with deformation is negligible. Deviations of the strain data from ideal behavior are attributed to a variety of partitioning effects discussed at length below. Validity of the shape analyses depends in part on the number of measurements in a given direction (strains based on fewer than 10 measurements should be interpreted cautiously). Some skewness in the data sets might have resulted from sampling bias. Such effects are not addressed here.

Figure 8.1: Distribution of longitudinal strains in pre-leucogranite lithologies of the lower plate. Irrotational strains in the Guacomea granodiorite are included. Blank regions are generally underlain by younger granites, except in the northwern Sierra Jojoba, where metavolcanic rocks were not sampled.

Figure 8.2: Distribution of longitudinal strains related to the Middle Tertiary deformation. Measurements are from the porphyritic two mica granitoids and from the leucogranite suite.

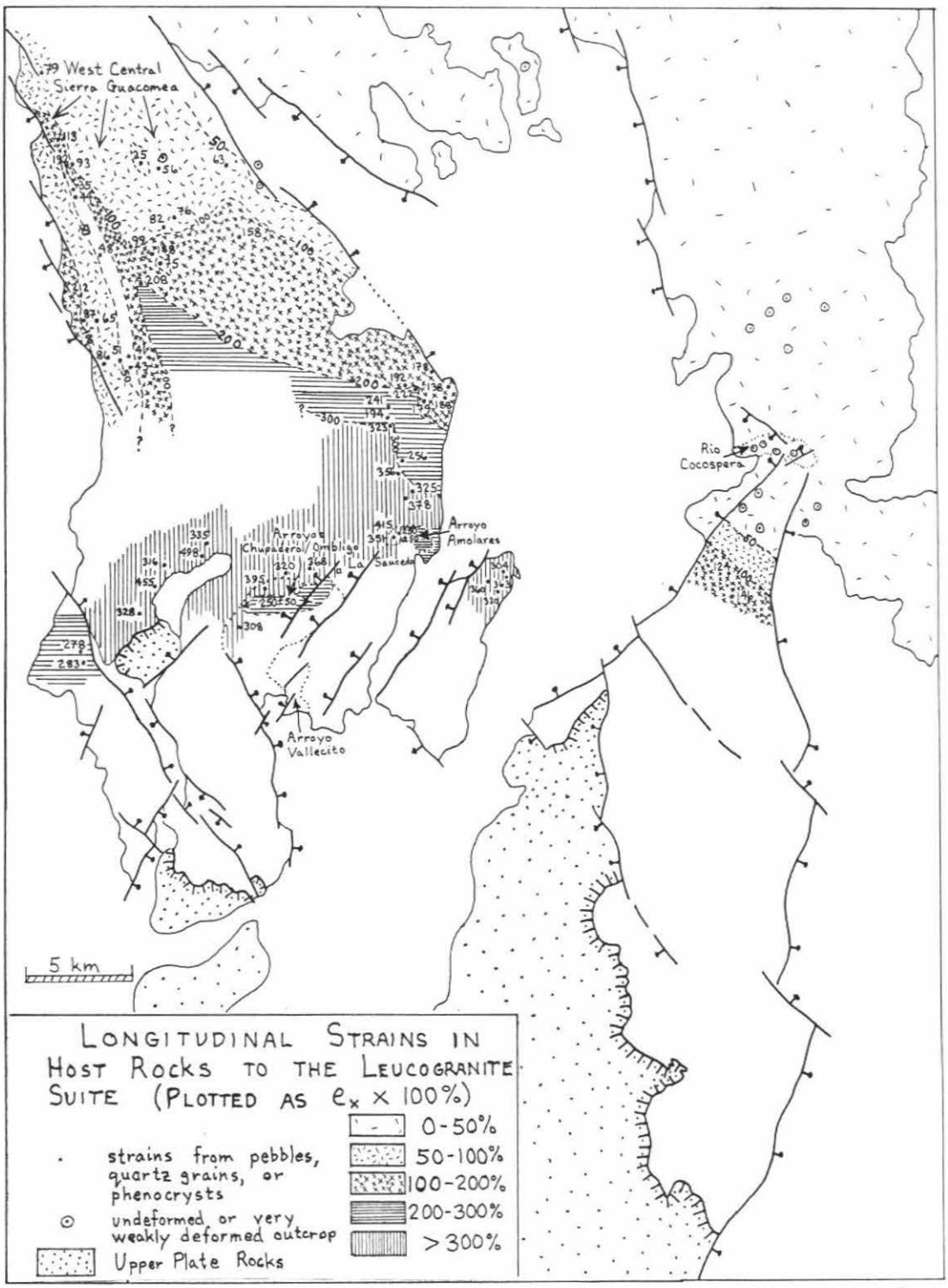
West Central
Sierra Guacomea
Rio
Cocospera
Arroyo
Chupadero
Ombligo
Arroyo
Amolares
Arroyo
Vallecito
5 km
LONGITUDINAL STRAINS IN HOST ROCKS TO THE LEUCOGRANITE SUITE (PLOTTED AS $e_x \times 100\%$)
0-50%
50-100%
100-200%
200-300%
>300%
strains from pebbles, quartz grains, or phenocrysts
undeformed or very weakly deformed outcrop
Upper Plate Rocks

Figure 8.1

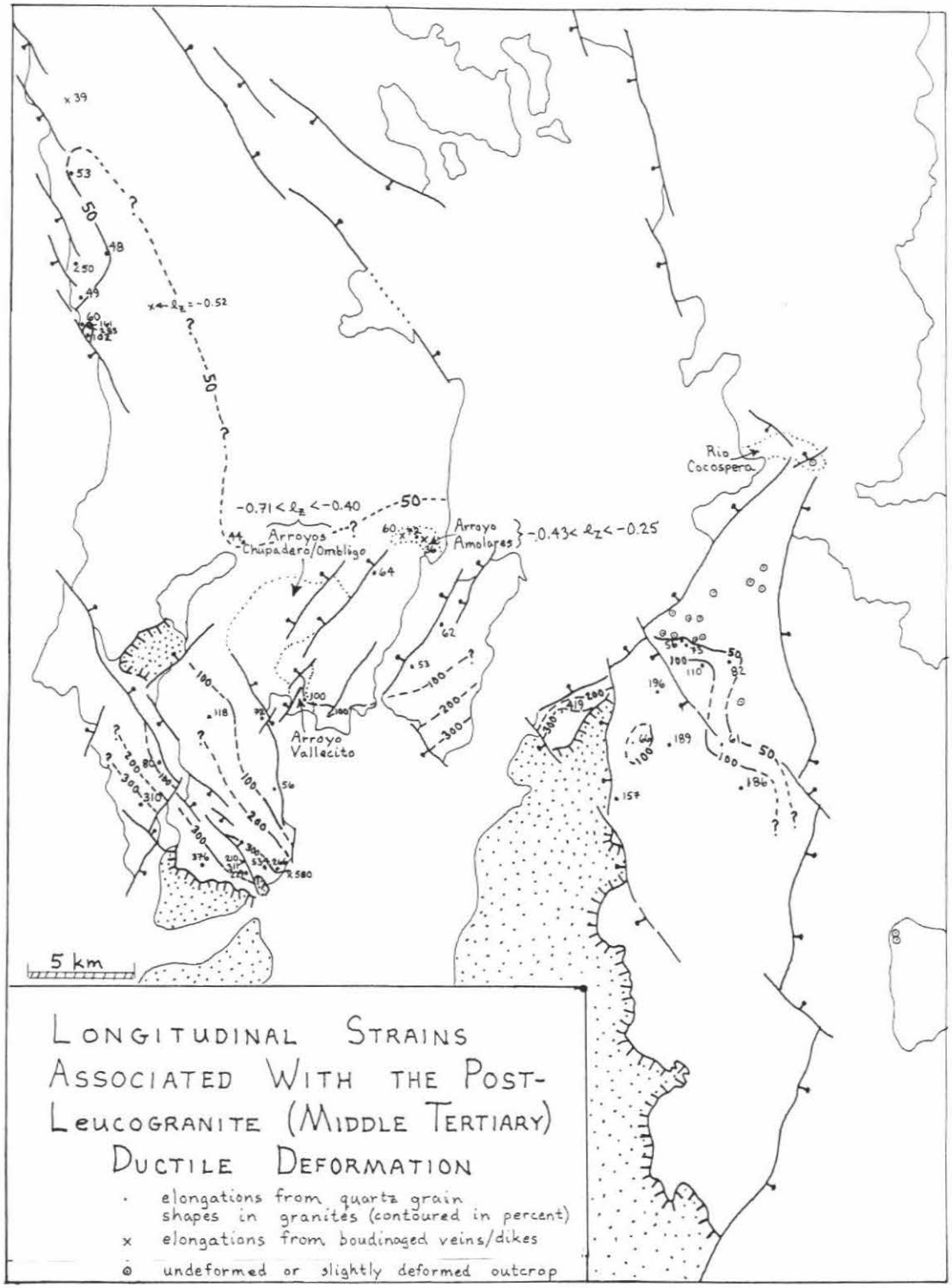
x 39
53
50
48
250
49
60
x ← ℓ_z = -0.52
50
-0.71 < ℓ_z < -0.40
50
Arroyos Chupadero/Ombligo
Arroyo Amolares
-0.43 < ℓ_z < -0.25
Rio Cocospera
64
62
53
100
200
300
Arroyo Vallecito
118
56
100
200
300
310
376
580
189
186
157
5 km
LONGITUDINAL STRAINS ASSOCIATED WITH THE POST-LEUCOGRANITE (MIDDLE TERTIARY) DUCTILE DEFORMATION
. elongations from quartz grain shapes in granites (contoured in percent)
x elongations from boudinaged veins/dikes
⊙ undeformed or slightly deformed outcrop

Figure 8.2

FINITE STRAINS IN THE PRE-LATE CRETACEOUS SUPRACRUSTAL SERIES

Deformed volcanic, hypabyssal, and sedimentary rocks of the supracrustal series contain a diversity of distinctive markers suitable for finite strain analysis. Quartz and/or feldspar phenocrysts and conglomerate clasts are approximated as ellipsoidal particles in the following calculations. Adaptations of the R_f/Φ technique (Ramsey, 1967; Lisle, 1985; de Paor, 1988) are utilized to determine the irrotational strain parameters (e_x, e_y, and e_z) and the k values (Flinn, 1962). These derived quantities are useful in assessing the geometry and variability of the bulk strain absorbed in the supracrustal rocks since Middle Cretaceous time.

R_f/Φ theory was first developed mathematically by Ramsey (1967). The fundamental equations describe the change in shape of any ellipsoid of any initial shape and orientation as it deforms **passively** within a **homogeneously straining** medium. Essentially, each particle will deform and rotate an amount dependent on the magnitude and orientation of the superimposed strain. The R_f/Φ technique is easily applied in the field: one only needs to measure the axial ratios (R_f) of several deformed markers (50 or more are best), and their long axis orientations (Φ) relative to a reference plane such as schistosity. Typically, only the deformed state is known, but from a standardized R_f/Φ plot the tectonic strain can be accurately estimated, and the initial variation in particle shapes can be determined. Also, the presence or absence of a pre-tectonic shape fabric may be qualitatively deduced from the inherent asymmetry or symmetry of the plot (see Lisle, 1985). The Magdalena region is special in that initial particle shape distributions predicted from the R_f/Φ theory may be checked against **actual**

shape distributions in undeformed parts of the same section.

MEASUREMENTS FROM THE RHYOLITE AND GRANITE PORPHYRY UNITS

Method: The orientations and shapes of feldspar and/or quartz phenocrysts were statistically determined in various samples of metamorphosed quartz porphyry and granite porphyry. Hand specimens were sliced parallel to lineation and perpendicular to foliation, thereby affording a view of the XZ principle plane of the finite strain ellipsoid. The sliced surfaces were coated with verithane (liquid plastic) to enhance the textural contrast between deformed phenocrysts and their recrystallized matrix. For each strain marker, R_f (the axial ratio) and Φ (the angle between the long axis and the schistosity) were measured and recorded.

Many of the samples were also sliced perpendicular to both foliation and lineation, i.e., parallel to the YZ principle plane of the finite strain ellipsoid. Measurements in this plane are necessary to completely characterize the strain in three dimensions, and thus quantify the deviation of the deformation from plane strain. For those samples where only the XZ plane was measured, values of maximum elongation (e_x) were calculated assuming plane strain deformation.

R_f/Φ measurements proved to be easier (and probably more accurate) in thin section. The outlines of recrystallized quartz and feldspar phenocrysts are usually well defined relative to a finer grained groundmass (see Figure 8.3a). Where the phenocrysts and groundmass are recrystallized to similar grain sizes, the area of the deformed marker is generally marked by an absence of mica.

Figure 8.3a: Photomicrograph of deformed rhyolite porphyry, showing highly elongate, recystallized quartz and feldspar phenocrysts (labeled Q and F, respectively).

Figure 8.3b: Photomicrograph of undeformed rhyolite porphyry, showing original shapes of quartz and feldspar phenocrysts.

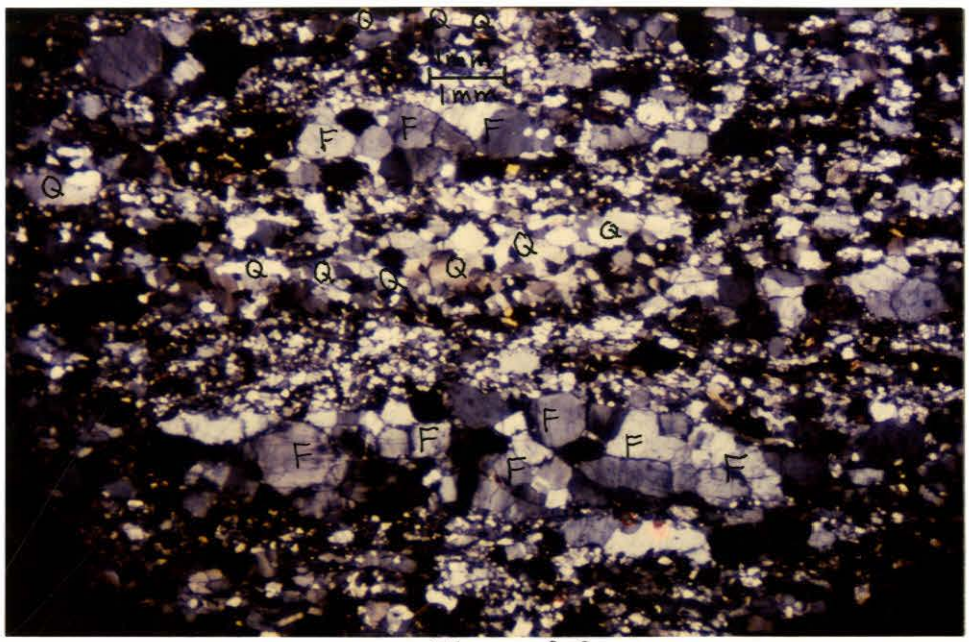

Figure 8.3a

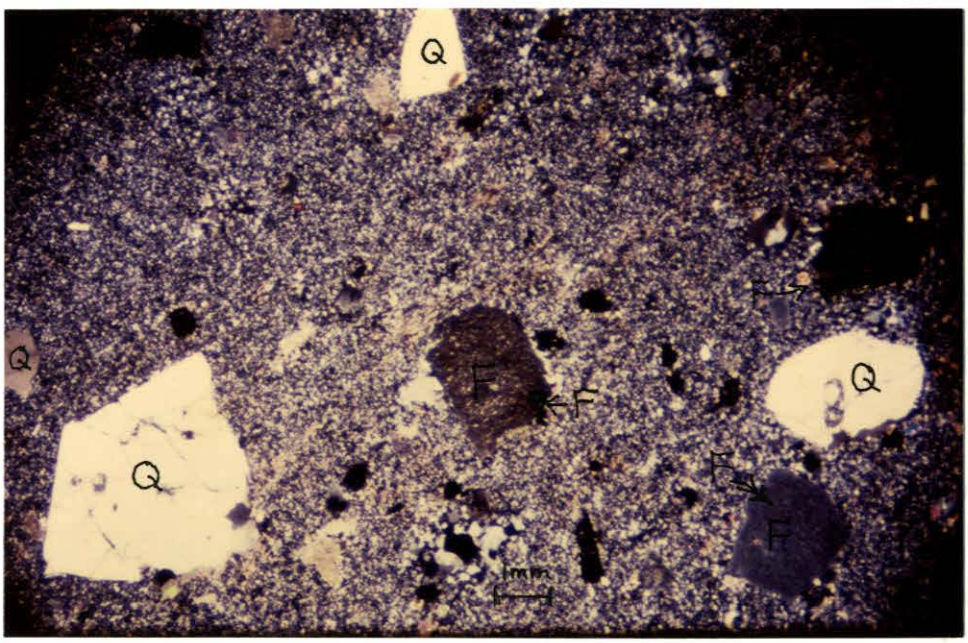

Figure 8.3b

Finally, for independent control on the R_f/Φ analyses, the shapes of randomly oriented feldspar and quartz phenocrysts were measured in several **undeformed** samples of rhyolite (see Figure 8.3b) and granite porphyry. These data demonstrate the range and variability of initial ellipticity (R_i) inherent in the strain markers.

Data Analysis: R_f/Φ data are suited for two alternative modes of finite strain analysis: simple numerical methods involving statistical averages, and more elaborate graphical methods designed to extract information about initial particle shapes and/or initial preferred orientation. A primary objective of the data analysis is to determine tectonic strains in the XZ and YZ planes. For this purpose, the harmonic mean of the R_f values probably gives as good an estimate of the strain as any other method, particularly at high strains (Lisle, 1985). However, in areas where only the deformed state can be measured, it is prudent to use graphical techniques such as the shape sector grid method of Lisle (1985) or the hyperbolic net method of de Paor (1988). These more time consuming R_f/Φ plots allow one to visually assess the data distribution as well as deduce the pre-tectonic geometric configuration of the strain markers.

Raw strain data from rocks of the Magdalena region are compiled in Appendix C. The data are displayed in separate R_f/Φ plots for each measured sample and direction. Some of these plots are specifically referred to in succeeding discussions regarding initial shape distributions and deviations from ideality. Calculated averages and strain parameters for each data set are tabulated in Appendix D. These strains are integrated with the results of measurements from the rhyolite cobble conglomerate unit and the quartz-sandstone-volcanic conglomerate unit to produce the summary strain map of Figure 8.1.

R_i/Θ plots from undeformed rhyolite and granite porphyry samples give a sense of the initial variability in particle shapes. It is observed that that the long axes of phenocrysts are randomly oriented. Quartz phenocrysts are almost spherical (R_i between 1.0 and 1.6), while feldspar shapes are more elongate and irregular (R_i between 1.25 and 2.0). Comparison of these initial shape data with R_f/Φ plots from the deformed section provides a means of assessing the validity of the R_f/Φ analyses. For these lithologies it can be argued that the range in R_i's predicted by the R_f/Φ plots (see Lisle, 1985, for description of the technique) is consistent with the **actual** initial shape variability (i.e., the R_f/Φ plots yield theoretical R_i values of 1.6 or less for the quartz markers, and 2.0 or less for the feldspars).

The R_f/Φ data from deformed rhyolite and granite porphyries exemplify two important sources of heterogeneity:

(1) Strain values derived from the deformed phenocrysts generally **underestimate** the true tectonic strain. This condition is due to the partitioning of strain into the more deformable, finer grained groundmass. The effect is most conspicuous in deformed parts of the rhyolite cobble conglomerate unit. Here, the phenocryst constituents of the stretched cobbles exhibit axial ratios much smaller than their hosts (see Figure 8.7, next subsection). Clearly, the groundmass has absorbed more of the strain.

(2) In almost all cases, the quartz phenocrysts are less deformed than the feldspars. Figure 8.4 compares the measured axial ratios of quartz and feldspar markers from the same samples. The respective ratios are plotted as a function of distance from a northwesterly line marking the first appearance of strain in the supracrustal series (this line is labeled "metamorphic front" on Plate 4). Most of the samples exhibit $R_{feldspar}/R_{quartz}$ ratios between 1 and 2. However, $R_{feldspar}/R_{quartz}$ is significantly higher in four samples that display strong

noncoaxial fabrics. A likely reason for this disparity is proposed in Figure 8.5. In a regime of coaxial deformation, the phenocrysts are subjected to a symmetric stress field, and do not rotate much after their initial allignment within the XY plane (foliation plane). Strain is absorbed fairly equally in both phenocryst types; however, the feldspars do seem to recrystallize and stretch more readily. In areas of strong noncoaxial deformation the quartz phenocrysts, being initially subspherical, tend to roll in a direction consistent with the rotational sense of the strain. The feldspars, being more angular and inequant, are confined to foliation planes and thereby absorb more of the associated finite elongation.

Figure 8.4: Comparison of strained quartz and feldspar phenocrysts in the metamorphosed rhyolite and granite porphyry units. The ratio of $R_{feldspar}$ to R_{quartz} is plotted as a function of distance southwest from the first appearance of schistosity in this unit (see Plate 4). Samples with penetrative noncoaxial fabrics are indicated.

Figure 8.5: Model illustrating the different strain behavior of quartz and feldspar phenocrysts in rhyolites subjected to coaxial and noncoaxial deformations.

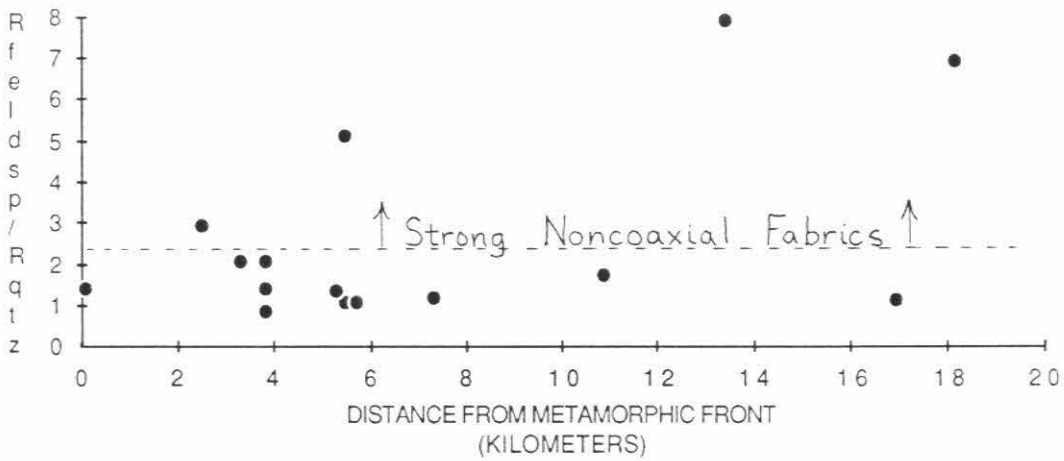

Figure 8.4

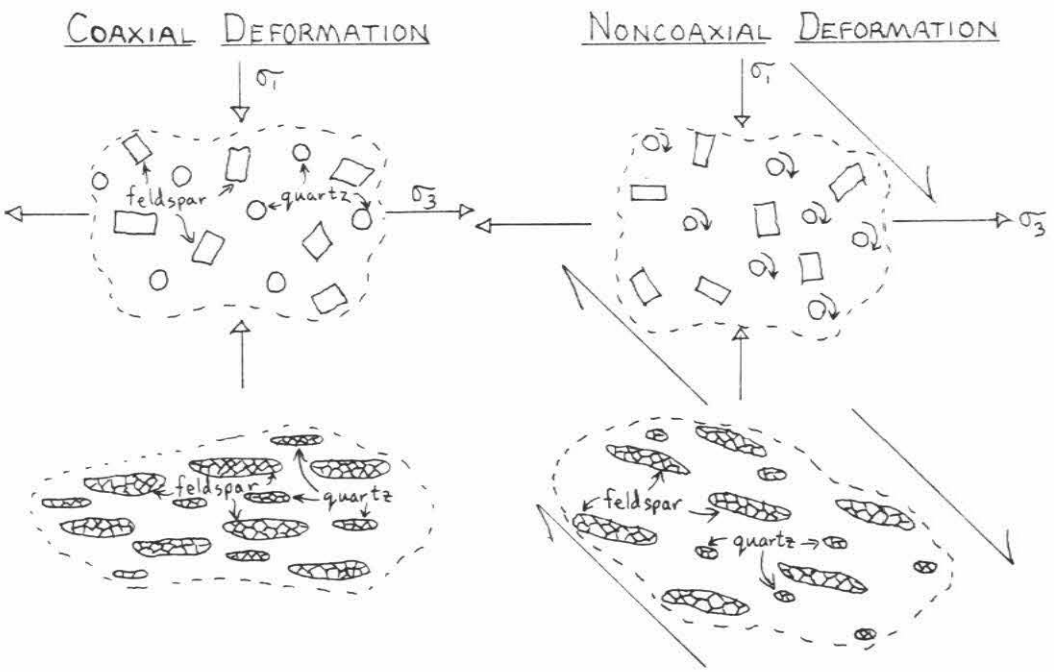

Figure 8.5

MEASUREMENTS FROM THE RHYOLITE COBBLE CONGLOMERATE UNIT

Method: R_f/Φ data were collected from exposures of stretched volcanic conglomerate encountered in the lower plate. Measurements were performed either on outcrops or on oriented photographs. Surfaces corresponding to the XZ and YZ planes of the finite strain ellipsoid were preferentially selected for analysis. As in the preceding subsection, the data are plotted on R_f/Φ graphs in Appendix C. Calculated R_f averages and strain parameters are compiled in Appendix D. One outcrop of undeformed rhyolite cobble conglomerate was measured to provide control on the initial shape distribution of the strain markers.

Data Analysis: The initial shape data were collected near Puerto la Bandera, where rhyolite conglomerate overlies rhyolite porphyry along a subhorizontal depositional contact (see Figure 8.6a). Bedding in the conglomerate is defined by a weak preferred orientation of cobbles parallel to the contact. R_i/Θ plots demonstrate the statistical alignment of clasts, and indicate that initial ellipticities ranged from 1.0 to 1.8.

In the deformed section (see Figure 8.6b), R_f/Φ plots exhibit a symmetric clustering of markers about the plane of schistosity. Tectonic strains derived from graphical fitting techniques (Lisle, 1985; de Paor, 1988) tend to be very similar to those calculated via the harmonic mean method. The range in R_i predicted by the R_f/Φ plots is within the limits established in the undeformed setting.

Of particular interest to the analysis is the partitioning of strain between phenocrysts and groundmass in the stretched rhyolite cobbles. As

Figure 8.6a: Photograph of undeformed rhyolite cobble conglomerate in depositional contact with underlying rhyolite porphyry. The site is located immediately southeast of Puerto La Bandera. Hammer is 18 inches long.

Figure 8.6b: Photograph of deformed rhyolite cobble conglomerate, from Arroyo Agua Zarca. Tape is 1 inch wide.

Figure 8.6a

Figure 8.6b

proposed earlier, the phenocrysts yield lower R values than the cobbles because, by virtue of their relative rigidity, the phenocrysts do not deform as easily as their finer grained groundmass. Because the volcanic conglomerate is clast supported, the stretched cobbles are believed to closely represent the bulk tectonic strain (there is very little sedimentary matrix in which to partition the deformation). The volcanic conglomerate unit therefore yields maximum finite strains to which lesser elongations of associated phenocrysts can be compared. In Figure 8.7, average R_f values of deformed quartz and feldspar phenocrysts are plotted against R_f values from corresponding stretched volcanic conglomerate exposures. The resultant curves indicate the degree to which the phenocrysts underestimate the strain. The figure provides a valuable calibration device. An average R_f value measured from deformed quartz and/or feldspar phenocrysts in the metamorphosed quartz porphyry unit may be converted to a "true" R_f value by simply determining the abscissa of that particular point on the appropriate curve.

MEASUREMENTS FROM THE COCOSPERA CONGLOMERATE

Method: Conglomerates of the Cocospera Formation were studied extensively in both the undeformed and deformed settings. All R_i/Θ and R_f/Φ measurements were conducted on joint surfaces oriented perpendicular to bedding or schistosity. Unlike the measurements from the volcanic conglomerate unit, axial ratios were determined along a wide spectrum of azimuths perpendicular to the XY plane. R_f/Φ or R_i/Θ plots and calculated strain parameters for each data set are organized in Appendices C and D.

Data Analysis: Because the three dimensional shapes and orientations of conglomerate clasts are known in both the final and initial

Figure 8.7: Graph illustrating the partitioning of strain between rhyolite cobbles of the deformed volcanic conglomerate unit and constituent quartz and feldspar phenocrysts.

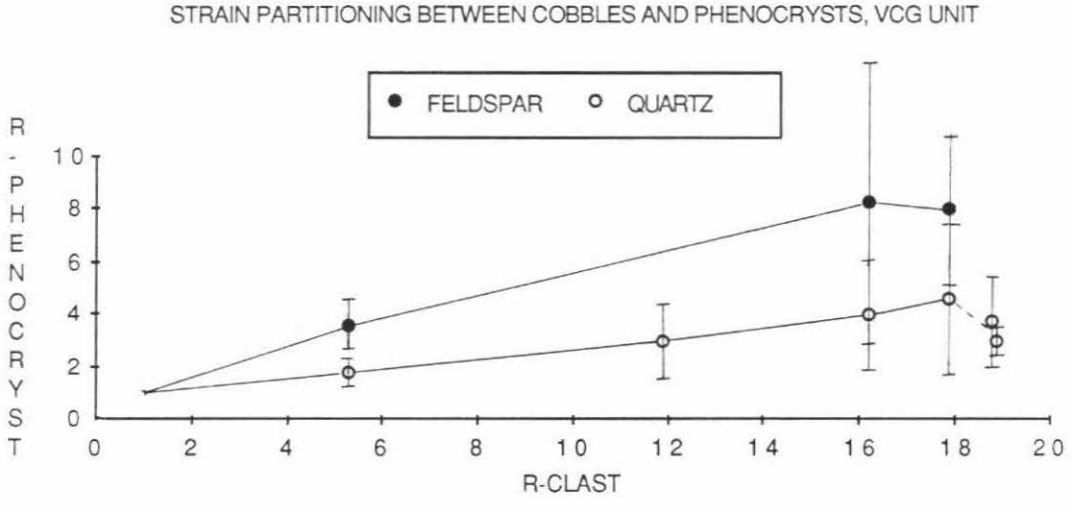
STRAIN PARTITIONING BETWEEN COBBLES AND PHENOCRYSTS, VCG UNIT
FELDSPAR
QUARTZ
R-PHENOCRYST
R-CLAST
0
2
4
6
8
10
12
14
16
18
20

Figure 8.7

states, the data are suited for a more sophisticated type of analysis. Essentially, an average "initial fabric ellipsoid" (with uncertainties) may be determined for the undeformed setting, and then mathematically removed from "final fabric ellipsoids" corresponding to various deformed settings, thus yielding the true tectonic strains (Wheeler, 1986). Important features of this analysis are illustrated graphically throughout the following discussion.

The initial fabric ellipsoid is calculated from data measured in the Rio Cocospera canyon. In this area, elongate conglomerate clasts display a moderate preferred orientation symmetric about bedding (see Figure 8.8a; see also the R_i/Θ plots in Appendix C). On some bedding planes, the long axes of clasts are weakly aligned in a N30E direction. Many of the quartzite cobbles are broken by steep, conjugate extensional fractures which tend to strike northwest. The fractures imply that some strain was associated with the rotation of clasts into the bedding plane. The observed preferred orientation of clasts may be due to one or more of three alternative mechanisms: (1) alignment or imbrication during original sedimentation, (2) compaction after burial, or (3) low intensity tectonic strain. Unfortunately, the relative importance of these mechanisms (all of which might have been active at different times) cannot be determined. Figure 8.9 shows the azimuthal variation in R_i within the XY plane. The cobbles are slightly more elongate in the NE-SW direction. From this plot, the dimensions of the initial fabric ellipsoid are measured. The resultant X:Y:Z ratio (with uncertainties) embodies 67% of the data. In the terminology of Wheeler (1986), the undeformed setting has a "triaxially symmetric" shape fabric.

Gilmont (1978) measured the actual three dimensional shapes of 252 unoriented pebbles collected from five unspecified locations in the Cocospera Formation. On a sphericity form diagram, most of these pebbles plot in the

Figure 8.8a: Photograph of weakly deformed Cocospera conglomerate from the Rio Cocospera canyon. Tape is 1 inch wide.

Figure 8.8b: Photograph of highly deformed Cocospera conglomerate from Arroyo Amolares. Tape is 1 inch wide.

Figure 8.9: Plot showing the azimuthal variation of axial ratios for 385 pebbles in the Rio Cocospera canyon. Each data point represents the arithmetic mean of an R_i population measured from a specific outcrop. The error bars indicate one standard deviation dispersion about the mean. The data are plotted in the plane of bedding (where maximum axial ratios are observed). Dimensions of the maximum and minimum initial fabric ellipsoids are outlined. The observed direction of pebble alignment within the bedding plane is indicated.

Figure 8.8a

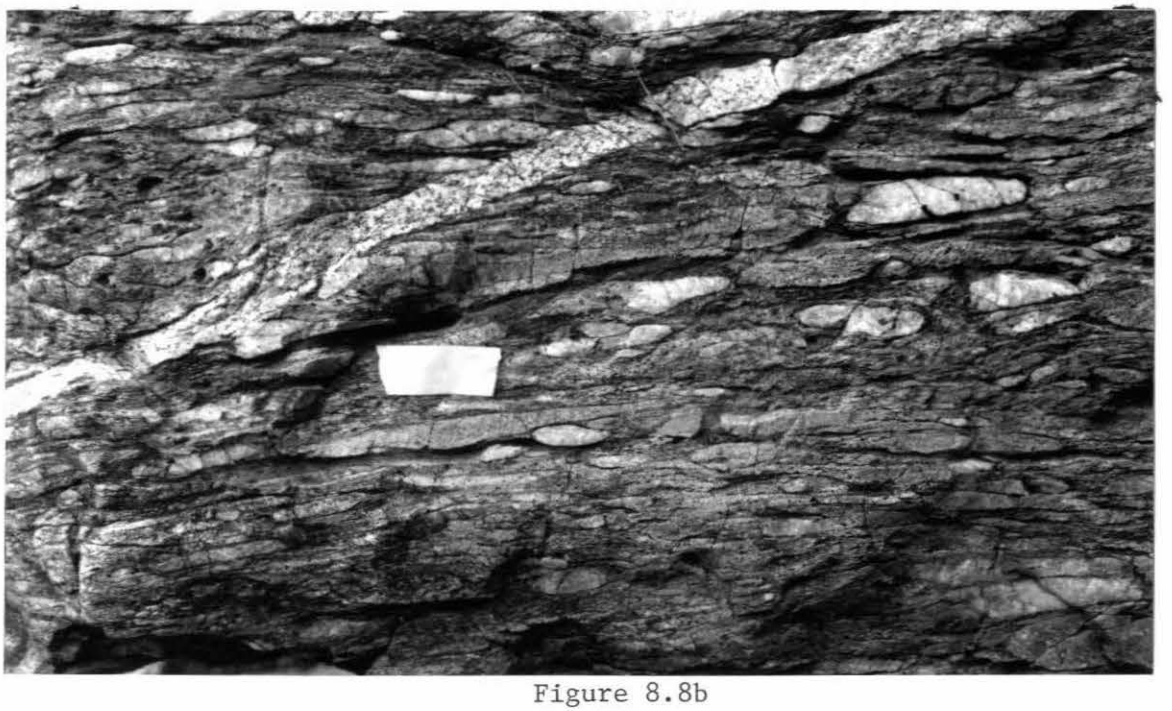

Figure 8.8b

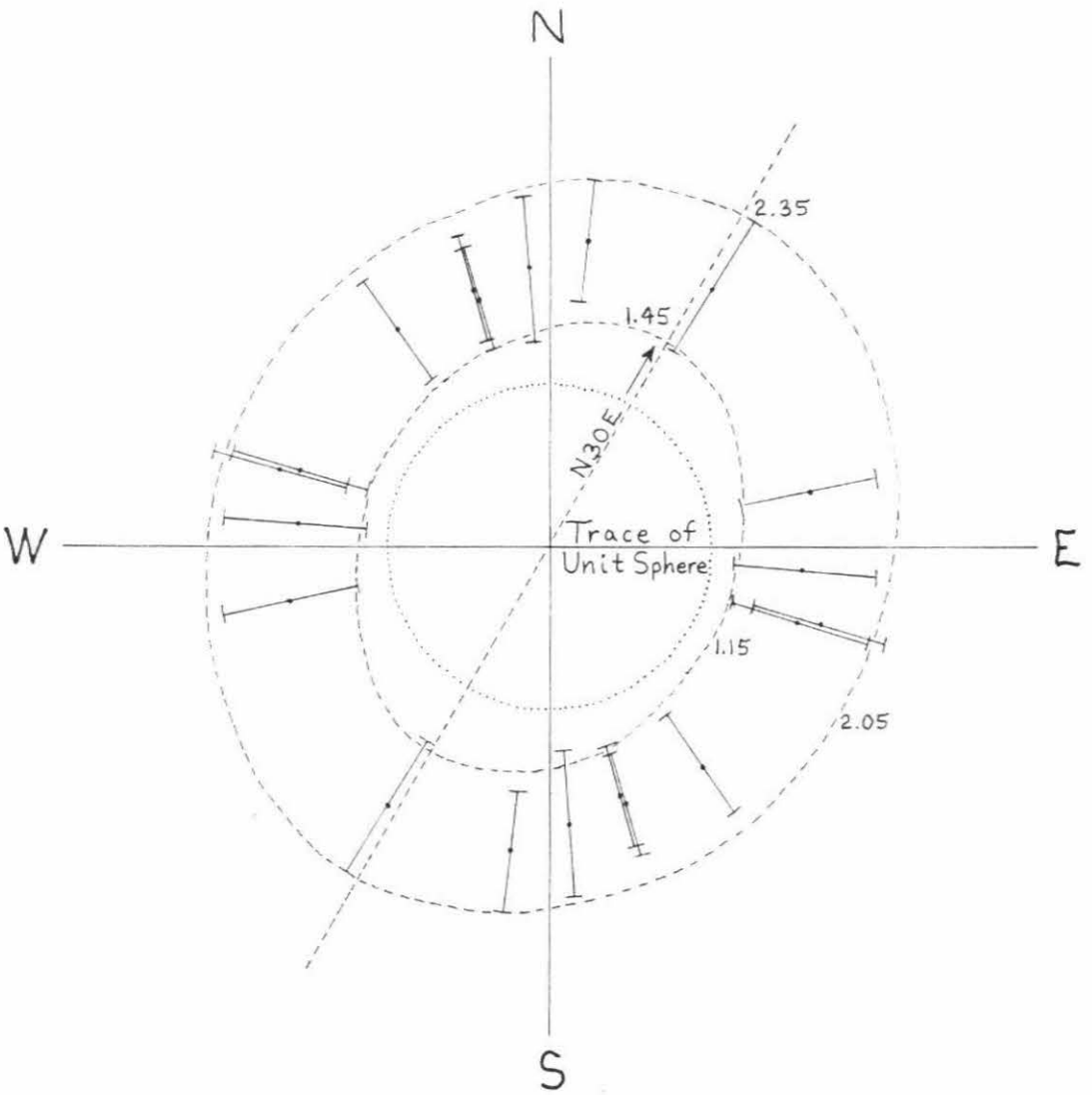

Figure 8.9

"bladed" shape field (see Figure 8.10). The average pebble shape (with one standard deviation uncertainties) calculated from Gilmont's data is: X = 4.5±2.2 cm, Y = 3.3±1.8 cm, and Z = 2.3±1.2 cm. Normalized to the scale of the fabric ellipsoid derived from my oriented measurements, these data yield a slightly more elongate initial shape ellipsoid.

Fabric ellipsoids are also determined for two separate geographical domains of the deformed section where the conglomerates are well exposed. Figures 8.11 and 8.12 summarize the data from Arroyo Amolares and Arroyos Chupadero/Ombligo, respectively. In these areas, lineations are consistently oriented N50±5E, and axes of highly deformed pebbles are virtually parallel to the schistosity (see Figure 8.8b). The maximum elongation directions of the two fabric ellipsoids are coincident with the lineation.

To determine the strain differences between the undeformed site and the deformed site, the initial fabric ellipsoid is "subtracted' from the two final fabric ellipsoids. In general this process involves tensor algebra, where:

(Final Shape and Orientation) =
(Initial Shape and Orientation)
x (Tectonic Strain),

and the quantities in the brackets are 3 by 3 matrices. However, in the Magdalena area, the elongation directions are nearly coincident in the initial and final settings, so the irrotational strain difference may be approximated by the equation:

$$R_{final} = R_{initial} \times R_{tectonic}.$$

The mean tectonic strains in the deformed domains are thus easily calculated from the average fabric ellipsoids determined above (see Table 8.1). Maximum tectonic strains are calculated by mathematically removing the

Figure 8.10: Three dimensional shape analysis of 252 undeformed, unoriented pebbles from the Cocospera Formation (compiled from Gilmont, 1978). The average pebble shape is calculated. The normalized fabric ellipsoid assumes that the long, intermediate, and short axes of the pebbles have been preferentially aligned during deposition and compaction.

Figure 8.11: Azimuthal variation of axial ratios for 673 deformed pebbles in Arroyo Amolares. Each data point represents the arithmetic mean of an R_f population measured from a specific outrop. The error bars indicate one standard deviation dispersion about the mean. The data are plotted in the plane of schistosity (where maximum axial ratios are observed). Dimensions of the maximum and minimum deformed fabric ellipsoids are outlined. The average observed lineation is indicated.

Figure 8.12: Plot of 655 deformed pebbles from Arroyos Chupadero/Ombligo. Symbols are the same as in Figure 8.11.

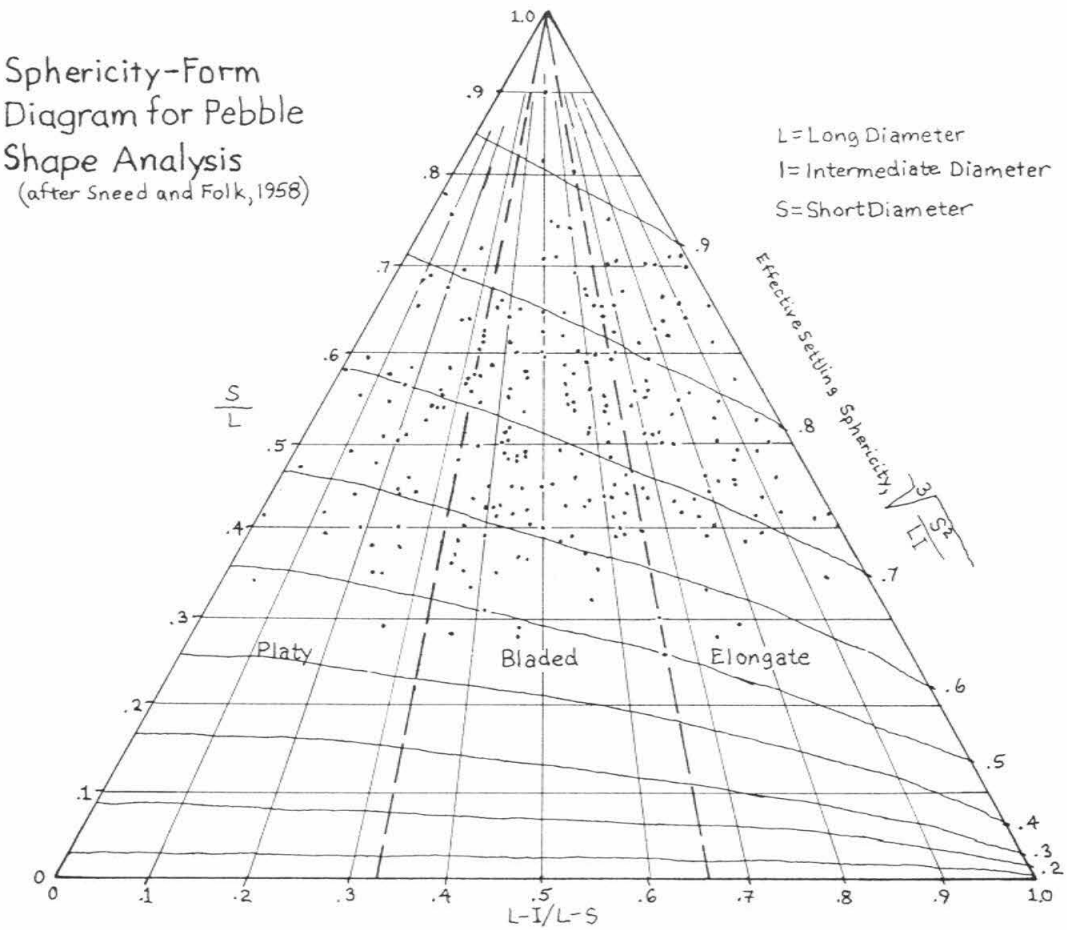

252 Pebbles From The Cocospera Formation
(GILMONT, 1978)

Average Shape	Normalized Fabric Ellipsoid
L = 4.5 ± 2.2 cm	X = 1.96
I = 3.3 ± 1.8 cm	Y = 1.43
S = 2.3 ± 1.2 cm	Z = 1.0

Figure 8.10

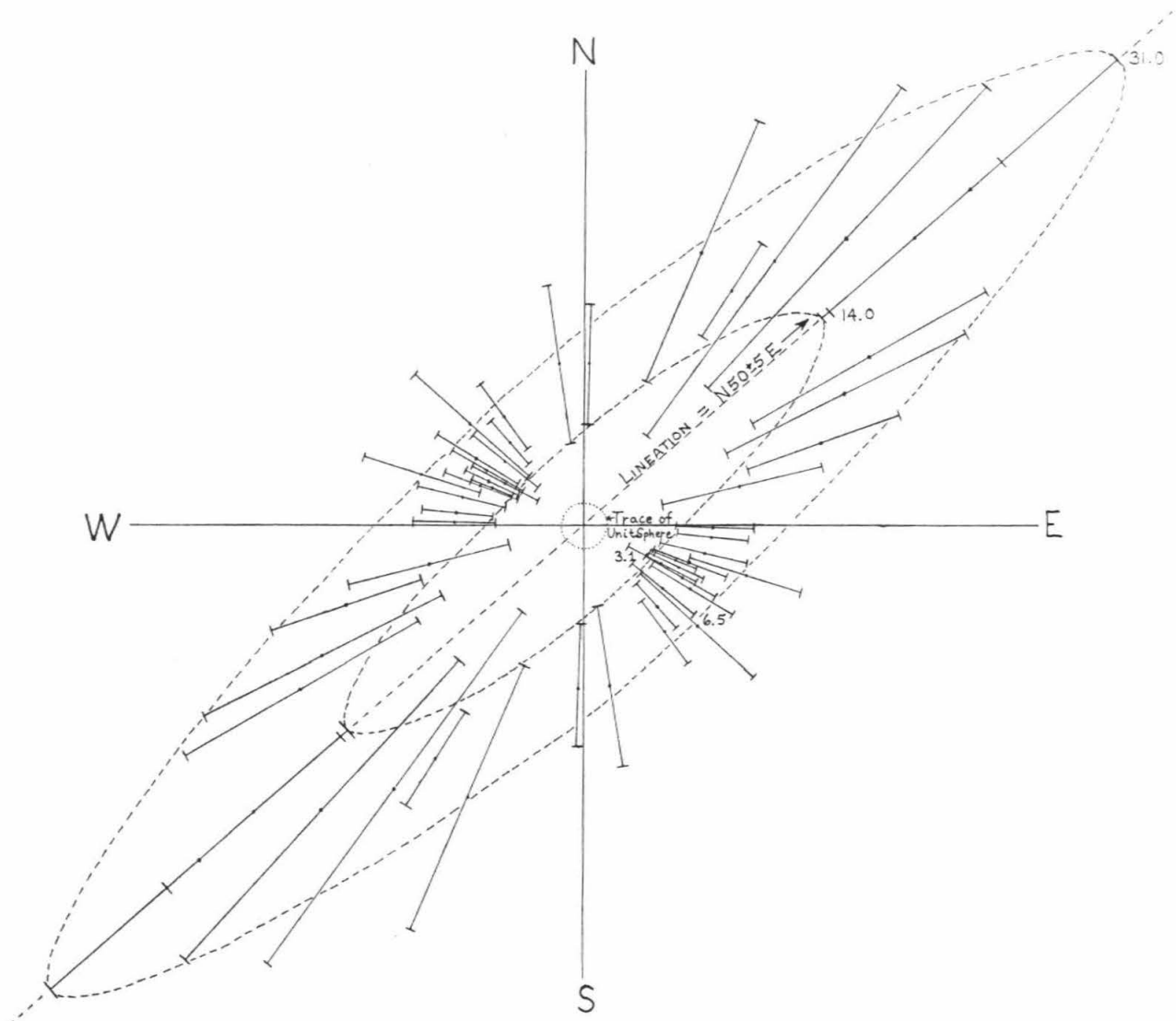

Figure 8.11

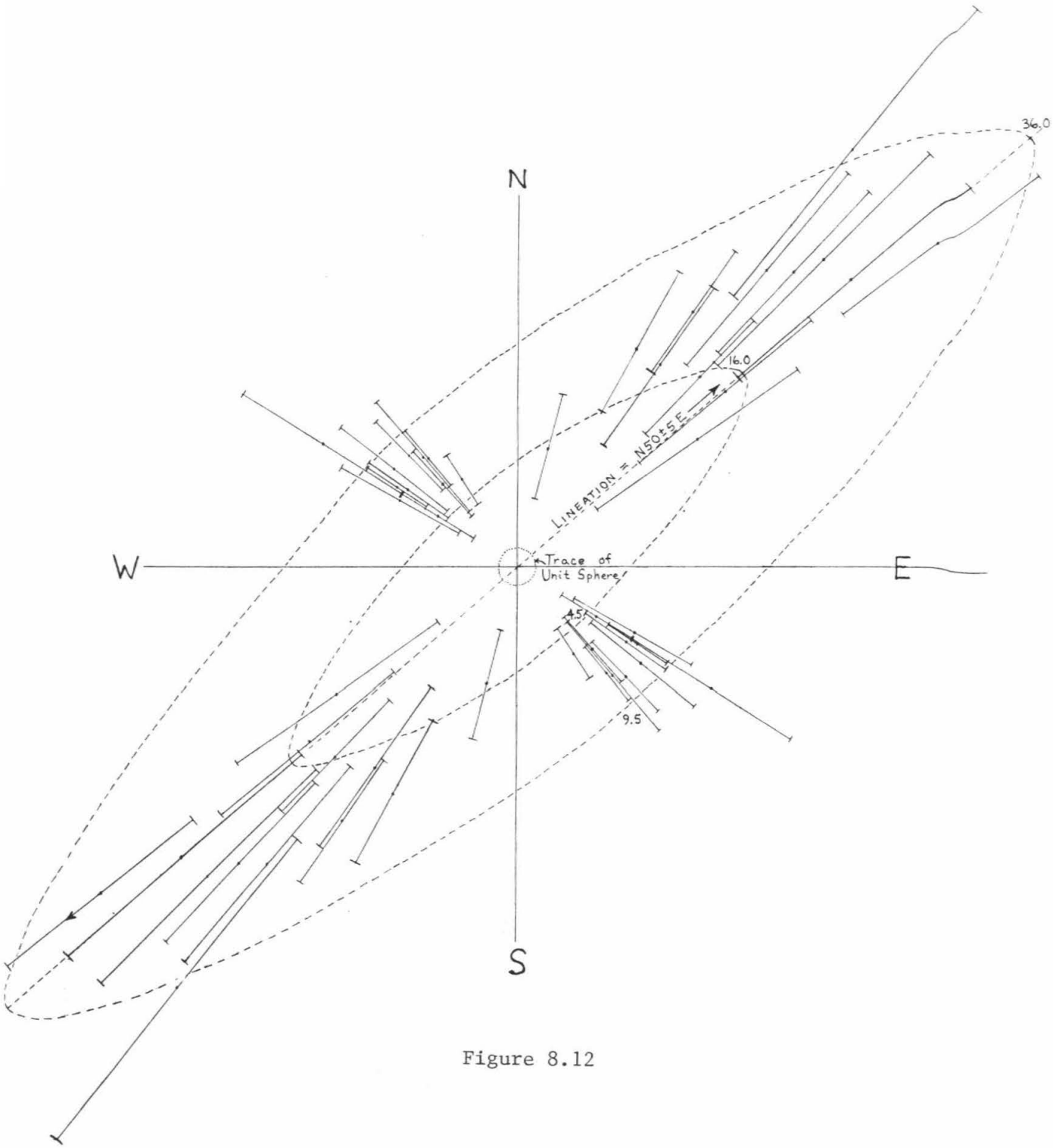

Figure 8.12

average initial fabric ellipsoid from the largest final ellipsoid. Likewise, minimum tectonic strains are calculated by removing the average initial ellipsoid from the smallest final ellipsoid. For each case k values are also calculated.

Tectonic strains determined from the fabric ellipsoid method may be compared to strains calculated using the harmonic mean method. Figures 8.13-8.14 show the azimuthal variation of $R_{harmonic}$ in the XY plane for the two deformed domains. The outlined maximum and minimum ellipses encompass more than 95% of the harmonic means, but probably only about 2/3 of the individual measurements (compare with Figures 8.11-8.12). The resulting strain parameters differ somewhat from the maximums and minimums calculated earlier, but the mean values obtained from one method are within the uncertainties of the other, and vice versa (see Table 8.1).

The large uncertainties demonstrated above are attributed to heterogeneous partitioning of strain. Because the measured conglomerates were clast supported, matrix effects are not believed to be important. However, the markers do exhibit differing strain behavior with respect to **clast composition** and **size**. In Figures 8.15a-c, short axes are plotted versus long axes for XZ and YZ surfaces in the two deformed domains. These plots demonstrate that quartz clasts tend to deform less readily than sandstone or volcanic clasts. Also, large quartzite cobbles appear to be less deformed than small quartzite pebbles, while the inverse seems to be the case for volcanic and sandstone clasts. Nevertheless, the finite strain data from the Cocospera conglomerate provide a valuable representation of the bulk deformation in the supracrustal series.

Figure 8.13: Azimuthal variation in $R_{harmonic}$ for the pebbles of Figure 8.11, plotted in the plane of schistosity. The ellipses approximate the dimensions of the maximum and minimum tectonic strain ellipsoid.

Figure 8.14: Azimuthal variation in $R_{harmonic}$ for the pebbles of Figure 8.12.

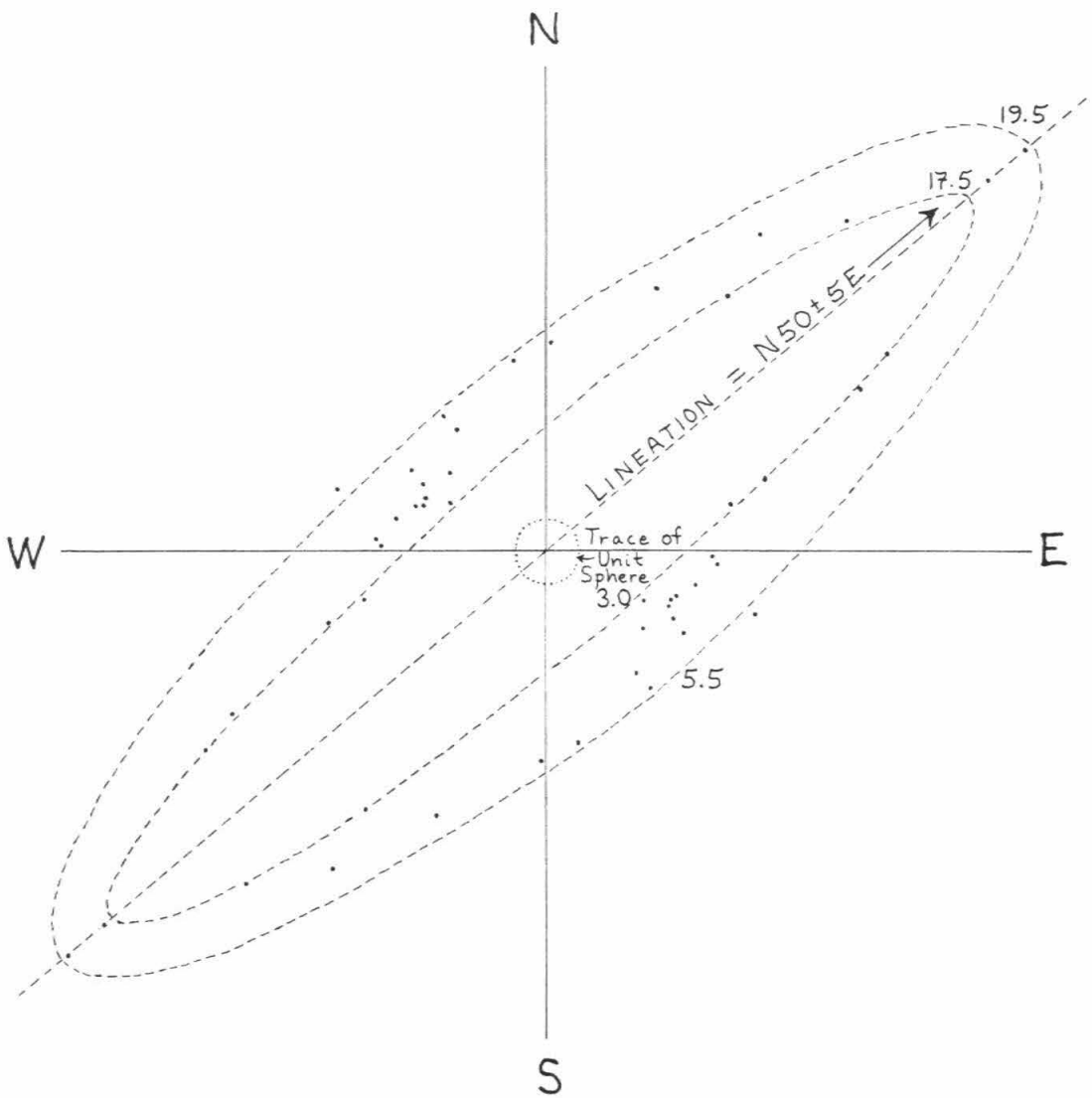

Figure 8.13

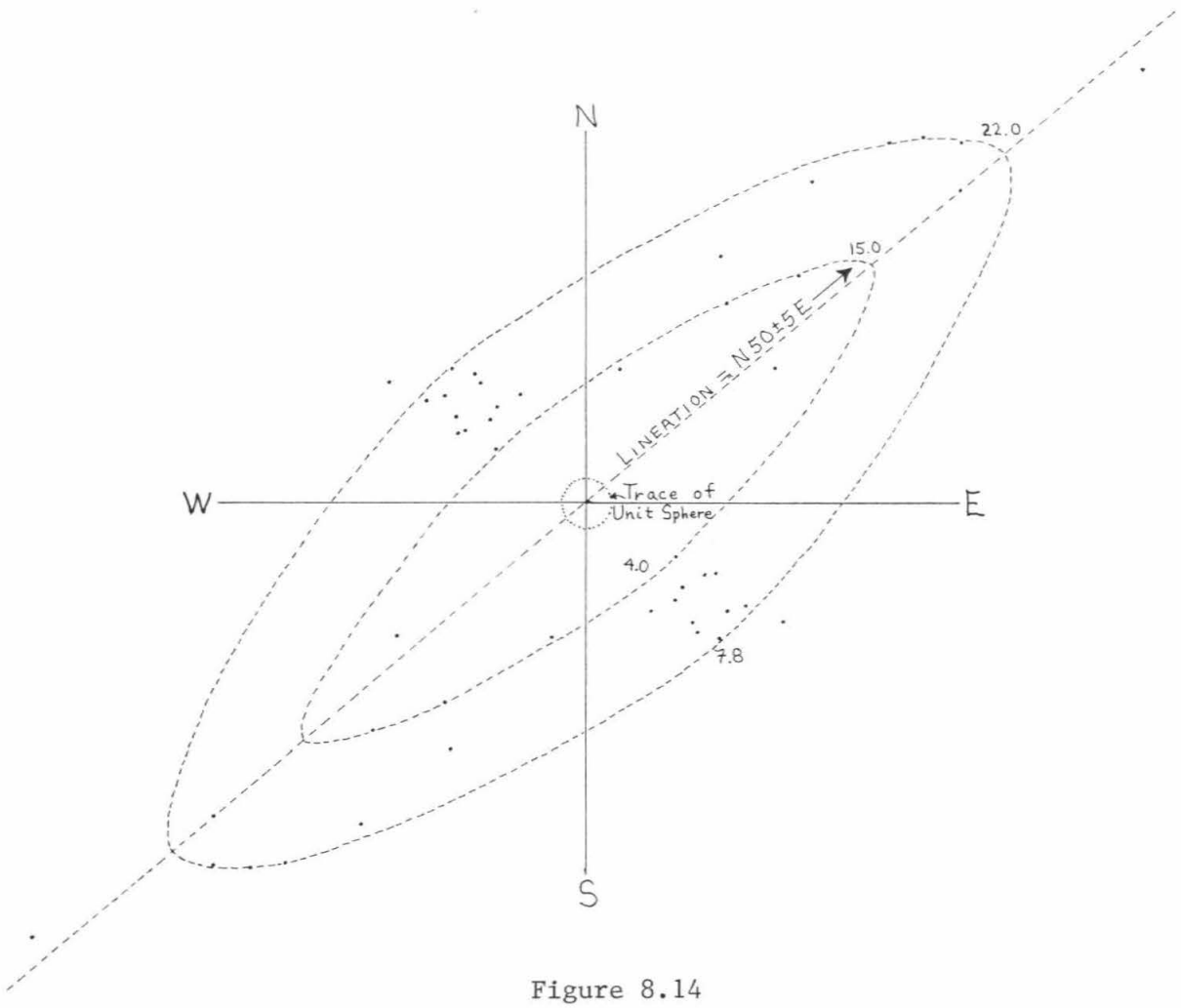

Figure 8.14

SITE		SHAPE FABRIC METHOD				HARMONIC MEAN METHOD			
		Measured Shapes		Tectonic Strain (Initial Shape Removed)		Mean Shape = Tectonic Strain			
		R_{xz}	R_{yz}	R_{xz}	R_{yz}	R_{xz}		R_{yz}	
Rio Cocospera	Max	3.4	2.1						
	Min	1.5	1.2						
	Ave	1.9	1.6						
Arroyo Amolares	Max	31.0	6.5	16.3	4.1	19.5		5.5	
	Min	14.0	3.1	7.4	1.9	17.5		3.0	
Arroyos Chupadero/ Ombligo	Max	36.0	9.5	18.9	5.9	22.0		7.8	
	Min	16.0	4.5	8.4	2.8	15.0		4.0	
		ℓ_x	ℓ_y	ℓ_z	k	ℓ_x	ℓ_y	ℓ_z	k
Arroyo Amolares	Max	+3.02	+0.01	−0.75	0.96	+3.10	+0.16	−0.79	0.57
	Min	+2.07	−0.21	−0.59	3.22	+3.67	−0.20	−0.73	+2.42
Arroyos Chupadero/ Ombligo	Max	+2.93	+0.23	−0.79	0.45	+2.97	+0.40	−0.82	0.27
	Min	+1.93	−0.02	−0.65	1.11	+2.83	+0.02	−0.74	0.92

Table 8.1: Summary of finite strain data for pebbles of the Cocospera Formation. Strain parameters derived from the shape fabric method are compared to those derived from the harmonic mean method.

Figure 8.15a: Plot of X dimension vs. Z dimension for three pebble types of Arroyo Amolares.

Figure 8.15b: Plot of X dimension vs. Z dimension for three pebble types of Arroyos Chupadero/Ombligo.

Figure 8.15c: Plot of Y dimension vs. Z dimension for three pebble types of Arroyos Chupadero/Ombligo.

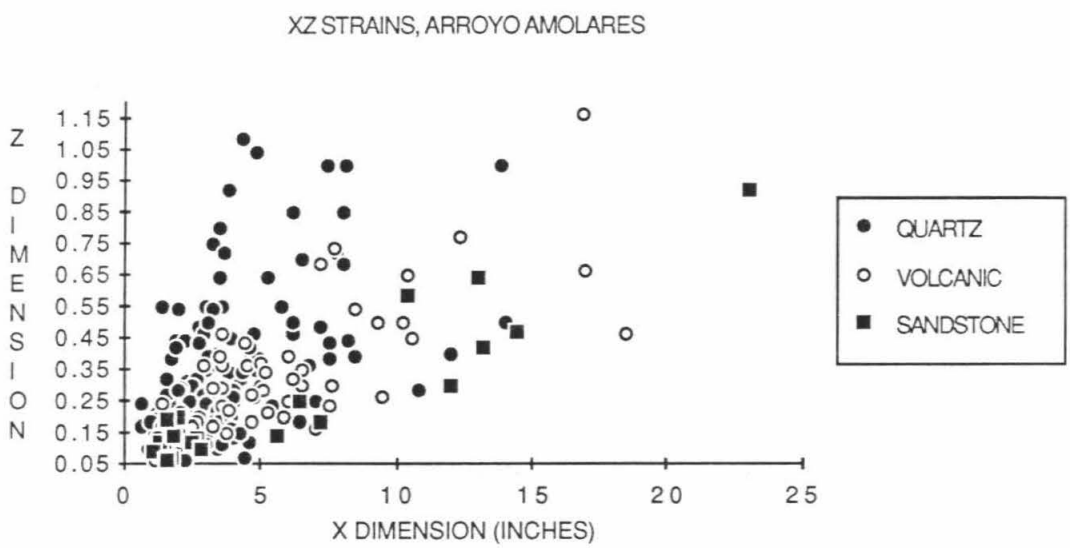
XZ STRAINS, ARROYO AMOLARES
Z DIMENSION
1.15
1.05
0.95
0.85
0.75
0.65
0.55
0.45
0.35
0.25
0.15
0.05
0
5
10
15
20
25
X DIMENSION (INCHES)
QUARTZ
VOLCANIC
SANDSTONE

Figure 8.15a

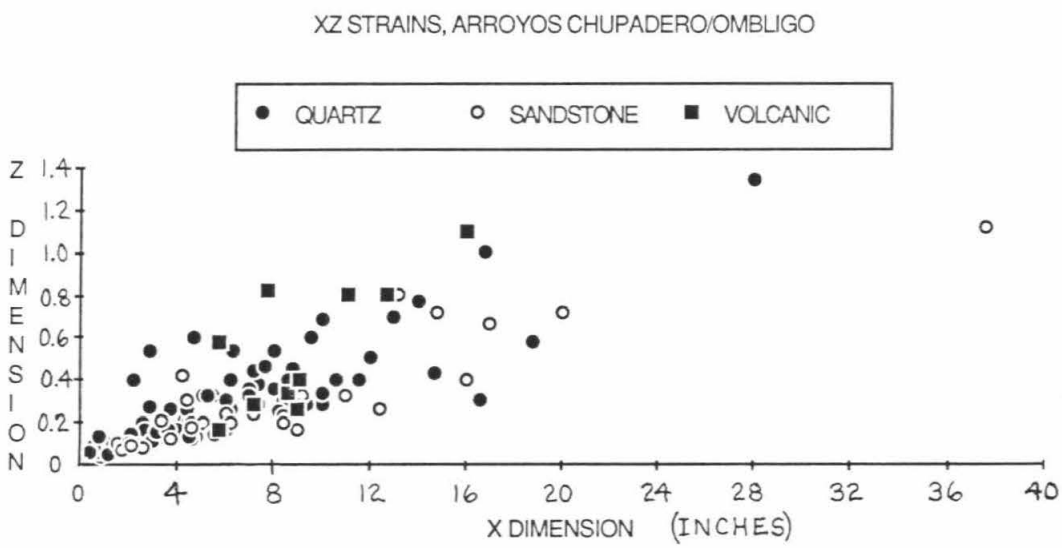
XZ STRAINS, ARROYOS CHUPADERO/OMBLIGO
QUARTZ
SANDSTONE
VOLCANIC
Z DIMENSION
1.4
1.2
1.0
0.8
0.6
0.4
0.2
0
0
4
8
12
16
20
24
28
32
36
40
X DIMENSION (INCHES)

Figure 8.15b

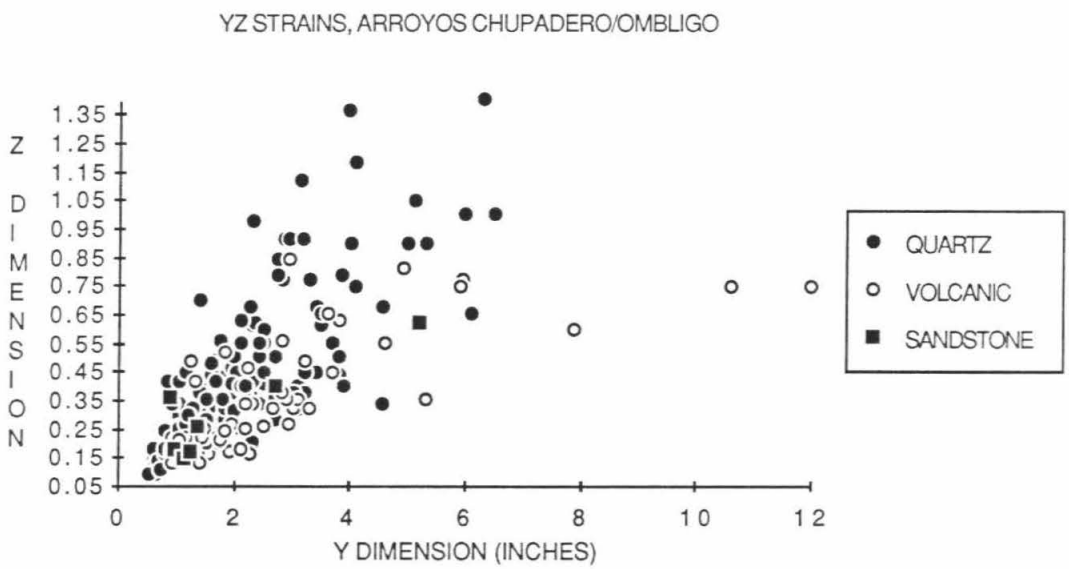
YZ STRAINS, ARROYOS CHUPADERO/OMBLIGO
Z DIMENSION
1.35
1.25
1.15
1.05
0.95
0.85
0.75
0.65
0.55
0.45
0.35
0.25
0.15
0.05
0
2
4
6
8
10
12
Y DIMENSION (INCHES)
QUARTZ
VOLCANIC
SANDSTONE

Figure 8.15c

SUMMARY OF THE SUPRACRUSTAL STRAINS

The variation of finite strain within the lower plate supracrustal series is summarized in map view and in two integrated structural sections. Strains are plotted in the form of percent elongations (i.e., e_x x 100%). Strains from some of the rhyolite porphyries have been recalculated using the calibration curve developed earlier.

Figure 8.1 shows a southwestward increasing finite strain gradient in the supracrustal series. Elongations increase gradually to about 200%, then, within the region of strong noncoaxial overprint, the values are abruptly upgraded to 300% or 400%. Deformed supracrustal rocks suitable for R_f/ϕ analysis were not encountered in the far southwestern area.

Vertical variations in strain are displayed in representative structural columns from two areas. Supracrustal strain gradients are plotted adjacent to gradients measured from associated granitic bodies (see next section). Figure 8.16 portrays the central part of the metamorphic core (near La Sauceda/Arroyo Amolares) while Figure 8.17 corresponds to the west central Sierra Guacomea. Two important features are evident in both areas:

(1) strains in the supracrustal series increase downward to a maximum at the contact with structurally deeper granitic sills, and

(2) the leucogranites are significantly less strained than their country rocks. These vertical strain profiles place important constraints on the destraining process discussed at the close of this chapter.

Figure 8.16: Longitudinal strain profiles in the central Sierra Magdalena. Rock units as in Figure 6.4. Stippled envelopes show the range in strain values for the quartz pebble conglomerate and volcanic conglomerate units. Strains in the granites are derived from quartz grain shapes and boudinaged dikes or sills. Dotted segments are extrapolated from regional trends.

Figure 8.17: Longitudinal strain profiles in the west central Sierra Guacomea. Rock units as in Figure 6.6. Approximate sample locations and sample numbers are indicated by circled x's. High strains at the base of the Guacomea granodiorite are associated with late northeast directed discrete normal sense shear zones.

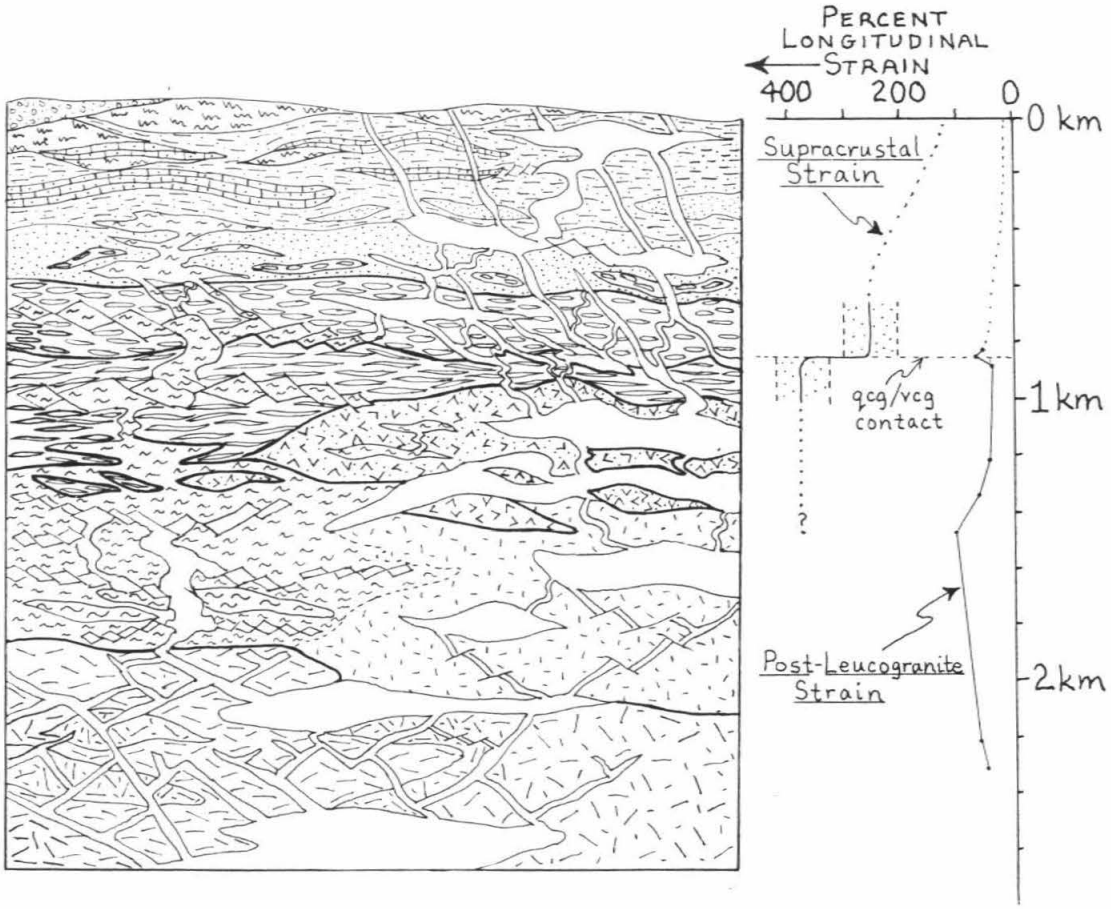
PERCENT
LONGITUDINAL
STRAIN
400
200
0
0 km
Supracrustal
Strain
qcg/vcg
contact
1km
?
Post-Leucogranite
Strain
2km

Figure 8.16

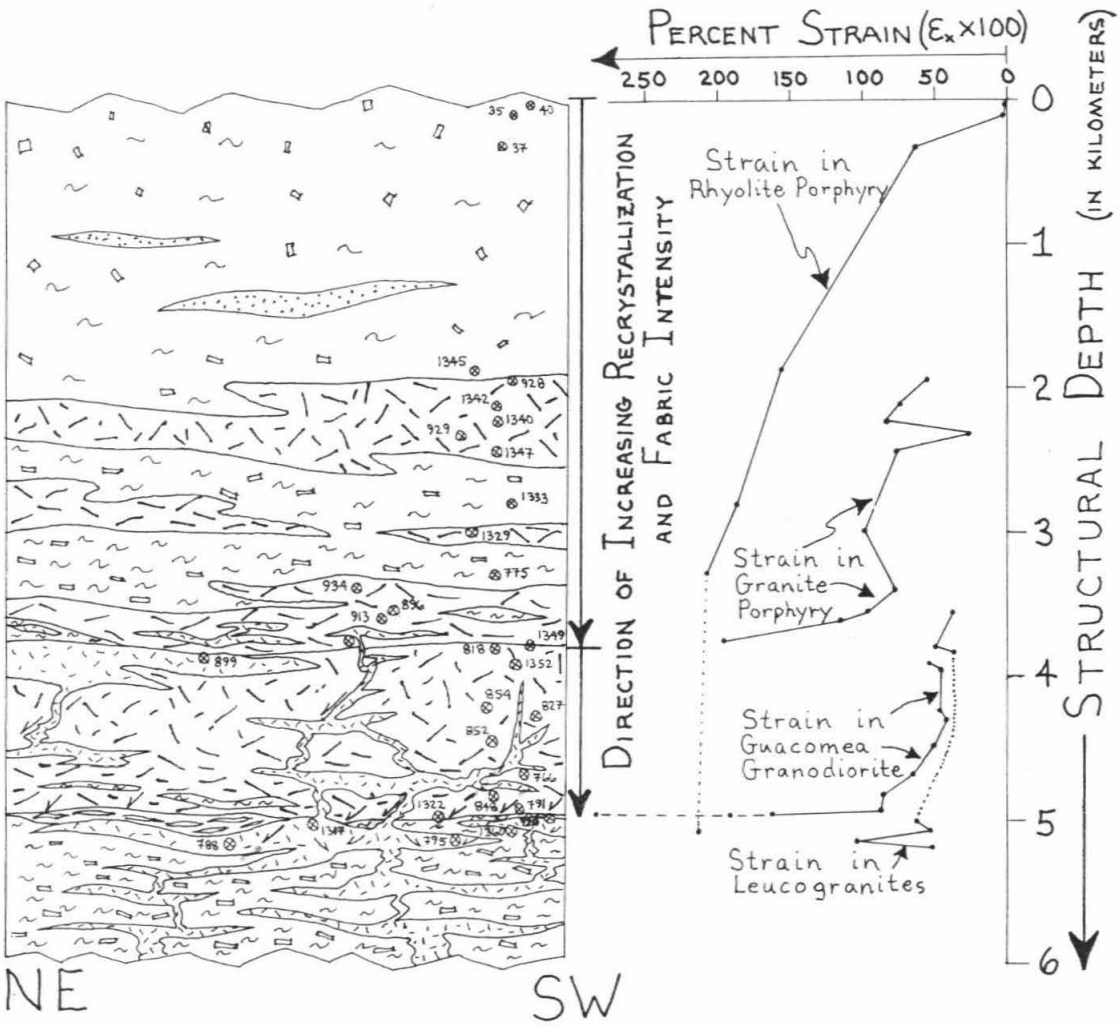
PERCENT STRAIN (εx×100)
250
200
150
100
50
0
STRUCTURAL DEPTH (IN KILOMETERS)
0
1
2
3
4
5
6
DIRECTION OF INCREASING RECRYSTALLIZATION AND FABRIC INTENSITY
Strain in Rhyolite Porphyry
Strain in Granite Porphyry
Strain in Guacomea Granodiorite
Strain in Leucogranites
NE
SW

Figure 8.17

FINITE STRAINS IN THE GRANITIC ORTHOGNEISSES

Strains in the granite orthogneiss complex are believed to have accumulated during Late Oligocene time, after emplacement of the leucogranite suite. The geometry of this deformation is quantified below. Because of the significant asymmetries involved, the data are analyzed by methods involving both irrotational strain theory (i.e., R_f/Φ analysis) and rotational strain theory (simple shear analysis). The irrotational and rotational strain fabrics are intimately related, and record a synchronous evolution. These interrelationships are developed in detail below.

IRROTATIONAL STRAINS

Irrotational strains may be determined by measuring the change in shape of markers that have known initial dimensions. Granites of the lower plate provide a variety of useful markers. Quartz grains are approximated as ellipsoids in an R_f/Φ analysis, and boudinaged or buckled leucogranite dikes (or veins) are measured to determine minimum finite elongations or contractions in particular directions. The resulting strains and their orientations place important constraints on the geometry of the associated noncoaxial deformation.

Method of Quartz Grains: R_f/Φ measurements were performed on quartz grains in three kinds of deformed granitoids: porphyritic biotite granodiorite, porphyritic two mica granite, and fine grained leucogranite. Most of the data were collected from various large sills at structural levels deeper than the supracrustal series. A few small leucogranite sills intrusive into the supracrustal series were also measured.

Considerable time and resources were saved by assuming that deformation in the granites was largely **plane strain**. In this special case it is only necessary to measure markers in the XZ principle plane. Validity of the plane strain assumption is supported by analysis of a few samples which were also sliced along the YZ plane.

About 90% of the R_f/Φ data were measured in thin sections oriented parallel to lineation and perpendicular to foliation (see Figure 8.18a). The remainder were measured from similarly oriented surfaces in hand specimens. Orientations of the quartz grains were recorded relative to the average biotite and feldspar foliation (in thin section this surface was statistically determined). Long axes were also measured relative to sets of syndeformational shear bands (see next section). Data plots and derived strain quantities are compiled in Appendices C and D.

Several randomly oriented surfaces in undeformed granite were analyzed to determine the range in initial quartz grain shapes and sizes. The shapes of quartz grains in a given planar section are generally subelliptical to subspherical (see Figure 8.18b). Associated R_i/Θ plots show that long axis distributions are random, and the initial ellipticities range between 1.0 and 1.6. These values are consistent with the range in R_i's predicted by R_f/Φ plots from deformed regions.

Method of Dikes and Veins: Arrays of boudinaged and buckled dikes (or veins) provide a means of directly measuring percent elongation or shortening at various positions in the lower plate (see Figures 8.19-8.22). Stretched and shortened veins occur in all lithologies affected by the post-leucogranite strain. Geometries of the veins were described as completely as possible in the field, and their orientations relative to local foliation and lineation were measured. Asymmetries were carefully noted where

Figure 8.18a: Photomicrograph of deformed two mica granite, showing elongate, recrystallized quartz grains (Q) used for finite strain analysis. View is perpendicular to foliation and parallel to lineation. S = mylonitic foliation; C = southwest vergent shear planes.

Figure 8.18b: Photomicrograph of undeformed two mica granite, showing original subspherical shape of quartz grains (Q).

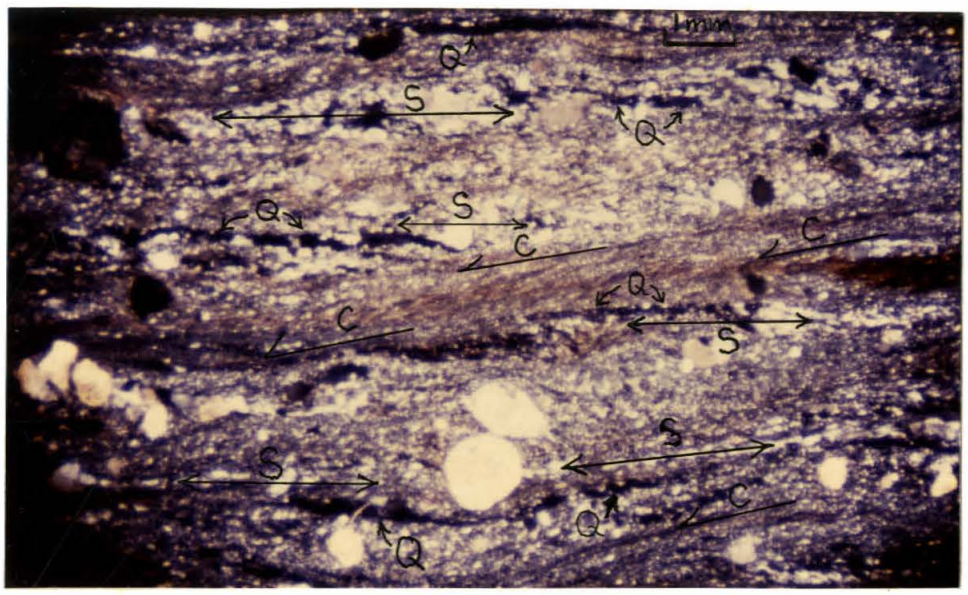

Figure 8.18a

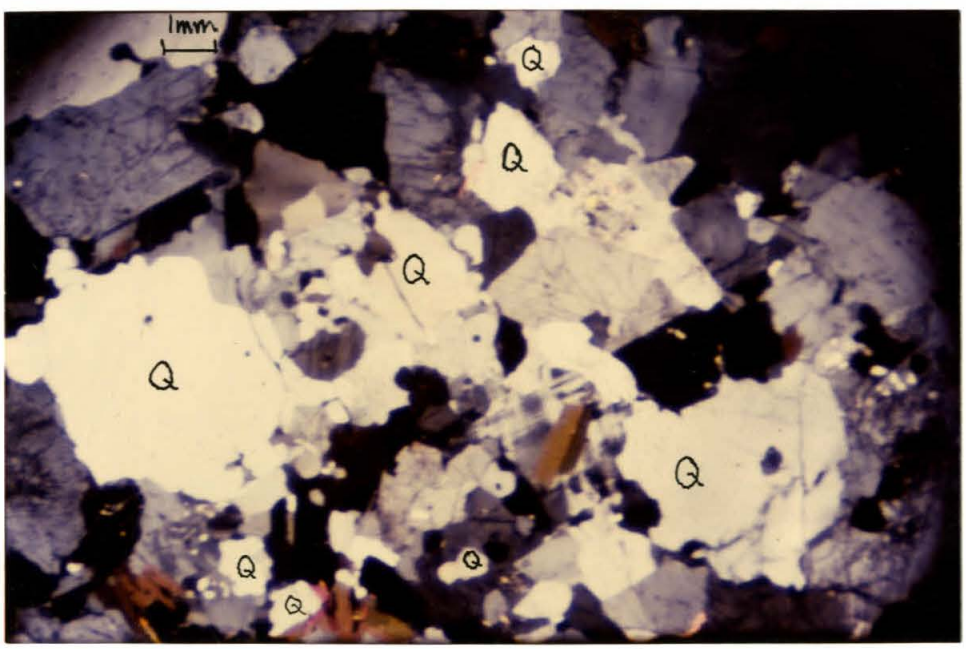

Figure 8.18b

encountered. The boudinaged veins are best quantified by measuring a strike and dip, and a finite elongation perpendicular to boudin axes. However, in practice it was easier to measure the direction and plunge of a boudinaged vein on an outcrop surface, and determine the finite elongation in that direction. Buckled veins are quantified by measuring the orientation of the buckling plane, the trend and plunge of associated fold axes (which are usually within the plane of buckling), and the finite shortening perpendicular to the fold axes.

Finite elongations determined from the boudinaged dikes and veins should be regarded as minimum values which underestimate the bulk strain. This disparity is due to the fact that the boudinaged material is more competent than its medium, and therefore strain is preferentially partitioned into the medium (a competence contrast is necessary to develop boudins in the first place). Many leucogranite veins and dikes were initially oriented at high angles to the extension direction. Hence, a significant amount of strain was probably absorbed by rigid body rotation of the veins prior to their decomposition into boudins (see rotational analysis, next section). Also, it should be noted that many of the measured elongations are somewhat discordant to the local foliation and lineation; i.e., longitudinal strain was not always determined along the maximum extension direction of the finite strain ellipsoid.

By a similar argument, magnitudes of shortening measured from buckled dikes or veins are also minimums. The buckled veins display variable geometries dependent on their thickness and the type of country rock. Some examples are shown in Figures 8.19-8.22. The competence contrast between the leucogranites and each host lithology can be estimated from the fold morphologies (see Ramsey and Huber, 1987, pp. 392-404). It can be argued that

Figure 8.19: Photograph of boudinaged leucogranite sills in stretched volcanic conglomerate host, Arroyo Amolares. Tape is 1 inch wide.

Figure 8.20: Photograph of leucogranite dike buckled perpendicular to foliation in host biotite feldspar schist, Arroyo Chupadero. Hammer is 18 inches long.

Figure 8.21: Photograph of leucogranite vein buckled at a high angle to foliation in stretched quartz pebble conglomerate host, Arroyo Amolares. Tape is 1 inch wide.

Figure 8.22: Photograph of pegmatite dike shortened perpendicular to foliation in fine grained leucogranite host, Arroyo Ombligo. Hammer is 18 inches long.

Figure 8.19

Figure 8.20

Figure 8.21

Figure 8.22

the leucogranites are significantly more competent than the metasedimentary or metavolcanic lithologies, but are only slightly more competent than their granite hosts. This is probably the reason why buckled veins were rarely observed within the large granite bodies; most veins of the proper orientation exhibit mesoscopic evidence for layer parallel shortening (see Figure 8.22).

Data Summary: Figure 8.2 is a compilation map showing irrotational strains associated with the post-leucogranite deformation. The data set is somewhat limited, but enough strains are determined in the Sierras Magdalena and Madera to permit first order contouring. The contours track a significant south or southwest increasing strain gradient which reaches a maximum in close proximity to the Magdalena detachment fault. Figures 8.16, 8.17, and 8.23 show the strains recorded by granites at various structural levels in specific geographic domains of the lower plate. In the southern Sierra Magdalena the granites display an upward increasing strain gradient. Near La Sauceda/Arroyo Amolares, the leucogranites are significantly less deformed than their metavolcanic and metasedimentary country rocks, implying that they were emplaced late in the deformational sequence. Likewise, in the west central Sierra Guacomea, the strain gradient in the granites is less intense than in the metamorphic host rocks.

In Plate 3A, the irrotational strain gradients are plotted to scale on five NE-SW geologic cross sections through the Magdalena core complex. These illustrations allow one to assess in three dimensions the relative importance of the two strain events at different geographic and structural positions. Of particular interest is the symmetry of both gradients about the horizon(s) occupied by large leucogranite sills. In the central and northern areas, strains in the supracrustal series achieve maximum values just above their

Figure 8.23: Longitudinal strain profile associated with the Middle Tertiary deformation in the southern Sierra Magdalena. Rock units as in Figure 6.5. Strains are derived from quartz grain shape measurements in granites and from boudinaged leucogranite veins.

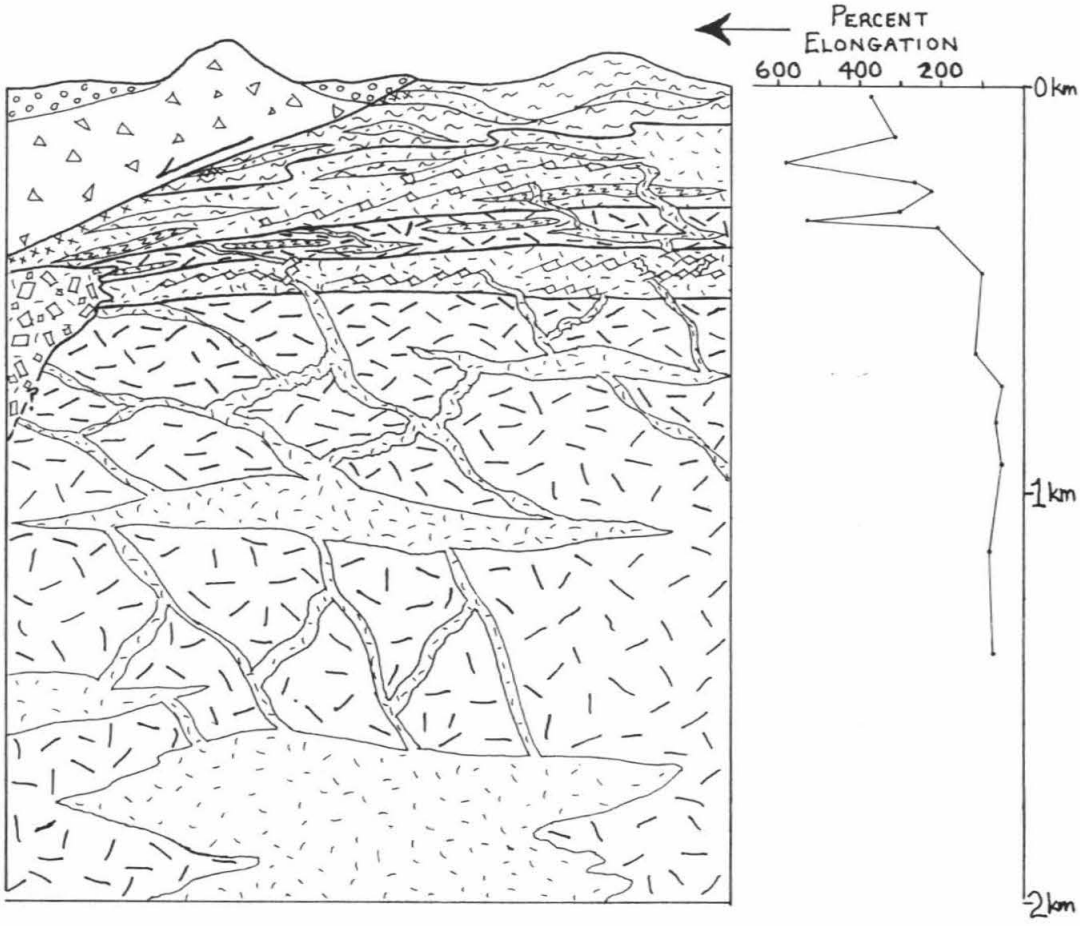

Figure 8.23

contact with the leucogranite horizon. An overlapping strain gradient of lesser intensity but similar trend is recorded by leucogranite dikes within this same interval of the supracrustal section. Farther south, only the younger strain gradient is preserved. Here the strains intensify upward in almost a mirror image of the shallower gradients, reaching a maximum at the level of the largest leucogranite sill.

Analysis of the irrotational strain patterns in Plate 3A leads to the conclusion that early strains accumulated in the supracrustal series, then leucogranite sills were injected along high strain horizons, then a later deformation affected the whole section in such a way that the greatest strains were concentrated near and within the leucogranites. As will be shown in the next section, the late strain gradients define a zone of simple shear focused about the leucogranites. Because of the rotational deformation involved, the core complex cannot yet be destrained to a pre-leucogranite state. Lateral displacements due to simple shear must be accounted for in addition to the changes in shape recorded by the irrotational strains.

ROTATIONAL STRAINS

Structural evidence for noncoaxial deformation is preserved throughout large regions of the lower plate. Common noncoaxial indicators include unidirectionally rotated dikes and veins, asymmetric boudinage, and asymmetric shear bands. Geometric variations in these features are mapped across the complex and are related to gradients in the finite strain. Plane strain models proposed below help explain the evolution of the rotational structures. These models also provide a means of extracting the simple shear component of the deformation. It should be emphasized that the solutions which stem from the models are **nonunique**; i.e., in each example it would be

possible to arrive at the same deformed geometry via a multitude of different deformation paths. However, I believe the solutions offered below are most compatable with local and regional geological observations.

Figure 8.24 illustrates the geometric behavior of idealized spherical and planar strain markers as they are subjected to plane strain. Two end member deformational mechanisms are possible: **simple shear** and **pure shear**. In this diagram the lines might represent three possible dike orientations, while the ellipse (which tracks the finite strain axes) might represent the orientation of mylonitic foliation, stretched pebble foliation, or schistosity. The two deformational sequences show the variability in angular relationships one might encounter in traversing a deformation zone. Assessing the relative importance of the two mechanisms in a given area is a tricky process. The drawing demonstrates how either deformation path, or various combinations of the two paths could produce a specific angular relationship between dikes and foliation. To quantify the component of noncoaxial deformation (simple shear), one requires information on the degree of asymmetry and the kinematic history. Generally, this involves assumptions about the initial orientation of markers relative to the kinematic framework. For example, unidirectional shear bands at low angles to the foliation are generally indicative of noncoaxial strain, with displacement parallel to the shear bands. Rotations or discrete offsets of planar markers in one preferred direction also provide information on the direction and magnitude of shear strain. In the following analyses, asymmetries between foliation and either dikes or shear bands are utilized to deduce the simple shear component of the post-leucogranite deformation.

Figure 8.24a: Geometry of a simple shear deformation path illustrating the symbols used in text. γ = shear strain; σ_1 = orientation of maximum principle stress; σ_3 = orientation of minimum principle stress; α and α' are the initial and final orientations of dikes relative to the shear plane; β and β' are the initial and final orientations of sills relative to the shear plane; X = major axis of the finite strain ellipsoid; Z = minor axis of the finite strain ellipsoid; θ' is the angle between the X direction of the finite strain ellipsoid and the shear plane.

Figure 8.24b: Geometry of a pure shear deformation path. Symbols as in Figure 8.24a, with two additions: e_X = maximum elongation (extensional strain); e_Z = shortening strain.

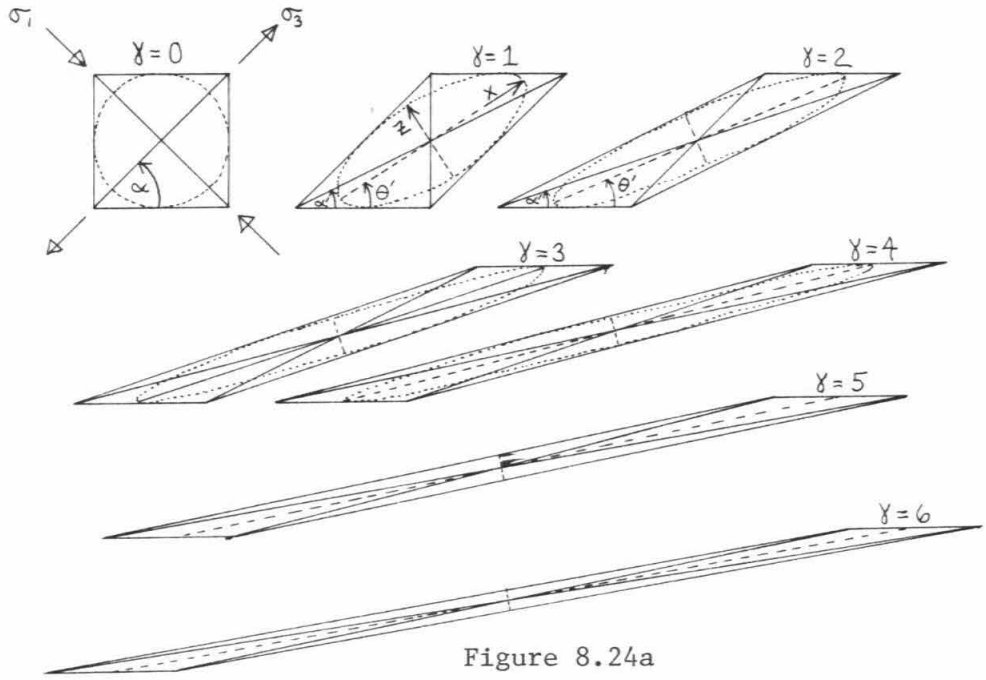

Figure 8.24a

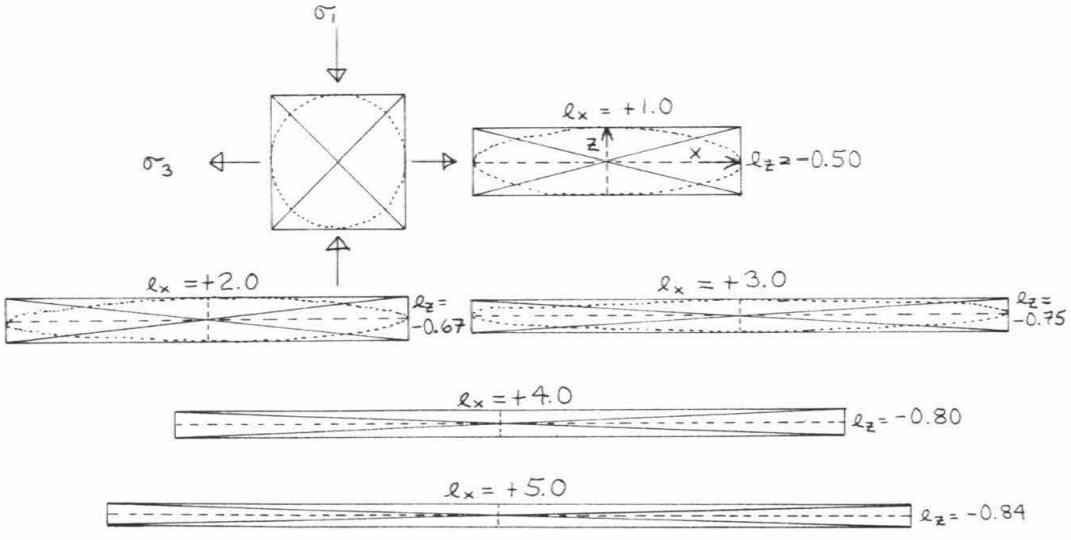

Figure 8.24b

SHEAR STRAINS FROM DEFORMED AND ROTATED PLANAR MARKERS

Dikes and Veins of the West Central Sierra Guacomea: East of Rancho la Joya, dikes and veins of leucogranite are deformed with their biotite granodiorite host. Quartz grain shape analysis shows that finite elongation within the granodiorite sill increases from 50% at the top to 85% at the base. In the lower part of the sill, the foliation dips 10° eastward. Leucogranite dikes within this structural interval display a similarly oriented foliation. Most of the dikes dip northeastward 49°±13° relative to the granodiorite foliation, and display drag features along their margins which indicate southwestward rotation. A few southwest dipping dikes have been buckled at high angles to the foliation.

Figure 8.25 summarizes the geometrical elements of the deformed setting. The asymmetry of the leucogranite dikes and veins relative to the bulk finite strain ellipsoid (represented by the granodiorite foliation) demonstrates that the deformation involved a component of southwestward rotational strain. Figures 8.26a and 8.26b illustrate two possible plane strain models (1 and 2) that permit shear strain to be quantified.

In Model 1, it is assumed that the granodiorite was undeformed at the time of dike emplacement, and all of the strain accumulated subsequently via simple shear. The granodiorite and dikes of the deformed setting are destrained along a simple shear path to the theoretical undeformed setting shown. The simple shear value of 1.3 required by this model provides a maximum shear strain for the lower portion of the Guacomea pluton. However, this number is a significant overestimation. Although the initial dike orientations predicted by Model 1 are consistent with their being

Figure 8.25: Geometry of structural elements in the Guacomea Granodiorite, showing observed strain behavior of two leucogranite dike sets. The range in present dike orientations is derived from the stereonet plot. The orientation of the bulk finite strain ellipsoid corresponds to the foliation and lineation in the granodiorite; the strain magnitude is derived from quartz grain shape measurements.

Figure 8.26a: Deformation model for the Guacomea Granodiorite. The model assumes that all strain accumulated via simple shear after emplacement of the leucogranites into **undeformed** granodiorite. e_α and e_β are the maximum longitudinal strains predicted for the two dike sets. R_f is the axial ratio of the bulk strain ellipsoid in the XZ plane.

Figure 8.26b: Preferred deformation model for the Guacomea granodiorite. The model assumes pure shear of the granodiorite followed by dike emplacement followed by southwest directed simple shear. Symbols as in Figure 8.26a.

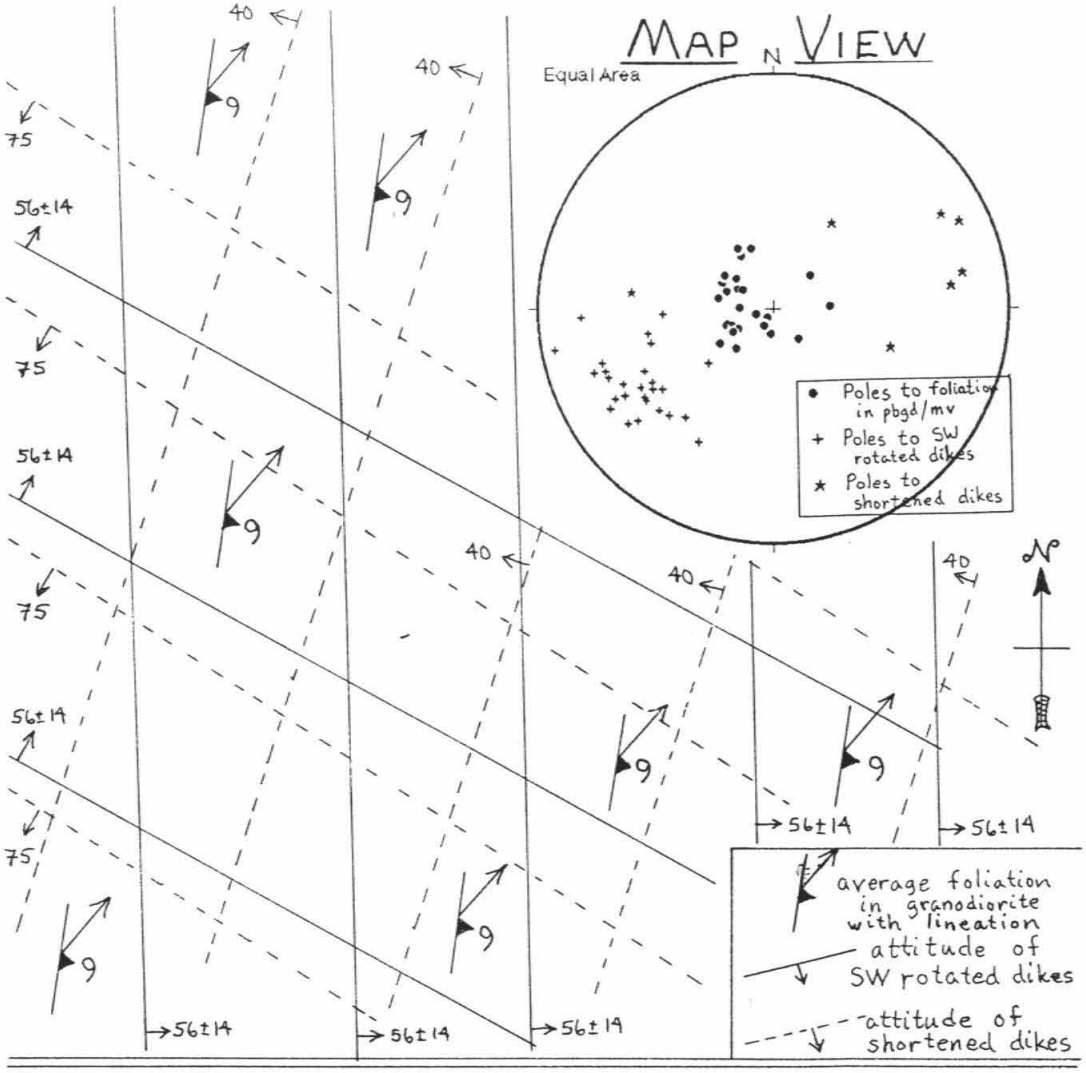

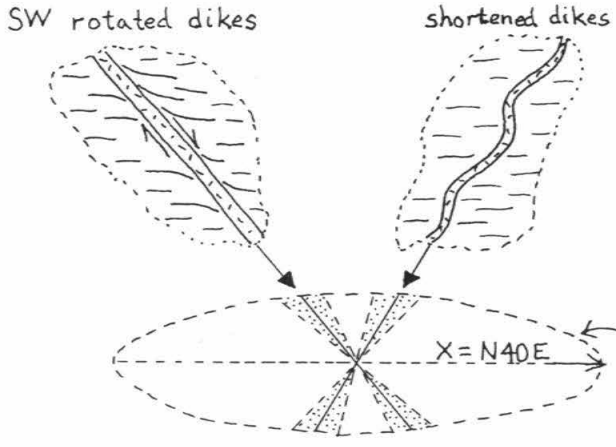

VIEW OF XZ PLANE

Figure 8.25

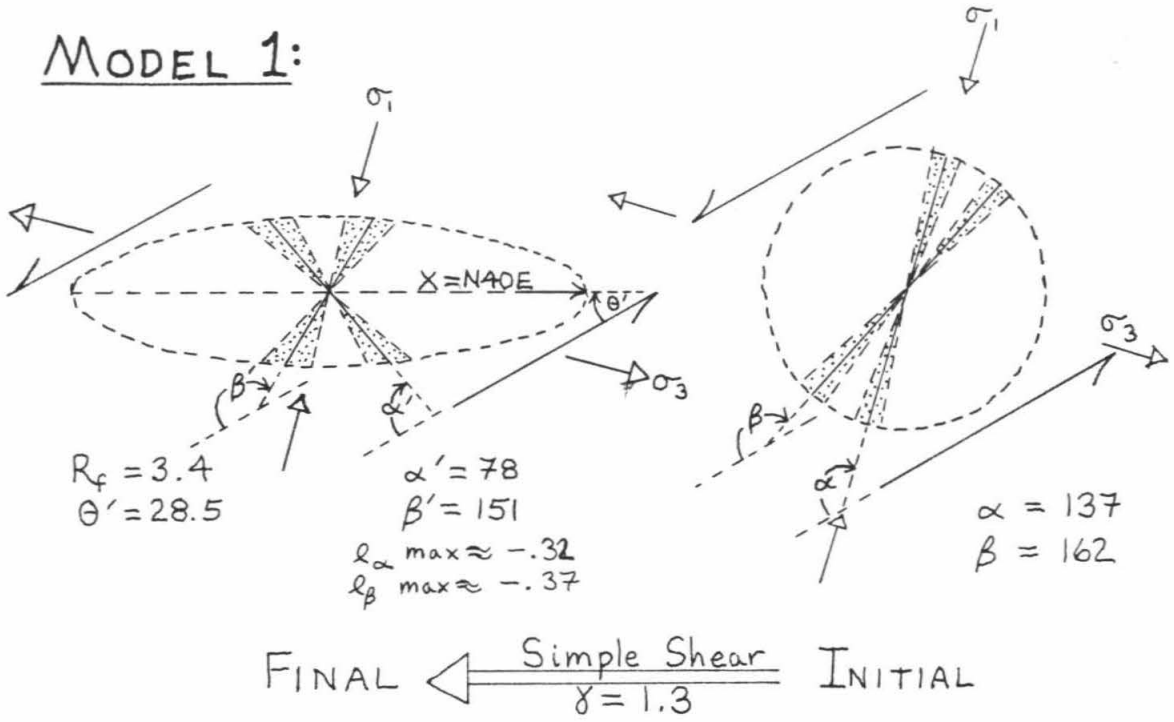

Figure 8.26a

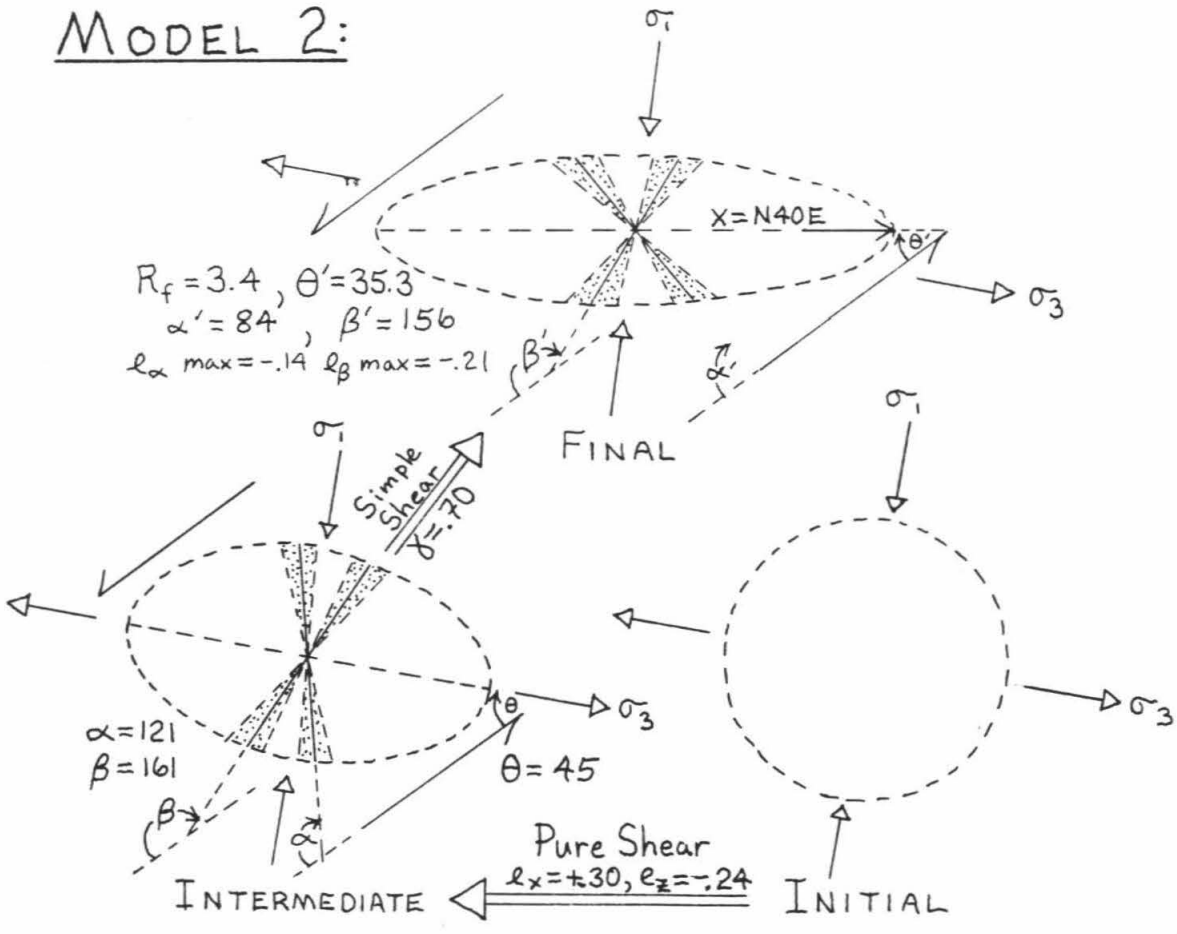

Figure 8.26b

emplaced along planes of minimum stress, the predicted subsequent strain behavior does not fit the field observations. Specifically, the dikes which ended up with northeast dips should have entered or passed through the shortening field during rotation. These dikes exhibit little evidence of the 32% shortening required by the model.

A more realistic model (Model 2) assumes pure shear deformation of the granodiorite prior to emplacement of the leucogranite dikes, followed by southwest directed simple shear of both rock units. The deformed setting may be destrained by a simple shear strain of 0.7 to produce an initial distribution of dikes symmetric about σ_1. The residual strain ellipse directly yields the magnitude of older deformation in the host granodiorite (here, e_X = +0.30, e_Z = -0.24). Model 2 still requires shortening of the dikes during rotation, however, the predicted e_Z's of -0.14 might easily have been accommodated by an inconspicuous mechanism of layer parallel shortening.

Dikes and Veins of Arroyo Amolares: In Arroyo Amolares, dikes and veins of leucogranite have been buckled, rotated, and boudinaged during noncoaxial deformation of their conglomeratic host rocks. A bulk strain of e_X = +2.44, e_Z = -0.71 is recorded by stretched pebbles which are elongate in a N50±5E direction. The configuration of dikes and veins relative to the pebble foliation is useful in destraining this section. Figure 8.27 illustrates the geometry of the deformed setting. One set of dikes is shortened 25% to 43% perpendicular to foliation. Other dikes have been rotated toward the southwest so that they dip 20° to 37° northeast relative to the foliation. Lastly, sills oriented at 10° or less to the foliation record finite elongations between 36% and 72%. Clearly, this geometry requires a significant amount of southwestward rotational strain subsequent to leucogranite emplacement. Two

Figure 8.27: Geometry of structural elements in Arroyo Amolares showing observed strain behavior of three sets of leucogranite dikes and sills. Present dike and sill orientations are derived from the stereonet plot. The orientation of the bulk finite strain ellipsoid corresponds to schistosity and lineation in the stretched quartz pebble conglomerate host; strain magnitude is derived from pebble shape measurements.

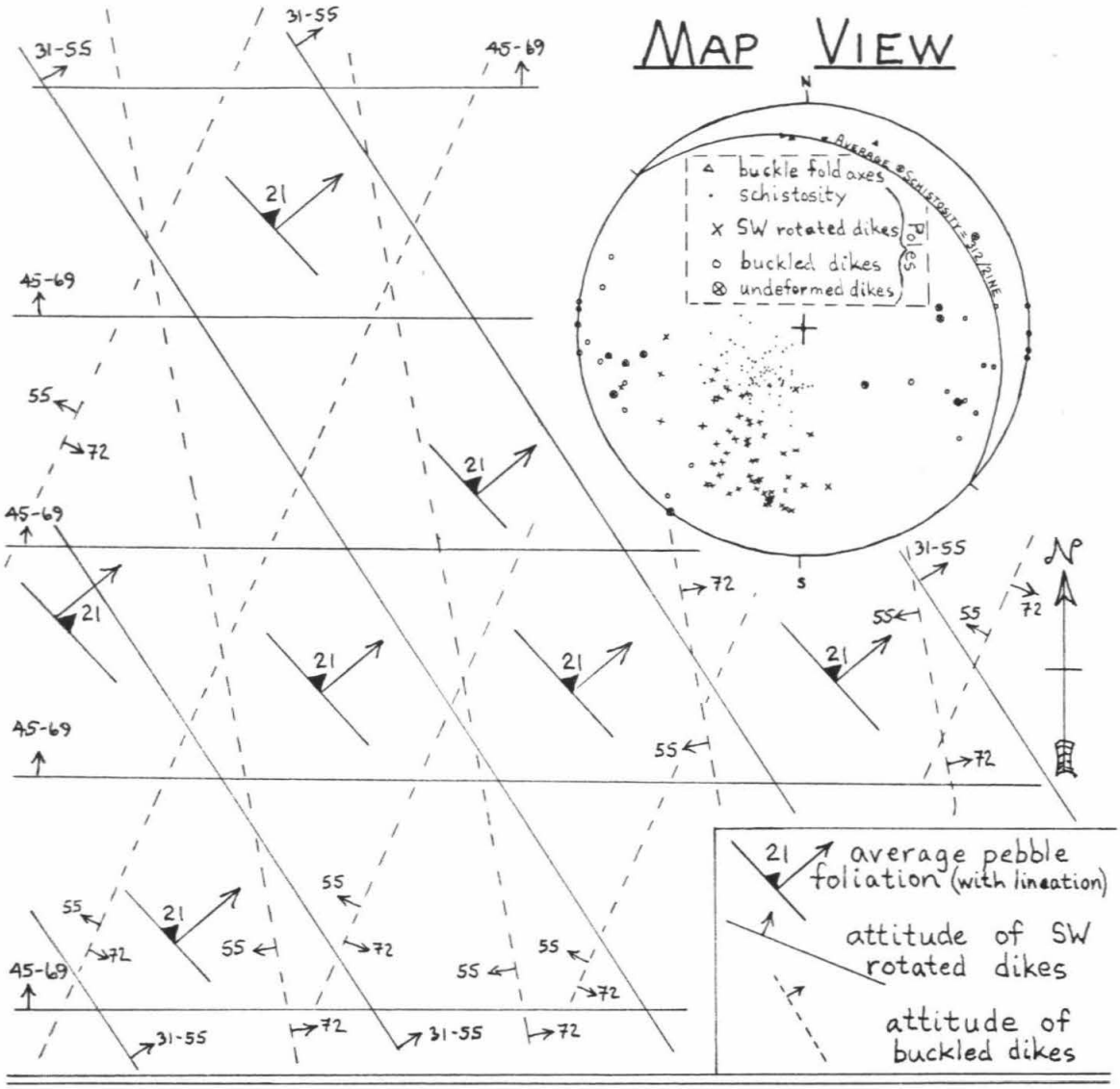
MAP VIEW
N
S
buckle fold axes
schistosity
SW rotated dikes
buckled dikes
undeformed dikes
POLES
AVERAGE SCHISTOSITY = 312/21NE
31-55
45-69
21
55
72
21 average pebble foliation (with lineation)
attitude of SW rotated dikes
attitude of buckled dikes

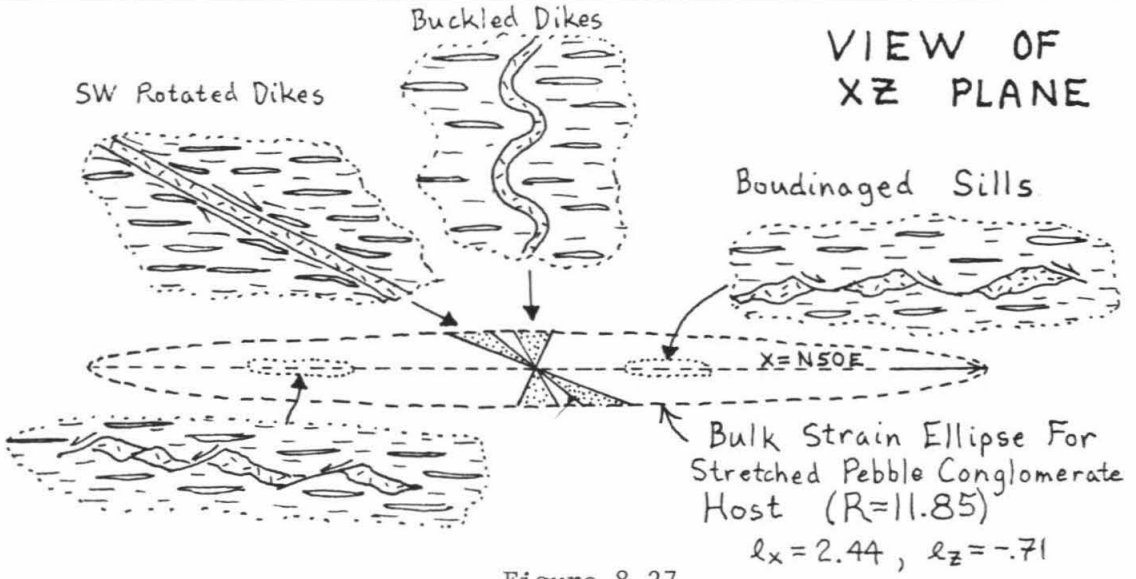
VIEW OF XZ PLANE
Buckled Dikes
SW Rotated Dikes
Boudinaged Sills
X = N50E
Bulk Strain Ellipse For Stretched Pebble Conglomerate Host (R=11.85)
$\ell_x = 2.44$, $\ell_z = -.71$

Figure 8.27

plane strain deformation models (Models 3 and 4) are illustrated in Figures 8.28a and 8.28b.

In Model 3, leucogranites are emplaced into undeformed conglomerate and the bulk strain accummulates entirely via simple shear. To produce the observed pebble elongations a shear strain of 3.2 is necessary. Destraining of the deformed section by this amount yields the theoretical initial geometry shown. Model 3 is deemed inappropriate for three reasons: (1) the predicted initial dike orientations are not symmetrically disposed about σ_1, (2) none of the dikes or veins observed in the field exhibit the 52% to 69% shortening recorded by their counterparts in the model, and (3) observed sills do not preserve the modeled elongations of +138% to +249%. The model does not work because the pebbles have absorbed a significant amount of finite strain prior to leucogranite emplacement.

Model 4 illustrates a more likely scenario: the leucogranites are emplaced as dikes and sills into a previously deformed conglomeratic section. The amount of post-leucogranite noncoaxial deformation may be determined by destraining the deformed setting along a simple shear path until a reasonable initial dike/sill/foliation configuration is reached. The solution shown in Model 4 is obtained with a simple shear strain of 1.2. This particular case yields a residual (pre-existing) pebble strain of e_X = +0.94, e_Z = -0.49. Predicted maximum elongations of sills and maximum shortenings of dikes are only slightly larger than measured values. Model 4 does not explain the fact that most of the northeast dipping dikes which should record a history of shortening are not obviously buckled. It is suspected that these dikes were shortened by means of some internal strain mechanism (layer parallel shortening?). Their coarse grained textures have certainly been disrupted. The response of the leucogranites to shortening strain seems to depend on

Figure 8.28a: Deformation model for Arroyo Amolares. The model assumes that all strain in the conglomerate accumulated via simple shear after dike and sill emplacement. e_α, e_β, and e_δ are the maximum longitudinal strains predicted for the three sets of dikes and sills. R_f is the axial ratio of the bulk strain ellipsoid in the XZ plane.

Figure 8.28b: Preferred deformational model for Arroyo Amolares. The model assumes pure shear of the conglomerate followed by dike and sill emplacement followed by southwest directed simple shear. During the second phase, the bulk shear plane is assumed to initiate at 45° to the pebble foliation. Symbols as in Figure 8.28a.

MODEL 3

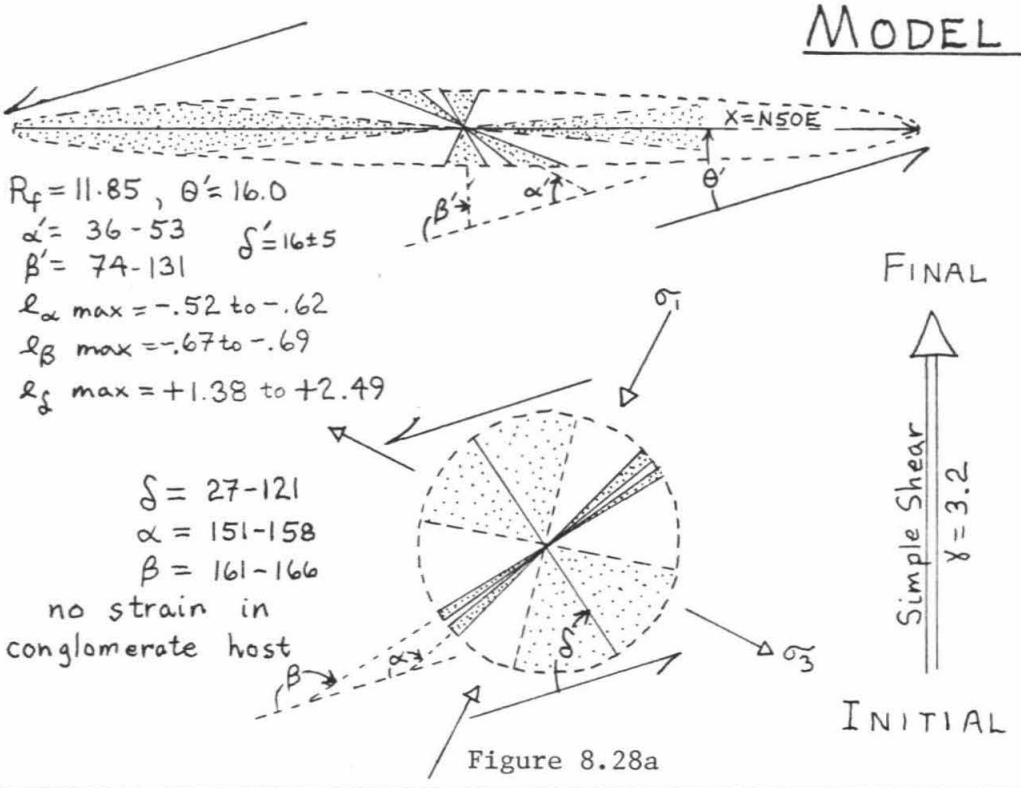

Figure 8.28a

MODEL 4

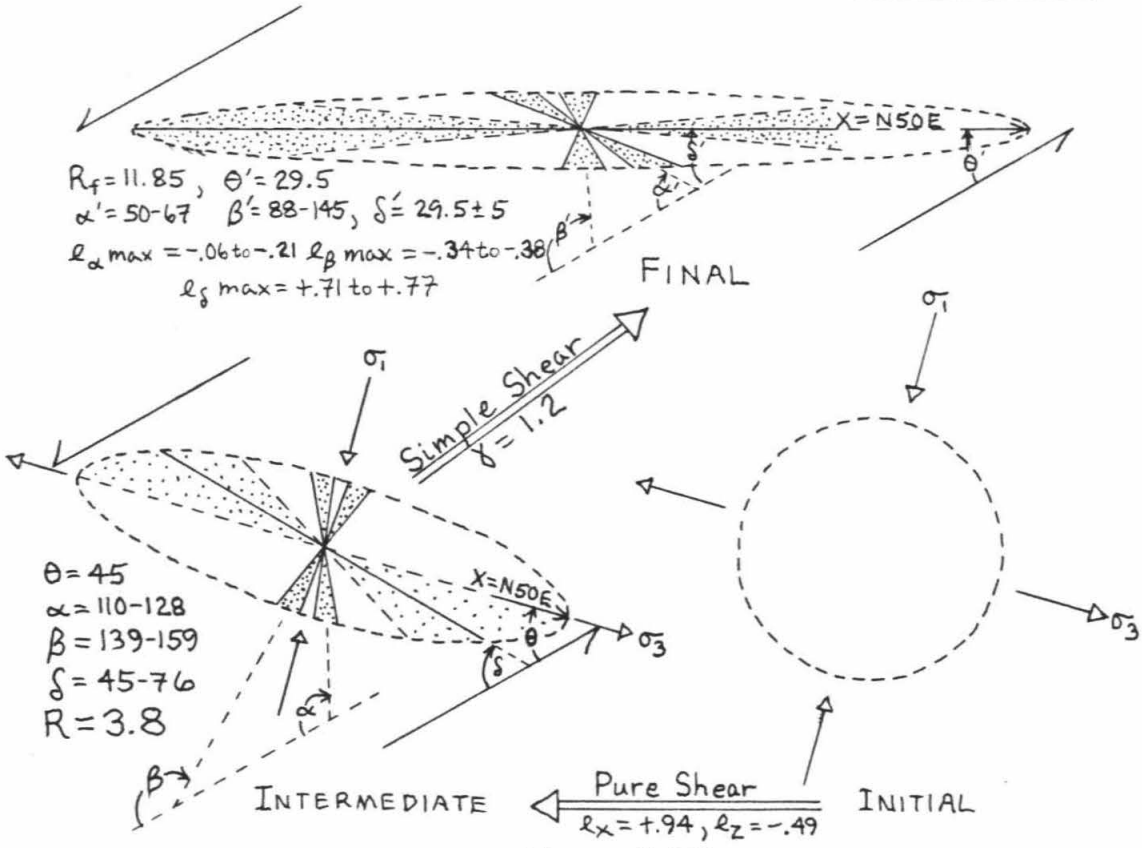

Figure 8.28b

layer thickness. Typically, thin veins are observed to be more significantly buckled than fat dikes.

Dikes and Veins Near La Sauceda/Canada Ombligo: In the vicinity of La Sauceda and Canada Ombligo, the quartz pebble conglomerate/volcanic conglomerate section preserves a more pronounced flattening strain, and the leucogranites appear to be more deformed. Here, maximum measured shortening strains range from 40% to 71%, and a larger proportion of the leucogranite bodies are oriented at low angles (less than 30°) to the pebble foliation (see Figures 8.29a and 8.29b). In many cases, it is difficult to determine if a given tabular leucogranite originated as a dike or a sill. Asymmetrically boudinaged leucogranite are commonly displaced along normal sense shear planes which act to rotate the veins into parallelism with the foliation of their host. These shear planes dip in almost all directions, indicating that a component of flattening strain was involved with late deformation (see Figure 8.30). A few special leocogranite veins preserve a progressive deformational sequence of buckling followed by rotation followed by asymmetric boudinage.

The relative symmetry of the leucogranite deformation in this area relative to the Arroyo Amolares suggests that a coaxial strain path should be considered as one end member. Model 5 (Figure 8.31) illustrates the consequences of a pure shear deformation superimposed on leucogranite dikes and veins of various initial orientations. Coaxial elongations of 100% and 200% produce maximum shortening strains of -0.50 and -0.67, respectively, consistent with the field data. However, a closer analysis indicates the model is flawed in two ways: (1) Pure shear geometry requires that for the range of likely strains the extended veins must make angles of less than 20° to the

Figure 8.29a: Equal area stereonet plot showing poles to rotated and boudinaged leucogranite dikes, sills, and veins from Arroyos Chupadero/Ombligo and vicinity. Those dikes outside the dashed curve are either buckled or apparently undeformed. All data have been rotated so that the schistosity in the metasedimentary host rocks is horizontal.

Figure 8.29b: Contoured version of Figure 8.30a.

Figure 8.30: Equal area stereonet showing poles to discrete ductile shear zones in metasedimentary rocks of Arroyos Chupadero/Ombligo. All poles have been rotated about the local schistosity; i.e., the schistosity is a horizontal plane in this plot.

Figure 8.31: Pure shear deformation model illustrating possible strain behavior of leucogranite dikes or sills in the vicinity of Arroyos Chupadero/Ombligo. Dikes in the shortening field are buckled while dikes (or sills) in the extension field are rotated and stretched via asymmetric boudinage.

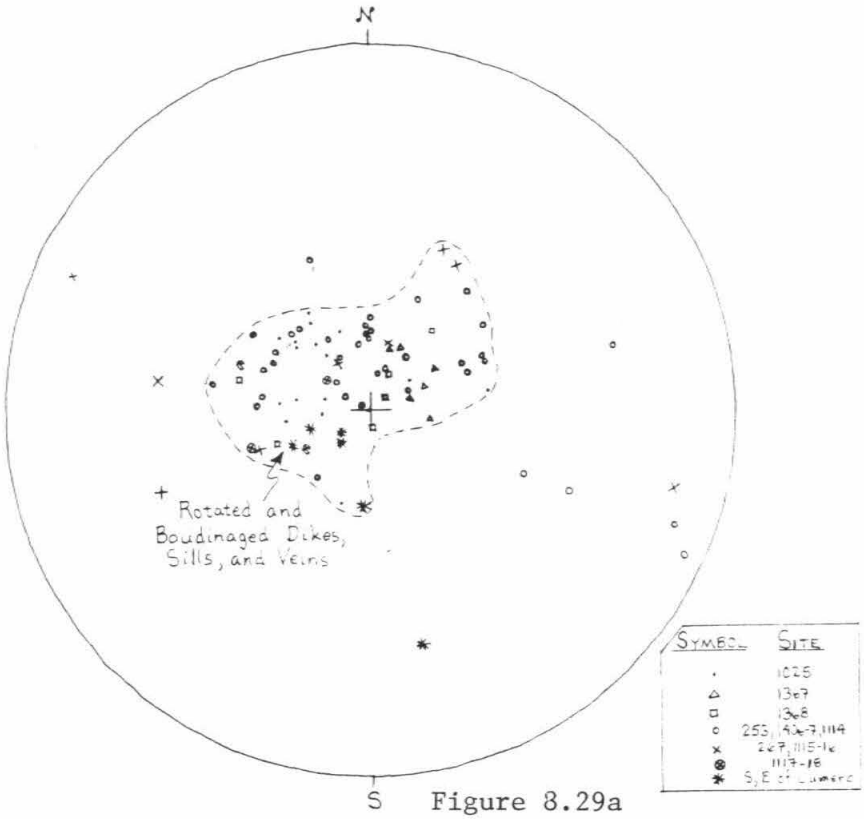

Figure 8.29a

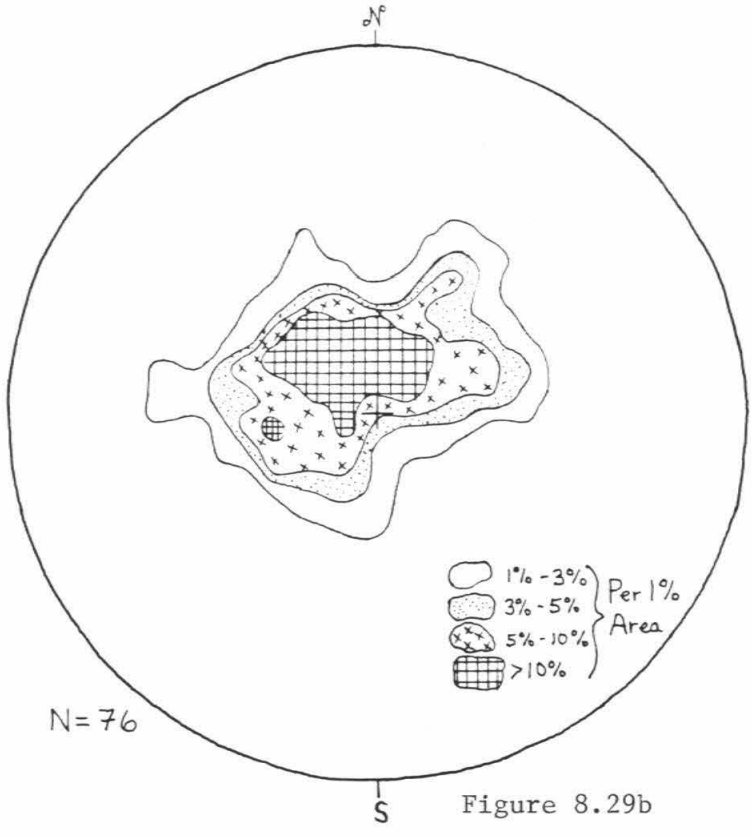

Figure 8.29b

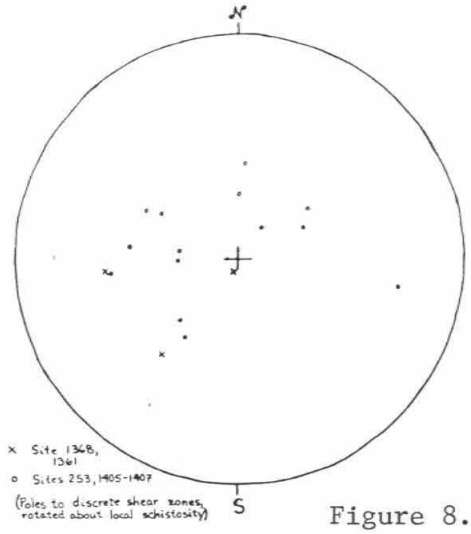

Figure 8.30

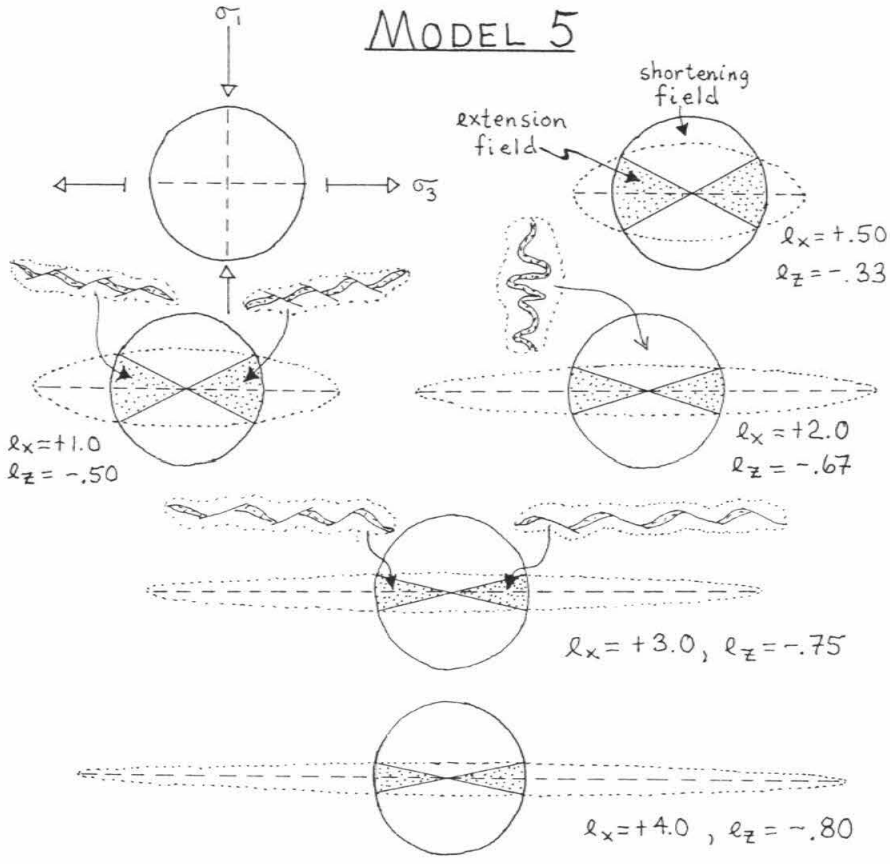

Figure 8.31

foliation. All other vein orientations should display evidence of shortening, and (2) in pure shear it is impossible for a vein to be **shortened and then lengthened**. Depending on its initial orientation, a vein may be **shortened only, lengthened and then shortened,** or **lengthened only**, after a given amount of finite strain. These two conditions are inconsistent with the field observations, hence proper analysis must involve rotational strain.

Model 6 (Figure 8.32) illustrates a way to arrive at the deformed vein/pebble configuration via southwest directed simple shear. In this model, the leucogranites are emplaced as dikes (perpendicular to σ_3) and as sills (parallel to σ_3) into a previously deformed conglomeratic section. As simple shear strain accumulates the dikes and sills both rotate southwestward at a rate faster than the pebble foliation. When the dikes enter the extensional field they are asymmetrically boudinaged via normal slip along southwest vergent shear planes. In contrast, the sills rapidly achieve a **southwest** dip relative to the foliation, and are subsequently displaced along **northeast** vergent shear planes as they extend. The effect of this "back slip" is to rotate some of the sills to steeper angles (20° to 30°) relative to foliation.

A special outcrop located 2 kilometers southwest of La Sauceda provides an opportunity to partition the superimposed simple shear strain component from the pre-existing pebble strain. Here, boudinaged folds in two leucogranite veins are ideally suited for the application of Model 6. In Figure 8.33a, the deformation of Vein 1 is removed along a simple shear path until the pebble foliation achieves an angle of 45° to the observed shear planes. At this stage the vein is oriented virtually parallel to σ_1. The total amount of shear strain involved with this proceure is 2.2. Residual strain in the quartz pebble conglomerate country rocks is: $e_X = +0.42$, $e_Z = -0.30$. This solution requires a maximum vein shortening of 29%, somewhat less than the measured buckling

Figure 8.32: Preferred simple shear deformation model illustrating possible strain behavior of leucogranite dikes and sills in Arroyos Chupadero/Ombligo. In this model, the dikes and sills are injected into a previously deformed conglomerate. The dikes are initially perpendicular to the pebble foliation while the sills are parallel to foliation. The black ellipse tracks the average shape of the deformed conglomerate pebbles as simple shear is superimposed. The dashed ellipse represents the finite strain due to simple shear alone. α' and β' record the orientations of the dikes and sills relative to the finite strain ellipsoid (and the pebble foliation) as simple shear progresses.

Figure 8.33a: Destraining model for a leucogranite vein in stretched quartz pebble conglomerate, Arroyo Chupadero. Simple shear is removed in increments along the observed shear planes until the pebble foliation achieves an angle of 45^{o} to the shear planes. At this stage the vein has an orientation virtually perpendicular to σ_3. The residual strain in the conglomerate is assumed to be due to an earlier episode of pure shear.

Figure 8.33b: Destraining model for a leucogranite vein in stretched quartz pebble conglomerate (same outcrop as vein in Figure 8.33a). Assuming the same shear plane orientation and the same simple shear as in the previous example, this vein must have originated at 81^{o} to σ_3.

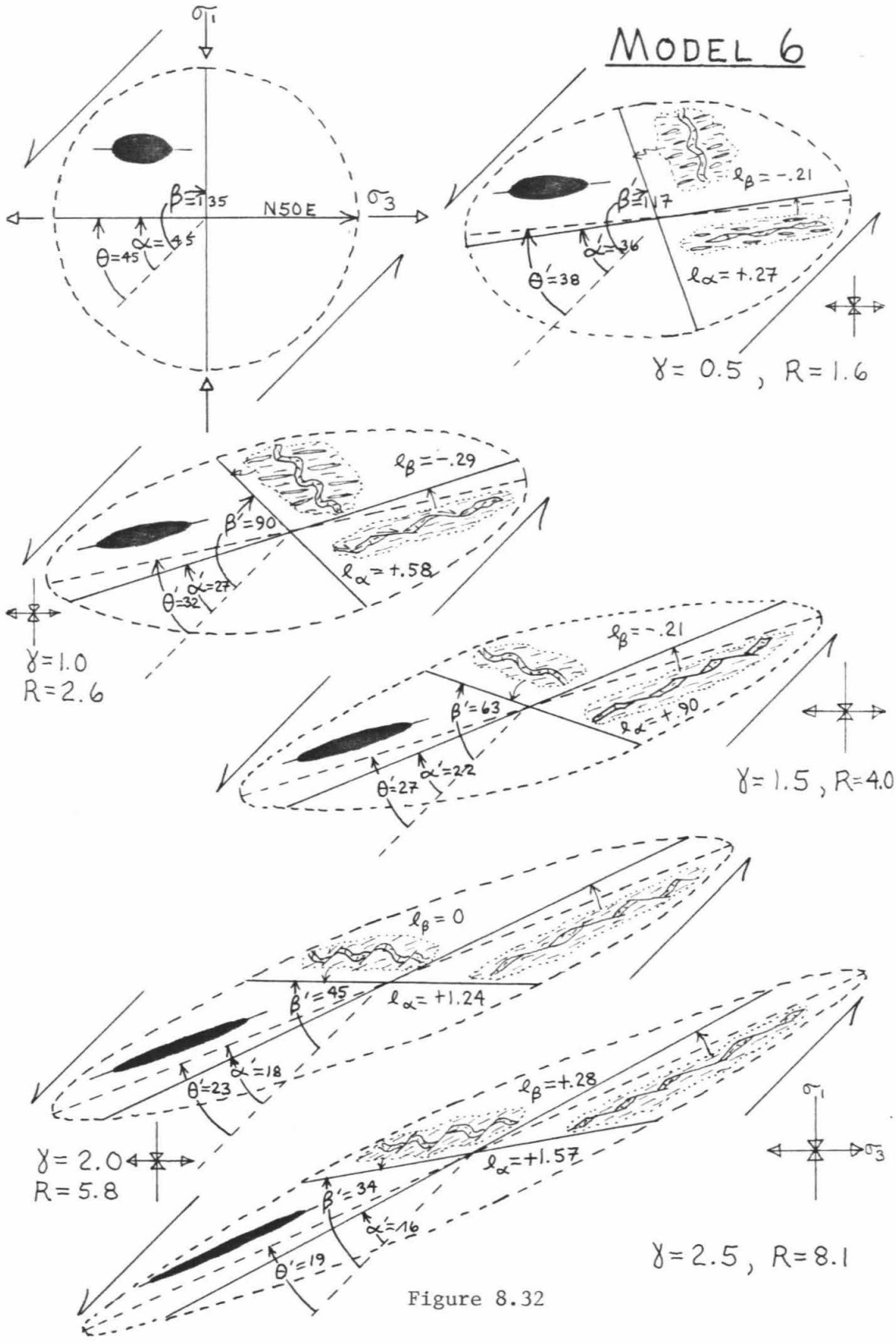
MODEL 6
σ1
σ3
N50E
β=135
α=45
θ=45
γ= 0.5 , R= 1.6
lβ=-.21
β'=117
α'=36
θ'=38
lα=+.27
γ=1.0
R=2.6
lβ=-.29
β'=90
α'=27
θ'=32
lα=+.58
γ= 1.5 , R=4.0
lβ=-.21
β'=63
α'=22
θ'=27
lα=+.90
γ= 2.0
R=5.8
lβ=0
β'=45
α'=18
θ'=23
lα=+1.24
γ= 2.5 , R=8.1
lβ=+.28
β'=34
α'=16
θ'=19
lα=+1.57

Figure 8.32

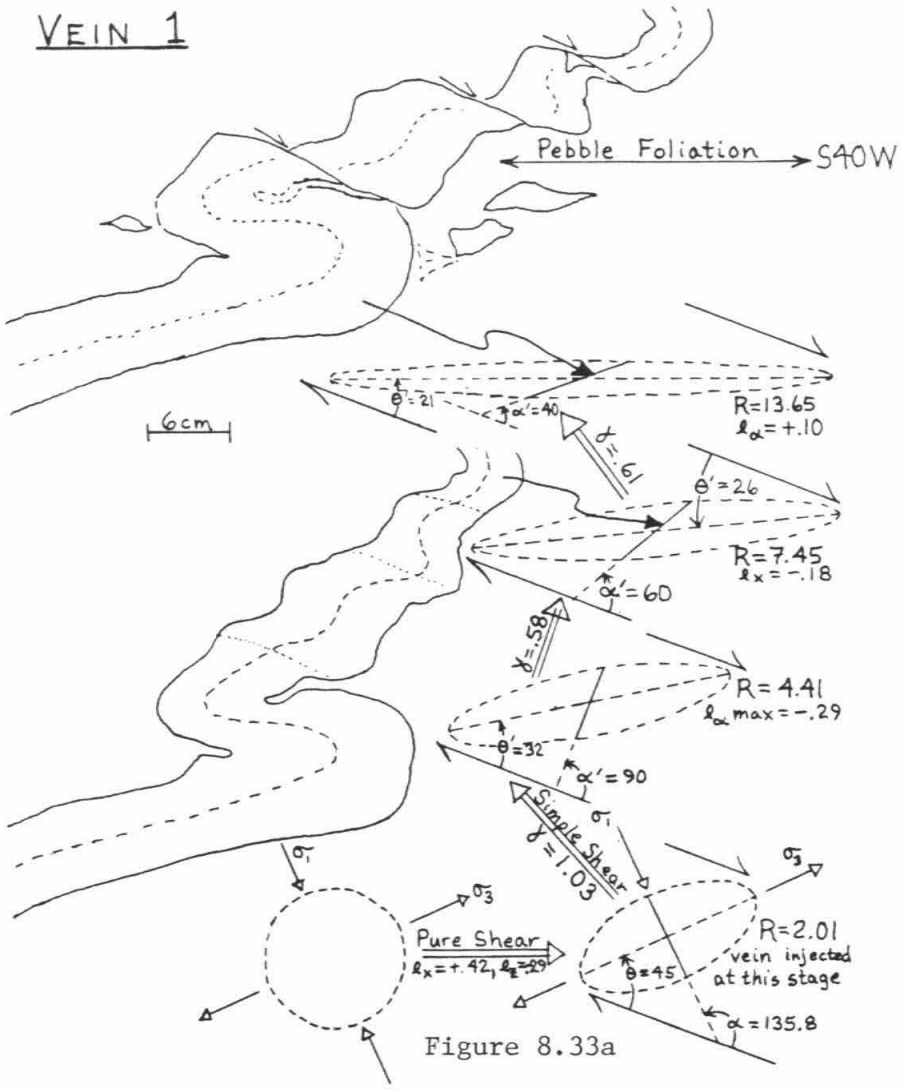

Figure 8.33a

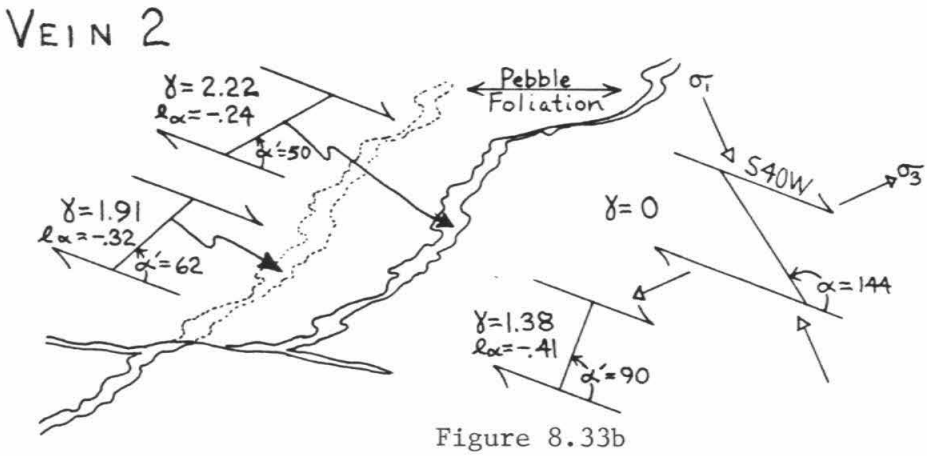

Figure 8.33b

strain of 40%. Some of the extra shortening may be due to an added component of flattening suspected in this area.

Vein 2 (from the same outcrop as Vein 1) offers a rough check on the above solution. A reconstruction of Vein 2 is illustrated in Figure 8.33b Removal of a shear strain of 2.2 results in an initial vein orientation less than 9° from σ_1 and a maximum shortening strain of 40% (quite plausible given the final shape of Vein 2). Neither Vein 1 nor Vein 2 have completely unfolded during their tenure within the extension field. Their observed final geometries are compatable with the orientation and magnitude of the modeled simple shear system.

Asymmetric Boudinage in Arroyo Vallecito: At somewhat deeper structural levels of the Sierra Magdalena, post leucogranite strain is recorded by networks of deformed pegmatite veins within fine grained biotite monzogranite sills. Three dimensional relationships are best exposed in Arroyo Vallecito. Here, most of the veins have undergone asymmetric boudinage, producing strings of diamond shaped boudins oriented subparallel to the finer scale compositional foliation of the leucogranite (see Figure 8.34a; see also Figure 7.12). Boudinage and vein rotation are accomplished by normal sense slip on discrete shear planes. These shear planes are lubricated with quartz, and generally verge either southwest or northeast. Also present in this arroyo are pegmatite veins which have been shortened perpendicular to foliation. Shortening strain is accommodated by displacement along conjugate normal sense shear planes oriented at about 45° to the axis of shortening (see Figure 8.34b).

Oriented tracings of boudinaged veins were collected from various outcrops in the field. All tracings correspond approximately to the XZ plane of

Figure 8.34a: Photograph showing boudinaged pegmatite veins in a fine grained leucogranite host, Arroyo Vallecito. Tape strips are 1 inch wide.

Figure 8.34b: Photograph showing pegmatite vein that has been shortened at a high angle to foliation in its leucogranite host. Strain is accommodated by normal sense slip on conjugate fractures. Scale bar indicates 1 inch.

Figure 8.34a

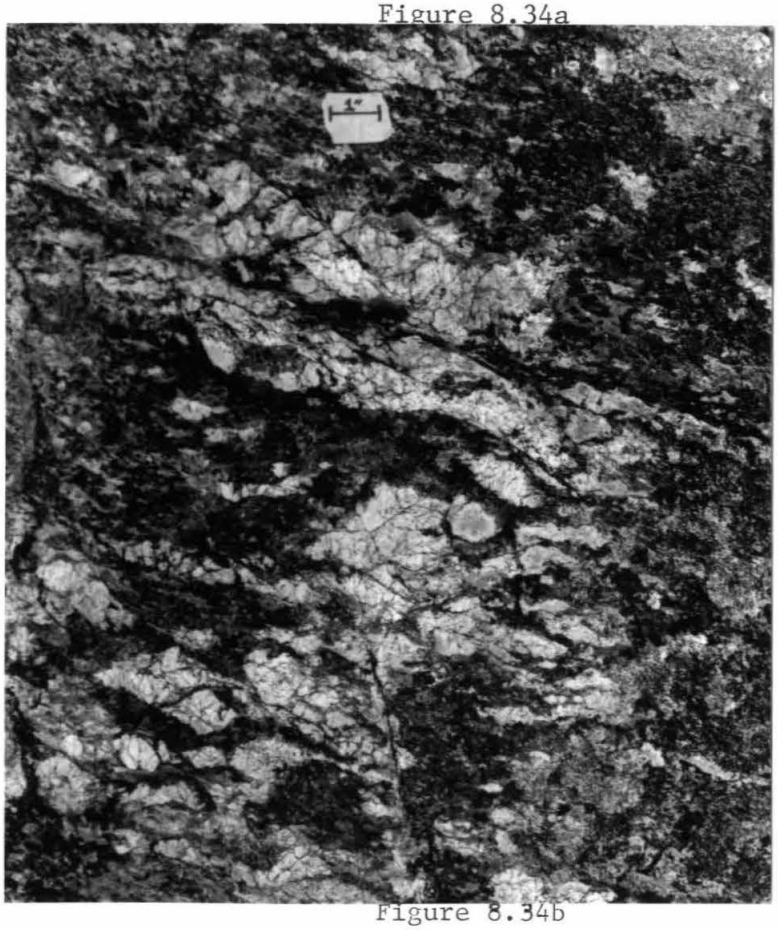

Figure 8.34b

the finite strain ellipsoid. The veins have been reconstructed by restoring observed slip on the shear planes (Figure 8.35 shows several examples). In Figure 8.36, final and initial vein orientations relative to the foliation are compiled. Also indicated are the directions and angles of rotation, and the calculated elongations. It can be seen that most of the veins record southwestward rotation, but a few display the opposite sense. Southwest vergent noncoaxial strain was clearly important in the deformation, but the presence of northeast directed shears suggests that some coaxial strain was involved.

Asymmetric boudins of Arroyo Vallecito are well suited for strain analysis, but solutions depend on the operative deformation mechanisms and the deformation path. The ideal asymmetric boudinage model should yield: (1) a plausible initial vein orientation, (2) a plausible initial orientation and subsequent development of the boudin separating shears, (3) the observed magnitudes of vein rotation and elongation, (4) the predominance of southwest directed shear and rotation, and (5) the observed finite strain in the host monzogranite (e_X = +1.00, e_Z = -0.50). Two end member plane strain models are proposed below. Model 7 (Figure 8.37) utilizes pure shear while Model 8 (Figure 8.38) involves simple shear. Both models assume that the leucogranite host was undeformed prior to emplacement of the pegmatite veins.

In Model 7, the boudinaged veins are initially oriented at angles of 30° or less to σ_3 (all other vein orientations would be shortened under the necessary finite strains of 100+%). As the veins extend, two possibilties exist for initial fracture development: (1) conjugate Coulomb fractures form at 45° to the vein axes, or (2) extension fractures develop at 90° to the vein axes. Inspection of Figure 8.37 leads to the conclusion that Model 7 is not applicable to Arroyo Vallecito. The predicted directions of slip and vein rotation are

Figure 8.35: Outcrop tracings of typical boudinaged pegmatite veins, Arroyo Vallecito. f = feldspar; q = quartz. The veins are reconstructed by restoring slip on the observed shear planes.

Figure 8.36: Illustration of the initial and final orientations and lengths of reconstructed vein segments, Arroyo Vallecito. All veins are oriented relative to the foliation in their fine grained leucogranite host. The directions and magnitudes of vein rotation are indicated, as are the finite elongations and the directions along which the veins were measured.

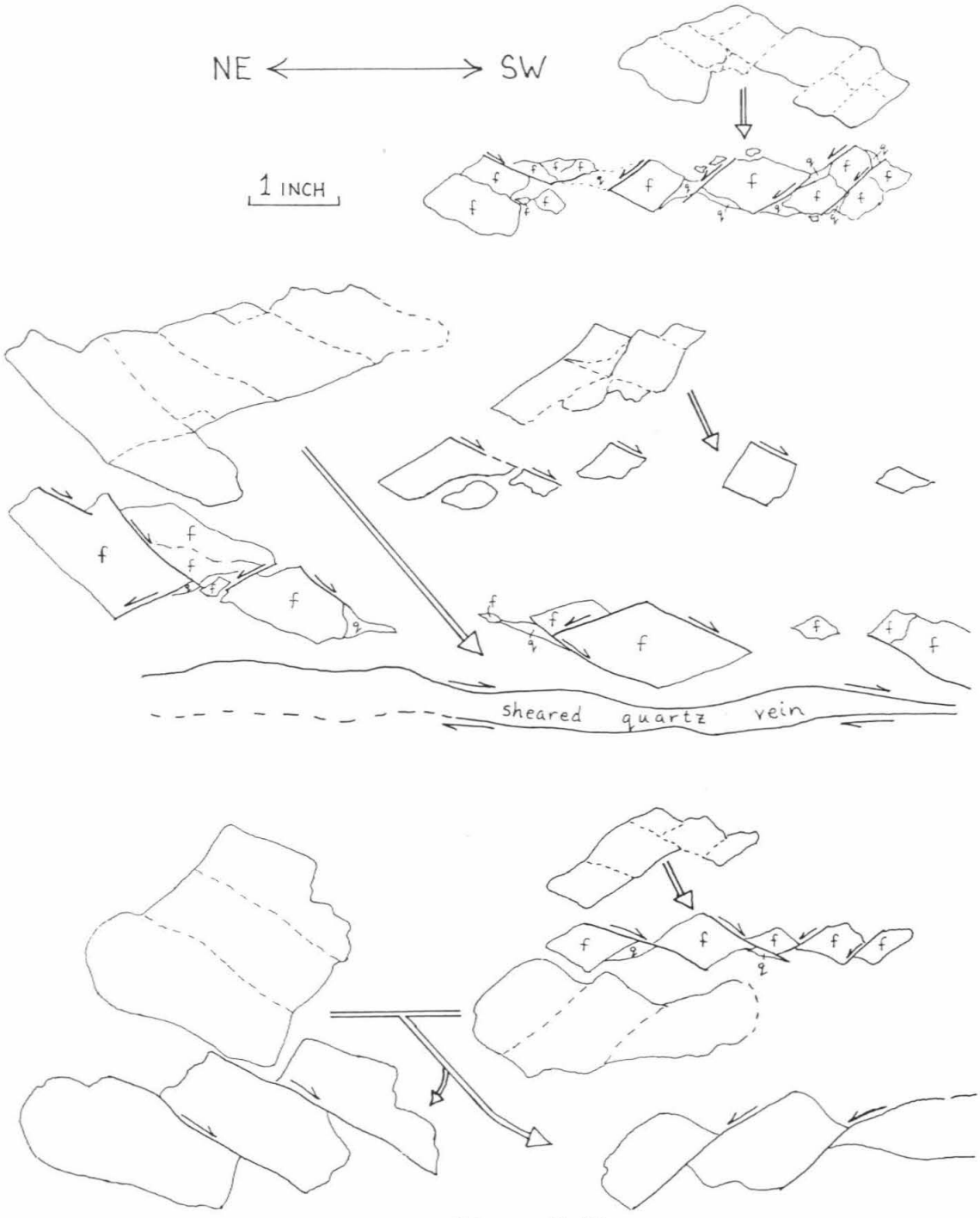

Figure 8.35

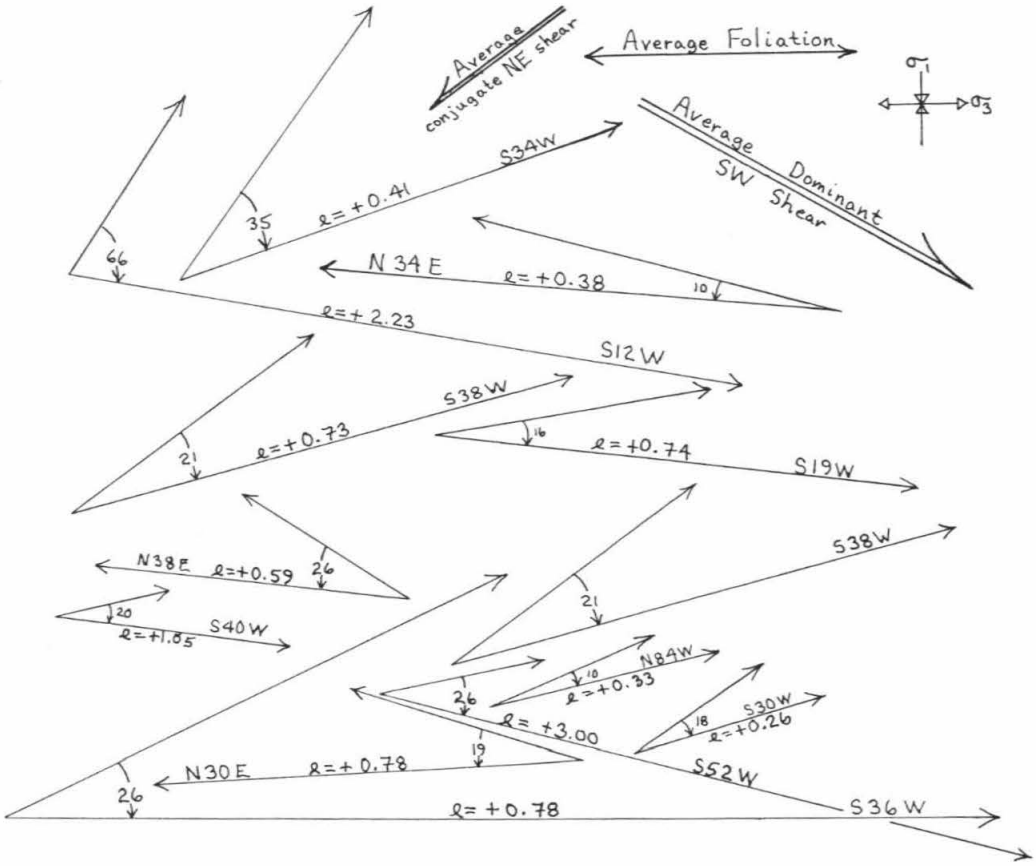
Average conjugate NE shear
Average Foliation
σ1
σ3
Average Dominant SW Shear
S34W
ℓ=+0.41
35
46
N34E
ℓ=+0.38
10
ℓ=+2.23
S12W
S38W
21
ℓ=+0.73
16
ℓ=+0.74
S19W
N38E
ℓ=+0.59
26
20
ℓ=+1.05
S40W
21
S38W
N84W
10
ℓ=+0.33
26
ℓ=+3.00
S30W
18
ℓ=+0.26
19
N30E
ℓ=+0.78
S52W
26
ℓ=+0.78
S36W

Figure 8.36

compatable with field observations, but the observed dominance of southwest vergent shear planes is not produced. The extension fracture mechanism certainly does not work, for the boudin separating shears must undergo extreme rotation (resulting in significant space problems). Finally, it seems unlikely that the veins would initially be emplaced at such low angles to σ_3.

In Model 8, all pegmatite veins are initially oriented at angles of 45^{o} or more to σ_3. Figure 8.38 illustrates the subsequent behavior of three differently oriented veins as the system is subjected to simple shear. The vein initially oriented parallel to the bulk shear plane will not deform. The vein oriented perpendicular to σ_3 will first enter the shortening field, where it develops conjugate Coulomb fractures. As this vein rotates southwestward into the extension field, one set of fractures becomes appropriately oriented for southwest slip. Displacement accumulates and the vein rotates toward σ_3 as deformation progresses. The vein initially oriented perpendicular to the shear plane is always within the extension field. This vein might initially develop extension fractures and/or Coulomb fractures. In the first situation, the extension fractures will be activated as shear planes almost immediately. In the second case, vein rotation equivalent to a shear strain of about 1.0 may be necessary before one set of Coulomb fractures becomes ideally oriented for normal slip.

Comparison of Models 7 and 8 with available field data argues strongly in favor of Model 8. Most of the geometrical relations in Arroyo Vallecito can be explained by simple shear. Depending on the range in initial vein attitudes, application of Model 8 yields shear strains between 2.0 and 3.0. One potential drawback of Model 8 is the persistence of a subordinate set of northeast rotated, northeast sheared vein segments. These features might be explained by superimposing a minor component of coaxial strain parallel to σ_1

Figure 8.37: Pure shear deformation model for asymmetric boudinage in Arroyo Vallecito. The veins must start out at very low angles to σ_3. Two modes of initial fracture development are considered, and the subsequent displacements and rotations of these fractures are illustrated. Finite elongations of the veins are indicated at various stages of the deformation sequence.

Figure 8.38: Preferred simple shear model for asymmetric boudinage, Arroyo Vallecito. Three initial vein orientations are considered, all at angles greater than 45^{o} to σ_3. The type of initial fracture development will be determined early on. The range in likely vein geometries is illustrated for each increment of simple shear. Associated finite elongations are indicated.

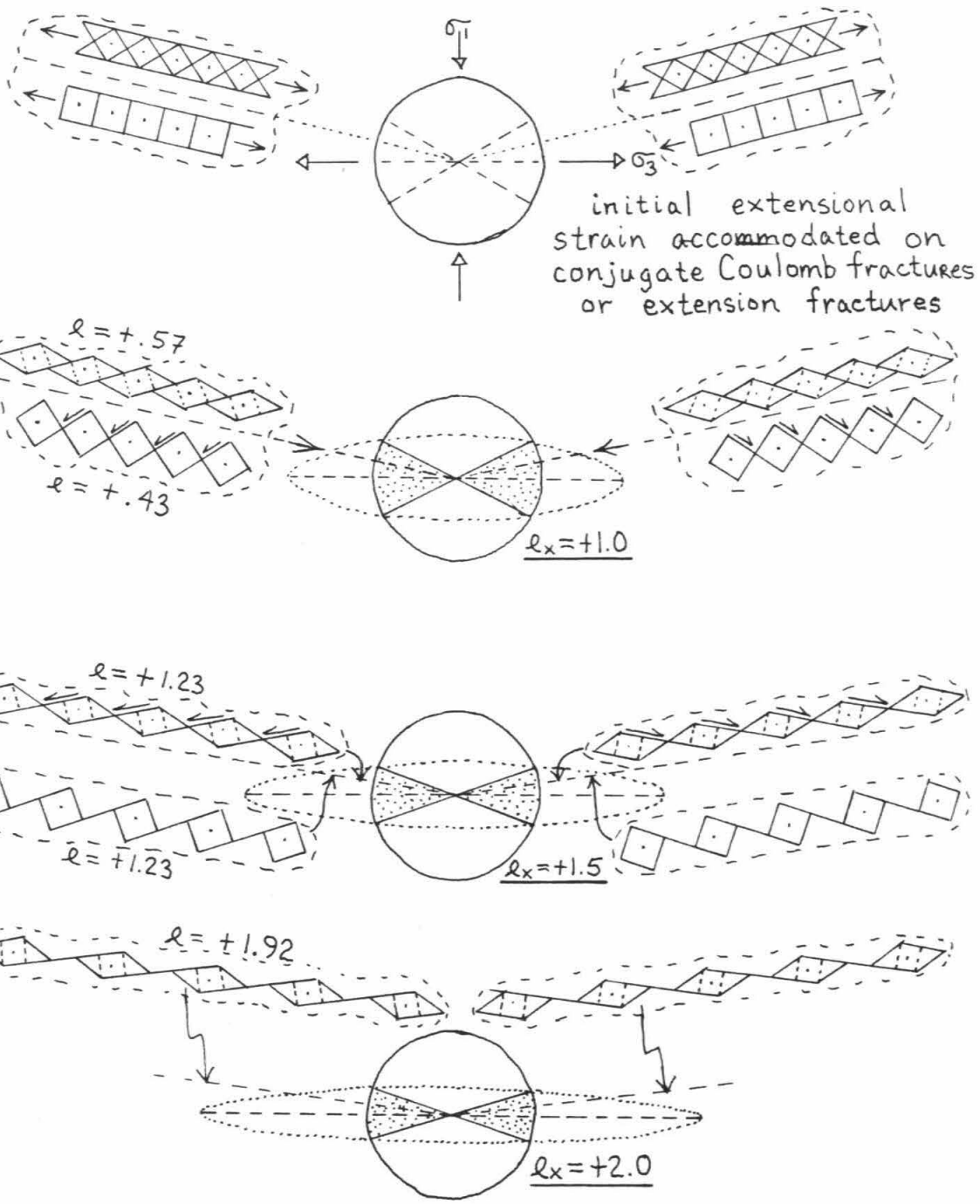

MODEL 7

Figure 8.37

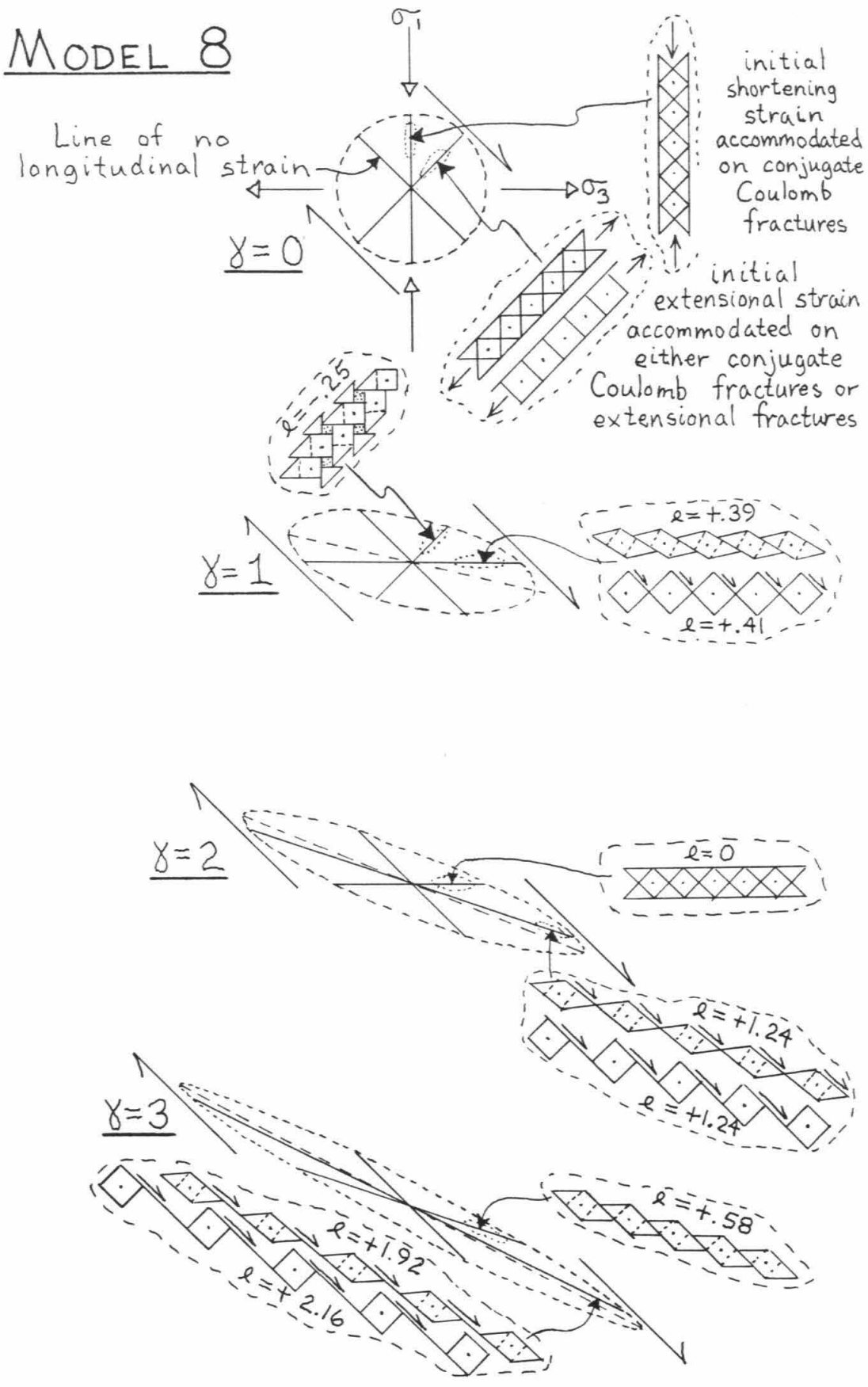
MODEL 8
Line of no longitudinal strain
σ_1
σ_3
γ=0
initial shortening strain accommodated on conjugate Coulomb fractures
initial extensional strain accommodated on either conjugate Coulomb fractures or extensional fractures
ε=.25
γ=1
ε=+.39
ε=+.41
γ=2
ε=0
ε=+1.24
ε=+1.24
γ=3
ε=+.58
ε=+1.92
ε=+2.16

Figure 8.38

during late stages of the deformation. One can imagine how northeast slip might take place on appropriately oriented Coulomb fractures. It seems that the northeast vergent shear planes are needed to even out strain incompatabilities that arise in a regime of bulk southwestward simple shear.

SHEAR STRAINS FROM S-C FABRICS

Over the past ten years, mylonitic S-C fabrics have been recognized in the lower plate granite gneisses of almost every Cordilleran metamorphic core complex. By virtue of their asymmetry, these fabrics are generally interpreted to have developed within noncoaxial shear zones. Much attention has been devoted to determining the sense of shear in these mylonites, but until recently little has been written about the more quantitative aspects of the rotational strain. The question of how much displacement is represented by a given shear zone may be partially resolved by strain analysis. Although the magnitude of brittle slip along the detachment surface cannot be directly measured, the amount of displacement taken up by ductile deformation in the lower plate can.

Naruk (1986) was first to apply simple shear zone theory of Ramsey and Graham (1970) to the kilometer scale shear zones. Naruk's approach is based on Ramsey's observation that within many centimeter-decimeter scale ductile shear zones, the angle between the foliation and the shear zone walls varies with shear strain in a manner consistent with simple shear deformation (see Ramsey and Huber, 1983, pp. 33-50). In the shear zones of the Catalina and Pinaleno metamorphic core complexes of southeastern Arizona, Naruk measured angular variations between mylonitic foliation (S) and shear bands (C) at various structural levels. Using the equation:

$$\gamma = 2/2\tan\Theta',$$ (Ramsey and Huber, 1983, p. 27),

and assuming that the C planes approximate the orientation of the shear zone boundary, he was able to calculate shear strain at different positions and integrate the displacement across the two shear zones

In the next few pages, I present data from the Magdalena area which support Naruk's assumption that shear strain can be directly determined from the angular relationship between S and C. In my analysis, the variation of S ^ C with finite strain is shown to approximate a simple shear law. It is noted that the dominant set of shear planes is parallel to the Magdalena detachment fault, so the detachment could be regarded as a shear zone boundary (though perhaps not the original one). Displacements across the Magdalena shear zone are calculated from measured shear strain versus depth profiles.

Description of Measurements: Most of the granites used in the earlier R_f/Φ analysis display one or two sets of shear planes at low angles to the foliation (see Figures 8.39a and 8.39b). While performing the quartz grain shape measurements, orientations of these shear bands were statistically determined. In XZ sections, the shear bands record normal senses of movement relative to the foliation. In XY sections, the shear bands are parallel to the foliation and show little evidence of offset. The C surfaces are generally defined by narrow, suplanar zones of concentrated shear strain along which biotite flakes, recrystallized quartz grains, and trails of crushed feldspar are deflected and sometimes offset minor amounts. Angular relationships between S and C are usually visible at both microscopic and mesoscopic scales, however, at low strains the shear bands are more easily differentiated with a microscope.

Most of the detailed S-C measurements used to create the curve of Figure 8.43 were performed on granite samples from the southern and central Sierra

Figure 8.39a: Tracing of an oriented sample of granite gneiss (actual size), showing well developed conjugate shear planes. f = feldspar. This sample records a finite elongation of about 60%, determined from quartz grain shape analysis.

Figure 8.39b: Tracing of an oriented sample of granite gneiss (actual size), showing well developed noncoaxial S-C fabric. This sample records a finite elongation of about 210% and a shear strain of 2.0.

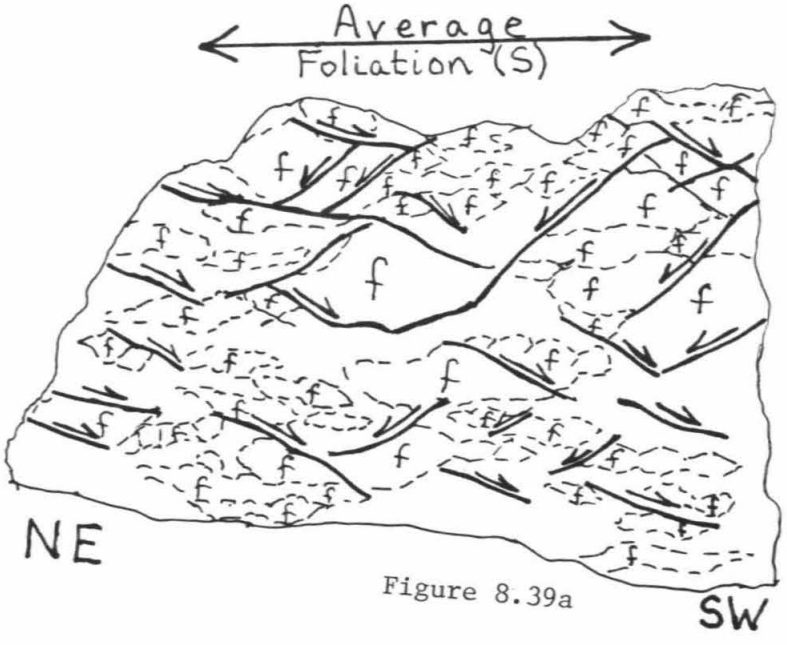

Figure 8.39a

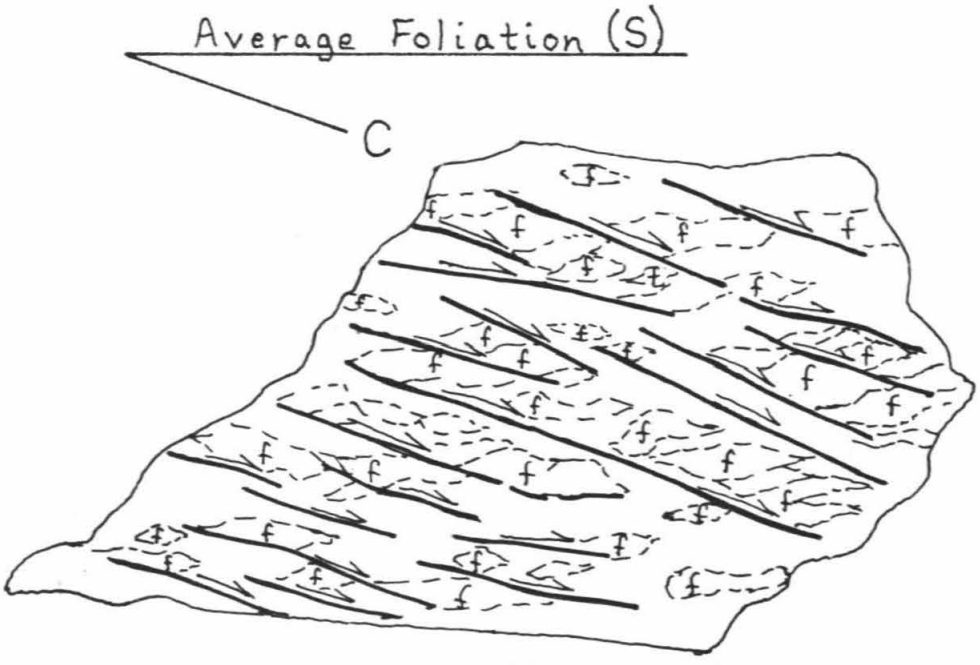

Figure 8.39b

Magdalena. All analyses are from surfaces sliced parallel to lineation and perpendicular to foliation. The S-C technique of shear strain determination developed below is later applied to hand specimens from the Sierra Madera.

Data Analysis: Variations in S-C fabrics within the southern and central Sierra Magdalena provide insight into the geometry and mechanics of noncoaxial deformation. Remembering that the irrotational strains derived from the quartz grains showed an upward increasing gradient, it is interesting to study shear band development as a function of structural level. Figure 8.40 shows shear band orientations observed along a northeast-southwest profile through the tilted granitic gneiss sequence north of Magdalena. The deepest, least strained granites display conjugate shear bands at 25° to 35° to the foliation. One set may be dominant, but coaxial shortening was clearly important in the deformation. At intermediate levels, the S-C fabrics are distinctively asymmetric, with a dominant set of shear planes oriented at 10° to 25° to the foliation. At the highest levels, the gneisses are essentially ultramylonites, with less than 10° discordance between S and C. Corresponding to the upward increase in asymmetry are several other gradients: (1) an increase in quartz grain elongation, (2) a decrease in porphyroclast/matrix ratio, (3) an increase in the degree of porphyroclast roundness, and (4) an increase in C plane density (marked by a decrease in shear band spacing).

The observation that the shear bands become progressively and systematically better developed as one traverses through zones of greater and greater finite strain is taken as evidence that the S and C planes evolved **synchronously**. In fact, the shear bands are a necessary mechanism for accommodating rotational strain as the foliations develop. Naruk et al., (1986)

Figure 8.40: Northeast-southwest profile through the southern Sierra Magdalena, illustrating the variability in shear band geometries observed at different structural levels. No vertical exaggeration.

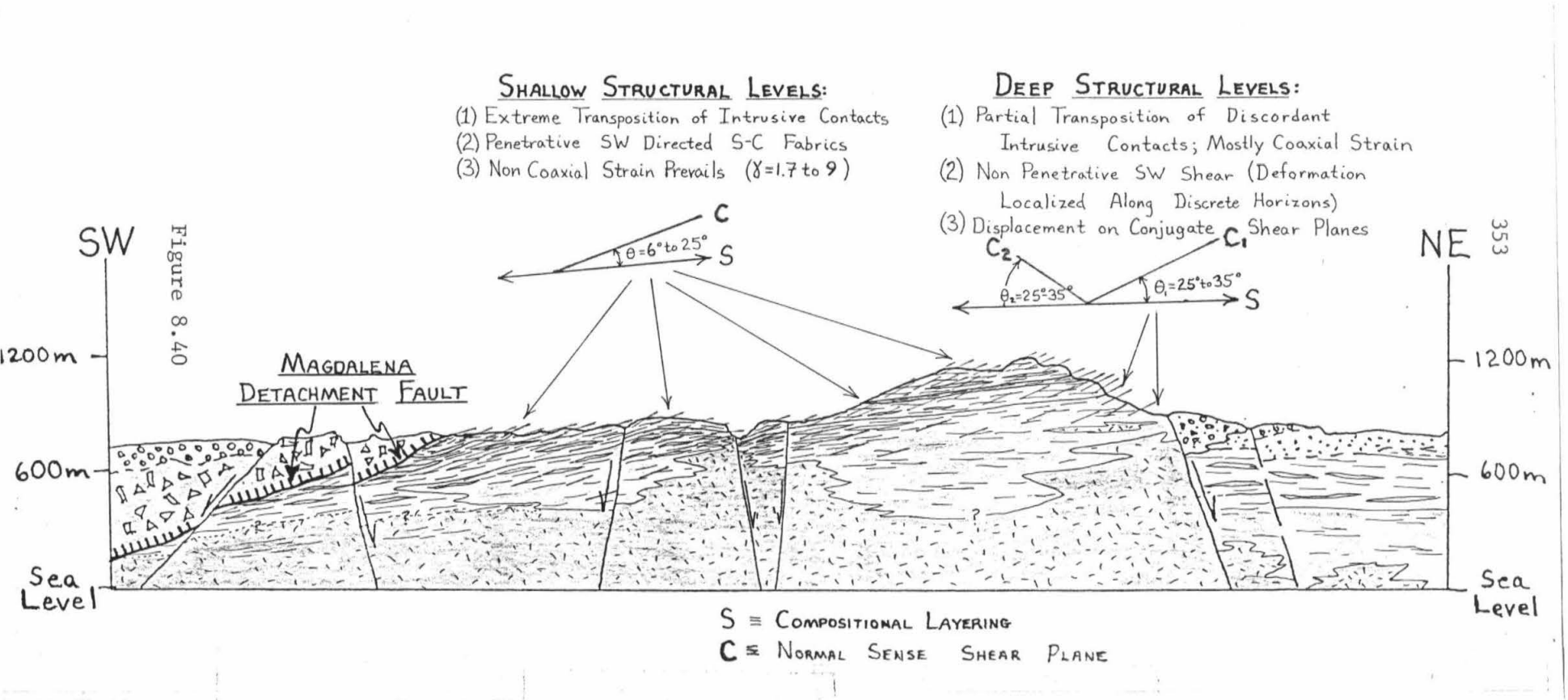
SHALLOW STRUCTURAL LEVELS:
(1) Extreme Transposition of Intrusive Contacts
(2) Penetrative SW Directed S-C Fabrics
(3) Non Coaxial Strain Prevails (γ=1.7 to 9)
DEEP STRUCTURAL LEVELS:
(1) Partial Transposition of Discordant Intrusive Contacts; Mostly Coaxial Strain
(2) Non Penetrative SW Shear (Deformation Localized Along Discrete Horizons)
(3) Displacement on Conjugate Shear Planes
C
θ=6° to 25°
S
C2
C1
θ2=25°-35°
θ1=25°to35°
S
SW
NE
1200m
600m
Sea Level
MAGDALENA DETACHMENT FAULT
1200m
600m
Sea Level
S ≡ COMPOSITIONAL LAYERING
C ≡ NORMAL SENSE SHEAR PLANE

Figure 8.40

reached a similar conclusion from studies of S-C fabrics in granites of several Arizona core complexes.

In Figure 8.41, I propose a model for the evolution of S-C fabrics in the Magdalena granites. The fabrics develop in an extensional environment, with σ_1 appproximately vertical and σ_3 horizontal and directed NE-SW. Initial deformation is accommodated by displacement along conjugate normal sense shear planes, resulting in a bulk coaxial shortening strain, with NE-SW extension. The shear bands become zones of weakness favorably oriented for slip in either a northeast or southwest direction. A slight rotation of the rock mass relative to the regional stress system is all that is needed to preferentially transfer slip to the southwest dipping set of shear planes. From this point on the strain accumulates noncoaxially, as rotation of foliation planes toward the dominant set of shear planes is accommodated by lesser antithetic slip along the conjugate set. The early stages of this model are similar to a drawing in Ramsey and Graham (1970), which depicts a region of crust evolving from a coaxial strain environment to a noncoaxial environment.

Figure 8.42 compares mesoscopic and microscopic S-C measurements from the same samples. Although the uncertainties overlap, there are certainly discrepancies between the two methods. These discrepancies are non systematic, i.e., one technique does not yield consistently lower values than the other, and the amount of disparity does not appear to depend on the strain intensity. The observed differences in measured Θ' values may be due to two effects: (1) the thin section samples a nonrepresentative portion of the larger hand specimen, and/or (2) at a larger scale the eye may correlate shear bands and foliations which are not obviously continuous at micro scale. In other words, the mesoscopic measurements give a general average of the S-C geometry over a larger area, while the micro measurements yield the true

Figure 8.41: Model for the development of S-C fabrics in the granites of the Magdalena core complex. The transition from coaxial deformation to noncoaxial deformation may be viewed either as a progression in time (pure shear followed by simple shear) or as a progression in space (pure shear at deep structural levels contemporaneous with simple shear at shallower levels).

Figure 8.42: Comparison of mesoscopic and microscopic S-C measurements from the same samples. Data points are arithmetic means; error bars indicate one standard deviation dispersion about the mean.

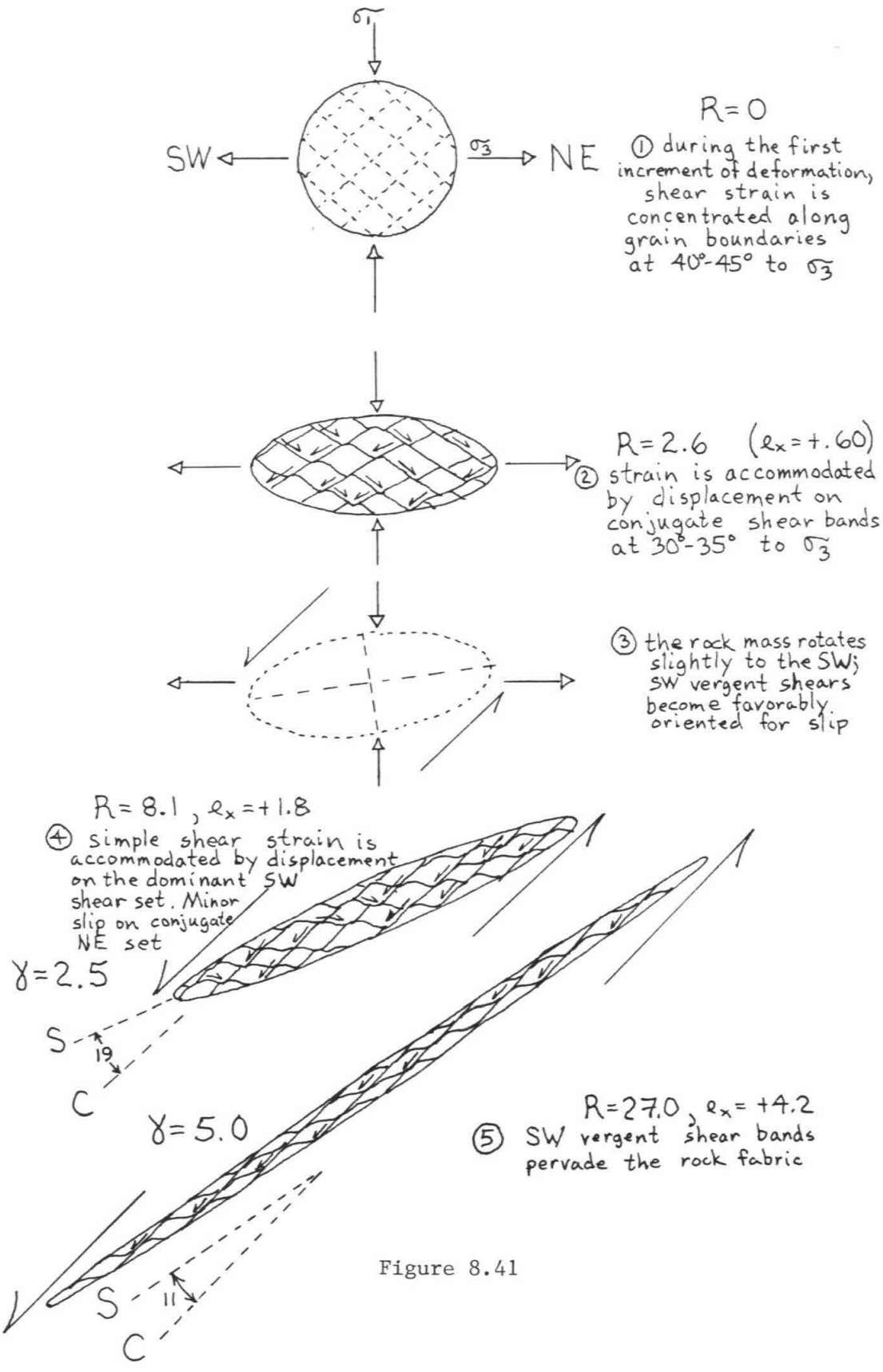
σ1
SW
σ3
NE
R=0
① during the first increment of deformation, shear strain is concentrated along grain boundaries at 40°-45° to σ3
R=2.6 (εx=+.60)
② strain is accommodated by displacement on conjugate shear bands at 30°-35° to σ3
③ the rock mass rotates slightly to the SW; SW vergent shears become favorably oriented for slip
R=8.1, εx=+1.8
④ simple shear strain is accommodated by displacement on the dominant SW shear set. Minor slip on conjugate NE set
γ=2.5
S
19
C
γ=5.0
R=27.0, εx=+4.2
⑤ SW vergent shear bands pervade the rock fabric
S
11
C

Figure 8.41

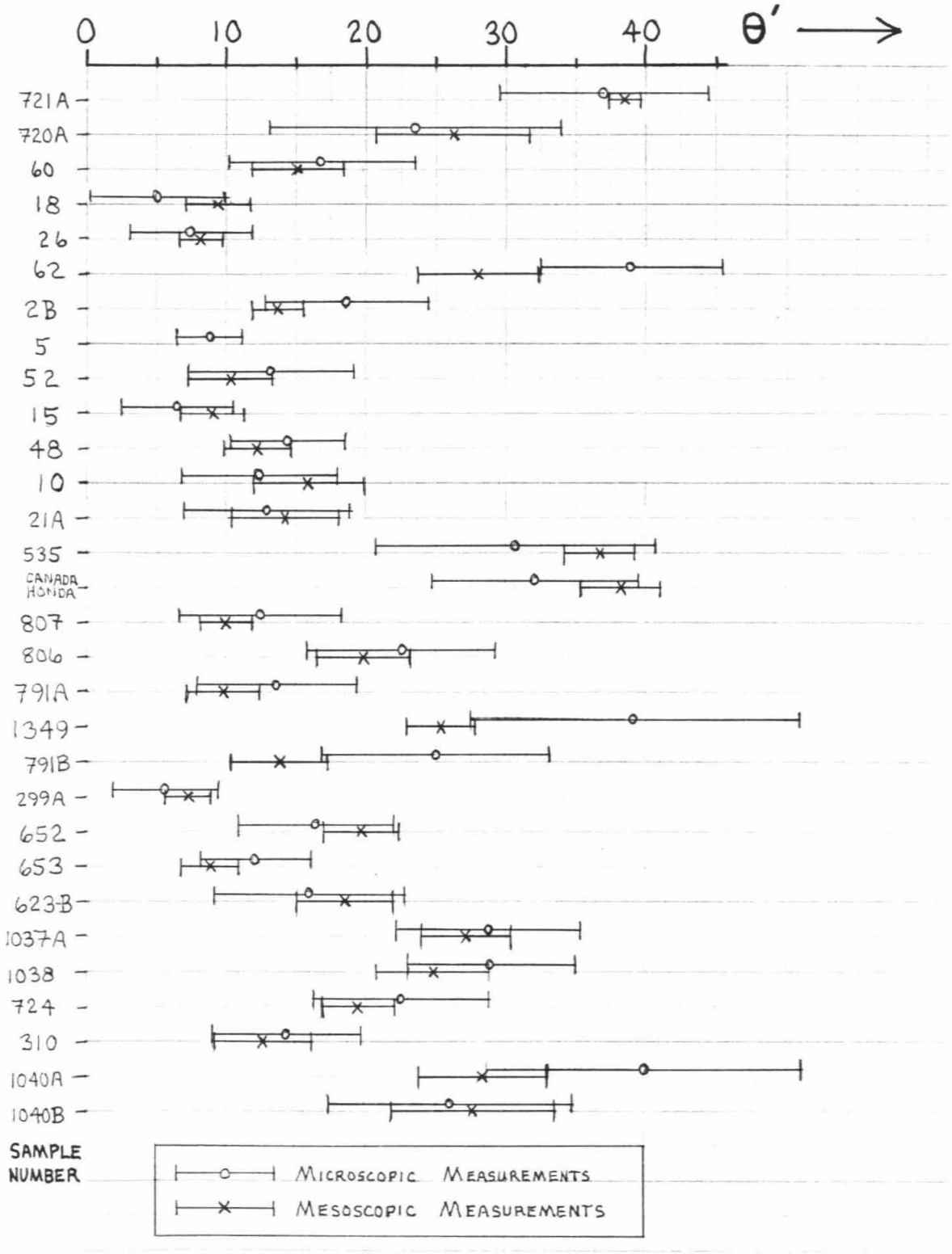
0
10
20
30
40
θ'
721A
720A
60
18
26
62
2B
5
52
15
48
10
21A
535
CANADA HONDA
807
806
791A
1349
791B
299A
652
653
623B
1037A
1038
724
310
1040A
1040B
SAMPLE NUMBER
MICROSCOPIC MEASUREMENTS
MESOSCOPIC MEASUREMENTS

Figure 8.42

variability in localized domains.

In Figure 8.43, the angle between S and C (i.e., Θ') is plotted as a function of R_{XZ} for all measured samples. At low strains the dominant shear plane of the conjugate set is used in the Θ' determination. Superimposed on the data set is a theoretical curve which tracks the angle between the X direction of the finite strain ellipsoid and the shear zone boundary as a function of R_{XZ} in a regime of homogeneous simple shear. Considering the measured S-C discordance to be equivalent to the X-shear plane discordance in a simple shear zone, this figure provides a quantitative measure of how significantly the deformation in the granites deviates from ideal simple shear.

Deviations from ideality are believed to be related to three effects: (1) At low strains the deformation is partly coaxial, i.e., some of the quartz grain elongation is accommodated by slip along surfaces antithetic to the dominant shear planes. Hence, the rock records more strain than it would due to activity of the dominant shear planes alone. (2) At high strains stretched quartz grains may break up into separate domains, or may be displaced along shear bands. Thus the measured values may underestimate the amount of finite strain accumulated during simple shear. (3) General scatter about the curve at all strains is due partly to heterogeneous deformation. A certain amount of nonuniform strain is implied by the fact that within a given sample the C planes are not completely parallel.

Figure 8.43: S-C calibration curve: graph of theta' versus strain ratio for variably deformed granites of the Magdalena core complex. θ' is the angle between S and C. R_{XZ} is the average axial ratio of deformed quartz grains. Each data point is the arithmetic mean of the measurement population for a given sample; error bars indicate one standard deviation dispersion about the mean. The low strain samples (R_{XZ} less than 3) generally exhibit conjugate shear planes; in these samples the dominant shear plane was chosen for the θ' determination.

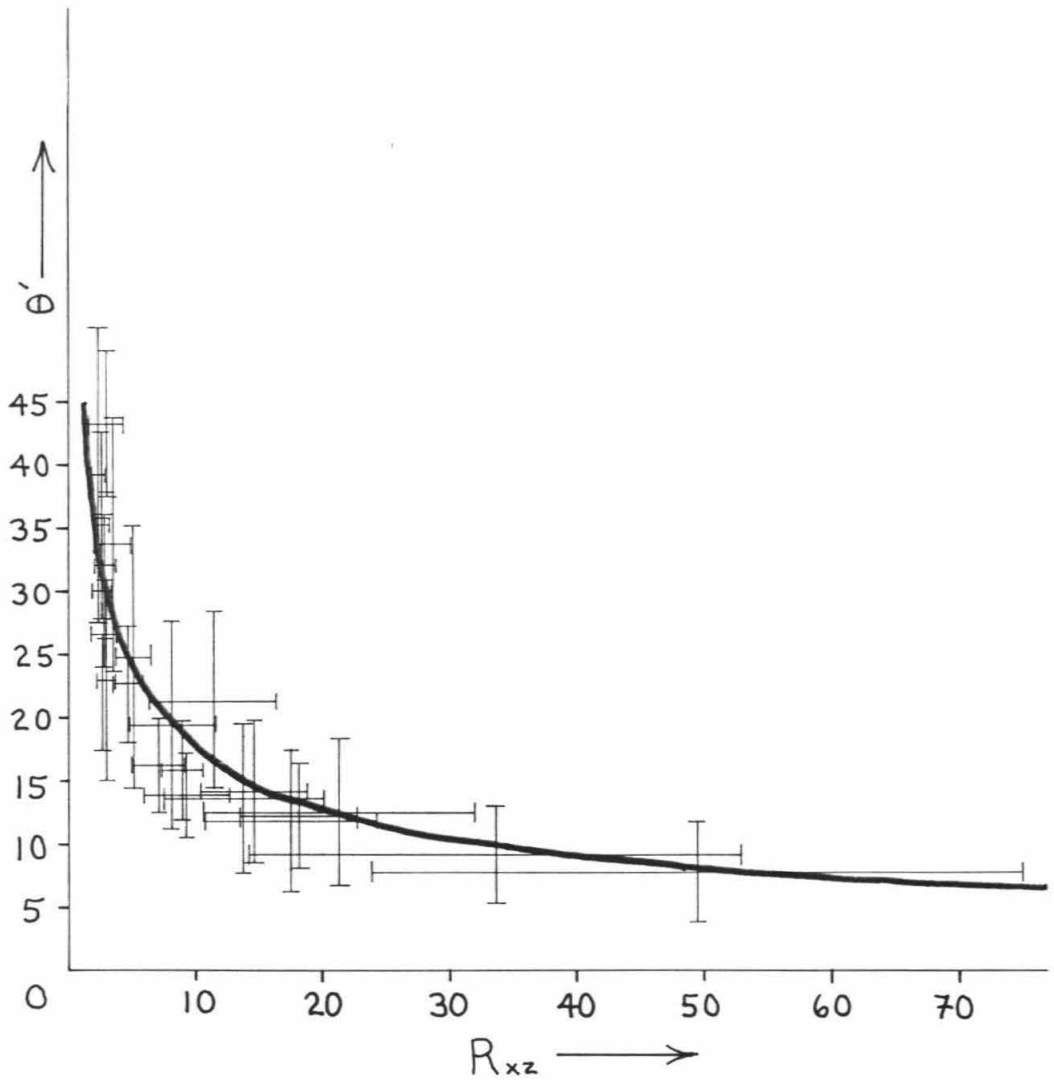

Figure 8.43

Despite the non ideal behavior cited above, in general the S-C data set is compatable with simple shear deformation. The measured Θ' values reasonably approximate the angular discordance between the finite strain ellipsoid and the bulk shear plane in a simple shear zone. Given this assertion, the equation:

$$\gamma = 2/2\tan\Theta'$$

may be used to determine the shear strain wherever asymmetric S-C fabrics are well developed in the granites.

Extension of the S-C Technique to the Sierra Madera: Accepting the S-C technique as a valid means of shear strain determination, oriented hand specimens of granite from the Sierra Madera were sliced along XZ planes for mesoscopic analysis. Θ' values were determined at all possible structural levels. Additional samples from the Sierra Magdalena were analyzed for geometric control. As observed earlier, the least strained samples occur at the deepest structural horizons, and tend to display conjugate shear bands. It appears that the lower boundary of the zone of noncoaxial deformation is everywhere gradational into an interval characterized by coaxial strain of minor intensity.

SUMMARY OF SHEAR STRAIN DISTRIBUTION

Figure 8.44a is a compilation map showing the distribution of all measured post-leucogranite shear strains in the lower plate. Rotational strains determined from deformed dikes and veins are plotted in addition to strains derived from S-C analysis. The highly asymmetric contoured pattern (Figure 8.44b) indicates that shear strain increases both toward the southwest and up section.

Figure 8.44a: Distribution of post-leucogranite southwest vergent shear strain in the lower plate. Shear strain values are derived from S-C measurements in granites and from rotated and deformed dikes. The high shear strains in the west central Sierra Guacomea are from samples collected along late northeast vergent discrete normal sense shear zones. Circled points indicate undeformed or very slightly strained samples.

Figure 8.44b: Contoured version of Figure 8.44a, showing also the distribution of the Late Cretaceous-Early Tertiary regional metamorphic fabric.

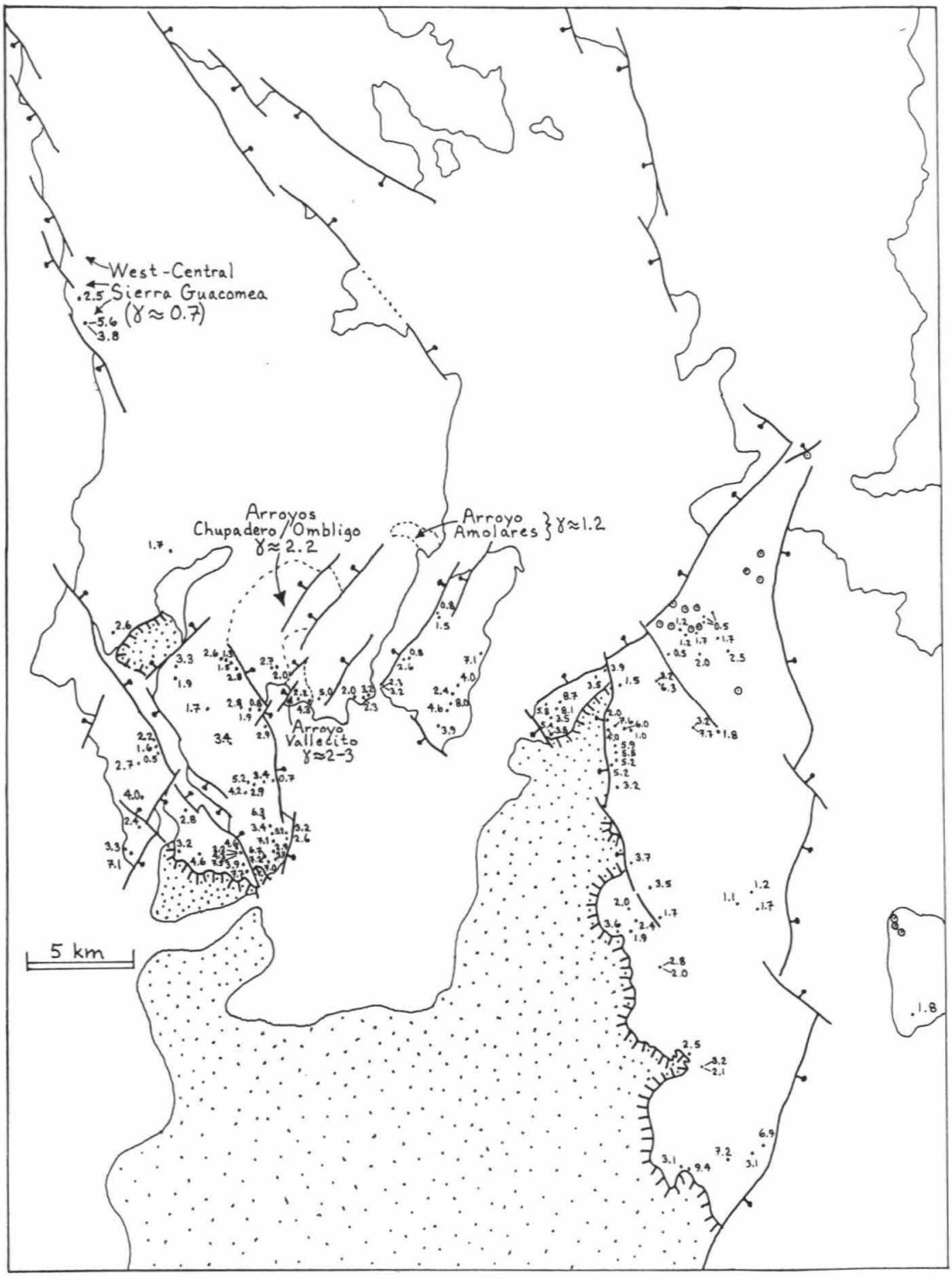
West-Central
Sierra Guacomea
(γ ≈ 0.7)
Arroyos
Chupadero/Ombligo
γ ≈ 2.2
Arroyo
Amolares
γ ≈ 1.2
Arroyo
Vallecito
γ ≈ 2-3
5 km

Figure 8.44a

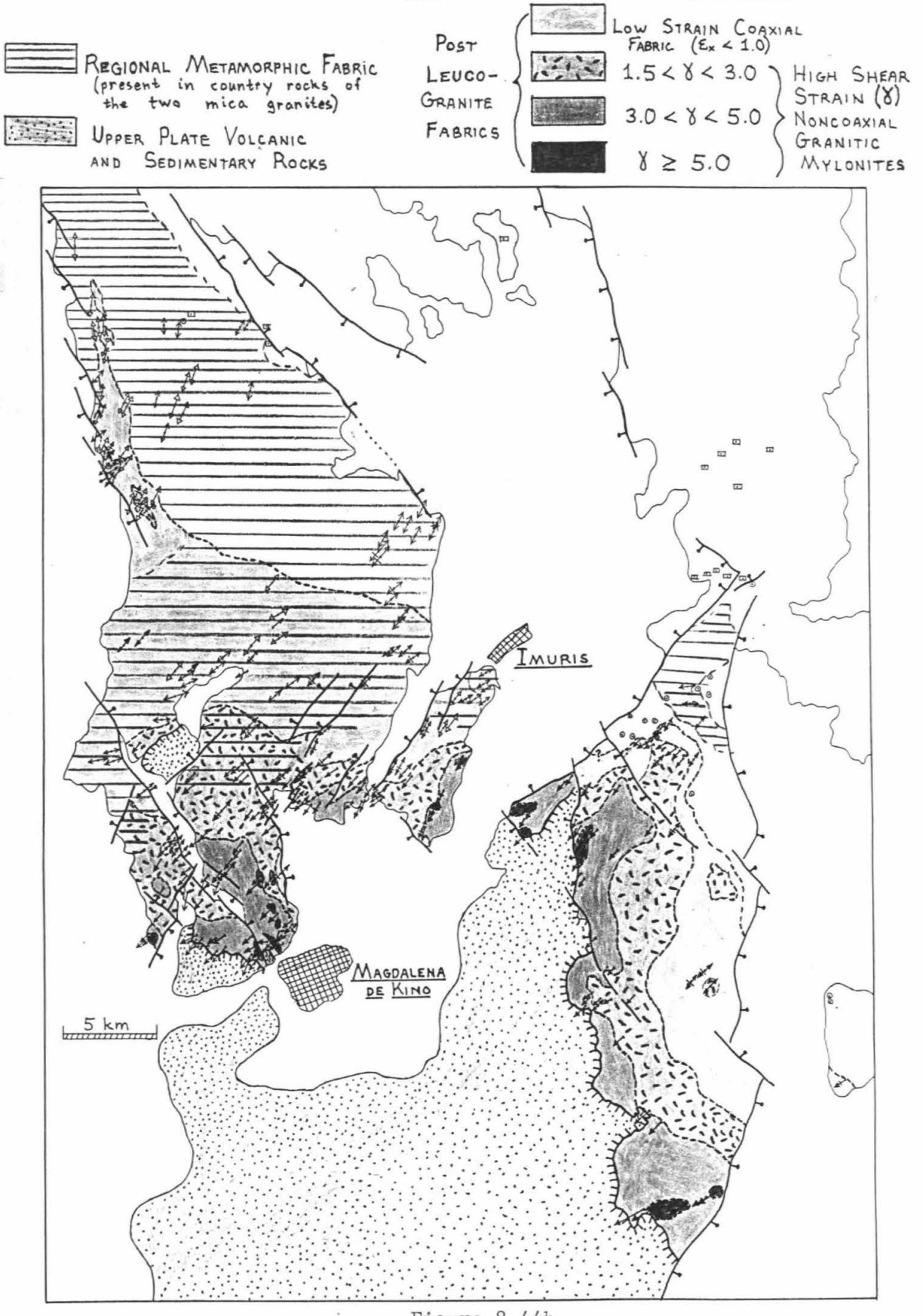
REGIONAL METAMORPHIC FABRIC
(present in country rocks of the two mica granites)
UPPER PLATE VOLCANIC AND SEDIMENTARY ROCKS
POST LEUCO-GRANITE FABRICS
LOW STRAIN COAXIAL FABRIC ($\varepsilon_x < 1.0$)
$1.5 < \gamma < 3.0$
$3.0 < \gamma < 5.0$
$\gamma \geq 5.0$
HIGH SHEAR STRAIN (γ) NONCOAXIAL GRANITIC MYLONITES
IMURIS
MAGDALENA DE KINO
5 km

Figure 8.44b

Quantitative estimates of displacement across the shear zone may now be calculated from shear strain versus depth plots. In Figures 8.45a and 8.45b, vertical shear strain profiles are presented for the Sierras Magdalena and Madera, respectively. The depth dimension is measured perpendicular to the shear planes in the mylonites. In general the shear planes are parallel to the Magdalena detachment fault, so zero depth is taken to coincide with the projection of the detachment surface. The simple shear displacement is equal to the area under the shear strain-depth curve. Mathematically, the displacement is given by the equation:

$$D = {}_0{}^{h}\!\int \gamma \, dh$$

(modified from Ramsey and Graham, 1970).

Application of this equation to the two shear strain profiles yields shear zone displacements of 7.9±4.3 for the southern and central Sierra Magdalena, and 10.4±6.6 for the Sierra Madera.

Figure 8.45a: Shear strain vs. depth profile for the Sierra Madera. Each data point represents an individual granite sample. Treating the Magdalena detachment fault as the upper boundary of a simple shear zone, the maximum and minimum displacements absorbed by ductile strain in the lower plate are graphically determined.

Figure 8.45b: Shear strain vs. depth profile for the southern and central Sierra Magdalena. Maximum and minimum displacements across this portion of the shear zone are graphically determined.

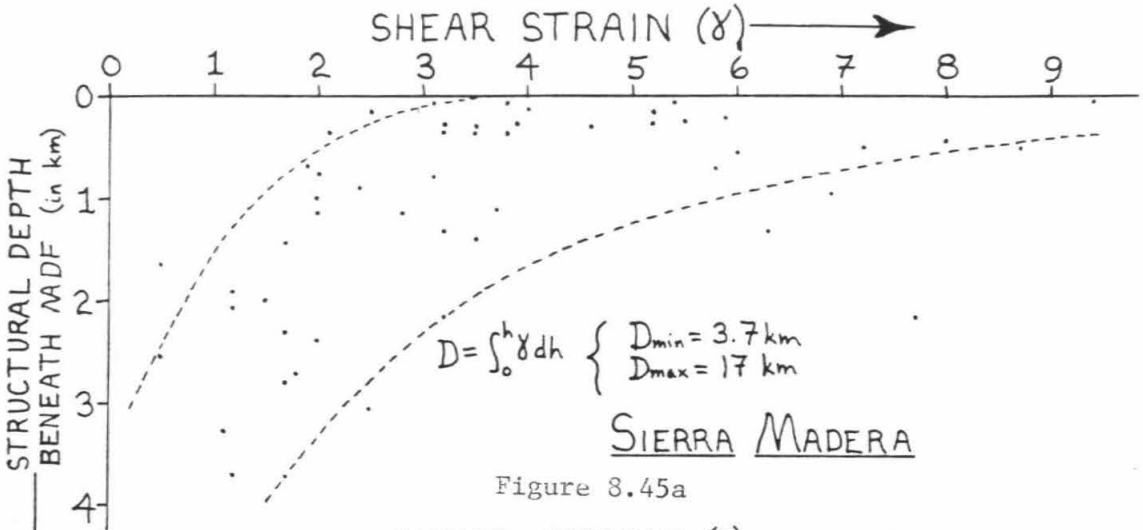

Figure 8.45a

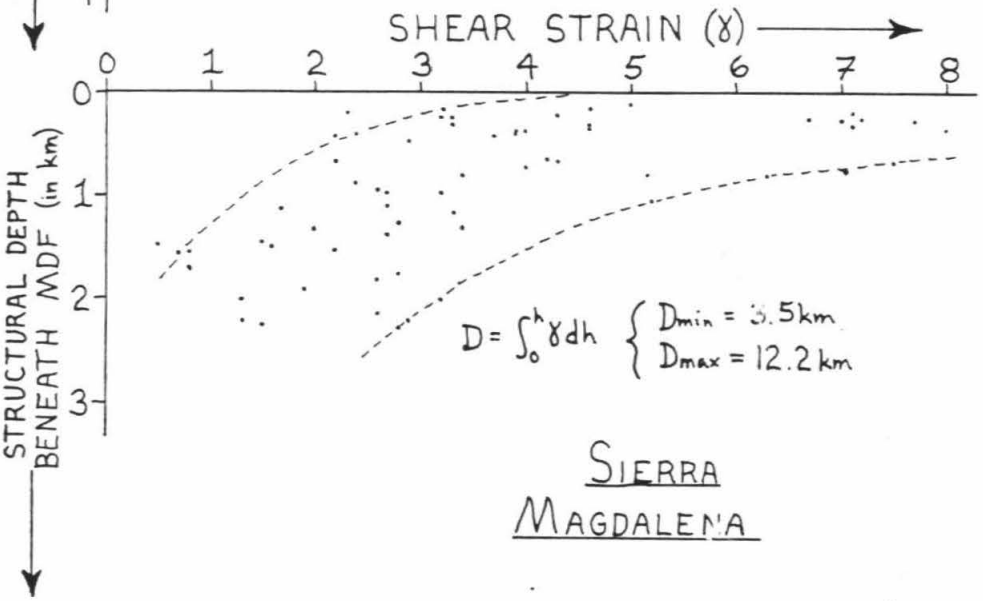

Figure 8.45b

LOWER PLATE STRAIN SYNTHESIS

Now that both the irrotational and rotational strain gradients associated with the post-leucogranite deformation have been determined, the cross sections of Plate 3A can be destrained to a geometry representative of the scenario at the time of leucogranite emplacement. Eight kilometers of southwest vergent simple shear are removed from a three kilometer wide structural interval of the southern and central Sierra Magdalena. Lesser amounts of simple shear are removed from the metamorphic sequences farther northeast. Ten kilometers of displacement are removed from the three cross sections of the Sierra Madera. Length and thickness changes (irrotational strains) associated with the noncoaxial deformation are also accounted for. Balanced, partially destrained solutions for four of the cross sections are illustrated in Plate 3 B.

The restored cross sections invite speculation about the nature of the tectonic environment prior to Middle Tertiary emplacement of the leucogranite suite. Although the geometry is somewhat dependant on the inferred shapes of rock units at depth and the boundary conditions chosen for the destraining process, some first order observations are apparent. In general, it can be argued that the Magalena region was in an unstable state at the end of Early Tertiary time. Specifically, the regions now affected by the greatest shear strains were topographically high, a result of basement cored uplift and regional shortening strain. The Early Tertiary porphyritic two mica granites probably enhanced the topography by inflating the crust in the vicinity of the previously disturbed region. The residual strains in the Jurassic-Lower Cretaceous supracrustal series are a reflection of this Late Cretaceous-Early Tertiary orogeny.

The geometric configuration of the restored leucogranites is highly suggestive of their being emplaced as dikes and sills along the axis of the "orogenic welt." The most extensive leucogranite sill occurs along the contact between the deformed supracrustal series and structurally deeper porphyritic two mica granites. Presumably this geometry is a consequence of preexisting structural anisotropies in the region.

Lastly, restoration of the upper plate sequences to their proper positions above the lower plate allows an estimation of bulk crustal extension resulting from the Middle Tertiary deformation. Depending on where the initial boundaries are chosen, it can be seen that a minimum of !00% + 50% extension has been absorbed across a 50 kilometer wide corridor.

CHAPTER 9:

TECTONIC SUMMARY

The tectonic evolution of the Magdalena metamorphic core complex is briefly summarized below. A series of schematic cross sections (Figures 9.1-9.6) illustrate essential features of the tectonostratigraphic history since Early Jurassic time. Regional stratigraphic correlations implicit in this model are based on observations and arguments developed in Chapters 6 and 7 (pertinent references are cited therein). The timing and kinematics of various deformational phases are derived from structural observations of Chapter 7. The geometry of deformation in three dimensions is constrained in part by the finite strain analysis of Chapter 8. In the final figure (Figure 9.7) Early through Middle Tertiary evolution of the Magdalena area is placed into a regional plate tectonic context, and a driving mechanism for core complex development is proposed.

INTERPRETATION OF TECTONIC SEQUENCE

(1) Early to Middle Jurassic evolution of the region was dominated by the development of a continental margin magmatic arc above a northeast dipping subduction zone. The rhyolite porphyry, quartz arenite, and rhyolite clast conglomerate units accumulated during this time. Sills of granite porphyry were emplaced late in the sequence.

(2) During the Late Jurassic-Earliest Cretaceous, a fault bounded? basin developed, probably along a northwestward trend. The Cocospera

Conglomerate represents alluvial fan debris shed from uplifted Middle Jurassic and older source terranes.

(3) During Early-Middle Cretaceous time the region was inundated by a sea. The sandstones, siltstones, shales, and limestones of the Represo Formation accumulated in a quiescent marine environment.

(4) A long lived orogeny affected the region during Late Cretaceous and Early Tertiary time. At deep structural levels the orogeny is reflected by emplacement of the Late Cretaceous Guacomea Granodiorite, subsequent metamorphism and ductile deformation, then Early Tertiary? post-kinematic emplacement of porphyritic two mica granite plutons. At shallow structural levels the tectonic sequence includes intense disruption of the Represo Formation, and accumulation of syntectonic debris in a foreland basin as the La Lamina thrust sheets were emplaced from the south. The andesites of the Sierra Ventana may have been erupted late in this sequence.

(5) A Middle Tertiary? thermal event is recorded by emplacement of the leucogranite suite at depth and extrusion of silicic pyroclastic rocks at the surface. This reactivation event probably is related to "thermal erosion" of the Farallon plate beneath southwestern North America as the East Pacific rise encroached upon the continental margin (see Figure 9.7). In the proposed model, hot asthenespheric material is placed in direct contact with the lower crust, facilitating melting at depth. The northwestward trend of the resulting leucogranite suite is believed to have been controlled by preexisting structural weaknesses in the continental crust. This model may apply regionally to the Arizona core complexes as well.

(6) Gravitational instabilities resulting from the Middle Tertiary thermal perturbation are believed to be the driving mechanism for development of the southwest vergent mylonite zone and subsequent

detachment of the upper crustal section. Significant displacement on the Magdalena detachment fault appears to have ceased by Early Miocene time.

(7) Middle Miocene and younger tectonic disturbances in the region include folding along northwest trends, northeast directed thrust faulting, and subsequent Basin and Range style block faulting. Strains associated with these Neogene disturbances are relatively minor in comparison to the Middle Tertiary extensional event.

Figure 9.1: Schematic cross sections illustrating the Jurassic through Middle Cretaceous tectonic evolution of the Magdalena region. Symbols in this and succeeding figures as in Figures 6.1, 6.3-6.6, and 6.8-6.9.

Figure 9.2: Schematic sections showing evolution of deeper crustal levels of the Magdalena region during the Late Cretaceous-Early Tertiary orogeny.

Figure 9.3: Schematic sections showing evolution of shallow crustal levels of the Magdalena region during the Late Cretaceous-Early Tertiary orogeny.

JURASSIC

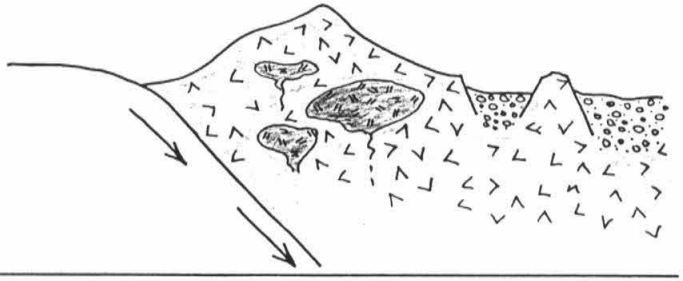

VOLCANIC ARC DEVELOPMENT:

-ACCUMULATION OF SUPRACRUSTAL ROCKS

-EMPLACEMENT OF GRANITIC PLUTONS

LATE JURASSIC-EARLY CRETACEOUS?

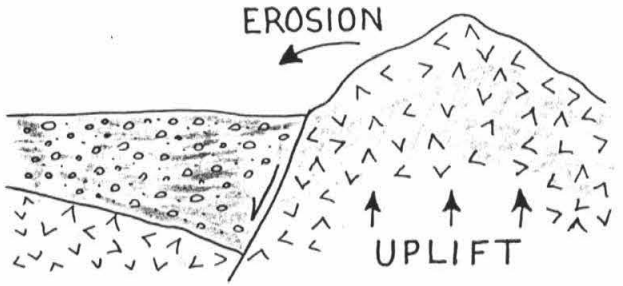

REGIONAL? TECTONIC DISTURBANCE:

-DEPOSITION OF CONGLOMERATE AND FINING UPWARD CLASTIC SECTION

EARLY TO MIDDLE CRETACEOUS

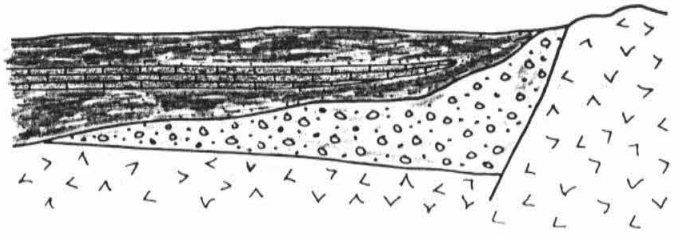

MARINE INCURSION:

-DEPOSITION OF BISBEE GROUP EQUIVALENT STRATA

Figure 9.1

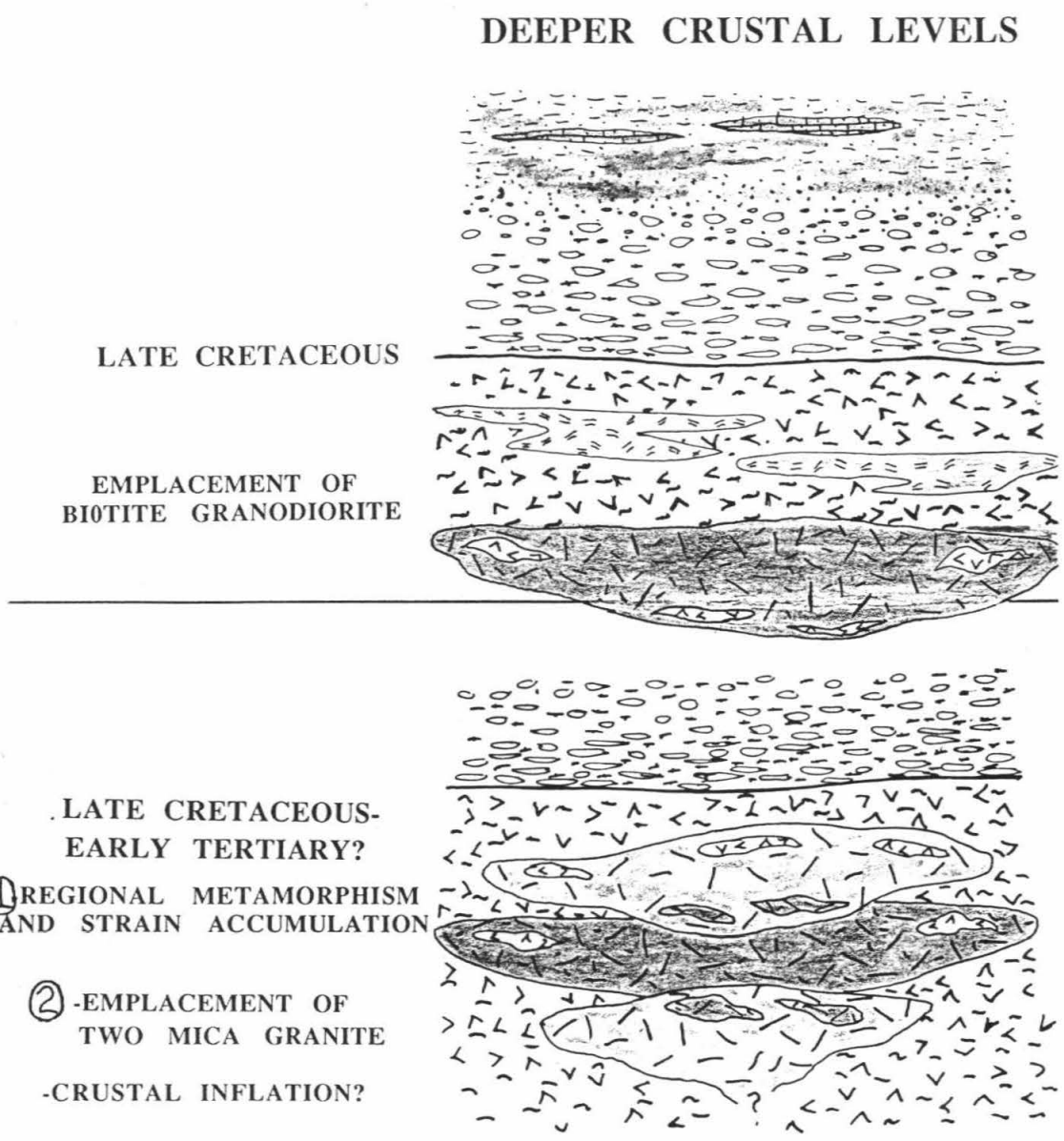
DEEPER CRUSTAL LEVELS
LATE CRETACEOUS
EMPLACEMENT OF
BIOTITE GRANODIORITE
LATE CRETACEOUS-
EARLY TERTIARY?
1 -REGIONAL METAMORPHISM
AND STRAIN ACCUMULATION
2 -EMPLACEMENT OF
TWO MICA GRANITE
-CRUSTAL INFLATION?

Figure 9.2

SHALLOW CRUSTAL LEVELS

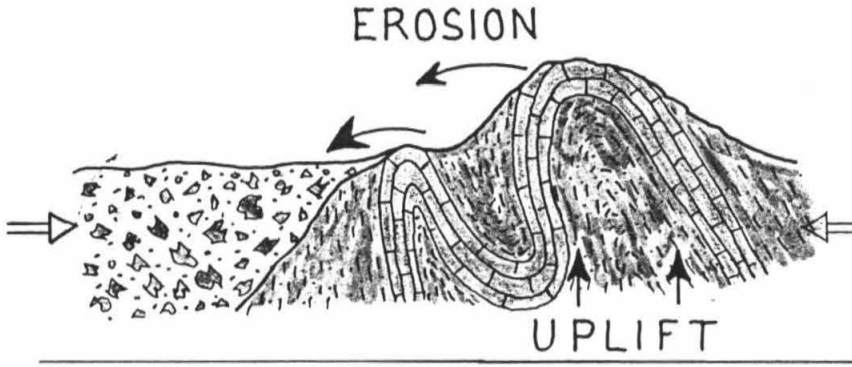

POST ALBIAN-PRE TERTIARY

-TECTONIC DISRUPTION OF BISBEE GROUP STRATA

-NORTH-SOUTH SHORTENING?

-PROXIMAL DEPOSITION OF SEDIMENTARY BRECCIA

Figure 9.3

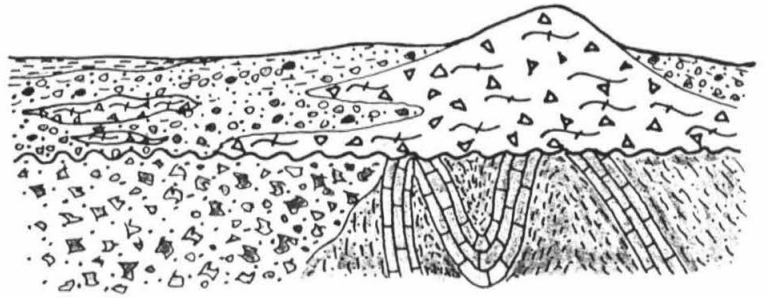

LATE CRETACEOUS-EARLY TERTIARY

-ANDESITIC VOLCANISM WITH COEVAL DEPOSITION OF RED BEDS IN A TECTONICALLY ACTIVE CONTINENTAL ENVIRONMENT

Figure 9.4: Schematic crustal profile of the Magdalena region, reconstructed for Middle Tertiary time. The onset of crustal extension is accompanied by emplacement of leucogranites at depth and andesitic and/or silicic volcanism at the surface.

Figure 9.5: Pre-detachment geometry of the Magdalena section, showing incipient ductile shear zone development.

Figure 9.6: Post-detachment geometry of the Magdalena section, emphasizing ductile strain in the lower plate.

RECONSTRUCTED STRATIGRAPHY

(MIDDLE TERTIARY TIME)

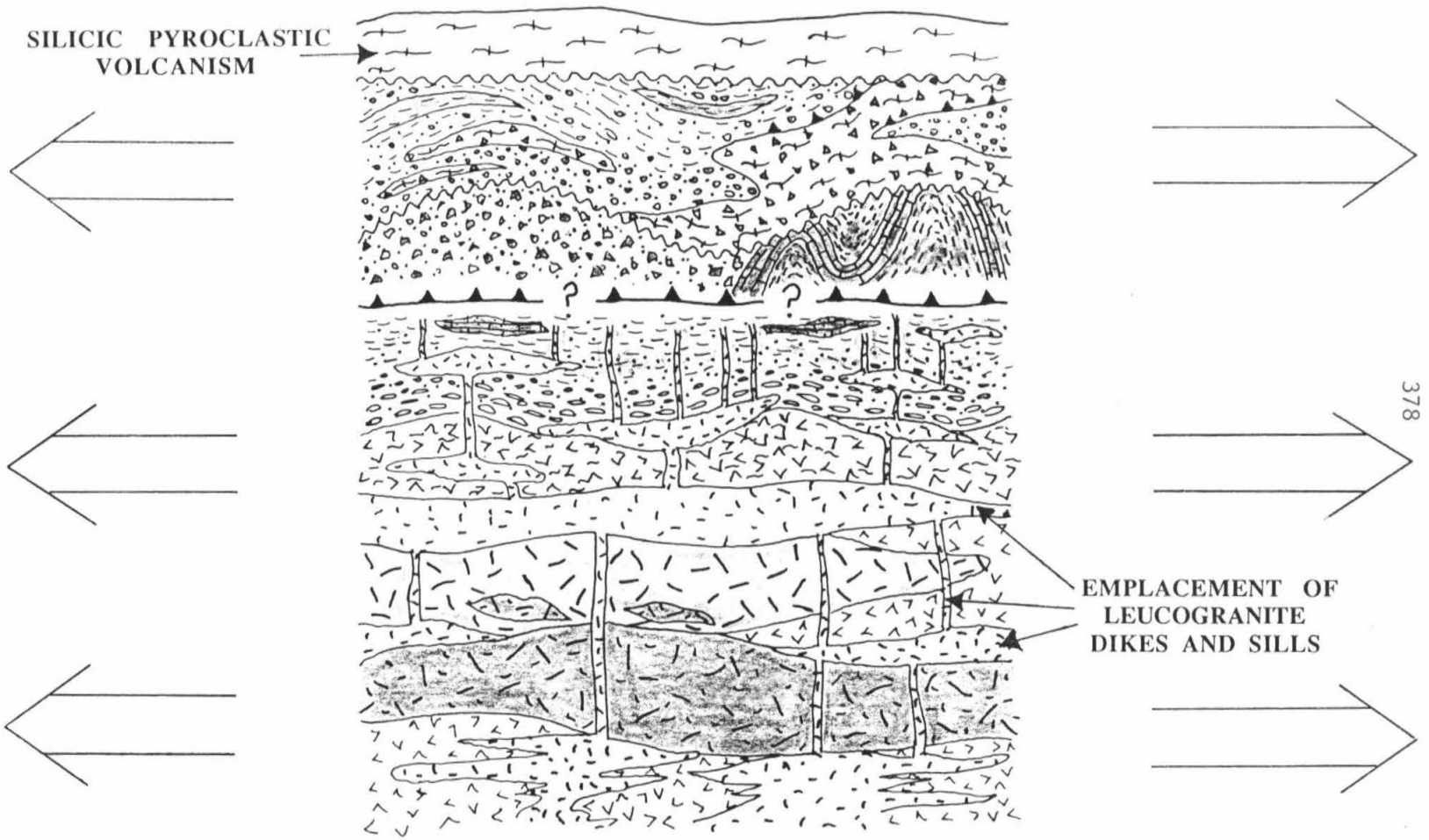

Figure 9.4

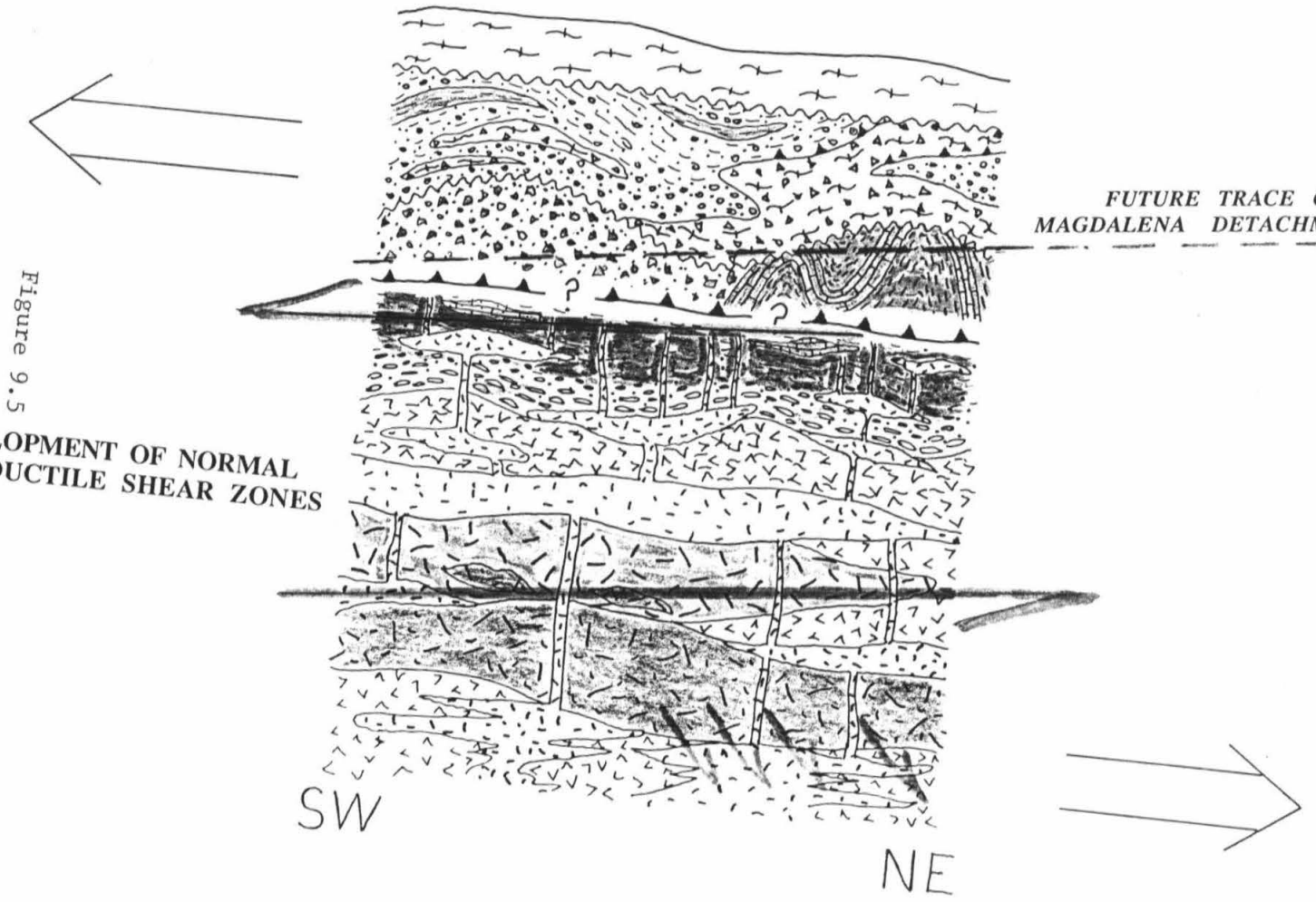

Figure 9.5

DEVELOPMENT OF NORMAL SENSE DUCTILE SHEAR ZONES

POST DETACHMENT TIME

(MIDDLE MIOCENE?)

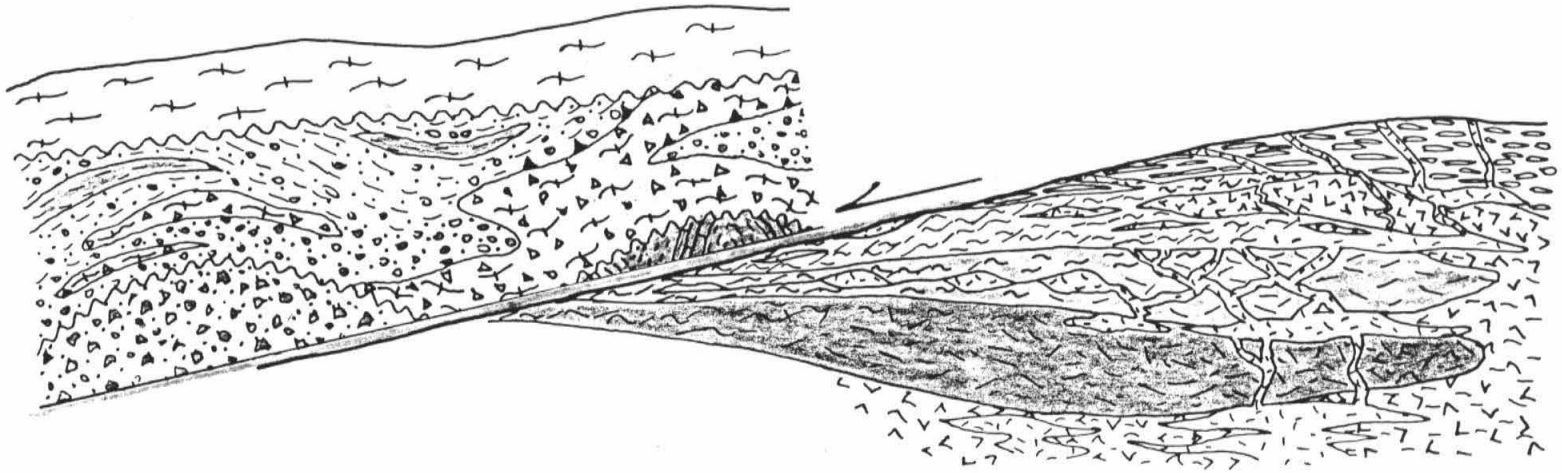

SW NE

Figure 9.6

Figure 9.7: Early through Middle Tertiary plate tectonic setting of the western North American continental margin (modified from Stock and Molnar, 1988), illustrating proposed driving mechanism(s) for metamorphic core complex evolution. In this model, Late Cretaceous-Early Tertiary compressional structures in the southwestern Cordillera are driven by rapid convergence of the Farallon Plate with the North American Plate. As the East Pacific Rise encroaches on the continental margin during the Middle Tertiary, the young subducted oceanic lithosphere begins to "thermally erode" beneath northern Sonora and southern Arizona. Hot asthenespheric material is placed in direct contact with overlying continental lithosphere. Melting is induced, and granites ascend through weak regions of the continental crust. Resulting linear thermal anomalies cause uplift along northwesterly trends while the crust begins to extend. Upper crustal strata become gravitationally unstable and are displaced in northeast and southwest directions along normal sense brittle/ductile shear zones.

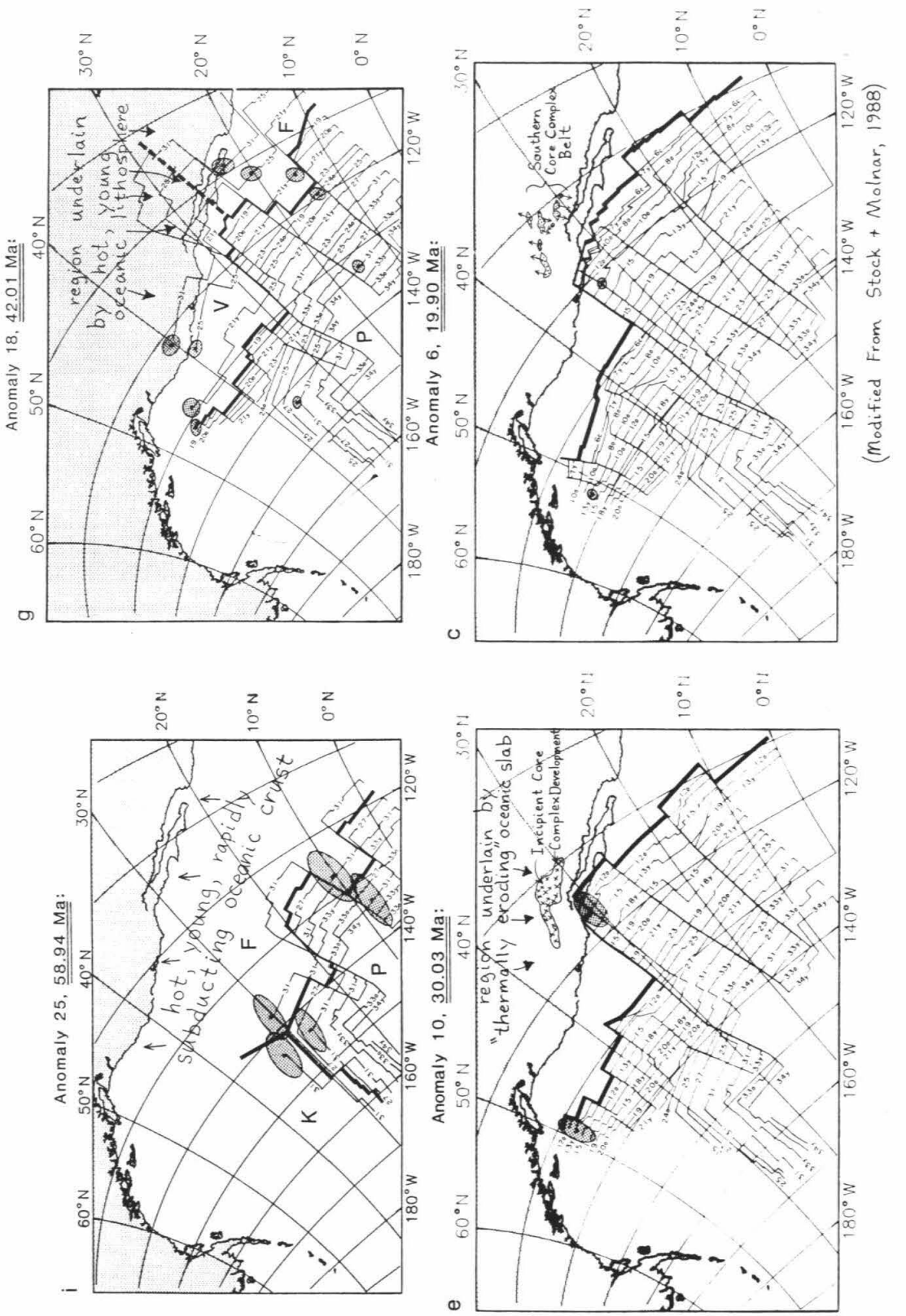
Anomaly 18, 42.01 Ma:
region underlain by hot, young lithosphere
oceanic
Anomaly 6, 19.90 Ma:
Southern Core Complex Belt
(Modified From Stock + Molnar, 1988)
Anomaly 25, 58.94 Ma:
hot, young, rapidly subducting oceanic crust
Anomaly 10, 30.03 Ma:
region underlain by "thermally eroding" oceanic slab
Incipient Core Complex Development
60° N
50° N
40° N
30° N
20° N
10° N
0° N
180° W
160° W
140° W
120° W
F
V
P
K

Figure 9.7

REFERENCES

Almazan-Vazquez, E. y Fernandez-Aguirre, M. A., 1988, Estratigrafia de la Hoja Arivechi, In: Almazan-Vazquez, E. y Fernandez-Aguirre, M. A. (editors), Resumenes, Segundo Simposio Sobre Geologia y Mineria de Sonora, p. 2.

Amaya-Martinez, R., Bojorquez-Ochoa, J. A., Castro-Rodriguez, A. A., Figueroa-Valenzuela, M. C., Grijalva-Haro, A. S., Morfin-Velarde, S., y Rosas-Haro, J. A., 1988, Estratigrafia del prospecto Aconchi, In: Almazan-Vazquez, E. y Fernandez-Aguirre, M. A. (editors), Resumenes, Segundo Simposio Sobre Geologia y Mineria de Sonora, pp. 3-4.

Anderson, T. H., Silver, L. T., and Cordoba, Diego A., 1969, Mesozoic magmatic events of the northern Sonora coastal region, Mexico: GSA Abstracts with Programs, v. 1, p. 3.

Anderson, T. H. and Silver, L. T., 1974, Late Cretaceous plutonism in Sonora, Mexico and its relationship to Circum-Pacific magmatism: GSA Abstracts with Programs, v. 6, p. 484.

Anderson, T. H. and Silver, L. T., 1977, U/Pb ages of granitic plutons near Cananea, Sonora: Economic Geology, v. 72, pp. 827-836.

Anderson, T. H., Silver, L. T., and Salas, G. A., 1977, Metamorphic core complexes of the southern part of the North American Cordillera--northwestern Mexico: GSA Abstracts with Programs, v. 9, p. 881.

Anderson, T. H. and Silver, L. T., 1978, Jurassic magmatism in Sonora, Mexico: GSA Abstracts with Programs, v. 10, p. 359.

Anderson, T. H. and Silver, L. T., 1979, The role of the Mojave-Sonora Megashear in the tectonic evolution of northern Sonora, In: Anderson, T. H. and Roldan-Quintana, J. (editors), GSA Field Trip Guidebook #27, Geology of northern Sonora, pp. 59-68.

Anderson, T. H., Silver, L. T., and Salas, G. A., 1980, Distribution and U-Pb isotope ages of some lineated plutons, northwestern Mexico: GSA Memoir 153, pp. 269-283.

Anderson, T. H. and Silver, L. T., 1983, An overview of Precambrian rocks in Sonora: Revista, Universidad Nacional Autonoma de Mexico, Instituto de Geologia, v. 5, pp. 131-140.

Anderson, T. H., Bajek, D. T., Chepega, J. R., Ichikawa, K. M., Rodriguez, J. L., Stephens, W. E., and Silver, L. T., 1984, Crystalline thrust sheets near the Mojave-Sonora Megashear, Sonora, Mexico: GSA Abstracts with Programs, v. 16, p. 430.

Anderson, T. H., Stephens, W., and Chepega, J., 1988, Newly recognized stratigraphic subdivisions of Jurassic and earliest Cretaceous(?) strata

west of Rio San Miguel, near Cucurpe, Sonora, In: Almazan-Vazquez, E. y Fernandez-Aguirre, M. A. (editors), Resumenes, Segundo Simposio Sobre Geologia y Mineria de Sonora, p. 5.

Bennett, V. and DePaulo, D. J., 1982, Tectonic implications of Nd isotopes in the Pelona, Rand, Orocopia, and Catalina Schists, southern California: GSA Abstracts with Programs, v. 14, p. 442.

Berthe, D., Choukroune, P., and Jegouzo, P., 1979, Orthogneiss, mylonite, and noncoaxial deformation of granites--The example of the South Amorican shear zone: Journal of Structural Geology, v. 1, pp. 31-42.

Bilodeau, W. L., 1978, The Glance Conglomerate, a Lower Cretaceous syntectonic deposit in southeastern Arizona, In: New Mexico Geol. Soc. 29th Annual Field Conference Guidebook, Land of Cochise, pp. 209-214.

Bilodeau, W. L., Kluth, C. F., and Vedder, L. K., 1987, Regional stratigraphic, sedimentologic, and tectonic relationships of the Glance Conglomerate in southeastern Arizona: Arizona Geol. Soc. Digest, v. 18, pp. 229-256.

Bouchez, J. L., 1977, Plastic deformation of quartzites at low temperature in an area of natural strain gradient: Tectonophysics, v. 39, pp. 25-50.

Burg, J. P., 1986, Quartz shape fabric variations and c-axis fabrics in a ribbon mylonite: arguments for an oscillating foliation: Journal of Structural Geology, v. 8, pp. 123-132.

Busby-Spera, C. J., 1988, Speculative tectonic model for the early Mesozoic arc of the southwest Cordilleran United States: Geology, v. 16, pp. 1121-1125.

Buwalda, J. P., 1916, New mammalian fossils from Miocene sediments near Tehachapi Pass in the southern Sierra Nevada: Univ. Calif., Dept. Geol. Bull., v. 10, pp. 75-85.

Buwalda, J. P., 1954, Geology of the Tehachapi Mountains, California: California Division of Mines Bulletin 170, pp. 131-142.

Bykerk-Kauffman, A. and Janecke, S. U., 1987, Late Cretaceous to Early Tertiary ductile deformation, Catalina-Rincon metamorphic core complex, southeastern Arizona: Geology, v. 15, pp. 462-465.

Carillo, R. Pablo , 1985, Geologia del area de Tubutama, Sonora: Tesis de Maestria, Facultad de Ciencias, UNAM, Mexico, D. F.

Clark, K. F., Dow, R. R., and Knowling, R. D., 1979, Fissure-vein deposits related to continental volcanic and subvolcanic terranes in Sierra Madre Occidental province, Mexico: Nevada Bureau of Mines, Report 33, pp. 189-201.

Clark, K. F., Foster, C. T., and Damon, P. E., 1982, Cenozoic mineral deposits and subduction-related magmatic arcs in Mexico: GSA Bulletin, v. 93, pp. 533-544.

Coney, P. J. and Reynolds, S. J., 1977, Cordilleran Benioff zones: Nature, v. 270, pp. 403-406.

Coney, P. J., 1979, The plate tectonic setting of southeastern Arizona, In: New Mexico Geol. Soc. 29th Field Conference Guidebook, Land of Cochise, pp. 285-290.

Cooley, M. E. and Davidson, E. S., 1963, The Mogollon Highlands--Their influence on Mesozoic and Cenozoic erosion and sedimentation: Arizona Geol. Soc. Digest, v. 6, pp. 7-36.

Cooper, J. R. and Silver, L. T., 1964, Geology and ore deposits of the Dragoon quadrangle, Cochise County, Arizona: USGS Prof. Paper 416, 196 pages.

Davis, G. A., Lister, G. S., and Reynolds, S. J., 1986, Structural evolution of the Whipple and South mountains shear zones, southwestern United States: Geology, v. 14, pp. 7-10.

Davis, G. A., 1988, Rapid upward transport of mid-crustal mylonitic gneisses in the footwall of a Miocene detachment fault, Whipple Mountains, southeastern California: Geologisches Rundschau, v. 77, pp. 191-210.

Davis, G. H., 1979, Laramide folding and faulting in southeastern Arizona: American Journal of Science, v. 279, pp. 543-569.

Davis, G. H., 1980, Structural characteristics of metamorphic core complexes, southern Arizona: GSA Memoir 153, pp. 35-77.

Davis, G. H., Gardulski, A. F., and Anderson, T. H., 1981, Structural and structural-petrological characteristics of some metamorphic core complex terranes in southern Arizona and northern Sonora, In: Ortlieb, L. and Roldan-Quintana, J. (editors), Field guides and papers prepared for the GSA Cordilleran Section meeting, Hermosillo, Sonora, Mexico, Geology of northwestern Sonora and southern Arizona, pp. 323-65.

Davis, G. H., 1983, Shear zone model for the origin of metamorphic core complexes: Geology, v. 11, pp. 342-347.

Dawson, M. R. and Jacobson, C. E., 1986, Trace element geochemistry of the metabasites from the Pelona-Orocopia-Rand Schists, southern California: GSA Abstracts with Programs, v. 18, p. 99.

De Jong, K. A., Escarcega-Escarcega, J. A., and Damon, P. E., 1988, Eastward thrusting, southwestward folding, and westward backsliding in the Sierra La Vibora, Sonora, Mexico: Geology, v. 16, pp. 904-907.

De Paor, D. G., 1988, R_f/phi analysis using an orientation net: Journal of Structural Geology, v. 10, pp. 323-333.

Dibblee, T. W., Jr., 1952, Geology of the Saltdale quadrangle, California: California Division of Mines Bulletin 160, pp. 7-43.

Dibblee, T. W., Jr., 1959, Preliminary geologic map of the Mojave quadrangle,

California: USGS Mineral Inv. Field Studies, Map MF-219.

Dibblee, T. W., Jr., 1967, Areal geology of the western Mojave desert, California: USGS Prof. Paper 522, pp. 1-152.

Dickinson, W. R., 1981, Plate tectonic setting of the southern Cordillera: Arizona Geol. Soc. Digest, v. 14, pp. 113-136.

Dickinson, W. R. and Klute, M. A., 1987, (editors), Mesozoic rocks of southern Arizona and adjacent areas, Arizona Geol. Soc. Digest 18, 394 pages.

Dokka, R. K., McCurry, M., Woodburne, M. O., Frost, E. G., and Okaya, D. A., 1988, A field guide to the Cenozoic structure of the Mojave desert, In: Weide, D. L. and Faber, M. L. (editors), GSA Cordilleran Section Field Trip Guidebook, This Extended Land, pp. 21-44.

Drewes, H, 1980, Tectonic map of southeast Arizona: USGS Map I-1109.

Ehlig, P. L., 1968, Causes of distribution of Pelona, Rand, and Orocopia Schists along the San Andreas and Garlock faults, In: Dickinson, W. R. and Grantz, A. (editors), Proceedings of conference on geologic problems of the San Andreas fault system, Stanford Univ. Pubs. Geol. Sci., v. 2, pp. 294-306.

Flores, Teodoro, 1929, Reconocimientos geologicos en la region central del estado de Sonora: Instituto Geologico de Mexico, Boletin numero 49, pp. 1-267.

Gans, P. B., 1987, An open system, two-layer crustal stretching model for the eastern Great Basin: Tectonics, v. 6, pp. 1-12.

Garcia y Barragan, J. C., Jacques-Ayala, C., De Jong. K. A., y Montano-Jimenez, T. R., 1988, Consideraciones preliminares sobre la geologia de la porcion oeste de los cerros El Amol, Altar, Sonora, In: Almazan-Vazquez, E. y Fernandez-Aguirre, M. A. (editors), Resumenes, Segundo Simposio Sobre Geologia y Mineria de Sonora, p. 22.

Gilmont, N. L., 1978, Geology of the Puerto La Bandera Area, Sonora, Mexico: Masters Thesis, University of Northern Arizona, Department of Geology.

Glazner, A. F., Bartley, J. M., and Walker, J. D., 1988, Geology of the Waterman Hills detachment fault, central Mojave desert, California, In: Weide, D. L. and Faber, M. L. (editors), GSA Cordilleran Section Field Trip Guidebook, This Extended Land, pp. 225-238.

Goldstein, A. G., 1988, Factors affecting the kinematic interpretation of asymmetric boudinage in shear zones: Journal of Structural Geology, v. 10, pp. 707-715.

Gonzalez-Leon, C. y Jacques-Ayala, C., 1988, La secuencia del Cretacico Temprano del area de Cerro de Oro, Sonora: implicaciones paleogeograficas, In: Almazan-Vazquez, E. y Fernandez-Aguirre, M. A. (editors), Resumenes, Segundo Simposio Sobre Geologia y Mineria de Sonora, pp. 23-24.

Goodlin, T. C. and Mark, R. A., 1987, Tectonic implications of stratigraphy and structure of Cretaceous rocks and overlying Mid-Tertiary cover in Hot Springs Canyon, Galiuro Mountains, southeastern Arizona: Arizona Geol. Soc. Digest, v. 18, pp. 177-189.

Hagstrum, J. T., Cox, D. P., and Miller, R. J., 1987, Structural reinterpretation of the Ajo mining district, Pima County, Arizona, based on paleomagnetic and geochronologic studies: Economic Geology, v. 82, pp. 1348-1361.

Hamilton, W., 1987, Crustal extension in the Basin and Range province, southwestern United States, In: Coward et al., (editors), Geol. Soc. London Spec. Pub., Continental Extensional Tectonics, pp. 155-176.

Hardy, L. R., 1981, Geology of the central Sierra de Santa Rosa, Sonora, Mexico, In: L.-Ortlieb and Roldan-Quintana (editors), Geology of northwestern Mexico and southern Arizona, Field guides and papers associated with the GSA Cordilleran section meeting in Hermosillo, Sonora.

Haxel, G. B. and Dillon, J., 1978, The Pelona-Orocopia Schist and Vincent-Chocolate Mountain thrust system, southern California, In: Howell, D. G. and McDougall, K. A. (editors), Pacific Section, Soc. Econ. Paleontologists and Mineralogists, Pacific Coast Paleogeography Symposium 2, Mesozoic paleogeography of the western United States, pp. 453-469.

Haxel, G. B., Gray, F., Briskey, J. A., Tosdal, R. M., and Wright, J. E., 1983, Two contrasting suites of Late Cretaceous and Early Tertiary granitoids, south-central Arizona: GSA Abstracts with Programs, v. 15, p. 410.

Haxel, G. B., Tosdal, R. M., May, D. J., and Wright, J. E., 1984, Latest Cretaceous and early Tertiary orogenesis in south-central Arizona: Thrust faulting, regional metamorphism, and granitic plutonism: GSA Bulletin, v. 95, pp. 631-653.

Haxel, G. B. and Tosdal, R. M., 1986, Significance of the Orocopia Schist and Chocolate Mountains thrust in the late Mesozoic tectonic evolution of the southeastern California-southwestern Arizona region: extended abstract: Arizona Geol. Soc. Digest, v. 16, pp. 52-61.

Haxel, G. B., Budahn, J. R., Fries, T. L., King, Bi-Shia W., White, L. D., and Aruscavage, P. J., 1987, Geochemistry of the Orocopia Schist, southeastern California: Summary, In: Dickinson, W. R. and Klute, M. A. (editors), Arizona Geol. Soc. Digest v. 18, Mesozoic rocks of southern Arizona and adjacent areas, pp. 49-64.

Hayama, Y., Shibata, K., and Takeda, H., 1984, K-Ar ages of the low grade metamorphic rocks in the Altar massif, northwest Sonora, Mexico: Journal Geol. Soc. Japan, v. 90, pp. 589-596.

Hayes, M. J., 1987, Depositional history of Upper Cretaceous Fort Crittendon Formation in southeastern Arizona: Arizona Geol. Soc. Digest, v. 18, pp. 315-326.

Hayes, P. T., 1970, Cretaceous paleogeography of southeastern Arizona and adjacent areas: USGS Prof. Paper 658-B.

Hayes, P. T. and Drewes, H., 1978, Mesozoic depositional history of southeastern Arizona, In: New Mexico Geol. Soc. Guidebook, 29th Field Conf., Land of Cochise, pp. 201-208.

Hershey, O. H., 1912, The Belt and Pelona series: Am. Jour. Sci. ser. 4, v. 34, pp. 263-273.

Hess, F. L., 1909, Gold mining in the Randsburg quadrangle, California: USGS Bulletin 430, pp. 23-47.

Hoisch, T. D., Miller, C. F., Heizler, M. T., Harrison, T. M., and Stoddard, E. F., 1988, Late Cretaceous regional metamorphism in southeastern California, In: Ernst, W. G. (editor), Rubey Volume VII, Metamorphism and crustal evolution of the western United States, pp. 538-571.

Hovey, E. O., 1905, The western Sierra Madre of the State of Chihuahua, Mexico: Amer. Geogr. Soc. Bull., v. 37, pp. 531-543.

Howard, K. A. and John, B. E., 1987, Crustal extension along a rooted system of imbricate normal faults: Colorado River extensional corridor, California and Arizona, In: Coward, M. P., Dewey, J. F., and Hancock, P. L. (editors), Geol. Soc. Spec. Pub. 28, Continental Extensional Tectonics, pp. 299-311.

Hulin, C. D., 1925, Geology and ore deposits of the Randsburg quadrangle of California: California State Mining Bureau, Bulletin 95.

Imlay, R. W., 1939, Paleogeographic studies in northeastern Sonora: GSA Bulletin, v. 50, pp. 1723-1744.

Jacobson, C. J. and Sorensen, S. S., 1986, Amphibole compositions and metamorphic history of the Rand Schist and the greenschist unit of the Catalina Schist, southern California: Contrib. Mineralogy Petrology, v. 92, pp. 308-315

Jacobson, C. J., Dawson, M. R., and Postlethwait, C. E., 1988, Structure, metamorphism, and tectonic significance of the Pelona, Orocopia, and Rand schists, southern California, In: Ernst, W. G. (editor), Rubey Volume VII, Metamorphism and crustal evolution of the western United States, pp.976-997.

Jacques-Ayala, C., 1986, Las rocas cretacicas del area de Caborca-Altar y sus deformaciones, In: Instituto de Geologia-UNAM, Estacion Regional del Noroeste, Hermosillo, Sonora, Nuevas Aportaciones a la Geologia de Sonora, pp. 56-68.

Jacques-Ayala, C. and Potter, P. E., 1987, Stratigraphy and structure of Lower Cretaceous rocks, Sierra el Chanate, northwest Sonora, Mexico: Arizona Geol. Soc. Digest, v. 18, pp. 203-214.

Jacques-Ayala, C. and Garcia y Barragan, J. C., 1988, Geology of the Cretaceous

rocks of Sierra El Chanate, northwest Sonora, In: Almazan-Vazquez, E. y Fernandez-Aguirre, M. A. (editors), Resumenes, Segundo Simposio Sobre Geologia y Mineria de Sonora, pp. 31-32.

James, A. I., 1985, The Origin and History of the Rand Thrust: Masters Thesis, University of California, Santa Barbara, Department of Geological Sciences.

Janecke, S. U., 1987, Mesozoic and Early Tertiary structural history of the Geesaman Wash area, northeastern Catalina-Rincon metamorphic core complex: Arizona Geol. Soc. Digest, v. 18, pp. 189-202.

Keller, P. C., Bockoven, N. T., and McDowell, F. W., 1982, Tertiary volcanic history of the Sierra del Gallego area, Chihuahua, Mexico: GSA Bulletin, v. 93, pp. 303-314.

King, R. E., 1939, A geological reconnaissance in the northern Sierra Madre Occidental of Mexico: GSA Bulletin, v. 50, pp. 1625-1722.

Kistler, R. W. and Peterman, Z. E., 1978, Reconstruction of crustal blocks of California on the basis of initial strontium isotopic compositions of Mesozoic granitic rocks: USGS Prof. Paper 1071, pp. 1-17.

Kitz, M. B. and Anderson, T. H., 1988, Deformation and stratigraphy of Lower Cretaceous basinal marine sediments, north-central Sonora, Mexico, In: Almazan-Vazquez, E. y Fernandez-Aguirre, M. A. (editors), Resumenes, Segundo Simposio Sobre Geologia y Mineria de Sonora, p. 34.

Lindberg, F. A., 1987, Cretaceous sedimentary geology of the Rucker Canyon area, Cochise County, Arizona: Arizona Geol. Soc. Digest, v. 18, pp. 283-300.

Lisle, R. J., 1985, Geological Strain Analysis, A Manual for R_f/phi Analysis: Pergamon Press.

Lister, G. S., 1977, Discussion: Crossed girdle c-axis fabrics in quartzites plastically deformed by plane strain and progressive simple shear: Tectonophysics, v. 39, pp. 51-54.

Lister, G. S., 1979, Fabric transitions in plastically deformed quartzites: competition between basal, prism, and rhomb systems: Bull. Mineral, v. 102, pp. 232-241.

Lister, G. S. and Snoke, A. W., 1984, S-C mylonites: Journal of Structural Geology, v. 6, pp. 617-638.

McDowell, F. W. and Clabaugh, S. E., 1979, Ignimbrites of the Sierra Madre Occidental and their relationship to the tectonic history of western Mexico: GSA Special Paper 180, pp. 113-124.

Miller, E. L., Gans, P. B. , and Garing, J., 1983, The Snake Range decollement: An exhumed mid-Tertiary brittle-ductile transition: Tectonics, v. 2, pp. 239-263.

Miranda, M., A. and Quiroz, F., 1988, Vulcanismo alcalino bimodal asociado a la tectonica cenozoica de cuencas y sierras en la region de Magdalena de Kino, Sonora, Mexico, In Resumenes: IX Convencion Geologica Nacional, Sociedad Geologica Mexicana, del 19 al 21 Octubre, Mexico, D.F.

Montano-Jimenez, T. R., 1988, Geologia del area de el Tigre, noreste de Sonora: Tesis de Maestria, Universidad de Sonora, Departamento de Geologia.

Naruk, S. J., 1986a, Finite strains and mylonitic fabrics in the Santa Catalina metamorphic core complex, southeastern Arizona: GSA Abstracts with Programs, v. 18, p. 163.

Naruk, S. J., 1986b, Strain and displacement across the Pinaleno Mountains shear zone, Arizona, USA: Journal of Structural Geology, v. 8, pp. 35-46.

Navarro-Fuentes, J. C. y Tellez-Duarte, M. A., 1988, Sobre la estratigrafia del Cretacico Temprano en el area de Santa Ana, Sonora, In: Almazan-Vazquez, E. y Fernandez-Aguirre, M. A. (editors), Resumenes, Segundo Simposio Sobre Geologia y Mineria de Sonora, p. 43.

Paschier, C. W., 1983, The reliability of asymmetric c-axis fabrics of quartz to determine sense of vorticity: Tectonophysics, v. 99, pp. T9-T18.

Paschier, C. W., and Simpson, C., 1986, Porphyroclast systems as kinematic indicators: Journal of Structural Geology, v. 8, pp. 831-844.

Postlethwait, C. E. and Jacobson, C. E., 1987, Early history and reactivation of the Rand thrust, southern California: Journal of Structural Geology, v. 9, pp. 195-205.

Ramsey, J. G., 1967, Folding and Fracturing of Rocks: McGraw Hill.

Ramsey, J. G. and Graham, R. H., 1970, Strain variation in shear belts: Can. Jour. Earth Sci., v. 7, pp. 786-813.

Ramsey, J. G. and Huber, M. I., 1983, The Techniques of Modern Structural Geology, Volume 1: Strain Analysis: Academic Press, Inc., pp. 1-307.

Ramsey, J. G. and Huber, M. I., 1987, The Techniques of Modern Structural Geology, Volume 2: Folds and Fractures: Academic Press, Inc., pp 308-700.

Rangin, C., 1977a, Sobre la presencia de jurasico superior con amonitas en Sonora septentrional: Revista, Univ. Nal. Auton. Mexico, Instituto de Geologia, v. 1, pp. 1-4.

Rangin, C., 1977b, Tectonicas sobrepuestas en Sonora septentrional: Revista, Univ. Nal. Auton. Mexico, Instituto de Geologia, v. 1, pp. 44-47.

Rehrig, W. A. and Reynolds, S. J., 1980, Geologic and geochronologic reconnaissance of a northwest trending zone of metamorphic core complexes in southern and western Arizona: GSA Memoir 153, pp. 131-57.

Reynolds, S. J., Keith, S. B., and Coney, P. J., 1980, Stacked overthrusts of

Precambrian crystalline basement and inverted Paleozoic sections emplaced over Mesozoic strata, west-central Arizona: Arizona Geol. Soc. Digest, v. 12, pp. 45-51.

Reynolds, S. J., Shaqfiqullah, M., Damon, P. E., and DeWitt, E., 1986a, Early Miocene mylonitization and detachment faulting, South Mountains, central Arizona: Geology, v. 14, pp. 283-286.

Reynolds, S. J., Spencer, J. E., Richard, S. M., and Laubach, S. E., 1986b, Mesozoic structures in west central Arizona: Arizona Geol. Soc. Digest, v. 16, pp. 35-51.

Reynolds, S. J., 1988, Geologic Map of Arizona, Arizona Geol. Survey Map 26.

Reynolds, S. J., Richard, S. M., Haxel, G. B., Tosdal, R. M., and Laubach, S. E., 1988, Geologic setting of Mesozoic and Cenozoic metamorphism in Arizona, In: Ernst, W. G. (editor), Rubey Volume VII, Metamorphism and crustal evolution of the western United States, pp. 466-501.

Richard, S. M., Reynolds, S. J., and Spencer, J. E., 1987, Mesozoic stratigraphy of the Little Harquahala and Harquahala Mountains, west central Arizona: Arizona Geol. Soc. Digest, v. 18, pp. 101-120.

Richard, S. M. and Sutter, J. F., 1988, Post-thrusting, Late Cretaceous syn-plutonic deformation and subsequent cooling, west central Arizona: GSA Abstracts with Programs, v. 20, p. A16.

Riggs, N., Mattinson, J. M., and Busby Spera, C. J., 1986, U/Pb ages of the Mount Wrightson Formation, southern Arizona, and possible correlation with the Navajo sandstone: Am. Geoph. Un., Trans. (EOS), v. 64, p. 1249.

Riggs, N., 1987, Stratigraphy, structure, and geochemistry of Mesozoic rocks in the Pajarito mountains, Santa Cruz county, Arizona: Arizona Geol. Soc. Digest, v. 18, pp. 165-176.

Riggs, N. and Busby-Spera, C. J., 1987, Tectonic setting of Lower Jurassic volcanic rocks in southern Arizona: GSA Abstracts with Programs, v. 19, p. 820.

Rodriguez-Castaneda, J. L., 1986, Interpretacion del contacto jurasico-cretacico en Sonora este-central: Paper and Field Trip Guide In: Instituto de Geologia-UNAM, Estacion Regional del Noroeste, Hermosillo, Sonora, Nuevas Aportaciones a la Geologia de Sonora, pp. 37-48; 69-91.

Rodriguez-Castaneda, J. L., Castillo-Mendoza, E., y Anderson, T. H., 1988, Caracteristicas estructurales y estratigraficas de rocas preterciarias entre los Rios San Miguel y Sonora, Sonora norte-central, In: Almazan-Vazquez, E. y Fernandez-Aguirre, M. A. (editors), Resumenes, Segundo Simposio Sobre Geologia y Mineria de Sonora, p. 52.

Roldan-Quintana, J., 1986, Estratigrafia de las rocas terciarias del noroeste de Sonora, In: Instituto de Geologia-UNAM, Estacion Regional del Noroeste, Hermosillo, Sonora, Nuevas Aportaciones a la Geologia de Sonora, pp. 49-

53.

Ross, D. C., 1982, The metamorphic and plutonic rocks of the southernmost Sierra Nevada, California, and their tectonic framework: USGS Prof. Paper (preprint).

Salas, G. A., 1968, Areal geology and petrology of the igneous rocks of the Santa Ana region, northwest Sonora: Bol. Soc. Geol. Mexicana, v. 31, pp. 11-63.

Saleeby, J. B. and Sams, D. B., 1987, U/Pb zircon, strontium, and oxygen isotopic and geochronological study of the southernmost Sierra Nevada batholith, California: Jour. Geoph. Res., v. 92, pp. 10443-10466.

Sams, D. B. and Saleeby, J. B., 1988, Geology and petrotectonic significance of crystalline rocks of the southernmost Sierra Nevada, California, In: Ernst, W. G. (editor), Rubey Volume VII, Metamorphism and crustal evolution of the western United States, pp. 865-893.

Savage, D. E., Downs, T., and Poe, O. J., 1954, Cenozoic land life of southern California: Calif. Div. Mines Bull. 170, pp. 43-58.

Sawyer, D. A., 1986, Late Cretaceous caldera volcanism and porphyry copper deposits, Silver Bell Mountains, southern Arizona: Arizona Geol. Soc Digest, v. 16, pp. 408-421.

Segerstrom, L., 1987, Geology of the Planchas de la Plata area, northern Sonora, Mexico: Arizona Geol. Soc. Digest, v. 18, pp. 153-164.

Shakel, D. W., Silver, L. T., and Damon, P. E., 1977, Observations on the history of the gneissic core complex, Santa Catalina Mtns., southern Arizona: GSA Abstracts with Programs, v. 9, pp. 1169-1170.

Sharry, J., 1981, The geology of the western Tehachapi Mountains, California: PhD Thesis, Massachusetts Institute of Technology, Cambridge, Mass., 215 pages.

Silver, L. T. and Anderson, T. H., 1974, Possible left-lateral early to middle Mesozoic disruption of the southwestern North American craton Margin: GSA Abstracts with Programs, v. 6, p. 955.

Silver, L. T. and Anderson, T. H., 1983, Further evidence and analysis of the role of the Mojave-Sonora Megashear(s) in Mesozoic Cordilleran tectonics: GSA Abstracts with Programs, v. 15, p. 273.

Silver, L. T., Sams, D. B., Bursik, M. I., Graymer, R. W., Nourse, J. A., Richards, M. A., and Salyards, S. L., 1984, Some observations on the tectonic history of the Rand Mountains, Mojave Desert, California: GSA Abstracts with Programs, v. 16, p. 333.

Silver, L. T. and Anderson, T. H., 1984, Evidence for a major Eocene crustal reactivation episode in northern Sonora, Mexico: GSA Abstracts with Programs, v. 16, p. 656.

Silver, L. T., 1986, Evidence for Paleogene low-angle detachment of the southern Sierra Nevada: GSA Abstracts with Programs, v. 18, p. 750.

Silver, L. T. and Nourse, J. A., 1986, The Rand Mountains "thrust" complex in comparison with the Vincent thrust-Pelona Schist relationship: GSA Abstracts with Programs, V. 18, p. 185.

Silver, L. T. and Chappell, B. W., 1988, The Peninsular Ranges Batholith: an insight into the evolution of the Cordilleran batholiths of southwestern North America: Transactions of the Royal Society of Edinburgh, Earth Sciences, v. 79, pp. 105-121.

Simpson, C. and Schmidt, S. M., 1983, An evaluation of criteria to deduce the sense of movement in sheared rocks: GSA Bulletin, v. 94, pp 1281-1288.

Simpson, C., 1984, Borrego Springs-Santa Rosa mylonite zone: a Late Cretaceous west directed thrust in southern California: Geology, v. 12, pp. 8-11.

Simpson, C., 1985, Deformation of granitic rocks across the brittle-ductile transition: Journal of Structural Geology, v. 7, pp. 503-511.

Simpson, C., 1986, Determination of movement sense in mylonites: Journ. Geol. Ed., v. 34, pp. 246-261.

Simpson, C., 1988, Analysis of two dimensional finite strain, In: Marshak, S. and Mitra, G. (editors), Basic Methods of Structural Geology, Prentice-Hall, Inc., pp. 317-338?

Smith, C. H. and Gehrels, G. E., 1987, Evidence for Late Cretaceous-Early Tertiary thrust faulting, peraluminous plutonism, and metamorphism in the Little Rincon Mountains, southeastern Arizona: GSA Abstracts with Programs, v. 19, p. 452.

Smith, G. I., 1964, Geology and volcanic petrology of the Lava Mountains, San Bernardino County, California: USGS Prof. Paper 457, 97 pages.

Stephens, W. E. and Anderson, T. H., 1986, Preliminary geologic map of the La Lamina thrust complex (provided by T. H. Anderson).

Stewart, J. H., 1978, Basin-range structure in western North America: A Review, GSA Memoir 152, pp. 1-31.

Stock, J. and Molnar, P., 1988, Uncertainties and implications of the Late Cretaceous and Tertiary positions of North America relative to the Farallon, Kula, and Pacific plates: Tectonics, v. 7, pp. 1339-1384.

Strekeisen, A. L., 1973, Classification and nomenclature for plutonic rocks: Geotimes, October issue.

Taliaferro, N. L., 1933, An occurrence of Upper Cretaceous sediments in northern Sonora, Mexico: Jounal of Geology, v. 41, pp. 12-37.

Titley, S. R., 1976, Evidence for a Mesozoic linear tectonic pattern in

southeastern Arizona: Arizona Geol. Soc. Digest, v. 10, pp. 71-101.

Tosdal, R. M., 1986, Mesozoic ductile deformations in the southern Dome Rock Mountains, northern Trigo Mountains, Trigo Peak, and Livingston Hills, southwestern Arizona, and Mule Mountains, southeastern California: Arizona Geol. Soc. Digest, v. 16, pp. 62-71.

Tosdal, R. M. and Miller, R. J., 1988, Thermal-tectonic terranes of the Ajo and Lukeville 1^{o} by 2^{o} quadrangles: K/Ar geochronology of Early Tertiary and older rocks: USGS Open File Report 88-217, pp. 5-8.

Tosdal, R. M., Haxel, G. B., and Wright, J. E., 1988, Jurassic geology of the Sonoran desert region, southern Arizona, southeastern California, and northernmost Sonora: Construction of a continental-margin magmatic arc, In: Jenny, J. P. and Reynolds, S. J. (editors), Geological Evolution of Arizona, Arizona Geol. Soc. Digest, v. 17, (in press).

Valentine, W. G., 1936, Geology of the Cananea Mountains, Sonora, Mexico: GSA Bulletin, v. 47, pp. 53-86.

Vargo, J. M., 1972, Structural geology of a portion of the eastern Rand Mountains, Kern and San Bernardino Counties, California: Masters Thesis, University of Southern California.

Wernicke, B., 1985, Uniform-sense normal simple shear of the continental lithosphere: Can. Jour. Earth Sci., V. 22, pp. 108-125.

Wheeler, J., 1986a, Average properties of ellipsoidal fabrics: implications for two and three dimensional methods of strain analysis: Tectonophysics, v. 126, pp. 259-270.

Wheeler, J., 1986b, Strain analysis in rocks with pretectonic fabrics: Journal of Structural Geology, v. 8, pp. 887-896.

Wright, J. E., Haxel, G. B., and May, D. J., 1981, Early Jurassic U/Pb isotopic ages for Mezozoic supracrustal sequences, Papago Indian Reservation, southern Arizona: GSA Abstracts with Programs, v. 13, p. 115.

Wright, J. E. and Haxel, G. B., 1982, A garnet-two-mica granite, Coyote Mountains, southern Arizona: geologic setting, uranium-lead isotopic systematics of zircon, and nature of granite source region: GSA Bulletin, v. 93, pp. 1176-1188.

Wright, J. E. and Snoke, A. W., 1986, Mid-Tertiary mylonitization in the Ruby Mountain-East Humboldt Range metamorphic core complex, Nevada: GSA Abstracts with Programs, v. 18, p. 795.

Wust, S. L., 1986, Regional correlation of extension directions in Cordilleran metamorphic core complexes: Geology, v. 14, pp. 828-830.